THE ASTROPHYSICAL JOURNAL

An International Review of Spectroscopy and Astronomical Physics

FOUNDED IN 1895 BY GEORGE E. HALE AND JAMES E. KEELER

EDITORS

PAUL W. MERRILL
Mount Wilson Observatory of the Carnegie Institution of Washington

HARLOW SHAPLEY
Harvard College Observatory Cambridge, Massachusetts

J. H. MOORE
Lick Observatory University of California

OTTO STRUVE
Yerkes Observatory of the University of Chicago

COLLABORATORS

S. B. NICHOLSON, *Mount Wilson Observatory;* D. B. MCLAUGHLIN, *University of Michigan;* J. A. PEARCE, *Dominion Astrophysical Observatory, Victoria;* S. A. MITCHELL, *Leander McCormick Observatory;* LYMAN SPITZER, JR., *Yale University;* W. W. MORGAN, *Yerkes Observatory;* CECILIA H. PAYNE-GAPOSCHKIN, *Harvard College Observatory;* H. N. RUSSELL, *Princeton University;* F. H. SEARES, *Mount Wilson Observatory*

VOLUME 99

JANUARY–MAY 1944

THE UNIVERSITY OF CHICAGO PRESS
CHICAGO, ILLINOIS

THE CAMBRIDGE UNIVERSITY PRESS, LONDON

PUBLISHED JANUARY, MARCH, MAY, 1944

COMPOSED AND PRINTED BY THE UNIVERSITY OF CHICAGO PRESS
CHICAGO, ILLINOIS, U.S.A.

Astron. observatory Wahr

CONTENTS

NUMBER 1

PAGE

NOTES ON THE THEORY OF NONCOHERENT SCATTERING. Lyman Spitzer, Jr. 1

COLORS OF EARLY-TYPE STARS IN THE SOUTHERN MILKY WAY. Francis J. Heyden, S.J. 8

SPECTROSCOPIC OBSERVATIONS OF AX PERSEI, RW HYDRAE, CI CYGNI, AND Z ANDROMEDAE. Paul W. Merrill 15

THE STATISTICS OF THE GRAVITATIONAL FIELD ARISING FROM A RANDOM DISTRIBUTION OF STARS. III. THE CORRELATIONS IN THE FORCES ACTING AT TWO POINTS SEPARATED BY A FINITE DISTANCE. S. Chandrasekhar 25

THE STATISTICS OF THE GRAVITATIONAL FIELD ARISING FROM A RANDOM DISTRIBUTION OF STARS. IV. THE STOCHASTIC VARIATION OF THE FORCE ACTING ON A STAR. S. Chandrasekhar 47

ON THE STABILITY OF BINARY SYSTEMS. S. Chandrasekhar 54

THE CONTINUOUS ABSORPTION COEFFICIENT OF THE NEGATIVE HYDROGEN ION. Louis R. Henrich 59

THE ULTRAVIOLET SPECTRUM OF VV CEPHEI. Otto Struve 70

RAPID CHANGES IN THE SPECTRUM OF HD 218393. Otto Struve 75

RADIAL VELOCITIES OF THE FOUR STARS OF THE TRAPEZIUM IN ORION. Otto Struve and John Titus 84

THE SPECTRUM OF SX CASSIOPEIAE. Otto Struve 89

A NOTE ON THE SHELL SPECTRUM OF 48 LIBRAE (HD 142983). W. A. Hiltner . . . 103

RECENT PROGRESS IN ASTROPHYSICS

"THE VARIATION IN THE PROFILES OF STRONG FRAUNHOFER LINES ALONG A RADIUS OF THE SOLAR DISK," BY J. HOUTGAST. Lyman Spitzer, Jr. 107

ASTROPHYSICAL RESEARCH IN FRANCE IN 1940–1942. P. Swings 115

SOLAR RESEARCH IN BELGIUM DURING 1942. P. Swings 118

NOTES

PRELIMINARY NOTE ON THE BEHAVIOR OF HELIUM IN THE SOLAR ATMOSPHERE. Suzanne E. A. van Dijke 121

REVIEWS 124

ERRATUM 124

NUMBER 2

ANALYSIS OF THE MILKY WAY IN CASSIOPEIA. Robert H. Baker and Elaine Nantkes . 125

THE SYSTEM OF β CORONAE BOREALIS. F. J. Neubauer 134

RADIAL VELOCITIES OF 283 STARS OF SPECTRAL CLASSES R AND N. Roscoe F. Sanford . 145

PAGE

THE SPECTRUM OF COMET WHIPPLE-FEDTKÉ-TEVZADZE (1942g). Andrew McKellar . . 162

ON THE SPECTRUM OF COMET 1940c. N. T. Bobrovnikoff 173

ON THE RADIATIVE EQUILIBRIUM OF A STELLAR ATMOSPHERE. S. Chandrasekhar . . 180

STELLAR ROTATION AND LARGE-SCALE CURRENTS. Wasley Krogdahl 191

NOTES ON STELLAR SPECTRA. Otto Struve 205

NEW ORBITS FOR THE SPECTROSCOPIC BINARIES HD 163181 AND HD 78316 (76 κ CANCRI). Otto Struve 210

THE SPECTROGRAPHIC PROBLEM OF U CEPHEI. Otto Struve 222

NOTE ON THE PROBLEM OF U CEPHEI. Zdeněk Kopal 239

NOTES

COLOR INDICES OF PROPER-MOTION STARS. W. J. Luyten, P. D. Jose, and J. F. Foster 244

ERRATA 244

NUMBER 3

HEBER DOUST CURTIS, 1872–1942. Robert R. McMath 245

LINE INTENSITIES AND THE SOLAR CURVE OF GROWTH. K. O. Wright 249

NOTE ON THE SPECTRUM OF α^2 CANUM VENATICORUM. W. A. Hiltner 256

THE SPECTRUM VARIABLE ϵ URSAE MAJORIS. J. W. Swensson 258

RADIAL VELOCITIES OF PROPER-MOTION STARS. Guido Münch 271

THE WOLF-RAYET SPECTROSCOPIC BINARY HD 214419. W. A. Hiltner 273

THE SPECTRUM OF NOVA PUPPIS 1942. Harold F. Weaver 280

THE SPECTRUM OF RX CASSIOPEIAE. O. Struve 295

RECENT PROGRESS IN ASTROPHYSICS

RUSSIAN INVESTIGATIONS OF ECLIPSING VARIABLES: "ON THE SMALLER EFFECTS IN ECLIPSING VARIABLES," BY D. J. MARTINOFF, AND "THE REFLECTION EFFECT IN ECLIPSING VARIABLES," BY M. G. ODINZOV. S. Gaposchkin 313

NOTES

NOTE ON THE SPECTRUM OF 12 COMAE BERENICES. Carlos U. Cesco and Jorge Sahade . 317

COMPLEX LINES IN THE SPECTRUM OF θ AURIGAE. W. A. Hiltner and W. W. Morgan . 318

THE CONTINUOUS ABSORPTION COEFFICIENT OF THE NEGATIVE ION OF HYDROGEN: A CORRECTION . . . Louis R. Henrich 318

REVIEWS 320

ERRATUM 321

INDEX 323

PAGE
162
173
180
191
205
210
222
239
244
244
245
249
256
258
271
273
280
295
313
317
318
318
320
321
323

THE ASTROPHYSICAL JOURNAL

AN INTERNATIONAL REVIEW OF SPECTROSCOPY AND ASTRONOMICAL PHYSICS

VOLUME 99 JANUARY 1944 NUMBER 1

NOTES ON THE THEORY OF NONCOHERENT SCATTERING

LYMAN SPITZER, JR.[1]
New York City
Received August 14, 1943

ABSTRACT

Consideration is given to the theory of noncoherent scattering. It is shown theoretically that this process is to be expected for almost all absorption lines of astronomical importance. The effect of this process on line profiles is also briefly examined. No major change in the curve of growth is to be expected, but the cores of strong lines will be much sharper than on the old theory; this sharpness diminishes toward the limb. The profiles of hydrogen lines in early-type stars and Shane's accurate data on the *Na* D lines in the solar spectrum are shown to be qualitatively consistent with this expectation.

Houtgast's suggestive paper on the center-limb variation of Fraunhofer lines, reviewed elsewhere in this issue,[2] raises anew the problem of noncoherent scattering in the formation of stellar absorption lines. It may be useful to review the present state of the theory and to consider the consequences that may be expected when the emission of radiation of a particular frequency by scattering atoms has no direct relation to the capture of quanta of the same frequency but depends only on the total amount of radiation captured in the line as a whole, i.e., when scattering atoms produce a continual interchange of energy between all the frequencies covered by an absorption line.

In the first place, it should be pointed out that the physical arguments for the presence of noncoherent scattering are quite strong. Theory indicates that coherent scattering may be expected when an atom is at rest, in the lowest quantum state, and in a radiation field which is not too strong. Then, when the atom absorbs a quantum of radiant energy, it must emit a quantum with exactly the same energy if it is to return to its initial state. By Heisenberg's uncertainty principle the finite life of the upper state implies that the energy of the absorbed and subsequently re-emitted quantum may be different from the energy involved in the electronic transition; i.e., the upper state acts as though it had a finite energy width, permitting the capture of quanta of various frequencies. But, if the life of the lower state is very long—and the restriction to lines arising from the ground state and to relatively weak radiation fields insures this—the scattering process must leave the atom with the same energy that it had originally.

If any of these assumptions is relaxed, the strict coherency disappears. In the hottest

[1] Formerly of Yale University, now engaged in research for the National Defense Research Committee.

[2] *Ap. J.*, 98, 107, 1943.

stars the energy density is sufficiently high so that the induced transition probabilities at the lower frequencies may be comparable with the spontaneous transition probabilities. This introduces an appreciable finite width for even the ground state. Also, for subordinate lines, the lower state will be an excited one and will have an appreciable finite width in the general case. Whenever the lower of the two levels producing the line has a finite width, the scattering process may leave the atom with a slightly different energy from that which it had initially, even though exactly the same electronic transition is involved in both the capture and the re-emission of radiation. Thus the absorbed and emitted quanta may be of slightly different frequencies.

In the long run, however, the atom cannot continually gain or lose energy. The sum of the energies of all the quanta absorbed must equal very closely the sum of the energies of all the scattered quanta. This is a much closer equality than would appear if the deviations from coherency were wholly random. If an atom, returning to its previous state, emits a quantum of frequency slightly *less* than the frequency previously absorbed, then in the next capture and emission of radiation the frequency of the emitted quantum is likely to be slightly *greater* than the frequency of the captured radiation. In other words, the atom has a "memory"; and, while it may not emit a quantum with exactly the same energy as that which it previously captured, it remembers how much excess energy was gained or lost in the process and tries to get rid of it or to regain it as soon as possible. The longer an atom spends in a particular state, the better its "memory" operates in eliminating any excess energy gained or lost in previous transitions. The term "excess energy" refers, of course, not to the total change of energy of the atom but rather to the difference between this and the total change computed from the difference of energies between the initial and final electron levels.

This type of noncoherent scattering which arises from natural line breadth has been discussed by several authors.[3] It involves interlocking between different lines and introduces many complications into the equation of radiative transfer. If radiation in one line flows from the center to the wings, then in another line the radiation is likely to flow from the wings back to the center. An additional complication is present in the fact that much of the radiation will tend to be coherently scattered, in general, unless the natural width of the upper level is much less than that of the lower level.

The presence of Doppler broadening also introduces noncoherent scattering in a rather complicated way. It is evident that, if a moving atom absorbs radiation from one direction and emits it in another, the frequencies of the absorbed and emitted quanta will differ in general even if the scattering, when viewed by an observer traveling with the atom, is coherent. The exact formulae for this case, in which the scattering from a stationary atom is coherent and the atoms are assumed to have a Maxwellian velocity distribution, have been derived and discussed by L. G. Henyey.[4]

Approximate results for the important case when the velocity broadening is large, compared to the resonance broadening, may be derived simply. Radiation emitted in the far violet wing of a line must come from atoms moving rapidly toward the observer, if each atom, when stationary, is assumed to absorb and emit radiation only of the central frequency. The velocity of such an atom in other directions will usually be less than the root-mean-square velocity. Let us consider the radiation absorbed by the particular atoms which are moving rapidly toward the observer. The quanta of radiation may be assumed to be moving along three mutually perpendicular axes—the two axes perpendicular to the line of sight, and the third one parallel. The velocities along each direction perpendicular to the line of sight have a Maxwellian distribution centered at zero velocity, and the radiation absorbed from these directions will have a corresponding frequency distribution; i.e., most of the quanta absorbed will be in the neighborhood of

[3] L. Spitzer, Jr., *M.N.*, **96**, 794, 1936; R. v. d. R. Woolley, *M.N.*, **98**, 624, 1938.

[4] *Proc. Nat. Acad. Sci.*, **26**, 50, 1940.

the line center, others will have frequencies corresponding to moderate distances from the central frequency, but very few will have a frequency corresponding to the far wings of the line and to a velocity substantially greater than the root-mean-square velocity. When the quanta absorbed from these directions by an atom moving rapidly toward the observer are emitted in the line of sight, radiation is transferred from the line center to the violet wing, thus producing noncoherent scattering.

On the other hand, the radiation moving along the line of sight will be absorbed only if it is either in the far violet wing and with a motion opposite to that of the atoms under consideration or equally far out in the red wing and overtaking the atom. In either case the quantum subsequently re-emitted toward the observer gives rise to coherent scattering, since the absorption line and the distribution of velocities may both be assumed symmetrical. The net result is that in the far wings (for frequency shifts greater than that corresponding to the root-mean-square velocity) the scattering may approximately be assumed two-thirds completely noncoherent and one-third completely coherent. This is the same result that appears in the absence of Doppler broadening when the lifetime of the lower state producing a line is one-half that of the upper state, with the natural width of each state inversely proportional, of course, to its mean life.

Pressure broadening gives rise to still a third case in which noncoherent scattering will appear. This is the simplest situation and, fortunately, probably the most important. From a physical standpoint the effect is clearest when the velocities of the perturbing atoms are quite small, and when as a result the profile of the broadened absorption coefficient reflects simply the statistical distribution of perturbers.[5] In this situation, if an electron jumps to a higher level when a perturbing atom or ion is quite close, the frequency of the absorbed quantum will be quite different from that if no perturbers were in the neighborhood. By the time the electron jumps down, the perturbing atom or ion may have gone far away, in which case the emitted quantum will have essentially the unperturbed frequency. The excess energy in this case is absorbed by the perturber, whose kinetic energy at infinity will be different from its initial value by precisely the energy difference between the absorbed and emitted quanta—provided, of course, that the absorbing atom returns to its original electronic state and that noncoherency in the unperturbed atom is neglected. The frequencies of absorbed and emitted quanta in this case are independent of each other, with respect to relatively small shifts from the unperturbed frequency, and the scattering will be completely noncoherent. This situation is directly applicable to the Stark-effect broadening of hydrogen lines in stellar atmospheres, since statistical broadening is usually assumed for this case.

When the velocities of the perturbers are large, impact broadening becomes important. It is very difficult to treat this situation rigorously;[6] but in the approximate treatment the broadening of the line corresponds to what would be found if the mean lives of the states producing the line were decreased and the widths of the atomic levels correspondingly increased by the perturbation. This might suggest that for lines widened by impact broadening the scattering is in part coherent, and in part noncoherent, as in the case where natural line breadth is important.

This method of approach is misleading, however, since from a fundamental standpoint the broadening arises not because of the width of any of the atomic energy levels but rather because there is a large number—in fact, a continuum—of energy levels, between which transitions are possible. The point is that the absorbing atom and the perturbing ions or atoms form a single system, and for each electronic state of the atom there are various states for the perturbers, corresponding to different kinetic energies. The per-

[5] For a discussion of "statistical" and "impact" broadening see H. Margenau and W. W. Watson, *Rev. Mod. Phys.*, **8**, 22, 1936.

[6] L. Spitzer, Jr., *Phys. Rev.*, **58**, 348, 1940.

turbation energy serves to provide a coupling between the electronic state of the atom and the motion of the perturbers in such a way that an electronic transition may be accompanied by a change in the perturbers' state function, corresponding to a change in their kinetic energy at infinity.

On this basis it is evident that any excess of energy involved in a difference between the energy of the photon absorbed or emitted and the energy distance from the initial to the final electronic states of the atom appears in a corresponding difference between the initial and final kinetic energies (at infinity) of the perturbers. Hence, when a quantum of frequency far from the line center is absorbed or emitted, there need be no departure from detailed conservation of energy. An electron jumping to a particular level must, of course, make its next transition away from that level; but the deviation of the emitted frequency from the frequency of the line center will have no relationship to the corresponding deviation for the next quantum emitted or absorbed. In other words, the scattering will be completely noncoherent.

To illustrate this general proposition, we may follow through the analysis in the special case in which the velocities are sufficiently slow so that the statistical results are approximately correct. While this analysis is not very helpful in computing line profiles, it may indicate by a specific example the meaning of the generalizations discussed above.

For simplicity, the absorbing atom will be assumed to have only two quantum states, 1 and 2, with energies E_1 and E_2, respectively, in the absence of the perturber, whose internal structure will be neglected and which will be assumed to be an ion. In state 1 the interaction between the atom and the ion will be assumed negligible. In state 2 the interaction or perturbation energy computed for a stationary ion at a distance r from the absorbing atom will be $E_p(r)$. The absorbing atom will be assumed stationary; the ion, whose mass is m_i, may be taken as free to move within the usual spherical *Hohlraum* of radius R.

When the velocity of the ion is not too great (or, more specifically, when the phase shift computed by classical methods for a single encounter is large compared to unity), the adiabatic approximation[7] may be applied. That is, first the atom is quantized in a system of rotating co-ordinates such that the z-axis passes from the center of the atom to the moving ion; the neglect of the rotation in this quantization is the adiabatic approximation referred to. Then the ion, moving in a potential field $E_p(r)$, is quantized. The total energy of the entire system is E. The wave equation for the ion, when the atom is in state 1, becomes

$$\nabla^2\psi_1+\frac{8\pi^2 m_i}{h^2}(E-E_1)\,\psi_1=0\,. \tag{1}$$

The restriction that ψ_1 vanish at the boundary, when $r = R$, restricts E to certain values which will be denoted by $E_a, E_b, E_c, \ldots$.

When the atom is in state 2, the wave equation for the ion is

$$\nabla^2\psi_2+\frac{8\pi^2 m_i}{h^2}[E-E_2'-E_p(r)]\,\psi_2=0\,, \tag{2}$$

where now the eigenvalues of E will be denoted by E_α, E_β, etc.

The transition probabilities are found in the usual way. That part of the general wave function which depends on the atom—that is, on the electronic co-ordinates—gives the total transition probability between the two states. The distribution of this probability with the frequency of the absorbed quantum will be given by a factor F_{12}, defined by the equation

$$F_{12}=\int\psi_1(E_\alpha)\,\overline{\psi}_2(E_\alpha)\,dV\,, \tag{3}$$

[7] W. Pauli, *Handb. d. Phys.*, **24**, No. 2, 161, Berlin: J. Springer, 1933.

integrated over the *Hohlraum*. The frequency ν of the quantum absorbed is determined by the difference between the initial and final energies and is simply

$$\nu = \frac{E_a - E_a}{h}. \tag{4}$$

Let us now consider first what happens when the velocity of the ion is very low, corresponding to a very high value of m_i. The "wave lengths" of ψ_1 and ψ_2 will be very small, and in equation (3) the integrand will make a contribution to F_{12} only when the wave lengths of ψ_1 and ψ_2 are equal, so that constructive interference appears. The condition for this is that

$$E_a - E_1 = E_a - E_2 - E_p(r), \tag{5}$$

or, using equation (4), that

$$\nu = \nu_{12} - \frac{E_p(r)}{h}, \tag{6}$$

where ν_{12} is $(E_1 - E_2)/h$, the frequency of the atomic transition in the absence of perturbation. In other words, F_{12} depends on the existence of regions where the perturbation energy is just equal to $h(\nu_{12} - \nu)$, and the value of F_{12} depends simply on the probability distribution of the perturber in space, which is the same "statistical" broadening case that was discussed qualitatively above.

In the more general case, F_{12} has a more complicated distribution. As m_i is decreased, the "wave lengths" of ψ_1 and ψ_2 are decreased, and the dependence of F_{12} on frequency begins to deviate from what would be expected on the basis of the statistical distribution of perturbers. When m_i becomes sufficiently small so that impact broadening replaces statistical broadening, however, the adiabatic approximation is no longer valid, and all the different rotational states (characterized by different values of the magnetic quantum number m), must be considered together, since the perturber induces transitions from one state to another. However, the same general principles apply, except that F_{12} becomes more complicated. It should be noted that for either statistical or impact broadening the mean lives of states 1 and 2 are exactly the same as would be found in the absence of any perturbation.

It is evident from this presentation that $\nu - \nu_{12}$ for the absorbed quantum has no relation to the corresponding value for the emitted quantum.[8] Whenever pressure broadening is important, one may infer that the scattering is completely noncoherent. This result is supported by the observations of W. Orthmann and P. Pringsheim,[9] to which Houtgast makes reference. These authors found by an indirect method that the breadth of the *Hg* resonance line emitted from a first mercury lamp, on excitation by radiation from a second mercury lamp, was independent of the presence of perturbing atoms in the second lamp used as the exciting source and was determined only by the pressure broadening produced by perturbing atoms in the first lamp.

The conclusion may be drawn, then, that for all cases of practical importance in stellar atmospheres the scattering is almost certainly noncoherent, at least in part, and that in many situations complete noncoherency is present. An analysis of the effects to be expected with this type of scattering is therefore much to be desired.

The following analysis does not constitute a theory of absorption lines on this new basis. These remarks are intended rather to point out certain possibilities in the field and to stimulate interest, so that, when circumstances permit, a more detailed theory may be worked out.

[8] When m_i becomes so large that the motion of the ion becomes negligible in a time compared with the natural mean life, this is no longer true. The frequency of the absorbed radiation then determines the position of the ion within a wave packet, whose divergence is small during the lifetime of the upper state. For any practical case, however, such a wave packet would diverge almost completely before the emission of a quantum.

[9] *Zs. f. Phys.*, **43**, 9, 1927.

The assumption of completely noncoherent scattering introduces additional complexities into the theory but offers corresponding simplifications. The exact computation of line contours becomes much more complicated, depending on the solution of an integral equation over all frequencies. Suitable approximations to this equation may perhaps be found in time. On the other hand, the interpretation of line profiles is much simplified by the fact that for each line the radiation field depends essentially on only one function —the radiation intensity in the line center, a quantity which will be denoted here by J_{ν_0} (Houtgast's use of a subscript c here might introduce some confusion with the intensity in the continuous background). If J_{ν_0} and the absorption and scattering coefficients are known as functions of optical depth, then the line profile is completely determined, both in integrated light and at each angle with the normal. Similarly, interlocking of different lines—a neglected field which is certainly important in some situations—is simplified in part if interlocking takes place between each line as a whole, not between the corresponding frequencies in each line.

The application of the curve of growth to stellar spectra will probably not be affected in general by the substitution of noncoherent for coherent scattering. This results from the fact that the shapes of the three sections—linear, Doppler, and resonance—of the curve of growth may be deduced from quite general considerations and are not dependent on the precise process of line formation. The detailed behavior of individual lines in a multiplet and the theoretical formulae which are fitted to each of the three sections may be expected to depend, however, on the noncoherency of the scattering process.

However, a detailed study of line contours will, of necessity, depend intimately on the effects introduced by noncoherent scattering. It may be of interest to examine a few results concerning line cores which follow rather simply from the theory of noncoherent scattering.

The equation of transfer for radiation of frequency ν becomes in the Eddington-Strömgren notation[10]

$$\cos\theta\,\frac{dI_\nu(\tau,\,\theta)}{\rho\,dx} = -(k_\nu + l_\nu)\,I_\nu + (\epsilon Q l_\nu + k_\nu)\,B_\nu + (1-\epsilon)\,l_\nu J_{\nu_0}\,, \tag{7}$$

which may also be written in the form

$$\frac{dI_\nu}{d\tau_\nu} - \sec\theta\,(1+\eta_\nu)\,I_\nu = -\sec\theta\,\{(1+\epsilon\eta_\nu Q)\,B_\nu(\tau_\nu) + (1-\epsilon)\,\eta_\nu J_{\nu_0}(\tau_\nu)\}\,. \tag{8}$$

Equation (8) may be solved for the emergent radiation; when η_ν, the ratio of the line-scattering coefficient l_ν to the continuous absorption coefficient k_ν, is constant with optical depth, we find

$$I_\nu(0,\,\theta) = \int_0^\infty e^{-(1+\eta_\nu)u}\,du\,\{(1+\epsilon Q\eta_\nu)\,B_\nu(u\cos\theta) + (1-\epsilon)\,\eta_\nu J_{\nu_0}(u\cos\theta)\}\,. \tag{9}$$

If we assume

$$B_\nu(\tau_\nu) = a + b\tau_\nu\,, \tag{10}$$

$$J_{\nu_0}(\tau_\nu) = g + h\tau_\nu\,, \tag{11}$$

and neglect ϵ as compared to unity, then, for large η_ν equation (9) becomes

$$I_\nu(0,\,\theta) = g + \epsilon aQ + \frac{a - g + (h + \epsilon bQ)\cos\theta}{\eta_\nu}\,, \tag{12}$$

plus terms in $1/\eta^2$. The quantity g, approximately the central intensity of the line, is much less than a for a sufficiently strong line; also, h is likely to be considerably greater than either a or b, since the intensity in the line center would be expected to rise very

[10] B. Strömgren, *Handb. d. Ap.*, **7**, 228, Berlin: J. Springer, 1936.

rapidly with optical depth just below the surface. The quantity ϵ is usually less than 10^{-2}, and both terms in ϵ in equation (12) will usually be negligible.

When the scattering is coherent, the term h in equation (12) disappears, and $I_\nu(0, \theta)$ rises relatively slowly with decreasing η_ν. The presence of this additional term provides a sharp core in the center of a strong absorption line, where the theory of coherent scattering predicts a broad core. This sharpness at the line center, moreover, should disappear for a line observed at the limb, where $\cos\theta$ vanishes.

There are several phenomena which may be explained by equation (12). It has already been pointed out[11] that this effect explains qualitatively the sharp, almost cusp-like cores of the hydrogen lines in the A-type stars. Shane's work [12] on the D lines shows relatively sharp line cores at the center of the sun; the attempt to explain these contours on the basis of coherent scattering led to a very high value, 0.013 A, for the damping constant, about a hundred times the classical value, and introduced various difficulties and inconsistencies. It is evident also from Shane's observations that the sharpness of the cores diminishes as the limb is approached in agreement with equation (12). The relevant data are given in Table 1, where the intensities at the limb have been multiplied

TABLE 1

INTENSITIES OF THE CORES OF THE D LINES

$\Delta\lambda$	D_1		D_2	
	$r/R_\odot = 0.00$	$r/R_\odot = 0.965$	$r/R_\odot = 0.00$	$r/R_\odot = 0.965$
0.00 A.....	0.058	0.058	0.052	0.052
.01.....	.060	.059	.053	.053
.02.....	.064	.060	.056	.053
.03.....	.069	.064	.060	.056
.04.....	.078	.068	.066	.059
0.05.....	0.094	0.075	0.073	0.062

by a constant factor for each line to make the central intensities equal at the center and at the limb. This does not quite reduce them to the same scale of absolute intensities, since from equation (12) a slight center-limb variation of absolute central intensity is to be expected. A more elaborate correction for the variation of the continuous background with θ is not necessary here.

It will be seen from Table 1 that within 0.02 A from the line center the profile at $\cos\theta = 1.00$ has risen some three or four times as far above its value at the line center as has the profile near the limb. Even at a distance of 0.04 A from the line center, the profile obtained from the center of the disk has risen twice as far as that near the limb. At increasingly greater distances the two curves approach each other, until at 0.16 A from the line center the absolute intensities are equal to within about 10 per cent of their values; at such great distances from the line center equation (12) is no longer applicable, since the linear expansion of $J_{\nu_0}(\tau_\nu)$ in equation (11) is valid only for very small values of τ_ν and may therefore be applied only to the inner parts of the line, which are formed very close to the surface.

From a qualitative standpoint the assumption of noncoherent scattering does not lead to any obvious inconsistency with the observations and promises to clarify various previously unexplained effects. One may conclude that further study of this almost unexplored field promises to be rewarding.

[11] L. Spitzer, Jr., *Pub. A.A.S.*, **10**, No. 3, 1941.

[12] *Lick Obs. Bull.*, No. 507, 1941.

COLORS OF EARLY-TYPE STARS IN THE SOUTHERN MILKY WAY

FRANCIS J. HEYDEN, S.J.[1]

Received September 17, 1943

Harvard College Observatory

ABSTRACT

Color excesses for 157 bright early-type stars have been computed from the color indices published by Knox-Shaw and the late E. G. Williams. The normal colors were derived from the system used by Stebbins, Huffer, and Whitford.

The factors for the conversion of the color excesses on the international scale to total absorptions for photovisual and photographic light have been taken equal to 4 and 5, respectively. Distance moduli have been computed on the basis of the absolute magnitudes adopted by Stebbins, Huffer, and Whitford.

The stars are all located in the southern Milky Way between galactic longitudes 215° and 330°. Only 19 out of the 157 stars show significant reddening. These are distributed as follows: one is in the η Carinae nebula, six are around the edges of the Coal Sack, and the remainder are near the cluster, NGC 6231, in the tail of Scorpio. These last show the heaviest obscuration, which amounts to 2.0 mag. in 300 parsecs, and hence confirm MacRae's results from a study of the parallactic motion of the cluster. A new determination of the distance of the η Carinae nebula places it near 600 parsecs, in contrast to Bok's original determination of 1100 parsecs.

Outside of the three regions mentioned the data show evidence that the space reddening is slight out to an average distance of 250 parsecs.

Knox-Shaw[2] has published the results of a color and magnitude survey of the bright O- and B-type stars in the southern Milky Way from galactic longitudes 215° to 330° and roughly between latitudes +15° and −15°. This region of the Milky Way was out of reach for the extensive photoelectric survey carried out a few years ago by Stebbins, Huffer, and Whitford.[3] The present data, therefore, complete the survey of the entire Milky Way for the early-type stars brighter than the sixth magnitude.

OBSERVATIONAL DATA

The observational program, planned and executed by the late E. G. Williams, provided for the determination of photographic magnitudes in the blue (λ 4100), green (λ 5150), and red (λ 6200) for each of 157 stars in the survey region and for 24 other early-type stars in the regions already covered by Stebbins, Huffer, and Whitford. These 24 stars permit a comparison between the photoelectric and photographic results, thus tying together the two surveys and providing a uniform system for a study of space reddening over the whole Milky Way.

The color indices found for the 24 comparison stars agree in the mean to within 0.01 mag. with the results of Stebbins, Huffer, and Whitford, after these had been reduced to the international system. The photovisual magnitudes of the 157 stars are close to the international system. From a comparison with magnitudes in the *Harvard Mimeograms*, Knox-Shaw finds that the probable error of a single color index is well within 0.10 mag.

In the present paper the color excesses of the 157 stars have been computed on the basis of Knox-Shaw's color indices and the colors adopted as normal by Stebbins, Huffer, and Whitford.[3] The normal photoelectric colors have been reduced to the international system by the formula

$$C = 1.5C_1 ,$$

where C_1 is the normal photoelectric color.

[1] Teaching Fellow at Harvard College Observatory.

[2] *M.N.*, **102**, No. 5, 1942.

[3] *Ap. J.*, **91**, 20–50, 1940; *Mt. W. Contr.*, No. 621.

The distance moduli, $m_0 - M$, have been determined from the mean absolute photovisual magnitudes, which were used by the photoelectric observers[3] and from the apparent magnitude corrected for total photovisual absorption by the relation

$$m_0 = m_{pv} - 4E .$$

The factor 4, used for passing from color excesses to absorption on the photovisual scale, may seem rather small. We have adopted it because it results in total absorptions that are on about the same scale as those used in previous investigations for this part of the sky. The excesses thus derived are also very nearly on the system used by Stebbins, Huffer, and Whitford. Recent investigations by Stebbins and Whitford[4] show that there is some latitude in the value of the ratio, A/E, because of the uncertainty of the zero point in the empirical $1/\lambda$ law.

Table 1 shows the values of normal color indices and mean absolute magnitudes used in deriving the data for Table 2. The spectra are taken almost entirely from the revised Victoria list.

TABLE 1

Spectrum	O	B0	B1	B2	B3	B4
Normal C.I.	−0.35	−0.33	−0.32	−0.30	−0.29	−0.27
M_V (adopted)	−4.5	−3.9	−3.6	−3.0	−2.2	−1.9
Spectrum	B5	B6	B7	B8	B9	A0
Normal C.I.	−0.26	−0.24	−0.21	−0.20	−0.18	−0.15
M_V (adopted)	−1.6	−1.4	−1.1	−0.8	−0.4	.....

The distance moduli, $m_0 - M$, of Williams' 24 comparison stars differ from the values of Stebbins, Huffer, and Whitford by 0.06 mag., in the mean. Some of the individual differences are as large as 1.0 mag. A large difference, of course, can be attributed to a combination of several factors, involving slight differences in spectral type, apparent magnitude, and color index. The uncertainties are at least within the range of the dispersion in absolute magnitude.

In Table 3 the distribution of the observed color excesses between +0.10 mag. and −0.10 mag. is shown for four average distances. At the bottom of each column are given the mean color excess and the dispersion around 0.00 mag. In constructing Table 3 it has been assumed that color excesses less than +0.10 mag. are not significant because of the probable errors in the individual magnitudes, and the mean excesses seem to justify the assumption. The majority of the stars tabulated in Table 3 are distributed between 200 and 300 parsecs and show no evidence, from the nearest to the most distant group, of any systematic increase of color excess with increasing distance.

Oort[5] has recommended a zero-point correction of +0.049 mag. for the normal colors which were used by Stebbins, Huffer, and Whitford. We have not applied this correction. It is therefore to be understood that our excesses and absorption are in all probability minimum values.

Only 19 out of the 157 early-type stars have excesses greater than +0.10 mag., and these presumably indicate real space reddening. These stars have been omitted in Table 3, but they have the same average distance modulus as the unreddened stars which make up the table.

ANALYSIS OF THE RESULTS

The 157 stars have been plotted according to their galactic co-ordinates in Figure 1. Open circles indicate color excesses less than +0.05 mag.; lightly shaded ones show

[4] *Ap. J.*, 98, 32, 1943.

[5] *B.A.N.*, No. 308, 1938.

TABLE 2

HD	E	m_0-M	HD	E	m_0-M
28873	−0.02	7.4	84816	−0.04	7.4
40494	− .01	6.7	85953	.00	8.2
42933	− .04	8.6	92938	+ .04	7.0
54893	+ .01	7.1	92964	+ .37	7.6
56779	− .02	7.5	93030	+ .01	7.3
57150	+ .07	6.8	93194	+ .07	6.9
57219	− .01	7.5	93845	− .05	6.4
61831	+ .01	7.0	96706*	+ .02	7.8
61925	+ .02	7.6	97670	+ .09	7.6
62226	+ .01	7.7	99264*	+ .14	7.3
63465	+ .02	7.4	100929*	+ .07	7.8
63578	+ .04	8.2	104841	+ .11	6.5
63922	+ .01	8.0	105435	.00	5.1
63949	+ .03	8.7	105521	.00	7.8
64503	.00	6.8	105937	− .05	6.5
64722*	+ .05	7.7	106231	− .06	7.6
64740	+ .01	6.9	106490	− .09	5.5
64760	+ .04	7.2	106983	− .08	6.8
64802	− .05	7.4	108248	− .09	.....
65460	− .05	7.9	108249		
65551	− .01	7.5	108257	− .05	7.2
65575	.00	5.9	108483	− .09	6.6
65818	+ .02	7.4	109668	.00	4.5
66194	+ .08	7.1	110432	+ .40	7.4
66591	+ .05	7.0	110879	− .04	5.5
66811	.00	6.9	110956	− .01	6.4
68217	− .08	7.9	111123	− .05	5.6
68243	− .06	6.9	112078	− .02	7.0
68273	− .01	6.5	112091	+ .03	.....
68324	− .04	7.7	112092		
68657	− .01	8.1	112244	+ .22	8.9
68980	+ .06	6.7	113120	+ .17	7.4
69081	− .01	7.5	113703	+ .05	6.8
69144	− .04	7.0	113791	− .03	6.7
69302	− .02	8.1	113904	+ .12	9.1
70556	− .08	7.8	115823	− .09	6.6
70930	+ .02	7.8	118716	− .05	5.7
71459	+ .04	7.6	120307	− .03	6.7
71510	.00	7.4	120324	+ .05	5.4
72067	− .02	8.1	120640	− .01	8.0
73390	+ .03	7.4	120991	+ .06	7.8
74195	− .03	6.0	121263	− .02	4.9
74375	+ .06	7.9	121743	− .02	6.2
74455	− .02	7.9	121790	− .06	6.4
74753	− .02	7.5	122451	.00	3.0
75311	− .03	6.9	122980	− .02	6.7
75821	− .05	9.3	124367	+ .08	7.0
76538	+ .07	7.1	124471	+ .07	8.5
77002	− .02	6.7	125238	− .10	6.2
78764	+ .04	6.9	126341	− .03	6.9
79275	− .01	8.1	127381	− .02	6.8
79351	− .04	5.9	127972	+ .03	4.6
79447	+ .01	6.3	129056	+ .03	5.3
79735	− .03	7.0	129116	.00	6.3
81188	− .03	4.9	131492	+ .03	7.5
82984	+ .03	7.3	132200	− .02	6.4
83058	.00	7.3	133955	− .01	6.4
83979	+0.04	7.2	134687	−0.09	6.8

* Henry Draper classification.

TABLE 2—*Continued*

HD	E	m_0-M	HD	E	m_0-M
135160*	+0.03	9.3	151985	−0.05	7.0
135240	+ .09	9.3	152234	+ .45	7.5
135591	+ .08	9.7	152236	+ .64	6.0
136298	− .08	5.9	152249	+ .40	8.6
136504	− .05	6.0	152408*	+ .39	8.8
136664	− .02	7.0	153716	+ .06	7.1
138690	− .03	5.4	156838	+ .01	7.8
138769	− .01	6.9	157042	+ .03	7.4
143118	− .06	6.0	157246	+ .04	6.9
144294	− .06	6.8	158408	− .07	5.3
148379	+ .66	6.4	158427	+ .03	5.1
148688	+ .53	6.8	158926	− .07	5.1
149038	+ .29	8.4	160578	− .08	5.0
149404	+ .58	7.7	161783	+ .07	7.6
150135* }	+ .41	.....	165024	+ .06	7.2
150136 }			166596	+ .03	7.6
150168*	+ .10	8.9	168905	− .07	7.1
150742	+ .09	7.5	169467	− .10	5.4
150745	+ .10	7.6	172910	− .02	6.7
150898	+ .05	9.3	173948	+ .07	6.0
151804	+ .23	8.8	189103	− .04	6.3
151890	−0.06	5.7	193924	+0.07	4.0

TABLE 3

Excess	100 Parsecs	No. of Stars		
		200 Parsecs	300 Parsecs	500 Parsecs
−0.10 to −0.08	4	5	2	0
− .07 to − .05	8	5	5	1
− .04 to − .02	6	15	6	3
− .01 to + .01	4	11	11	4
+ .02 to + .04	3	3	13	3
+ .05 to + .07	2	5	7	2
+0.07 to +0.10	0	1	4	3
Mean	−0.03	−0.01	+0.01	+0.02
Dispersion around 0.00	±0.05	±0.05	±0.05	±0.05

excesses between +0.05 mag. and +0.10 mag.; and heavily shaded ones, excesses greater than +0.10 mag.

This region of the Milky Way includes the area around the η Carinae nebula, the Coal Sack, the tail of Scorpio, and the six Selected Areas, 191–196, inclusive. The absorption has already been determined by other observers for these portions of the survey, so that it is possible to connect their results with the new data.

First of all, it is clear that the area between galactic longitudes 215° and 245° shows little evidence of selective absorption. None of the 50 stars observed by Williams which lie in this area, mostly just south of the galactic plane, has a significant color excess. The mean color excess of these stars is −0.002 mag. This indicates a negligible absorp-

tion out to the average distance of 250 parsecs. Mrs. Gaposchkin[6] has determined the absorption for two Selected Areas in this region: 191 at $l = 239°$, $b = -19°$, and 192 at $l = 248°$, $b = -6°$. The total obscuration for stars with distance modulus 16.5 in S.A. 191 is only 0.42 mag/kpc, but in S.A. 192 it amounts to 1.5 mag/kpc, and we note that there is a gap in the bright early-type stars in this region. There is an extensive dark nebula in Vela, near $l = 235°$, $b = +1.5°$, which Greenstein[7] finds to be situated at a distance of 600 parsecs with an average absorption of about 2 mag. The present data show only two bright stars in the vicinity of this nebula. Both have negative color excesses, and their distance moduli place them within 400 parsecs. They offer us no help in studying the absorption of the nebula but place it at a distance of more than 400 parsecs in agreement with Greenstein's result.

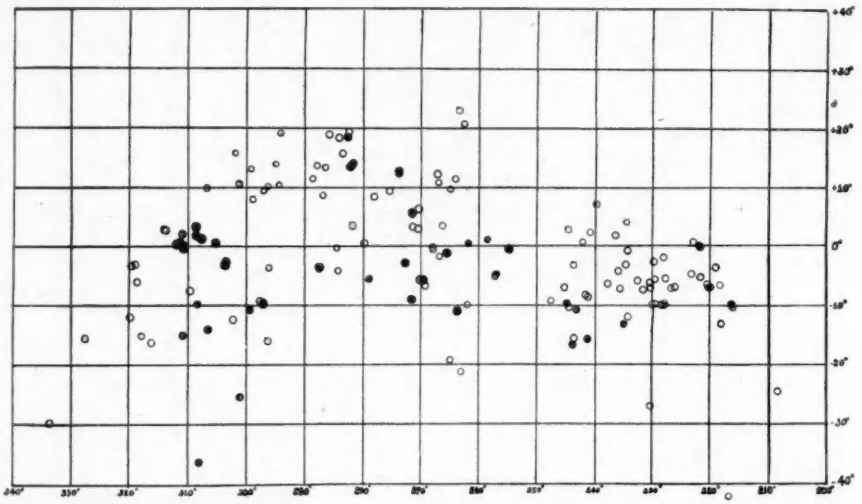

FIG. 1.—Co-ordinates are galactic longitudes and latitudes. Open circles indicate color excesses less than +0.05 mag.; lightly shaded ones show excesses between +0.05 mag. and +0.10 mag.; and heavily shaded ones, excesses greater than +0.10 mag.

If only the stars with distance moduli comparable to these 50 stars are considered in the survey of Stebbins, Huffer, and Whitford,[8] one finds an almost identical result for a long stretch of the Milky Way beginning at about longitude 120°. In fact, the complete data for this whole region, with the exception of areas where dark nebulae are obvious, show a total visual absorption that is smaller than 1 mag/kpc. This is also confirmed in two places by more detailed studies of the absorption. Bok[9] finds a total photographic absorption of 0.6 mag/kpc for the region of Monoceros; and McCuskey,[10] the value of 0.5 mag/kpc for the apparently unobscured regions of Taurus. It may well be that Williams' survey has added another 30° to this part of the Milky Way, where absorption is not serious out to at least 1000 parsecs.

From $l = 255°$ to $l = 280°$ and from $b = +10°$ to $b = -10°$ there are seven stars with color excesses larger than +0.10 mag. One of these, HD 92964, is situated in the bright nebulosity around the star η Carinae. Its color excess is +0.37 mag., indicating a total photovisual absorption of 1.5 mag. at a distance of about 600 parsecs. In a study

[6] *Ap. J.*, **90**, 321, 1939.

[7] *Harvard Ann.*, **105**, 360 1936.

[8] *Pub. Washburn Obs.*, Vol. **15**, Part 5, 1934.

[9] Paper given at Tonantzintla Observatory, 1942.

[10] *Ap. J.*, **89**, 568, 1939.

of this same nebula Bok[11] determined its distance from star counts and distance moduli of bright early-type stars. The distance which he found is 1100 parsecs. But at the time when Bok computed this distance the relation between color excess and total absorption was not known. Hence the distance moduli which he used were not sufficientlycorrected for absorption.

In Table 4 the bright early-type stars have been combined with some others whose color indices were also determined by Bok at the same time, and all of the distance moduli have been corrected for an absorption of $4E$. Mrs. Rieke[12] found absolute magnitudes for all these stars, including HD 92964, which occurs in the table by Williams and Knox-Shaw.

The mean absorption for the η Carinae nebulosity is 1.65, and its distance is 600 parsecs, or a little over half the value found by Bok. He did, however, suspect the presence of a nearer absorbing cloud at about 500 parsecs, indicated by the color excesses of three of the stars used in Table 4. The revised data now show quite definitely that the absorption affecting all these stars, some of which are probably responsible for the bright emission, is at a distance of about 600 parsecs.

TABLE 4

HD	M_{vis}	A_{vis}	m_0-M
92964	−4.4	1.48	8.4
93403	3.3	1.64	9.0
93873	2.5	2.50	7.8
94230	4.0	1.72	10.4
93250	3.1	1.88	8.5
93131	4.0	1.20	9.2
03206	−4.6	1.08	9.9
Mean	.....	1.65	9.0

There are six bright stars near the Coal Sack which from Williams' observations show excesses between +0.11 mag. and +0.22 mag. The six reddened stars yield a mean total photovisual absorption of 0.8 mag. at an average distance of 300 parsecs, which confirms the results of several independent observations in this region. Mrs. Gaposchkin[6] finds an average total photovisual absorption of 1.04 mag/kpc for S.A. 194, which is partly inside and partly on the edge of the Coal Sack. Unsöld[13] and Müller,[14] from a comparison between surface distribution of stars inside and outside the nebula, have derived an average total photovisual absorption of 1 mag. and a distance of 150 parsecs. Lindsay has devoted special attention to this region in recent years, and his early results confirm the average value of the absorption found by other observers. Both Lindsay and Mrs. Gaposchkin have found several areas within the Coal Sack where the obscuration is between 2 and 3 mag.

One of the richest regions for early-type stars is S.A. 193 ($l = 261°$, $b = +1°$), which lies between the Coal Sack and the η Carinae nebula. The absence of selective absorption in this region has been attested to by Mrs. Gaposchkin[6] and by Bok and Miss Wright.[9] Mrs. Gaposchkin finds a total photographic obscuration of 0.11 mag/kpc from a color survey of 771 stars, while Bok in his recent study admits a maximum photographic absorption of 0.4 mag. for a distance of 3000–4000 parsecs. Williams observed only two bright B3 stars in this area, both at an average distance of 300 parsecs. These two stars indicate a slight reddening or an average visual absorption of 0.30 mag.; but, in view of

[11] *Harvard Reprint*, No. 77, 1932.

[12] *Harvard Circ.*, No. 373, 1932.

[13] *Harvard Bull.*, No. 870, 1929.

[14] *Zs. f. Ap.*, 8, 66, 1934.

the fact that the color excesses of both stars are less than +0.10 mag., the obscuration which they indicate is not considered significant.

The most reddened B stars in Williams' survey are found close to the galactic plane near the tail of Scorpio, between $l = 305°$ and $l = 312°$. There are indications of heavy absorption in this region which appears covered by a network of dark patches superimposed on the background stars. At about galactic longitude 307° Williams' observations include four stars, two of which are of type B1 and two of type O. These have an average color excess of +0.52 mag., corresponding to a total visual absorption of 2.0 mag. at an average distance of 300 parsecs. Another group of four stars around $l = 311°$, apparently associated with the elongated cluster NGC 6231, shows almost the same amount of obscuration.

Stebbins, Huffer, and Whitford[3] determined colors for six B stars in this neighborhood, and the average absorption found from these is 1.5 mag. at a distance of 750 parsecs. MacRae[15] computed the distance of the cluster from parallactic motion and, in comparing his result of 300 parsecs with the distance of 600 parsecs, found by photometric methods, estimated that this difference could be explained only by an absorption of 1.7 mag. in 300 parsecs. Both of these independent results are confirmed by the present data.

Two more Selected Areas (195 and 196), in which Mrs. Gaposchkin determined red indices, are represented in Williams' survey by a few stars in each. Selected Area 195, at $l = 286°$, $b = -2°$, has no appreciable absorption according to the evidence of five stars at a mean distance of 400 parsecs, while three stars in S.A. 196, at $l = 298°$, $b = -12°$, show an obscuration of only 0.2 mag. at the same average distance. Mrs. Gaposchkin's data for these two Selected Areas provide definite proof that they are not unobscured out to greater distances. From the colors of stars whose mean distance is 3000 parsecs she finds an absorption of 2.5 mag/kpc in S.A. 195 and 1.0 mag/kpc in S.A. 196.

An extension of this survey between $l = 215°$ and $l = 330°$ to include early-type stars fainter than sixth magnitude should give a better picture of the details in the Carina-Centaurus neighborhood. Long-exposure photographs show many dense pockets and channels of obscuring matter, some of which are outlined by the blank areas in Figure 1 where no bright early-type stars are found. Shapley[16] has also shown that the B stars fainter than the seventh magnitude are distributed more evenly along the galactic plane than the brighter ones. On the other hand, the mere absence of bright early-type stars over a rather extensive area does not establish the presence of absorption. There is at least one region of slight obscuration along this section of the Milky Way, between galactic longitude 245° and 255°, in which no bright B stars are found. Bok[9] has analyzed the colors of 333 stars at $l = 249°$, $b = +1°$, in the center of this vacancy, and he finds a total reddening of +0.20 mag. out to a distance of 1200 parsecs. The total average absorption is therefore of the order of 0.5 mag/kpc.

There is no significant selective absorption out to an average distance of 250 parsecs in the apparently clear regions covered by the present data. Even near the η Carinae nebula where several early-type stars show definite reddening, Bok[9] has found several others which are unaffected by absorption. These are evidently foreground stars, and they have nearly the same average distance modulus as the reddened stars. Hence they indicate a minimum distance of 600 parsecs for the obscuration in the direction of η Carinae. Figure 1 shows several unreddened stars intermingled with the reddened stars around the edges of the Coal Sack and at least three more unobscured stars close to the heavily obscured stars in the tail of Scorpio. The patchy condition of the sky in these two regions suggests a very uneven distribution of dark clouds and prevents any definite conclusion concerning the minimum distance of the absorbing material.

[15] *Harvard Bull.*, No. 914, p. 21, 1940.

[16] *Harvard Circ.*, No. 239, 1922.

SPECTROSCOPIC OBSERVATIONS OF AX PERSEI, RW HYDRAE, CI CYGNI, AND Z ANDROMEDAE*

PAUL W. MERRILL
Mount Wilson Observatory
Received October 4, 1943

ABSTRACT

Data concerning the intensities and displacements of the chief bright lines in the blue-violet portion of the combination spectra of AX Per 013053, RW Hya 132824, CI Cyg 194635, and Z And 232848 are reported in considerable detail. Lines observed include those of *H*, *He* I, *He* II, *N* III, [*O* III], [*Ne* III], *Fe* II, [*Fe* V], and [*Fe* VII].

Bright-line stars with absorption spectra of late type may be arranged in five groups. Those characterized by bright lines of *He* II and/or [*O* III], [*Ne* III] are called "combination spectra." Data concerning probable periodic variations in the displacements of the bright lines in six combination spectra are summarized. Tentative generalizations are: (1) The displacements of most, if not all, of the lines are variable. (2) A typical range is 30 km/sec. Permitted lines exhibit smaller ranges than forbidden lines. (3) The fluctuations are of long period (one to three years). (4) Maxima and minima of the forbidden lines occur about one-fifth of the period after the corresponding phases of permitted lines.

In most stars the net spectroscopic effect of the incandescent atmosphere is the production of dark lines—dark because in each line the energy emitted by the atmosphere is less than that absorbed from the continuous spectrum of the photosphere. But, if the atmosphere be sufficiently brilliant relative to the photosphere, bright lines may appear in the integrated spectrum. The necessary brilliance may have an atomic or a general cause: circumstances differing from those of thermodynamic equilibrium may lead to a relatively great number of atoms in energy-levels which produce bright lines; or the atmosphere may be so much larger than the main body of the star that a considerable portion of it lies outside the cone joining the photosphere and the observer, i.e., in a position where emission cannot be balanced by absorption.

Stars near the ends of the sequence of stellar temperatures are much more likely to exhibit bright lines than those near the middle of the sequence. Bright-line stars are thus naturally divided into two great groups. In the high-temperature group the chief bright lines coincide with some of the stronger dark lines regularly found in normal stars of the same or slightly later types. They might be caused by the stimulating effect of the photospheric light on an unusually extensive atmosphere. In the low-temperature group, on the other hand, many of the bright lines do not correspond to any strong lines in the absorption spectrum. Indeed, some of the chief bright lines require an excitation far above that which the photosphere appears able to supply. This is true of the bright hydrogen lines in the spectra of long-period variables. Another engaging example of this anomaly is found in certain irregular variables with absorption spectra of type M upon which are superposed bright lines of ionized helium. The best known stars of this kind—AX Persei, RW Hydrae, CI Cygni, and especially Z Andromedae—have received considerable attention. The spectra are complex and, because they are variable, cannot be described once for all. Unpublished data derived from Mount Wilson spectrograms of these four stars, with brief summaries of previous investigations, are brought together in the present *Contribution*.

AX PERSEI 013053

An intense bright *Hα* line was discovered in the spectrum of AX Persei at Mount Wilson in 1930, and the anomalous combination of bright lines of ionized helium (and some

* *Contributions from the Mount Wilson Observatory, Carnegie Institution of Washington*, No. 688.

of the forbidden lines of gaseous nebulae) with the dark bands of titanium oxide was found a year later.[1, 2] In 1931 and 1932 the emission lines of *H*, *He* II, [*O* III], and [*Ne* III] were outstanding; those of *He* I and *N* III were of moderate intensity, while numerous *Fe* II lines were barely visible.[3]

Spectrograms taken at the McDonald Observatory during the years 1939–1943 have been discussed by Swings and Struve in a series of six articles,[4–9] published with the general title, "Spectrographic Observations of Peculiar Stars," I–VI. They give many details and describe interesting changes. Especially notable is their identification of lines of [*Ne* V], [*Fe* V], [*Fe* VI], and [*Fe* VII]. The presence in AX Persei of the highly ionized atoms producing these forbidden lines is most remarkable.

The Mount Wilson slit spectrograms, with the exception of low-dispersion plates taken on September 13 and October 2, 1931, are listed in Table 1.

TABLE 1

DISPLACEMENTS OF BRIGHT LINES IN AX PERSEI

(Km/Sec)

DATE	PLATE	DISP. AT $H\gamma$	*H*	*He* I	*He* II	*Fe* II	*Ca* II	*N* III	MEAN PERM.*	[*O* III]		[*Ne* III]	MEAN NEB.
										λ 4363	λ 4959 λ 5007		
		A/mm											
1931 Nov. 9	V 98	120	− 96	.....	−116	.....	.....	.....	(− 96)	− 86	.....	(−127)	− 90
1932 Aug. 16	C 6093	70	−103	−112	−106	−102	.....	− 99	−105	−118	−111	−116	−116
1940 Aug. 23	C 7562	75	− 98	−105	−108	−103	.....	− 98	−101	−106	.....	−129	(−114)
1941 Aug. 31	E 239	65	−121	−108	−133	−114	−119	− 99	−114	− 96	− 82	− 99	− 95
Dec. 7	E 361	65	−113	(−108)	−107	−112	.....	−115	−113	−111	−115	− 98	−104
1942 Oct. 22	E 637	65	−114	−126	−124	(−122)	.....	−118	−119	−133	−132	−136	−134
1943 Aug. 11	E 912	65	−118	−112	−130	−121	−121	−110	−116	− 95	− 86	− 91	− 91
Mean (omit V 98)	.....	.....	−111	−112	−118	−112	(−120)	−107	−111	−110	−105	−112	−109
Range (omit V 98)	.....	.....	23	21	27	20	.....	20	18	38	(50)	45	43

* Except *He* II.

Hydrogen and helium.—The bright lines of *H* and *He* II are always very strong. No striking variations in intensity have been observed. The lines of *He* I, all much weaker than λ 4686 *He* II, show a considerable change in intensity with respect to the continuous spectrum (see Table 2). The intensity of λ 4388 varies from about one-third to two-thirds that of λ 4471.

Iron.—Lines of *Fe* II and of [*Fe* II] are regularly present in low intensity, the permitted lines being somewhat stronger than usual on plate E 239 and especially on E 912. The line λ 4658 [*Fe* III] is probably present in very low intensity. Lines of [*Fe* V] are present in moderate intensity, being especially strong on E 637. Mean reduced wave lengths are: 3891.6[2] (5 plates); 3895.6 (2); 4071.9[0] (4). Since various lines yield different

[1] Merrill and Humason, *Pub. A.S.P.*, **44**, 56, 1932.

[2] Merrill, Humason, and Burwell, *Mt. W. Contr.*, No. 456; *Ap. J.*, **76**, 156, 1932.

[3] P. W. Merrill, *Mt. W. Contr.*, No. 460; *Ap. J.*, **67**, 44, 1933.

[4] I, *McDonald Obs. Contr.*, No. 22; *Ap. J.*, **91**, 546, 1940.

[5] II, *McDonald Obs. Contr.*, No. 37; *Ap. J.*, **94**, 291, 1941.

[6] III, *McDonald Obs. Contr.*, No. 42; *Ap. J.*, **95**, 152, 1942.

[7] IV, *McDonald Ob . Contr.*, No. 56; *Ap. J.*, **96**, 254, 1942.

[8] V, *McDonald Obs. Contr.*, No. 64; *Ap. J.*, **97**, 194, 1943.

[9] VI, *McDonald Obs. Contr.*, No. 72; *Ap. J.*, **98**, 91, 1943.

PLATE I

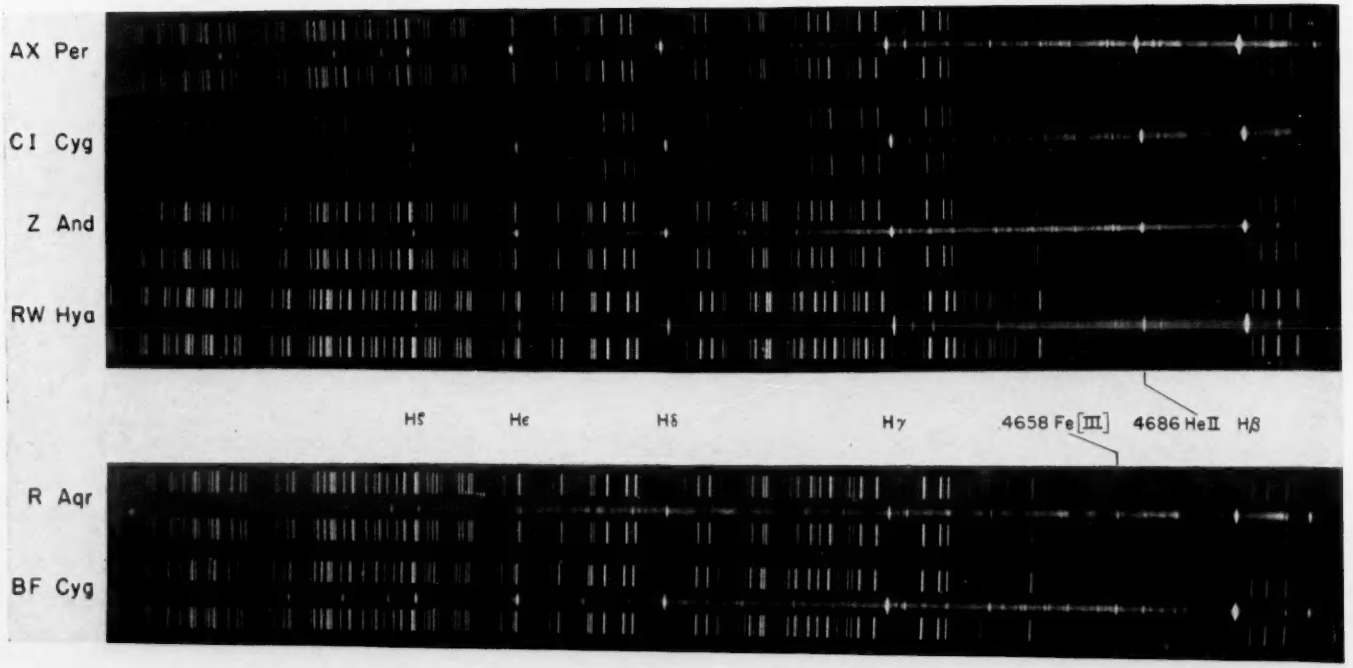

STARS HAVING COMBINATION SPECTRA

AX Per, E 912, Aug. 11, 1943
CI Cyg, E 914, Aug. 12, 1943
Z And, E 355, Dec. 6, 1941
RW Hya, E 73, March 7, 1941
R Aqr, E 360, Dec. 7, 1941
BF Cyg, E 635, Oct. 22, 1942

UNIV. OF MICH.

velocities, the corrections to be applied to the measured positions of lines of unknown wave length are slightly uncertain. On plates C 7562, E 239, E 361, and E 912 the velocity was assumed to be −110 km/sec; on E 637, −125 km/sec. The [*Fe* VII] line λ 3759.1 (mean observed wave length) is measurable on four plates, being remarkably strong on E 637 (see Table 2). This line is decidedly broad with a flat top and well-defined edges. Should this appearance be caused by duplicity, the separation of the components would be about 0.8 A.

Other bright lines.—Lines of *Ca* II are well marked on only two plates, E 239 and E 912. As might be expected, the lines of [*O* III], [*Ne* III], and [*Fe* VII] are relatively weak on these two plates. On the last four plates a line at λ 4725.0 (mean reduced wave length) is nearly as strong as the neighboring bright line λ 4713; but on plate C 7562 the λ 4725 line is missing. This is probably the same line listed in the spectra of gaseous nebulae at λ 4724.7 by A. B. Wyse[10] and identified as [*Ne* IV] in RX Puppis[5] (λ 4725.0) and Nova Serpentis[11] (λ 4725.6) by Swings and Struve. The companion line may be blended with *He* I λ 4713.

TABLE 2

ESTIMATED INTENSITIES OF CERTAIN BRIGHT LINES IN AX PERSEI

Date	Plate	*He* I	[*Fe* VII] λ 3759 / $H\iota$	[*Ne* III] λ 3869 / $H\zeta$
1931 Nov. 9.....	V 98	(1)	.....	(3)
1932 Aug. 16.....	C 6093	3	.....	5
1940 Aug. 23.....	C 7562	5	.....	2
1941 Aug. 31.....	E 239	4	1.5	0.3
Dec. 7.....	E 361	3	6	0.8
1942 Oct. 22.....	E 637	3+	10	2
1943 Aug. 11.....	E 912	3	4	0.3

Absorption spectrum.—The *TiO* bands are well marked, corresponding approximately to type M3, but the atomic lines are rather indistinct. No radical changes have been observed.

Displacements of bright lines.—The radial velocities derived from various groups of lines are listed in Table 1. Although discrepancies of a few kilometers per second in the velocities derived from these low-dispersion plates may be ascribed to errors of measurement, there can be no doubt concerning the reality of most of the larger differences. On the last two plates, for example, the velocities from permitted lines are −121 and −118 km/sec, respectively, while corresponding velocities from forbidden lines are −134 and −91 km/sec. The differential displacements on these two plates can easily be seen on the spectrocomparator. On both plates the lines are well defined.

The measured ranges of the permitted lines are about 23 km/sec; of the forbidden lines, 43 km/sec. Although some of this difference in range may be ascribed to the smaller number of lines in the forbidden groups, a considerable part of it is probably intrinsic. In spite of discrepancies on individual plates, like the ones noted in the preceding paragraph, the mean over-all displacements of the various groups of lines are nearly the same.

RW HYDRAE 132824

The light-curve[12] of RW Hydrae shows fluctuations with a mean period of 370 days; but the range, m_{pg}, *9.9–10.8*, is considerably less than that of a typical long-period variable. Bright hydrogen lines were noted at Harvard, where the spectrum was classified

[10] *Ap. J.*, **95**, 356, 1942. [11] *Ap. J.*, **96**, 468, 1942. [12] *Harv. Bull.*, No. 810, 1924.

from K5e to M2e. Bright lines of *He* I, *He* II, and [*O* III] were detected at Mount Wilson[1, 2] in 1931. These lines were less conspicuous than in AX Persei or CI Cygni. Observations in 1940 by Swings and Struve[13] revealed 14 permitted *O* III lines in the ultraviolet with the normal relative intensities of a recombination spectrum. Additional observations[5, 7] in 1941 and 1942 showed changes in the intensities of certain lines. The excellent spectrogram taken on February 1, 1942, by Swings and Struve[7] shows clearly both bright and dark lines.

The Mount Wilson spectrograms, listed in Table 3, reveal no very radical variations in the general appearance of the spectrum. Changes in the intensities of the bright lines

TABLE 3

DISPLACEMENTS OF BRIGHT LINES IN RW HYDRAE
(Km/Sec)

Date	Plate	Disp. at $H\gamma$	*H*	*He* I	*N* III	Mean	[*O* III] λ 4363	[*Ne* III] λ 3869	Mean Neb.
		A/mm							
1931 May 8	C 5725	70	(+11)	(+27)	.....	(+18)	.....	.....	.....
July 4	C 5776	70	(+ 2)	.....	.....	(+ 2)	.....	.....	.....
1932 Feb. 23	C 5965	70	− 5	−12	.....	− 7	(−11)	.....	(−11)
1935 May 10	C 6663	75	(+42)	+18	.....	+26	+23	.....	(+23)
1937 Feb. 27	C 6991	75	+ 8	+10	+ 1	+ 8	+34	.....	(+34)
Apr. 30	C 7035	75	+ 8	+ 8	.....	+ 8	−13	.....	(−13)
June 18	C 7066	70	+20	+28	.....	+23	− 9	.....	(− 9)
1938 June 8	C 7176	75	+ 5	.....	.....	(+ 5)	−10	.....	(−10)
1940 Apr. 17	C 7481	75	+ 5	+ 6	+ 7	+ 6	+23	+21	+22
1941 Mar. 7	E 73	65	+ 4	+11	+10	+ 7	+ 8	+ 2	+ 5
May 13	γ 23412	75	+18	+18	+23	+18	+ 2	+ 3	+ 2
May 15	E 121	65	+28	+32	(+48)	+30	+ 6	.....	(+ 6)
June 8	E 156	65	+23	+26	(+29)	+24	−11	(+ 6)	(− 5)
June 9	E 161	65	+29	+30	+37	+30	− 4	+ 7	+ 2
1943 Apr. 16	γ 25001	75	+ 8	+16	+ 2	+10	+29	+12	+20
Mean	.....	.....	+13	+16	+17	+14	+ 5	+ 8	+ 5

and in the distinctness of the dark lines may, however, be noted. For example, the estimated ratio of intensity $H\zeta$ λ 3889:[*Ne* III] λ 3869 varies from 10 to 2 or 3; that of [*O* III] λ 4363:*He* I λ 4388, from 1.5 to 0.6; that of *He* I λ 4388:*He* I λ 4471, from 2 to 1.

Displacements.—Table 3 shows that the displacements of the bright lines are not constant. On any one plate the velocities derived from lines of *H*, *He* I, and *N* III (λ 4097) appear to agree within errors of measurement. The lines λ 3869 [*Ne* III] and λ 4363 [*O* III] agree with each other but frequently disagree with the other group, the two sets of values exhibiting no obvious correlation. The over-all mean from the forbidden lines is slightly lower than that from the other group. The mean of rather scattering measurements of λ 4686 *He* II is +6 km/sec, in agreement with the mean value from the forbidden lines rather than with that from the other permitted lines.

[13] *Proc. Nat. Acad. Sci.*, **26**, 458, 1940.

On plate E 161, 6 absorption lines yielded the velocity +17 km/sec, in better agreement with the over-all mean velocity from permitted bright lines than with the bright-line velocity from the same plate. The type is approximately gM2ep. In a paper[7] dated May 1, 1943, Swings and Struve state: "The radial velocities of the emission and absorption lines are identical and are the same as in 1940."

CI Cygni

Bright lines were detected by Miss Annie J. Cannon in the spectrum of CI Cygni on an objective-prism photograph taken at Harvard in 1922. She wrote: "The hydrogen lines $H\beta$, $H\gamma$, $H\delta$, $H\epsilon$, and $H\zeta$ are bright, and two other bright lines have the approximate wave lengths 4686 and 4650. Several dark lines are also seen."[14]

Titanium oxide bands were photographed at Mount Wilson in 1931 following independent detection of the bright $H\alpha$ line.[1, 2] The spectrum resembled that of AX Persei, but the titanium bands were stronger, the forbidden lines weaker.[3] Observations by Swings and Struve[4, 7, 8] in the years 1939–1942 extended our knowledge of the spectrum, especially in the ultraviolet region. No marked changes were noted.

TABLE 4

SPECTROGRAMS OF CI CYGNI WITH DATA FROM BRIGHT LINES

Date	Plate	Disp. at $H\gamma$	Radial Velocity (Km/Sec)						Relative Intensities			
			H	*He* I	*He* II	*Fe* II	[*O* III] λ 4363	[*Ne* III] λ 3869	λ 3759 / $H\epsilon$	λ 3869 / $H\zeta$	λ 4363 / λ 4471	λ 4388 / λ 4471
		A/mm										
1931 Oct. 28	C 5879	70	+ 7	− 5	+ 2	(+14)	− 6	.....	.....	.....	2	1.3
1940 Aug. 25	C 7569	75	+30	− 1	+25	.....	− 2	−16	>3	(1)	6	0.2
1941 July 13	E 190	65	+ 5	+13	+ 5	+14	+23	+22	3	0.1	2	0.3
1942 Oct. 23	E 639*	65	+29	(+13)	(+23)	.....	(− 4)	.....	.....	(1)	3	0.3
1943 Aug. 12	E 914	65	+16	+28	+28	+32	+28	+28	4	0.1	1	0.8
Mean	.....	.....	+17	+ 9	+16	+20	+ 8	+11	.....	.....	.....	.....

* Weak exposure.

On the Mount Wilson spectrograms, listed in Table 4, lines of various elements are subject to moderate changes in intensity. On plate E 190, for example, lines of *He* I, *Fe* II, and *Ca* II are especially strong. Lines of [*Fe* II] are present in low intensity on two plates. A doubtful trace of λ 4658 [*Fe* III] was measured on E 190. A weak line of [*Fe* V] was measured at λ 3891.4 (mean reduced wave length) on C 7569 and E 190. The line [*Fe* VII] λ 3759.2 is strong and wide, with well-defined edges. The relative intensities of certain lines are indicated in the last four columns of Table 4.

Displacements.—The velocities derived from various lines differ from plate to plate but not in a uniform manner. The helium lines behave curiously. The results from *He* II lines closely resemble those from *H* lines, while those from *He* I are more like those from [*O* III] and [*Ne* III]. Meager data for *Fe* II and *Ca* II suggest that displacements of these lines agree with those of the lines of *He* I, but the result requires confirmation from more spectrograms. The grouping of *H* and *He* II and that of *He* I, [*O* III], and [*Ne* III] receive some slight confirmation from the means for all plates.

On plate E 914 the lines λλ 4515, 4520, 4556, and 4629 of the $b^4F - z^4F^\circ$ multiplet of *Fe* II yield a mean displacement of +50 km/sec, while 10 lines in other *Fe* II multiplets yield +30 km/sec. The cause of this discrepancy of 20 km/sec is unknown. The excitation potentials of the multiplets concerned are about the same. On plate E 190 the discrepancy is only 6 km/sec.

[14] *Harv. Bull.*, No. 778, 1922.

Z Andromedae 232848

The stronger bright lines in the spectrum of Z Andromedae ($H\beta$, $H\gamma$, $H\delta$, $H\epsilon$, and *He* II λ 4686) were discovered at Harvard in 1900. The spectrum was classified Ocp or Pec. An extensive investigation by H. H. Plaskett[15] was based on spectrograms taken at Victoria in the years 1923–1926. The plates revealed a rich bright-line spectrum, lines of *H*, *He* I, *Fe* II, [*Fe* II], *Ti* II, and *Si* II being ascribed to the "stellar part," those of *He* II, *N* III, *C* III, [*O* III], [*Ne* III], and [*Fe* III] to the "nebular part." The radial velocities derived from various lines presented a complex pattern; they were neither consistent on a given plate nor constant from year to year.

The titanium bands were apparently first detected[16] by the present writer in the illustrations accompanying Plaskett's article. Their presence was confirmed by F. S. Hogg upon re-examination of the original spectrograms.[17] Additional spectrograms taken by Hogg in 1932 and 1933 showed that "the *TiO* bands strengthened as the star faded. The emission lines have weakened relative to the continuous spectrum and irregularities in the velocity continue."[18]

A spectrogram obtained at the McDonald Observatory on September 14, 1939, showed a spectrum completely different from that observed by Plaskett. The combination spectrum with *TiO* bands and strong emission lines of *He* II and [*O* III] was replaced by a shell spectrum many of whose lines were of the P Cygni type. All the dark lines had large negative displacements.[19] After a few months the shell features disappeared and the spectrum resumed its original appearance. Identifications of the lines and the changing intensities from September, 1939, to January, 1943, are discussed in the series of papers by Swings and Struve.[4–9]

The Mount Wilson spectrograms, together with the measured displacements of various groups of emission lines, are recorded in Table 5.

1923.—The first spectrogram, for the use of which I am indebted to M. L. Humason, was taken on September 30, 1923, during the interval covered by Plaskett's early observations.[15] The spectrum on this plate and on a strongly exposed low-dispersion plate taken by E. P. Hubble on November 11, 1923, was closely similar to that shown in Plaskett's Plate VII *B*. The [*Ne* III] line λ 3869 is about one-half as intense as $H\zeta$. The [*O* III] line λ 4363 is four times as intense as *He* I λ 4388.

1939.—As noted by Struve and Elvey, the spectrum was now entirely different. The M-type features and many of the emission lines were suppressed by the strong shell-type spectrum. Even the exceedingly strong line *He* II λ 4686 cannot be seen on October 4 or October 23, 1939. It is barely visible on January 20, 1940. Data concerning displacements of the absorption lines are in Table 6. These displacements, presumably representing the outward velocities of an expanding envelope, were largest near the beginning of the outburst with values decreasing from September, 1939, to January, 1940 (see Table 6).

1940.—The shell spectrum, although only slightly weakened in January, had by May nearly disappeared. In July only a few traces of it, chiefly absorption at H and K, were left. By September the dark H and K lines were about gone; in October they were replaced by weak bright lines. It is noteworthy that, as the effect of the expanding shell disappeared, the spectrum became almost the same as it had been in 1923. The intensity ratio λ 3869 [*Ne* III]:λ 3889 $H\zeta$ decreased from 1.5 in May, 1940, to 0.6 by the end of the year. From July, 1940, to January, 1941, λ 4363 was five times as intense as λ 4388.

[15] *Dom. Ap. Obs.*, **4**, 119, 1928.

[16] The classification "Md?" given by Mrs. W. P. Fleming in *Harv. Circ.*, No. 54, 1901, may indicate that she suspected the presence of M-type bands. But see also a later note by E. C. Pickering in *Harv. Circ.*, No. 168, 1911.

[17] *Pub. A.S.P.*, **44**, 328, 1932.

[18] *Pub. A.A.S.*, **8**, 14, 1934.

[19] Struve and Elvey, *Pub. A.S.P.*, **51**, 297, 1939.

TABLE 5

Z ANDROMEDAE: DISPLACEMENTS OF EMISSION LINES
(Km/Sec)

Date	Mag.	Plate	Disp. at $H\gamma$	H	He I	Fe II	Ti II	Si II	Ca II	[O III] λ 4363	[Ne III]
			A/mm								
1923 Sept. 30...	9.8	C 2441‡	40	+ 7	(+30)	0	.....	.....	.....	− 1	.....
1939 Sept. 16*..	8.1	CQ 252	60	+23	.....	+ 3	− 8	+ 8	− 3	.....	.....
Oct. 3...	7.8	C 7389	75	(+38)	.....	.....	.....	.....	.....	.....	.....
Oct. 4...	7.8	C 7397	40	+40	.....	+10	+10	.....	+23	.....	.....
Oct. 18*..	7.8	CQ 271	60	+60	.....	+35	+28	.....	+36	.....	.....
Oct. 23...	7.9	C 7408	40	+37	.....	+18	+28	.....	+31	.....	.....
Dec. 5*..	8.0	CQ 290	60	+59	.....	+42	+50	+62	+28	.....	.....
1940 Jan. 20...	8.3	C 7438	40	+44	.....	+21	+18	+17	+33	.....	.....
May 29...	9.2	γ 22643§	75	+42	(+ 5)	(+19)	.....	(+16)	.....	− 3	+12
July 20...	9.5	C 7537	40	+28	+17	+ 1	+12	+ 6	.....	+ 6	+ 2
Sept. 17...	9.6	C 7583	40	+ 7	+ 4	− 7	− 2	− 6	+10	− 2	+ 4
Oct. 19...	9.6	C 7608	40	+ 5	+ 5	− 2	− 3	− 3	+17	− 6	+ 6
1941 Jan. 15...	9.6	γ 23272	75	− 3	− 9	−21	.....	−14	− 6	− 3	+ 2
July 13...	8.8	E 191§	65	+ 2	+ 4	(−14)	−10	−13	−14	.....	−22
July 14...	8.8	C 7686	40	+ 9	+ 5	− 6	− 8	.....	.....	−12	.....
Aug. 7...	8.6	C 7693	40	+ 7	+ 8	+ 1	− 2	+ 3	+20	− 7	− 7
Nov. 10...	9.0	γ 23877§	75	+19	+20	+ 9	.....	+14	+28	.....	−12
Dec. 6...	9.1	E 355	65	+16	+19	+ 9	.....	+11	+45	− 4	+ 2
1942 Oct. 23...	10.2	E 640	65	−14	− 9	− 9	.....	+ 2	+24	− 5	− 2
Dec. 2...	10.0	γ 24744	75	−16	+ 2	− 5	.....	(− 3)	(+ 9)	− 2	+ 8
1943 Aug. 11...	9.1	E 911	65	− 9	− 2	− 9	−15	− 8	+23	−23	− 1
Partial mean†	.....	.....	.....	+ 4	+ 6	− 4	− 4	− 1	+16	− 6	− 2

* McDonald Observatory (Swings and Struve, *Ap. J.*, **91**, 608 1940).

† Beginning with C 7537.

‡ Negative by M. L. Humason.

§ Overexposed.

TABLE 6

Z ANDROMEDAE: DISPLACEMENTS OF ABSORPTION LINES
(Km/Sec)

Date	Plate	H	Ca II	Fe II	Ti II	Mg II
1939 Sept. 16*.....	CQ 252	−81	−68	−140	−118	−93
Oct. 3.....	C 7389	−80	−80	.....	− 66	−93
Oct. 4.....	C 7397	−61	−68	− 76	− 52	−94
Oct. 18*.....	CQ 271	−72	−67	− 63	− 65	−20
Oct. 23.....	C 7408	−70	−61	− 86	− 48	−71
Dec. 5*.....	CQ 270	−55	−41	− 72	− 58	−53
1940 Jan. 20.....	C 7438	−48	−37	.....	.....	.....

* McDonald Observatory (Swings and Struve, *Ap. J.*, **91**, 608, 1940).

1941.—The lines of [*Ne* III] and of [*O* III], especially λ 4363, were weaker than in 1940. Otherwise there was not much change. The [*Ne* III] line λ 3869 was only one-fourth as intense as *Hζ*; λ 4363 was slightly stronger than λ 4388, slightly weaker than λ 4471.

1942.—The line λ 4363 [*O* III] and the [*Ne* III] lines were much stronger, as was λ 3759 *O* III (perhaps blended with [*Fe* VII]). Lines of [*Fe* V] were somewhat stronger, while those of *He* I and *Fe* II were weaker. Lines of doubly ionized atoms were evidently favored during this year. The line λ 3869 is about half as strong as *Hζ*; λ 4363 is three or four times as strong as λ 4388, twice as strong as λ 4471.

1943.—Lines of *Fe* II were stronger, while those of [*O* III] (especially λ 4363) and [*Ne* III] were weaker. The spectrum was much the same as in 1941.

The intensity of λ 4363 [*O* III] undergoes changes which parallel those of [*Ne* III] lines. The changes of λ 4959 and λ 5007 of [*O* III] seem less marked, possibly because my plates do not show these lines well. From 1940 to 1943 the helium singlet line λ 4388 is about one-half as intense as the triplet line λ 4471.

Displacements.—Radial velocities derived from various groups of bright lines (Table 5) present a baffling complexity. The actual pattern of the changing velocities will evidently be made clear only by very extensive observation. The following remarks refer to the spectrum from July 20, 1940, to August 11, 1943. Mean values for certain elements not included in Table 4 are: *Mg* II, −5 km/sec; *N* III, −5; *Mg* I, +7 (low weight); *He* II, −17 (low weight). The combined mean for *H* and *He* I is +5 km/sec; that for *Fe* II, *Ti* II, *Si* II, *Mg* II, *N* III, [*O* III], and [*Ne* III] is −4. The mean for *Ca* II, +16 km/sec, is quite different. This element is outstanding in another way. The observed range for most lines is about 30 km/sec; that for *Ca* II is nearly twice as great. Data for the dark lines at the time of the 1939 outburst are in Table 6.

Discussion

A convenient grouping of stars having late-type absorption spectra with superposed bright lines is indicated in Table 7. Group V was added at the suggestion of Mr. A. H. Joy.

TABLE 7

Groups of Bright-Line Stars with Absorption Spectra of Late Type

I. *Ca* II bright
Giants α Boo gK0
Subgiants λ And G7
Dwarfs Companion to Castor dM1e (*H* also bright)

II. *Fe* II bright (*H* also bright)
Permitted lines T Tau dGep (*Ca* II also bright)
Forbidden lines WY Gem M3ep

III. *He* II and/or [*O* III], [*Ne* III] bright (*H* also bright)
Z And Mep

IV. Long-period variables
R Leo M8e
R Cyg Se
R Lep N6e

V. SS Cygni variables
RU Peg dGep

The groups are not mutually exclusive. The T Tauri stars in group II regularly exhibit bright lines of *Ca* II; it would therefore be possible to remove them from group II and to combine them with the dMe stars of group I. Bright lines of *Fe* II like those characteristic of group II are found, usually with variable intensities, in many spectra of group III and frequently in spectra of long-period variables, notably in Me variables at minimum light. The long-period variables R Aquarii, RW Hydrae, and UV Aurigae belong also in group III.

Stars of group III are said to have "combination" spectra. It is a question whether the term should be extended to spectra in the other groups. My suggestion is that, for the time being, the restricted usage be continued. Stars assigned to group III are:

Z And	T CBr	RW Hya	AX Per
R Aqr	BF Cyg	SY Mus?	RX Pup?
UV Aur	CI Cyg	AG Peg	BD+67°922

With one exception these stars are variables whose light-curves have long-period or irregular fluctuations. Several are subject to groups of fairly regular fluctuations interrupted by relatively quiescent intervals; this behavior may be typical of stars with combination spectra.

Bright lines of many elements occur in combination spectra. Among the more important are those of *H*, *He* I, *He* II, *N* III, *O* III, [*O* III], [*Ne* III], [*Ne* V], *Fe* II, [*Fe* II], [*Fe* III], [*Fe* V], and [*Fe* VII]. The remarkable intensity of lines requiring high excitation constitutes the chief problem of these aberrant spectra. The presence of forbidden lines is notable because it indicates that the density of the emitting gas is low, the volume large.

The displacements of the lines in the spectrum of AG Pegasi (BD+11°4673) have been investigated in considerable detail; less extensive measurements have been made in five other spectra. The following summary indicates what has been learned about probable periodic variations.

Z Andromedae.—Meager data for the years 1940–1943 indicate a range of 30 km/sec and a probable period of about 680 days. The period is not well defined; it might be as short as the 650-day light-period suggested by Richard Prager.[20] The curve for the nebular lines follows that for permitted lines by perhaps 150 days.

BF Cygni.[21]—The range for the nebular lines is nearly 60 km/sec, fully twice that for permitted lines. The period seems clearly to be between 700 and 800 days and may coincide with the light-period of 754 days derived by Luigi Jacchia.[22] The curve for the nebular lines follows that for *H* and *He* I by perhaps 120 days.

CI Cygni.—The data are very inadequate. The lines of *H* and *He* II have an observed range of about 25 km/sec; those of *He* I, [*O* III], and [*Ne* III], about 40 km/sec. There may be a fluctuation in a period of 800 or 900 days, with the curve for the nebular lines following that for *H* by about 200 days.

RW Hydrae.—The range obtained from the lines of *H*, *He* I, and *N* III is about 40 km/sec; that from the nebular lines, perhaps slightly greater. The period may be 370 days or longer, with the nebular lines out of phase with the others.

AG Pegasi (BD+11°4673).[23]—The amplitude of the curve obtained from *H* lines is about 40 km/sec; that for the curve from *Fe* II lines, less than 10 km/sec. A period of 800 days is well defined. The curves for various elements show notable differences in phase.

AX Persei.—The data are meager. The observed range obtained from the permitted lines is 23 km/sec; that from the forbidden lines, nearly twice as great. The probable period, about 880 days, seems definitely greater than the light-periods of 600 and 650 days mentioned by E. M. Lindsay.[24] The curve for the nebular lines follows that for the other lines by perhaps 160 days.

[20] *Pop. Astr.*, **47**, 335, 1939.

[21] P. W. Merrill, *Mt. W. Contr.*, No. 687; *Ap. J.*, **98**, 334, 1943.

[22] *Harv. Bull.*, No. 915, 1941.

[23] P. W. Merrill, *Mt. W. Contr.*, Nos. 381, 659; *Ap. J.*, **69**, 330, 1929; **95**, 386, 1942.

[24] *Harv. Bull.*, No. 888, 1932.

Tentative generalizations concerning the displacements of bright lines in combination spectra are:

1. The displacements of most, if not all, of the lines are variable.

2. A typical range is 30 km/sec. Permitted lines exhibit smaller ranges than forbidden lines, metallic lines having especially small ranges. In certain lines, dark borders of the P Cygni type are connected with positive displacements of the bright components.

3. The fluctuations are of long period—say 1–3 years. Quick changes of displacement, if present, are small.

4. The cyclical changes of various groups of lines may differ in phase as well as in amplitude. Maxima and minima of the forbidden lines occur about one-fifth of the period after the corresponding phases of permitted lines.

A working hypothesis to explain the slow fluctuations in the displacements of the bright lines in combination spectra is that of pulsations in an extensive, tenuous atmosphere in which the spectroscopic effects are stratified, the nebular lines being produced in the outer zones. If, as A. S. Eddington has suggested,[25] the period of a long-period variable coincides with the natural vibration period of volume pulsation, it seems possible that the longer period of a combination star may coincide with the vibration period of a star with a more tenuous atmosphere. An alternative explanation may, of course, be sought in the double-star hypothesis. At present it would appear inadvisable to accept either hypothesis without reserve.

[25] *Internal Constitution of the Stars*, p. 206, Cambridge, 1926.

THE STATISTICS OF THE GRAVITATIONAL FIELD ARISING FROM A RANDOM DISTRIBUTION OF STARS

III. THE CORRELATIONS IN THE FORCES ACTING AT TWO POINTS SEPARATED BY A FINITE DISTANCE

S. CHANDRASEKHAR
Yerkes Observatory
Received September 27, 1943

ABSTRACT

In this paper we consider the theory of the correlations in the forces acting at two points separated by a finite distance in a system containing a random distribution of stars. A problem central in this theory is the evaluation of the average force acting at a point and in the same direction as the force acting at another specified point. It is shown how this and other similar problems in the theory of *spatial correlations* can be solved. An application of this theory to the problem of the stability of wide binaries is contained in a later paper.

1. *Introduction.*—In the two earlier papers[1] of this series we have analyzed certain statistical features of the fluctuating gravitational field acting on a star. More specifically, the particular problems considered in the earlier papers arose out of an attempt to answer certain questions relating to the speed of fluctuations in the force per unit mass $\boldsymbol{F}$ acting on a star and required the evaluation of all the first and the second moments of $\dot{\boldsymbol{F}}$, the rate of change of $\boldsymbol{F}$ for a given $\boldsymbol{F}$. While the specification of these moments of $\dot{\boldsymbol{F}}$ are sufficient for the purposes of determining the instantaneous rates of change of $\boldsymbol{F}$ that are to be expected, they are very far from providing all the information that is necessary for a complete statistical description of the fluctuating force acting on a star.[2] For the entire stochastic variation of $\boldsymbol{F}$ with time can be described fully only in terms of the average force $\bar{\boldsymbol{F}}_t$ acting at any later time t, given that a force of some prescribed intensity acted at time $t = 0$. In other words, we need a complete "integration" of the stochastic equations of $\boldsymbol{F}$.

Now the problem of specifying the average force $\bar{\boldsymbol{F}}_t$ acting at time t (for a given $\boldsymbol{F}_0$ at time $t = 0$) is essentially equivalent to determining the correlations in the force acting at a given point but at two instants separated by a finite interval of time. Accordingly, it would appear that the solution to the problem of the stochastic variation of $\boldsymbol{F}$ acting on a star can be derived from that of the somewhat simpler one of the correlations in the force acting simultaneously at two points separated by a finite distance. For the correlations between $\boldsymbol{F}_0$ and $\boldsymbol{F}_t$ will be determined in terms of the distribution function $W(\boldsymbol{F}_0, \boldsymbol{F}_t)$, where

$$\boldsymbol{F}_0 = G\sum_i M_i \frac{\boldsymbol{r}_i}{|\boldsymbol{r}_i|^3} \tag{1}$$

and

$$\boldsymbol{F}_t = G\sum_i M_i \frac{\boldsymbol{r}_i + \boldsymbol{V}_i t}{|\boldsymbol{r}_i + \boldsymbol{V}_i t|^3}. \tag{2}$$

[1] *Ap. J.*, **95**, 489, 1942, and **97**, 1, 1943: these two papers will be referred to as I and II, respectively. For a more general account of the basic ideas see S. Chandrasekhar, *Rev. Mod. Phys.*, **15**, 1, 1943, and also an essay entitled "New Methods in Stellar Dynamics," *Annals of the New York Academy of Sciences*, **45**, 131, 1943.

[2] See, e.g., the remarks in S. Chandrasekhar, *Ap. J.*, **97**, 255, 1943 (§ 3 of this paper).

In equations (1) and (2) r_i and V_i denote respectively the position and the velocity of a typical field star *relative* to the one under consideration. On the other hand, the problem of the spatial correlations requires the consideration of the distribution function $W(F_0, F_1)$, where F_0 is again defined as in equation (1), while

$$F_1 = G\sum_i \frac{r_i - r_1}{|r_i - r_1|^3}, \tag{3}$$

where r_1 now denotes the position of the second point considered relative to the first. Comparing equations (2) and (3), it is apparent that the two theories associated respectively with the quantities F_t and F_1 differ formally from each other only in one respect, namely, that, while when considering F_t we have to allow for an appropriate asymmetric distribution of the relative velocities V_i, we have no such problem of averaging when considering F_1, since r_1 is a certain prescribed constant vector. It is therefore seen that the consideration of spatial correlations provides us with a problem basic to the whole general theory. But, even apart from this, the theory of spatial correlations has its own independent interest for stellar dynamics. Thus, questions relating to the stability of wide binaries can be answered satisfactorily only in terms of such a theory.[3] We shall accordingly devote this paper entirely to the development of the theory of spatial correlations. The more difficult problem of the stochastic variation of F acting on a star is taken up in the paper following this one.[4]

2. *The general formula for* $\mathbf{W(F_0, F_1)}$.—As we have already indicated, the problem of spatial correlations requires us to consider the probability that a force F_0 will act at a point and that simultaneously a force F_1 will act at a second point distant $|r_1|$ from the first. The general expression for the corresponding probability distribution $W(F_0, F_1)$ can be readily written down by an application of Markoff's method.[5] We have

$$W(F_0, F_1) = \frac{1}{64\pi^6}\int_{|\rho|=0}^{\infty}\int_{|\sigma|=0}^{\infty} e^{-i(\rho\cdot F_0 + \sigma\cdot F_1)} A(\rho, \sigma)\, d\rho d\sigma, \tag{4}$$

where

$$A(\rho, \sigma) = \lim_{R\to\infty}\left[\frac{3}{4\pi R^3}\int_{|r|<R} e^{iGM\left\{\frac{r\cdot\rho}{|r|^3} + \frac{(r-r_1)\cdot\sigma}{|r-r_1|^3}\right\}} dr\right]^{4\pi R^3 N/3}. \tag{5}$$

In equations (4) and (5) ρ and σ are two auxiliary vectors and N denotes the average number of stars per unit volume. (It should be noted here that in writing equation [5] we have assumed that all the stars have the same mass M. However, the generalizations needed to allow for a distribution over the masses is fairly straightforward and will be indicated later.) By a series of transformations customary in this theory we can express $A(\rho, \sigma)$ in the form[6]

$$A(\rho, \sigma) = e^{-C(\rho, \sigma)}, \tag{6}$$

where the characteristic function $C(\rho, \sigma)$ is given by

$$C(\rho, \sigma = N\int_{-\infty}^{+\infty}\left[1 - e^{iGM\left\{\frac{r\cdot\rho}{|r|^3} + \frac{(r-r_1)\cdot\sigma}{|r-r_1|^3}\right\}}\right] dr. \tag{7}$$

[3] See a later paper appearing in this same issue (p. 54).

[4] See p. 47; this paper will be referred to as IV.

[5] Cf. S. Chandrasekhar, *Rev. Mod. Phys.*, **15**, 1, 1943. (See particularly chap. i, § 3, and chap. iv, §§ 2 and 3.)

[6] Cf., e.g., II, § 1, particularly the transformations leading from eq. (6) to eq. (12).

An alternative form for $C(\boldsymbol{\rho}, \boldsymbol{\sigma})$ is

$$\left.\begin{aligned} C(\boldsymbol{\rho}, \boldsymbol{\sigma}) = N\int_{-\infty}^{+\infty} [1 - e^{iGM\boldsymbol{r}\cdot\boldsymbol{\rho}/|\boldsymbol{r}|^3}]\, d\boldsymbol{r} \\ + N\int_{-\infty}^{+\infty} e^{iGM\boldsymbol{r}\cdot\boldsymbol{\rho}/|\boldsymbol{r}|^3} [1 - e^{iGM(\boldsymbol{r}-\boldsymbol{r}_1)\cdot\boldsymbol{\sigma}/|\boldsymbol{r}-\boldsymbol{r}_1|^3}]\, d\boldsymbol{r}\,. \end{aligned}\right\} \quad (8)$$

The first of the two integrals which occur in the foregoing equation is equivalent to the one we have already evaluated in I (eqs. [55]–[58]). We thus have

$$C(\boldsymbol{\rho}, \boldsymbol{\sigma}) = \tfrac{4}{15}(2\pi GM)^{3/2} N |\boldsymbol{\rho}|^{3/2} + N\int_{-\infty}^{+\infty} e^{iGM\boldsymbol{r}\cdot\boldsymbol{\rho}/|\boldsymbol{r}|^3} [1 - e^{iGM(\boldsymbol{r}-\boldsymbol{r}_1)\cdot\boldsymbol{\sigma}/|\boldsymbol{r}-\boldsymbol{r}_1|^3}]\, d\boldsymbol{r}\,. \quad (9)$$

Equations (4), (6), and (9) formally solve the problem. However, an explicit evaluation of the entire probability distribution $W(\boldsymbol{F}_0, \boldsymbol{F}_1)$ will require a complete knowledge of the characteristic function $C(\boldsymbol{\rho}, \boldsymbol{\sigma})$. But, if we are interested only in the moments of $\boldsymbol{F}_1$, we need only the behavior of $C(\boldsymbol{\rho}, \boldsymbol{\sigma})$ for $|\boldsymbol{\sigma}| \to 0$. For these purposes we can therefore expand

$$1 - e^{iGM(\boldsymbol{r}-\boldsymbol{r}_1)\cdot\boldsymbol{\sigma}/|\boldsymbol{r}-\boldsymbol{r}_1|^3}\,, \quad (10)$$

which occurs under the integral sign in equation (9) in a power series in $\boldsymbol{\sigma}$. Retaining only the first term in this expansion, we have

$$C(\boldsymbol{\rho}, \boldsymbol{\sigma}) = \tfrac{4}{15}(2\pi GM)^{3/2} N |\boldsymbol{\rho}|^{3/2} + D(\boldsymbol{\rho}, \boldsymbol{\sigma}) + O(|\boldsymbol{\sigma}|^2)\,, \quad (11)$$

where

$$D(\boldsymbol{\rho}, \boldsymbol{\sigma}) = -iGMN\int_{-\infty}^{+\infty} e^{iGM\boldsymbol{r}\cdot\boldsymbol{\rho}/|\boldsymbol{r}|^3} \frac{(\boldsymbol{r}-\boldsymbol{r}_1)\cdot\boldsymbol{\sigma}}{|\boldsymbol{r}-\boldsymbol{r}_1|^3}\, d\boldsymbol{r}\,. \quad (12)$$

In equation (12) it is convenient to introduce two new variables, $\boldsymbol{R}$ and $\boldsymbol{S}$, in place of $\boldsymbol{\rho}$ and $\boldsymbol{\sigma}$. Let

$$\boldsymbol{R} = GM\boldsymbol{\rho} \quad \text{and} \quad \boldsymbol{S} = GM\boldsymbol{\sigma}\,. \quad (13)$$

Equation (12) becomes

$$D(\boldsymbol{R}\ \boldsymbol{S}) = -iN\int_{-\infty}^{+\infty} e^{i\boldsymbol{r}\cdot\boldsymbol{R}/|\boldsymbol{r}|^3} \boldsymbol{S}\cdot\frac{(\boldsymbol{r}-\boldsymbol{r}_1)}{|\boldsymbol{r}-\boldsymbol{r}_1|^3}\, d\boldsymbol{r}\,, \quad (14)$$

or, alternatively,

$$D(\boldsymbol{R}, \boldsymbol{S}) = iN\int_{-\infty}^{+\infty} e^{i\boldsymbol{r}\cdot\boldsymbol{R}/|\boldsymbol{r}|^3} \left(\boldsymbol{S}\cdot\operatorname{grad}\frac{1}{|\boldsymbol{r}-\boldsymbol{r}_1|}\right) d\boldsymbol{r}\,. \quad (15)$$

Integrating by parts, we obtain

$$D(\boldsymbol{R}, \boldsymbol{S}) = -iN\int_{-\infty}^{+\infty} \frac{1}{|\boldsymbol{r}-\boldsymbol{r}_1|}\, \boldsymbol{S}\cdot\operatorname{grad}(e^{i\boldsymbol{r}\cdot\boldsymbol{R}/|\boldsymbol{r}|^3})\, d\boldsymbol{r}\,. \quad (16)$$

Explicitly, equation (16) has the form

$$D(\boldsymbol{R}, \boldsymbol{S}) = N\int_{-\infty}^{+\infty} \frac{e^{i\boldsymbol{r}\cdot\boldsymbol{R}/|\boldsymbol{r}|^3}}{|\boldsymbol{r}-\boldsymbol{r}_1|} \left\{\frac{\boldsymbol{S}\cdot\boldsymbol{R}}{|\boldsymbol{r}|^3} - 3\,\frac{(\boldsymbol{r}\cdot\boldsymbol{R})\,(\boldsymbol{r}\cdot\boldsymbol{S})}{|\boldsymbol{r}|^5}\right\} d\boldsymbol{r}\,. \quad (17)$$

It is of interest to note that, according to equation (17), $D(\boldsymbol{R}, \boldsymbol{S})$ regarded as a function of $\boldsymbol{r}_1$ satisfies the differential equation

$$\text{div grad } D = 4\pi N e^{i\boldsymbol{r}\cdot\boldsymbol{R}/|\boldsymbol{r}|^2}\left\{\frac{\boldsymbol{S}\cdot\boldsymbol{R}}{|\boldsymbol{r}|^3} - 3\,\frac{(\boldsymbol{r}\cdot\boldsymbol{R})\,(\boldsymbol{r}\cdot\boldsymbol{S})}{|\boldsymbol{r}|^5}\right\}. \tag{18}$$

It is possible that the existence of this differential equation of the Poisson type has a deeper significance than is apparent at first sight.

3. *The evaluation* $D(\boldsymbol{\rho}, \boldsymbol{\sigma})$.—To evaluate the integral defining $D(\boldsymbol{R}, \boldsymbol{S})$, we shall chose a Cartesian system of co-ordinates in which the z-axis is in the direction of $\boldsymbol{R}$ (i.e., $\boldsymbol{\rho}$) and the xz-plane contains the vector $\boldsymbol{r}_1$. Let the components of $\boldsymbol{S}$ in this system of co-ordinates be S_1, S_2, and S_3. With this choice of the orientation of the co-ordinate system and transforming to polar co-ordinates, equation (17) reduces to

$$\left.\begin{aligned} D(\boldsymbol{R}, \boldsymbol{S}) = -N|\boldsymbol{R}|\int_0^{\infty}\int_{-1}^{+1}\int_0^{2\pi}\frac{e^{i|\boldsymbol{R}|\mu/r^2}}{|\boldsymbol{r}-\boldsymbol{r}_1|\,r}\,[2S_3P_2(\mu) \\ + 3\mu(1-\mu^2)^{1/2}(S_1\cos\varphi + S_2\sin\varphi)]\,dr\,d\mu\,d\varphi\,, \end{aligned}\right\} \tag{19}$$

where we have used μ to denote $\cos\vartheta$. Further, the P_n's denote, as usual, the Legendre functions.

We now expand $|\boldsymbol{r}-\boldsymbol{r}_1|^{-1}$, which occurs under the integral sign in equation (19) in spherical harmonics. We have

$$\frac{1}{|\boldsymbol{r}-\boldsymbol{r}_1|} = \frac{1}{\tilde{r}}\sum_{l=0}^{\infty} x^l P_l(\cos\Theta)\,, \tag{20}$$

where

$$\tilde{r} \text{ is the larger of } r \text{ and } r_1 \tag{21}$$

and

$$x = \left\{\begin{matrix} r/r_1 & \text{if} & r < r_1 \\ r_1/r & \text{if} & r > r_1 \end{matrix}\right\}. \tag{22}$$

Further, in equation (20) Θ denotes the angle between the directions of $\boldsymbol{r}$ and $\boldsymbol{r}_1$. Accordingly,

$$\cos\Theta = \cos\vartheta\cos\vartheta_1 + \sin\vartheta\sin\vartheta_1\cos\varphi\,, \tag{23}$$

where

$$\vartheta_1 = \measuredangle(\boldsymbol{R}, \boldsymbol{r}_1)\,. \tag{24}$$

Moreover, by the addition theorem of spherical harmonics

$$P_l(\cos\Theta) = P_l(\mu)P_l(\mu_1) + 2\sum_{m=1}^{l}\frac{(l-m)!}{(l+m)!}P_l^m(\mu)P_l^m(\mu_1)\cos m\varphi\,, \tag{25}$$

where we have written μ_1 for $\cos\vartheta_1$. Combining equations (19), (20), and (25), we have

$$\left.\begin{aligned} D(\boldsymbol{R}, \boldsymbol{S}) = -N|\boldsymbol{R}|\int_0^{\infty}\int_{-1}^{+1}\int_0^{2\pi}\frac{e^{i|\boldsymbol{R}|\mu/r^2}}{r\,\tilde{r}}\,[2S_3P_2(\mu) + 3\mu(1-\mu^2)^{1/2} \\ \times(S_1\cos\varphi + S_2\sin\varphi)]\left[\sum_{l=0}^{\infty} x^l\left\{P_l(\mu)P_l(\mu_1) + 2\sum_{m=1}^{l}\frac{(l-m)!}{(l+m)!}\right.\right. \\ \left.\left.\times P_l^m(\mu)P_l^m(\mu_1)\cos m\varphi\right\}\right]dr\,d\mu\,d\varphi\,. \end{aligned}\right\} \tag{26}$$

Integration over φ is now readily performed, and we get

$$D(\boldsymbol{R},\boldsymbol{S}) = -2\pi N|\boldsymbol{R}|\int_0^{\infty}\int_{-1}^{+1}\frac{e^{i|\boldsymbol{R}|\mu/r^2}}{r\tilde{r}}\left[2S_3P_2(\mu)\sum_{l=0}^{\infty}x^lP_l(\mu)P_l(\mu_1)\right.$$
$$\left.+\,3S_1\mu(1-\mu^2)^{1/2}\sum_{l=1}^{\infty}\frac{(l-1)!}{(l+1)!}x^lP_l^1(\mu)P_l^1(\mu_1)\right]dr\,d\mu\,. \qquad (27)$$

Now, introduce the new variable

$$z = |\boldsymbol{R}|\,r^{-2} \qquad (28)$$

and let

$$z_1 = |\boldsymbol{R}|\,r_1^{-2} = GM|\rho|\,r_1^{-2}\,. \qquad (29)$$

With this change of the variables, equation (27) takes the more convenient form

$$D(\boldsymbol{R},\boldsymbol{S}) = -\pi N|\boldsymbol{R}|^{1/2}\int_0^{\infty}\int_{-1}^{+1}e^{iz\mu}\frac{\tilde{z}^{1/2}}{z}\left[2S_3P_2(\mu)\sum_{l=0}^{\infty}\xi^{l/2}P_l(\mu)P_l(\mu_1)\right.$$
$$\left.+\,3S_1\mu(1-\mu^2)^{1/2}\sum_{l=1}^{\infty}\xi^{l/2}\frac{(l-1)!}{(l+1)!}P_l^1(\mu)P_l^1(\mu_1)\right]dz\,d\mu\,, \qquad (30)$$

where

$$\tilde{z} \text{ is the smaller of } z \text{ and } z_1 \qquad (31)$$

and

$$\xi = \begin{cases} z/z_1 & \text{if } z < z_1 \\ z_1/z & \text{if } z > z_1 \end{cases}. \qquad (32)$$

To perform the integration over μ, we expand $\exp(iz\mu)$ in spherical harmonics. We have the well-known expansion

$$e^{iz\mu} = \left(\frac{\pi}{2z}\right)^{1/2}\sum_{n=0}^{\infty}(2n+1)\,i^nJ_{n+1/2}(z)P_n(\mu)\,, \qquad (33)$$

in which the $J_{n+1/2}$'s are the Bessel functions of half odd-integral orders. Hence,

$$D(\boldsymbol{R},\boldsymbol{S}) = -\frac{\pi^{3/2}N|\boldsymbol{R}|^{1/2}}{2^{1/2}}\int_0^{\infty}dz\,\frac{\tilde{z}^{1/2}}{z^{3/2}}\left[2S_3\sum_{l=0}^{\infty}\xi^{l/2}P_l(\mu_1)\int_{-1}^{+1}d\mu P_2(\mu)P_l(\mu)\right.$$
$$\times\sum_{n=0}^{\infty}(2n+1)\,i^nJ_{n+1/2}(z)P_n(\mu) + 3S_1\sum_{l=1}^{\infty}\xi^{l/2}P_l^1(\mu_1)$$
$$\left.\times\frac{(l-1)!}{(l+1)!}\int_{-1}^{+1}d\mu\mu(1-\mu^2)^{1/2}P_l^1(\mu)\sum_{n=0}^{\infty}(2n+1)\,i^nJ_{n+1/2}(z)P_n(\mu)\right]. \qquad (34)$$

It is seen that in the foregoing equation we have to perform integrations over the product of three tesseral harmonics, the upper suffix of one being the sum of the upper suffixes of the other two. Such integrals have been studied by J. A. Gaunt.[7] However, the par-

[7] *Phil. Trans. Roy. Soc.* (London), Ser. A, **228**, 151, 1929. (See particularly the appendix to this paper, pp. 192–196.)

ticular results needed for our purposes can be derived more directly. Thus, using the recursion formulae

$$\left.\begin{aligned} \mu P_n^m &= \frac{1}{2n+1}\left[(n-m+1)P_{n+1}^m + (n+m)P_{n-1}^m\right], \\ (1-\mu^2)^{1/2}P_n^m &= \frac{1}{2n+1}\left(P_{n+1}^{m+1} - P_{n-1}^{m+1}\right), \end{aligned}\right\} \tag{35}$$

we readily obtain the equations

$$\left.\begin{aligned} P_2 P_n &= \frac{3(n+1)(n+2)}{2(2n+1)(2n+3)}P_{n+2} + \frac{n(n+1)}{(2n+3)(2n-1)}P_n \\ &\qquad + \frac{3n(n-1)}{2(2n+1)(2n-1)}P_{n-2}, \\ \mu(1-\mu^2)^{1/2}P_n &= \frac{n+1}{(2n+1)(2n+3)}P_{n+2}^1 + \frac{1}{(2n+3)(2n-1)}P_n^1 \\ &\qquad - \frac{n}{(2n+1)(2n-1)}P_{n-2}^1. \end{aligned}\right\} \tag{36}$$

Substituting these formulae in equation (34) and using the orthogonality properties of the Legendre functions, we find

$$\left.\begin{aligned} D(\boldsymbol{R},\boldsymbol{S}) = &-\frac{\pi^{3/2}|\boldsymbol{R}|^{1/2}N}{2^{1/2}}\int_0^\infty dz\,\frac{\tilde{z}^{1/2}}{z^{3/2}}\Bigg[2S_3\sum_{l=0}^\infty i^l \xi^{l/2}P_l(\mu_1) \\ &\times\Bigg\{-\frac{3l(l-1)}{(2l+1)(2l-1)}J_{l-3/2} + \frac{2l(l+1)}{(2l+3)(2l-1)}J_{l+1/2} \\ &-\frac{3(l+2)(l+1)}{(2l+1)(2l+3)}J_{l+5/2}\Bigg\} + 2S_1\sum_{l=1}^\infty i^l \xi^{l/2}P_l^1(\mu_1) \\ &\times\Bigg\{-\frac{3(l-1)}{(2l+1)(2l-1)}J_{l-3/2} + \frac{3}{(2l+3)(2l-1)}J_{l+1/2} \\ &+\frac{3(l+2)}{(2l+1)(2l+3)}J_{l+5/2}\Bigg\}\Bigg]. \end{aligned}\right\} \tag{37}$$

Returning to our original variables $\boldsymbol{\rho}$ and $\boldsymbol{\sigma}$ (cf. eq. [13]), it is apparent that we can express $D(\boldsymbol{\rho},\boldsymbol{\sigma})$ in the form

$$D(\boldsymbol{\rho},\boldsymbol{\sigma}) = -\sigma_3\sum_{l=0}^\infty A_l(|\boldsymbol{\rho}|;z_1)P_l(\mu) - \sigma_1\sum_{l=1}^\infty B_l(|\boldsymbol{\rho}|;z_1)P_l^1(\mu), \tag{38}$$

where

$$\left.\begin{aligned} A_l = i^l 2^{1/2}\pi^{3/2}(GM)^{3/2}N|\boldsymbol{\rho}|^{1/2}\int_0^\infty dz\,\xi^{l/2}\frac{\tilde{z}^{1/2}}{z^{3/2}}\Bigg[&-\frac{3l(l-1)}{(2l+1)(2l-1)}J_{l-3/2} \\ &+\frac{2l(l+1)}{(2l+3)(2l-1)}J_{l+1/2} - \frac{3(l+2)(l+1)}{(2l+1)(2l+3)}J_{l+5/2}\Bigg] \end{aligned}\right\} \tag{39}$$

and

$$B_l = i^l 2^{1/2}\pi^{3/2}(GM)^{3/2}N|\rho|^{1/2}\int_0^\infty d\,z\,\xi^{1/2}\frac{\tilde{z}^{1/2}}{z^{3/2}}\left[-\frac{3(l-1)}{(2l+1)(2l-1)}J_{l-3/2}\right.$$
$$\left.+\frac{3}{(2l+3)(2l-1)}J_{l+1/2}+\frac{3(l+2)}{(2l+1)(2l+3)}J_{l+5/2}\right]. \tag{40}$$

Further, in equation (38) we have suppressed the suffix "1" in μ_1, thus now letting μ denote the cosine of the angle between the directions of ρ and r_1.

4. *The expression for* $A(\rho, \sigma)$ *for* $|\sigma| \to 0$.—According to equation (4), $A(\rho, \sigma)$ is the six-dimensional Fourier transform of the distribution function $W(F_0, F_1)$. Consequently, for the purposes of this equation the vectors ρ and σ must be referred to a fixed

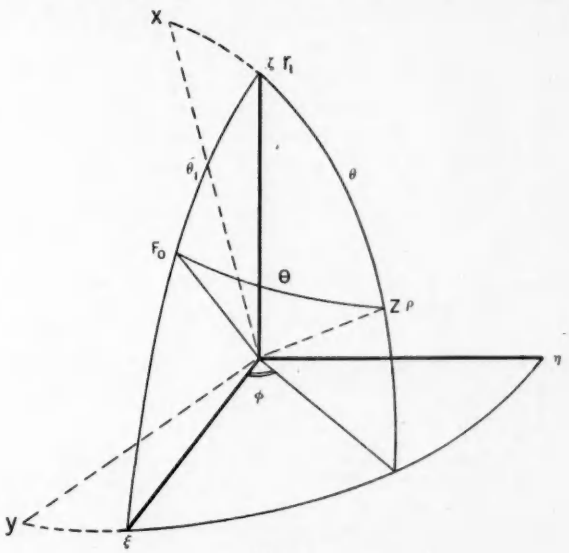

FIG. 1

system of co-ordinates. But in equation (38) for $D(\rho, \sigma)$ we have expressed $\sigma = (\sigma_1, \sigma_2, \sigma_3)$ in a variable system of co-ordinates depending on the direction of ρ. We shall now pass from this variable xyz-system to a fixed $\xi\eta\zeta$-system (see Fig. 1). This fixed $\xi\eta\zeta$-system is so chosen that the ζ-axis is in the direction of r_1 and the $\xi\zeta$-plane contains the vector F_0. Let ρ be along an arbitrary direction in this system of co-ordinates. The linear transformation which allows us to pass from the xyz- to the $\xi\eta\zeta$-system is clearly

$$\left.\begin{aligned}\sigma_1 &= -\sigma_\xi\cos\vartheta\cos\varphi-\sigma_\eta\cos\vartheta\sin\varphi+\sigma_\zeta\sin\vartheta\,,\\ \sigma_2 &= +\sigma_\xi\sin\varphi-\sigma_\eta\cos\varphi\,,\\ \sigma_3 &= +\sigma_\xi\sin\vartheta\cos\varphi+\sigma_\eta\sin\vartheta\sin\varphi+\sigma_\zeta\cos\vartheta\,.\end{aligned}\right\} \tag{41}$$

Thus, in this fixed system of co-ordinates $D(\rho, \sigma)$ has the form

$$\left.\begin{aligned}D(\rho,\sigma) = &-(\sigma_\xi\sin\vartheta\cos\varphi+\sigma_\eta\sin\vartheta\sin\varphi+\sigma_\zeta\cos\vartheta)\sum_{l=0}^{\infty}A_lP_l(\mu)\\ &+(\sigma_\xi\cos\vartheta\cos\varphi+\sigma_\eta\cos\vartheta\sin\varphi-\sigma_\zeta\sin\vartheta)\sum_{l=1}^{\infty}B_lP_l^1(\mu)\,.\end{aligned}\right\} \tag{42}$$

Finally, combining equations (6), (11), and (42), we obtain

$$A(\boldsymbol{\rho}, \boldsymbol{\sigma}) = e^{-a|\boldsymbol{\rho}|^{3/2}}\left[1+(\sigma_\xi \sin\vartheta\cos\varphi+\sigma_\eta\sin\vartheta\sin\varphi+\sigma_\zeta\cos\vartheta)\sum_{l=0}^{\infty}A_l P_l(\mu)\right.$$
$$\left. -(\sigma_\xi\cos\vartheta\cos\varphi+\sigma_\eta\cos\vartheta\sin\varphi-\sigma_\zeta\sin\vartheta)\sum_{l=1}^{\infty}B_l P_l^1(\mu)+O(|\boldsymbol{\sigma}|^2)\right], \tag{43}$$

where

$$a = {}_1^4{}_5\,(2\pi GM)^{3/2}N\,. \tag{44}$$

We can express (43) more simply in the form

$$A(\boldsymbol{\rho}, \boldsymbol{\sigma}) = e^{-a|\boldsymbol{\rho}|^{3/2}}[1 - D(\boldsymbol{\rho}, \boldsymbol{\sigma}) + O(|\boldsymbol{\sigma}|^2)]\,, \tag{45}$$

where $D(\boldsymbol{\rho}, \boldsymbol{\sigma})$ is defined as in equation (42).

5. *The first moments of* $\mathbf{F}_1$.—To determine the average values of $\boldsymbol{F}_1$ (for a given $\boldsymbol{F}_0$) in any specified direction, it would clearly be sufficient to evaluate the first moments of the components of $\boldsymbol{F}_1$ (namely, $F_{1,\xi}$, $F_{1,\eta}$, and $F_{1,\zeta}$) along the three principal directions of the $\xi\eta\zeta$-system as defined in § 4.

According to equation (4),

$$\int_{-\infty}^{+\infty} W(\boldsymbol{F}_0, \boldsymbol{F}_1)\, F_{1,\tau}\, dF_1 = \frac{1}{64\pi^6}\int_{-\infty}^{+\infty}\int_{-\infty}^{+\infty}\int_{-\infty}^{+\infty} e^{-i(\boldsymbol{\rho}\cdot\boldsymbol{F}_0+\boldsymbol{\sigma}\cdot\boldsymbol{F}_1)} A(\boldsymbol{\rho}, \boldsymbol{\sigma})\, F_{1,\tau}\, d\boldsymbol{\rho}\, d\boldsymbol{\sigma}\, dF_1\,, \tag{46}$$

where we have used τ to denote either of ξ, η, or ζ. From this equation we readily derive (cf. II, eqs. [73]–[76])

$$\int_{-\infty}^{+\infty} W(\boldsymbol{F}_0, \boldsymbol{F}_1)\, F_{1,\tau}\, dF_1 = -\frac{i}{8\pi^3}\int_{-\infty}^{+\infty} e^{-i\boldsymbol{\rho}\cdot\boldsymbol{F}_0}\left[\frac{\partial}{\partial\sigma_\tau}A(\boldsymbol{\rho}, \boldsymbol{\sigma})\right]_{|\boldsymbol{\sigma}|=0} d\boldsymbol{\rho}\,; \tag{47}$$

or, using equation (45) for $A(\boldsymbol{\rho}, \boldsymbol{\sigma})$, we have

$$\int_{-\infty}^{+\infty} W(\boldsymbol{F}_0, \boldsymbol{F}_1)\, F_{1,\tau}\, dF_1 = \frac{i}{8\pi^3}\int_{-\infty}^{+\infty} e^{-i\boldsymbol{\rho}\cdot\boldsymbol{F}_0-a|\boldsymbol{\rho}|^{3/2}}\frac{\partial D}{\partial\sigma_\tau}\, d\boldsymbol{\rho}\,, \tag{48}$$

since $D(\boldsymbol{\rho}, \boldsymbol{\sigma})$ is linear in $\boldsymbol{\sigma}$. On the other hand, the left-hand side of the foregoing equation defines $\overline{F}_{1,\tau}$, for

$$W(\boldsymbol{F}_0)\,\overline{F}_{1,\tau} = \int_{-\infty}^{+\infty} W(\boldsymbol{F}_0, \boldsymbol{F}_1)\, F_{1,\tau}\, dF_1\,. \tag{49}$$

Hence,

$$W(\boldsymbol{F}_0)\,\overline{F}_{1,\tau} = \frac{i}{8\pi^3}\int_{-\infty}^{+\infty} e^{-i\boldsymbol{\rho}\cdot\boldsymbol{F}_0-a|\boldsymbol{\rho}|^{3/2}}\frac{\partial D}{\partial\sigma_\tau}\, d\boldsymbol{\rho}\,; \tag{50}$$

or, using polar co-ordinates, we have

$$W(\boldsymbol{F}_0)\,\overline{F}_{1,\tau} = \frac{i}{8\pi^3}\int_0^{\infty}\int_{-1}^{+1}\int_0^{2\pi} e^{-i|\boldsymbol{\rho}||\boldsymbol{F}_0|\cos\Theta-a|\boldsymbol{\rho}|^{3/2}}\frac{\partial D}{\partial\sigma_\tau}|\boldsymbol{\rho}|^2 d|\boldsymbol{\rho}|\, d\mu\, d\varphi\,, \tag{51}$$

where Θ denotes the angle between the directions of $\boldsymbol{F}_0$ and $\boldsymbol{\rho}$. Putting (cf. I, eq. [134], and II, eq. [81])

$$|\boldsymbol{\rho}|\,|\boldsymbol{F}_0| = x\,; \qquad |\boldsymbol{F}_0| = a^{2/3}\beta = Q_H\beta \tag{52}$$

in equation (51), we obtain

$$W(\boldsymbol{F}_0)\,\overline{F}_{1,\tau} = \frac{i}{8\pi^3 a^2\beta^3}\int_0^\infty\int_{-1}^{+1}\int_0^{2\pi} e^{-ix\cos\Theta-(x/\beta)^{3/2}}\,\frac{\partial D}{\partial\sigma_\tau}\,x^2\,dx\,d\mu\,d\varphi\,. \tag{53}$$

Substituting for $W(\boldsymbol{F}_0)$ in the foregoing equation from I, equation (117), we obtain the general formula

$$\overline{F}_{1,\tau} = \frac{i}{2\pi^2\beta H(\beta)}\int_0^\infty\int_{-1}^{+1}\int_0^{2\pi} e^{-ix\cos\Theta-(x/\beta)^{3/2}}\,\frac{\partial D}{\partial\sigma_\tau}\,x^2\,dx\,d\mu\,d\varphi\,, \tag{54}$$

where it might be recalled that $H(\beta)$ is the "Holtsmark function,"

$$H(\beta) = \frac{2}{\pi\beta}\int_0^\infty e^{-(x/\beta)^{3/2}}x\,\sin x\,dx\,. \tag{55}$$

To carry out the integrations over μ and φ in equation (54), we first expand $\exp(-ix\cos\Theta)$ in spherical harmonics. We have (cf. eqs. [25] and [33])

$$\left.\begin{aligned} e^{-ix\cos\Theta} = \left(\frac{\pi}{2x}\right)^{1/2}\sum_{n=0}^\infty (2n+1)\,(-i)^n J_{n+1/2}(x)\Big\{&P_n(\mu)\,P_n(\mu_1) \\ &+2\sum_{m=1}^n\frac{(n-m)!}{(n+m)!}\,P_n^m(\mu)\,P_n^m(\mu_1)\cos m\varphi\Big\}\,, \end{aligned}\right\} \tag{56}$$

where

$$\mu_1 = \cos\vartheta_1\,; \qquad \vartheta_1 = \sphericalangle(\boldsymbol{F}_0, \boldsymbol{r}_1)\,. \tag{57}$$

Combining equations (54) and (56) and substituting for D from equation (42), we obtain

$$\left.\begin{aligned} \overline{F}_{1,\tau} = -\frac{i}{2\pi^2\beta H(\beta)}\left(\frac{\pi}{2}\right)^{1/2}&\int_0^\infty\int_{-1}^{+1}\int_0^{2\pi} dx\,d\mu\,d\varphi\,e^{-(x/\beta)^{3/2}}x^{3/2} \\ \times\Bigg[\sum_{n=0}^\infty (-i)^n(2n+1)\,J_{n+1/2}(x)\Big\{&P_n(\mu)\,P_n(\mu_1) \\ &+2\sum_{m=1}^n\frac{(n-m)!}{(n+m)!}\,P_n^m(\mu)\,P_n^m(\mu_1)\cos m\varphi\Big\}\Bigg] \\ \times\begin{cases} \left[\sin\vartheta\cos\varphi\sum_{l=0}^\infty A_l P_l(\mu) - \cos\vartheta\cos\varphi\sum_{l=1}^\infty B_l P_l^1(\mu)\right] & (\tau=\xi) \\ \left[\sin\vartheta\sin\varphi\sum_{l=0}^\infty A_l P_l(\mu) - \cos\vartheta\sin\varphi\sum_{l=1}^\infty B_l P_l^1(\mu)\right] & (\tau=\eta) \\ \left[\cos\vartheta\sum_{l=0}^\infty A_l P_l(\mu) + \sin\vartheta\sum_{l=1}^\infty B_l P_l^1(\mu)\right] & (\tau=\zeta) \end{cases}. \end{aligned}\right\} \tag{58}$$

The integration over φ can be carried out directly, and we are left with

$$\left.\begin{aligned}\bar{F}_{1,\xi} = -\frac{i}{\pi\beta H(\beta)}\left(\frac{\pi}{2}\right)^{1/2}\sum_{n=1}^{\infty}(-i)^n P_n^1(\mu_1)\int_0^{\infty}dx\, e^{-(x/\beta)^3/2}x^{3/2}J_{n+1/2}(x)\\ \times(2n+1)\frac{(n-1)!}{(n+1)!}\int_{-1}^{+1}d\mu P_n^1(\mu)\left\{\sum_{l=0}^{\infty}A_l(1-\mu^2)^{1/2}P_l(\mu)\right.\\ \left.-\sum_{l=1}^{\infty}B_l\mu P_l^1(\mu)\right\},\end{aligned}\right\} \tag{59}$$

$$\bar{F}_{1,\eta} = 0\,, \tag{60}$$

and

$$\left.\begin{aligned}\bar{F}_{1,\zeta} = -\frac{i}{\pi\beta H(\beta)}\left(\frac{\pi}{2}\right)^{1/2}\sum_{n=0}^{\infty}(-i)^n P_n(\mu_1)\int_0^{\infty}dx\, e^{-(x/\beta)^3/2}x^{3/2}J_{n+1/2}(x)\\ \times(2n+1)\int_{-1}^{+1}d\mu P_n(\mu)\left\{\sum_{l=0}^{\infty}A_l\mu P_l(\mu)+\sum_{l=1}^{\infty}B_l(1-\mu^2)^{1/2}P_l^1(\mu)\right\}.\end{aligned}\right\} \tag{61}$$

The result (60) is, of course, to be expected. Using the recursion formulae (35) and the orthogonality relations among the Legendre functions, we can readily effect the integrations over μ in equations (59) and (61). We find

$$\left.\begin{aligned}\bar{F}_{1,\xi} = -\frac{2i}{\pi\beta H(\beta)}\left(\frac{\pi}{2}\right)^{1/2}\sum_{n=1}^{\infty}(-i)^n P_n^1(\mu_1)\int_0^{\infty}e^{-(x/\beta)^3/2}x^{3/2}J_{n+1/2}(x)\\ \times\left[\frac{1}{2n-1}\{A_{n-1}-(n-1)B_{n-1}\}-\frac{1}{2n+3}\{A_{n+1}+(n+2)B_{n+1}\}\right]dx\end{aligned}\right\} \tag{62}$$

and

$$\left.\begin{aligned}\bar{F}_{1,\zeta} = -\frac{2i}{\pi\beta H(\beta)}\left(\frac{\pi}{2}\right)^{1/2}\sum_{n=0}^{\infty}(-i)^n P_n(\mu_1)\int_0^{\infty}e^{-(x/\beta)^3/2}x^{3/2}J_{n+1/2}(x)\\ \times\left[\frac{n}{2n-1}\{A_{n-1}-(n-1)B_{n-1}\}+\frac{n+1}{2n+3}\{A_{n+1}+(n+2)B_{n+1}\}\right]dx\,.\end{aligned}\right\} \tag{63}$$

It is seen that the foregoing expressions for $\bar{F}_{1,\xi}$ and $\bar{F}_{1,\zeta}$ can be written somewhat more compactly if we introduce the quantities

$$C_l = \frac{1}{2l+1}\{A_l - lB_l\} \quad\text{and}\quad D_l = \frac{1}{2l+1}\{A_l+(l+1)B_l\}\,. \tag{64}$$

Then

$$\left.\begin{aligned}\bar{F}_{1,\xi} = -\frac{2i}{\pi\beta H(\beta)}\left(\frac{\pi}{2}\right)^{1/2}\sum_{n=1}^{\infty}(-i)^n P_n^1(\mu)\int_0^{\infty}e^{-(x/\beta)^3/2}x^{3/2}J_{n+1/2}(x)\\ \times[C_{n-1}-D_{n+1}]\,dx\end{aligned}\right\} \tag{65}$$

and

$$\left.\begin{aligned}\bar{F}_{1,\zeta} = -\frac{2i}{\pi\beta H(\beta)}\left(\frac{\pi}{2}\right)^{1/2}\sum_{n=0}^{\infty}(-i)^n P_n(\mu)\int_0^{\infty}e^{-(x/\beta)^3/2}x^{3/2}J_{n+1/2}(x)\\ \times[nC_{n-1}+(n+1)D_{n+1}]\,dx\,,\end{aligned}\right\} \tag{66}$$

where we have further suppressed the suffix "1" in μ_1, thus letting μ denote the cosine of the angle between the directions of $\boldsymbol{r}_1$ and $\boldsymbol{F}_0$.

Using equations (39) and (40), we shall now obtain explicit formulae for C_l and D_l. First, we notice that the factor which occurs in front of the integrals on the right-hand sides of the equations (39) and (40) can be re-written as (cf. eqs. [44] and [52])

$$i^l \frac{15}{8}\left(\frac{x}{\beta}\right)^{1/2} Q_H . \tag{67}$$

Next, evaluating C_l and D_l as defined in equation (64), we find that

$$C_l = i^l \frac{15 Q_H}{8(2l+3)(2l+1)}\left(\frac{x}{\beta}\right)^{1/2}\int_0^\infty d z\, \xi^{l/2}\frac{\tilde{z}^{1/2}}{z^{3/2}}\left[l J_{l+1/2} - 3(l+2) J_{l+5/2}\right] \tag{68}$$

and

$$D_l = i^l \frac{15 Q_H}{8(2l-1)(2l+1)}\left(\frac{x}{\beta}\right)^{1/2}\int_0^\infty d z\, \xi^{l/2}\frac{\tilde{z}^{1/2}}{z^{3/2}}\left[-3(l-1) J_{l-3/2} + (l+1) J_{l+1/2}\right], \tag{69}$$

where it might be recalled that the range of integration over z has to be broken at z_1, according to the scheme (31) and (32). Thus, the "infinite" integrals occurring on the right-hand sides of the foregoing equations are really functions of z_1 and therefore also of $|\boldsymbol{\rho}|$ and $|\boldsymbol{r}_1|$, according to equation (29). In terms of our new variables x and β (eq. [52]), we can express z_1 as follows:

$$z_1 = \frac{GM\,|\boldsymbol{\rho}|\,|\boldsymbol{F}_0|}{|\boldsymbol{r}_1|^2 |\boldsymbol{F}_0|} = \frac{GM}{|\boldsymbol{r}_1|^2 Q_H}\frac{x}{\beta}; \tag{70}$$

or, alternatively,

$$z_1 = \frac{15^{2/3}}{4^{2/3} 2\pi N^{2/3} |\boldsymbol{r}_1|^2}\frac{x}{\beta}. \tag{71}$$

This suggests that we measure $|\boldsymbol{r}_1|$ in units of the distance

$$l = \frac{15^{1/3}}{4^{1/3}(2\pi)^{1/2}} N^{-1/3} = 0.619804 N^{-1/3}. \tag{72}$$[8]

If s denotes $|\boldsymbol{r}_1|$ measured in this unit, we clearly have

$$z_1 = \frac{x}{s^2\beta}. \tag{73}$$

Thus, the integrals occurring in the formulae for C_l and D_l are functions of x, s, and β only through the combination $x/s^2\beta$.

Equations (60), (65), (66), (68), and (69) together provide the complete formal solution to the problem of spatial correlations.

6. *The first moment of* $\mathbf{F}_1$ *in the direction of* $\mathbf{F}_0$ *and its average.*—A quantity of considerable interest is the average value of $\boldsymbol{F}_1$ in the direction of $\boldsymbol{F}_0$. Since (see Fig. 1)

$$F_{1,\,\boldsymbol{F}_0} = \cos\vartheta F_{1,\,\xi} + \sin\vartheta F_{1,\,\eta}, \tag{74}$$

we have

$$\overline{F}_{1,\,\boldsymbol{F}_0} = \mu\overline{F}_{1,\,\xi} + (1-\mu^2)^{1/2}\overline{F}_{1,\,\eta}. \tag{75}$$

[8] Since the average distance $\overline{D}$ between the stars is $0.55396 N^{-1/3}$ (cf. S. Chandrasekhar, *Rev. Mod. Phys.*, **15**, 1, 1943, eq. [676]), it follows that the unit of distance adopted is of the same order as $\overline{D}$.

Hence, according to equations (65) and (66),

$$\left.\begin{aligned}\bar{F}_{1,\,\mathbf{F}_0} = -\frac{2i}{\pi\beta H(\beta)}\left(\frac{\pi}{2}\right)^{1/2}\Bigg\{\sum_{n=1}^{\infty}(-i)^n P_1^1(\mu)\,P_n^1(\mu)\int_0^{\infty} e^{-(x/\beta)^{3/2}}x^{3/2}J_{n+1/2}(x)\\ \times[C_{n-1}-D_{n+1}]\,dx+\sum_{n=0}^{\infty}(-1)^n P_1(\mu)\,P_n(\mu)\int_0^{\infty}e^{-(x/\beta)^{3/2}}x^{3/2}J_{n+1/2}(x)\\ \times[nC_{n-1}+(n+1)\,D_{n+1}]\,dx\Bigg\}.\end{aligned}\right\}\quad(76)$$

Now, from the point of view of the applications of the theory, greatest interest is attached to $\bar{F}_{1,\,\mathbf{F}_0}$ only after it has been further averaged over all mutual orientations of the vectors $\mathbf{F}_0$ and $\mathbf{r}_1$.[9] When this additional averaging is performed, it is seen that the only two terms in the infinite series in equation (76) which survive are those with $n = 1$. We are thus left with

$$\bar{\bar{F}}_{1,\,\mathbf{F}_0} = -\frac{2}{\pi\beta H(\beta)}\left(\frac{\pi}{2}\right)^{1/2}\int_0^{\infty}e^{-(x/\beta)^{3/2}}x^{3/2}J_{3/2}(x)\,C_0\,dx\,. \quad(77)$$

On the other hand (cf. eq. [68]),

$$C_0 = -Q_H\,\frac{15}{4}\left(\frac{x}{\beta}\right)^{1/2}\int_0^{\infty}dz\,\frac{\tilde{z}^{1/2}}{z^{3/2}}J_{5/2}(z)\,. \quad(78)$$

Hence, combining equations (77) and (78), we obtain the relatively simple formula

$$\bar{\bar{F}}_{1,\,\mathbf{F}_0} = \frac{15Q_H}{2\pi\beta^{3/2}H(\beta)}\left(\frac{\pi}{2}\right)^{1/2}\int_0^{\infty}e^{-(x/\beta)^{3/2}}x^2J_{3/2}(x)\,\mathcal{Q}\left(\frac{x}{s^2\beta}\right)dx\,, \quad(79)$$

where we have used $\mathcal{Q}(y)$ to denote the function

$$\mathcal{Q}(y) = \int_0^{\infty}\frac{\tilde{z}^{1/2}}{z^{3/2}}J_{5/2}(z)\,dz\,. \quad(80)$$

Letting

$$\mathbf{F}_1 = Q_H\boldsymbol{\beta}_1 \text{ and } \mathbf{F}_0 = Q_H\boldsymbol{\beta}\,, \quad(81)$$

we can re-write equation (79) more conveniently in the form

$$\bar{\bar{\beta}}_{1,\,\boldsymbol{\beta}} = \frac{15}{2\pi\beta^{3/2}H(\beta)}\int_0^{\infty}e^{-(x/\beta)^{3/2}}x^{3/2}\left(\frac{\sin x}{x}-\cos x\right)\mathcal{Q}\left(\frac{x}{s^2\beta}\right)dx\,, \quad(82)$$

where we have further substituted explicitly for $J_{3/2}(x)$.

We now proceed to a closer discussion of the equations (80) and (82).

i) $\mathcal{Q}(y)$ *and its asymptotic behavior.*—According to the scheme (31) and (32), the equation defining $\mathcal{Q}(y)$ has explicitly the form

$$\mathcal{Q}(y) = \int_0^{y}\frac{1}{z}J_{5/2}(z)\,dz + y^{1/2}\int_y^{\infty}\frac{1}{z^{3/2}}J_{5/2}(z)\,dz\,. \quad(83)$$

[9] E.g., see the paper "On The Stability of Binary Systems" appearing later in this same issue of the *Astrophysical Journal* (p. 54).

Using the formula

$$\frac{d}{dz}(z^{-n}J_n) = -z^{-n}J_{n+1}, \tag{84}$$

well known in the theory of Bessel functions, we can directly evaluate the second of the two integrals occurring on the right-hand side of equation (83), while the first can be simplified by an integration by parts. The two integrated parts cancel each other, and we are left with

$$\mathcal{Q}(y) = \tfrac{1}{2}\int_0^y \frac{1}{z^2} J_{3/2}(z)\, dz\,; \tag{85}$$

or, using the formula for $J_{3/2}$, we have

$$\mathcal{Q}(y) = \frac{1}{(2\pi)^{1/2}}\int_0^y \frac{1}{z^{7/2}} (\sin z - z\cos z)\, dz\,. \tag{86}$$

After two further integrations by parts the foregoing equation can be reduced to the form

$$\mathcal{Q}(y) = \frac{4}{5(2\pi)^{1/2}}\int_0^y \frac{\cos z}{z^{1/2}}\, dz - \frac{1}{5}\left(\frac{2}{\pi}\right)^{1/2}\frac{1}{y^2}[(1+2y^2)\sin y - y\cos y]\,, \tag{87}$$

or, somewhat differently,

$$\mathcal{Q}(y) = \frac{1}{5}\left[4\mathcal{F}(y) - \frac{1}{y}J_{3/2}(y) - 2J_{1/2}(y)\right], \tag{88}$$

where we have used $\mathcal{F}(y)$ to denote the *Fresnel integral*,

$$\mathcal{F}(y) = \frac{1}{(2\pi)^{1/2}}\int_0^y \frac{\cos z}{z^{1/2}}\, dz = \frac{1}{2}\int_0^y J_{-1/2}(z)\, dz\,. \tag{89}$$

The form (88) for $\mathcal{Q}(y)$ is particularly convenient for the purposes of numerically evaluating the function.

From equation (88) and the known asymptotic expansions for the Fresnel integral[10] it can be readily shown that

$$\mathcal{Q}(y) = \frac{2}{5} - \frac{1}{(2\pi)^{1/2}}\frac{\sin y}{y^{5/2}} + O(y^{-7/2}) \qquad (y\to\infty) \tag{90}$$

and

$$\mathcal{Q}(y) = \frac{1}{3}\left(\frac{2}{\pi}\right)^{1/2} y^{1/2} + O(y^{5/2}) \qquad (y\to 0)\,. \tag{91}$$

ii) *The asymptotic behavior of* $\bar{\bar{\beta}}_{1,\,\beta}$ *for* $s\to 0$ *and* $s\to\infty$.—It is of interest to consider the asymptotic behavior of $\bar{\bar{\beta}}_{1,\,\beta}$. First, considering the behavior for $s\to 0$, we have, according to equations (82) and (90),

$$\bar{\bar{\beta}}_{1,\,\beta} \to \frac{3}{\pi\beta^{3/2}H(\beta)}\int_0^\infty e^{-(x/\beta)^{1/2}} x^{3/2}\left(\frac{\sin x}{x} - \cos x\right) dx\,. \tag{92}$$

[10] Cf. G. N. Watson, *Theory of Bessel Functions*, p. 545, Cambridge, England, 1922.

The integral occurring on the right-hand side of this equation can be expressed simply in terms of the Holtsmark function. For, writing it in the form

$$-\tfrac{2}{3}\beta^{3/2}\int_0^\infty \frac{d}{dx}[e^{-(x/\beta)^{3/2}}]\,(\sin x - x\cos x)\,dx \tag{93}$$

and integrating by parts, we have

$$\left.\begin{aligned}\int_0^\infty e^{-(x/\beta)^{3/2}}x^{1/2}(\sin x - x\cos x)\,dx &= \tfrac{2}{3}\beta^{3/2}\int_0^\infty e^{-(x/\beta)^{3/2}}x\sin x\,dx\\ &= \frac{\pi}{3}\beta^{5/2}H(\beta)\,.\end{aligned}\right\} \tag{94}$$

Hence,

$$\bar{\bar{\beta}}_{1,\,\mathbf{B}}\to\beta \quad \text{as} \quad s\to 0\,, \tag{95}$$

a result which is to be expected. On the other hand, according to equations (82) and (91), we have for $s\to\infty$

$$\bar{\bar{\beta}}_{1,\,\mathbf{B}}\to\frac{5}{2\pi\beta^2 H(\beta)}\left(\frac{2}{\pi}\right)^{1/2}\frac{1}{s}\int_0^\infty e^{-(x/\beta)^{3/2}}x\,(\sin x - x\cos x)\,dx \qquad (s\to\infty)\,. \tag{96}$$

In other words,

$$\bar{\bar{\beta}}_{1,\,\mathbf{B}}\propto s^{-1} \quad \text{for} \quad s\to\infty\,, \tag{97}$$

the constant of proportionality depending, however, on β; this behavior for $S\to\infty$ has important consequences for the applications of the theory.[11]

7. *The average value of* $\mathbf{F}_1$, $\mathbf{F}_0$ *for all* $\mathbf{F}_0$ *and the correlation in the forces acting simultaneously at two different points.*—In the preceding section we have evaluated the average value of $\bar{F}_{1,\,\mathbf{F}_0}$ for all mutual directions between $\boldsymbol{F}_0$ and $\boldsymbol{r}_1$. The result of this averaging was to yield a function $\bar{\bar{F}}_{1,\,\mathbf{F}_0}$ of the two variables $|\boldsymbol{F}_0|$ and $|\boldsymbol{r}_1|$. If we now average $\bar{\bar{F}}_{1,\,\mathbf{F}_0}$ still further over all initial values of $|\boldsymbol{F}_0|$ (with the appropriate weight function $W(|\boldsymbol{F}_0|)$), we shall obtain a function of $|\boldsymbol{r}_1|$ only which will describe the correlation in the forces acting simultaneously at points separated by a distance $|\boldsymbol{r}_1|$. For,

$$\bar{\bar{\bar{F}}}_{1,\,\mathbf{F}_0}=\int_0^\infty \bar{\bar{F}}_{1,\,\mathbf{F}_0}\,W(|\boldsymbol{F}_0|)\,d|\boldsymbol{F}_0|\,; \tag{98}$$

and this is clearly the same as

$$\bar{\bar{\bar{F}}}_{1,\,\mathbf{F}_0}=\int_{-\infty}^{+\infty}\int_{-\infty}^{+\infty}\boldsymbol{F}_1\cdot\mathbf{1}_{\boldsymbol{F}_0}\,W(\boldsymbol{F}_0,\boldsymbol{F}_1)\,d\boldsymbol{F}_0 d\boldsymbol{F}_1\,, \tag{99}$$

where we have used $\mathbf{1}_{\boldsymbol{F}_0}$ to denote a unit vector in the direction of $\boldsymbol{F}_0$.

Since the distribution of $|\boldsymbol{F}_0|$ is directly governed by the Holtsmark function $H(\beta)$ (cf. I, eq. [115]), we have

$$\bar{\bar{\bar{\beta}}}_{\mathbf{B}}(s)=\frac{\bar{\bar{\bar{F}}}_1}{Q_H}=\int_0^\infty \bar{\bar{\beta}}_{1,\,\mathbf{B}}H(\beta)\,d\beta\,, \tag{100}$$

[11] See IV, p. 52.

where it might be recalled that s measures $|r_1|$ in units of the distance l introduced in equation (72). Substituting for $\bar{\bar{\beta}}_{1,\,\mathfrak{B}}$ from equation (82), we can write

$$\bar{\bar{\beta}}_{\mathfrak{B}}(s) = \int_0^\infty I(\beta)\, d\beta\,, \tag{101}$$

where

$$I(\beta) = \frac{15}{2\pi\beta^{3/2}} \int_0^\infty e^{-(x/\beta)^2/2} x^{3/2} \left(\frac{\sin x}{x} - \cos x\right) \mathfrak{Q}\left(\frac{x}{s^2\beta}\right) dx\,. \tag{102}$$

Putting $x = \beta y$ in equation (102), we can express $I(\beta)$ alternatively in the form

$$I(\beta) = \int_0^\infty \Phi(y) \left(\frac{\sin \beta y}{y} - \beta \cos \beta y\right) dy\,, \tag{103}$$

where, for the sake of brevity, we have written

$$\Phi(y) = \frac{15}{2\pi} e^{-y^2/2} y^{3/2} \mathfrak{Q}\left(\frac{y}{s^2}\right). \tag{104}$$

Integrating by parts the term in $\cos \beta y$ in equation (103), we find

$$I(\beta) = \int_0^\infty \Phi(y)\, \frac{\sin \beta y}{y}\, dy + \int_0^\infty \Phi'(y) \sin \beta y\, dy\,, \tag{105}$$

where Φ' denotes the derivative of Φ.

Now, multiplying both sides of equation (105) by $\sin \beta z/\beta z$ (where z is some positive constant) and integrating over β from 0 to ∞, we obtain

$$\left.\begin{aligned} \int_0^\infty I(\beta) \frac{\sin \beta z}{\beta z}\, d\beta = \int_0^\infty \int_0^\infty \Phi(y) \frac{\sin \beta y \sin \beta z}{\beta y z}\, d\beta\, dy \\ + \int_0^\infty \int_0^\infty \Phi'(y) \frac{\sin \beta y \sin \beta z}{\beta z}\, d\beta\, dy\,. \end{aligned}\right\} \tag{106}$$

Since

$$\int_0^\infty \frac{\sin \beta y \sin \beta z}{\beta}\, d\beta = \tfrac{1}{4} \log \left(\frac{y+z}{y-z}\right)^2, \tag{107}$$

equation (106) reduces to

$$\left.\begin{aligned} \int_0^\infty I(\beta) \frac{\sin \beta z}{\beta z}\, d\beta = \int_0^\infty \Phi(y) \frac{1}{4yz} \log \left(\frac{y+z}{y-z}\right)^2 dy \\ + \int_0^\infty \Phi'(y) \frac{1}{4z} \log \left(\frac{y+z}{y-z}\right)^2 dy\,, \end{aligned}\right\} \tag{108}$$

a formula which is valid for all positive z. Passing now to the limit $z = 0$, we obtain

$$\int_0^\infty I(\beta)\, d\beta = \int_0^\infty \Phi(y) \frac{dy}{y^2} + \int_0^\infty \Phi'(y) \frac{dy}{y}\,. \tag{109}$$

Integrating by parts the second of the two integrals occurring on the right-hand side, we find that

$$\int_0^\infty I(\beta)\,d\beta = 2\int_0^\infty \Phi(y)\frac{dy}{y^2}. \tag{110}$$

According to equations (101), (104), and (110), we therefore have

$$\bar{\bar{\beta}}_{\mathbf{B}}(s) = \frac{15}{\pi}\int_0^\infty e^{-y^{3/2}}\mathcal{Q}\left(\frac{y}{s^2}\right)\frac{dy}{y^{1/2}}. \tag{111}$$

We shall find that the function $\bar{\bar{\beta}}_{\mathbf{B}}(s)$ plays an important role in the applications of the theory. We shall therefore discuss the integral defining this function somewhat closely.

First, we shall derive a useful alternative form of equation (111). Writing $y = xs^2$ in this equation and substituting for $\mathcal{Q}(x)$ according to equation (85), we find that $\bar{\bar{\beta}}_{\mathbf{B}}(s)$ can be expressed as a double integral in the form

$$\bar{\bar{\beta}}_{\mathbf{B}}(s) = \frac{15}{2\pi}\,s\int_0^\infty \frac{dx}{x^{1/2}}\,e^{-x^3/2s^3}\int_0^x \frac{dz}{z^2}\,J_{3/2}(z)\,, \tag{112}$$

or, inverting the order of the integration,

$$\bar{\bar{\beta}}_{\mathbf{B}}(s) = \frac{15}{2\pi}\,s\int_0^\infty \frac{dz}{z^2}\,J_{3/2}(z)\int_z^\infty \frac{dx}{x^{1/2}}\,e^{-x^3/2s^3}. \tag{113}$$

Putting

$$t = x^{3/2}s^3\,, \tag{114}$$

equation (113) becomes

$$\bar{\bar{\beta}}_{\mathbf{B}}(s) = \frac{5}{\pi}\int_0^\infty \frac{dz}{z^2}\,J_{3/2}(z)\int_{s^3z^{3/2}}^\infty dt\,t^{-2/3}e^{-t}\,, \tag{115}$$

which is the form required. Since the incomplete Γ-function is defined by

$$\Gamma_x(p+1) = \int_0^x e^{-t}t^p dt\,, \tag{116}$$

we can re-write equation (115) alternatively in the form

$$\bar{\bar{\beta}}_{\mathbf{B}}(s) = \frac{5}{\pi}\int_0^\infty \frac{dz}{z^2}\,J_{3/2}(z)\,[\Gamma(\tfrac{1}{3}) - \Gamma_{s^3z^{3/2}}(\tfrac{1}{3})]\,. \tag{117}$$

i) *The asymptotic expansion for* $\bar{\bar{\beta}}_{\mathbf{B}}(s)$ *for* $s \to 0$.—The behavior of $\bar{\bar{\beta}}_{\mathbf{B}}(s)$ for $s \to 0$ can be derived from equation (117) by using an appropriate expansion for the incomplete Γ-function which occurs under the integral sign in this equation. Thus, since

$$\left.\begin{aligned}\Gamma_{s^3z^{3/2}}(\tfrac{1}{3}) &= \int_0^{s^3z^{3/2}} e^{-t}t^{-2/3}dt\\ &= \int_0^{s^3z^{3/2}}\left(1 - t + \frac{t^2}{2!} - \ldots.\right)t^{-2/3}dt\\ &= 3\,s\,z^{1/2} - \tfrac{3}{4}s^4z^2 + O(s^7)\,,\end{aligned}\right\} \tag{118}$$

we have

$$\bar{\bar{\beta}}_{\mathfrak{B}}(s) = \frac{5}{\pi}\int_0^\infty \frac{dz}{z^2} J_{3/2}(z)\,[\Gamma(\tfrac{1}{3}) - 3sz^{1/2} + \tfrac{3}{4}s^4z^2 + \ldots.] \quad (s\to 0)\,. \quad (119)$$

Substituting explicitly for $J_{3/2}$ in the foregoing equation, we obtain

$$\bar{\bar{\beta}}_{\mathfrak{B}}(s) = \frac{5}{\pi}\left(\frac{2}{\pi}\right)^{1/2}\int_0^\infty \frac{dz}{z^{7/2}}(\sin z - z\cos z)\,[\Gamma(\tfrac{1}{3}) - 3sz^{1/2} + \tfrac{3}{4}s^4z^2 + \ldots.]\,. \quad (120)$$

Now the integrals

$$\int_0^\infty \frac{dz}{z^j}\,(\sin z - z\cos z) \quad (121)$$

for $j = 7/2$, 3, and $3/2$ are readily expressible in terms of known integrals and have respectively the values

$$\frac{4}{5}\left(\frac{\pi}{2}\right)^{1/2}, \quad \frac{\pi}{4}, \quad \text{and} \quad \left(\frac{\pi}{2}\right)^{1/2} \qquad (j = \tfrac{7}{2},\ 3,\ \tfrac{3}{2})\,. \quad (122)$$

Accordingly, equation (120) leads to the following asymptotic expansion for $\bar{\bar{\beta}}_{\mathfrak{B}}(s)$ valid for $s \to 0$:

$$\bar{\bar{\beta}}_{\mathfrak{B}}(s) = \frac{4}{\pi}\Gamma(\tfrac{1}{3}) - \frac{15}{4}\left(\frac{2}{\pi}\right)^{1/2}s + \frac{15}{4\pi}s^4 + \ldots.. \quad (123)$$

Numerically, this series has the form

$$\bar{\bar{\beta}}_{\mathfrak{B}}(s) = 3.41093 - 2.992067\,s + 1.193662\,s^4 + \ldots.. \quad (124)$$

According to equation (123),

$$\bar{\bar{\beta}}_{\mathfrak{B}}(0) = \frac{4}{\pi}\Gamma(\tfrac{1}{3})\,. \quad (125)$$

On the other hand, it is clear that, as $s \to 0$, $\bar{\bar{\beta}}_{\mathfrak{B}}(s)$ must simply tend to the first moment of the Holtsmark function (cf. eqs. [95] and [100]). We have thus incidentally proved that

$$\int_0^\infty \beta H(\beta)\,d\beta = \frac{4}{\pi}\Gamma(\tfrac{1}{3})\,. \quad (126)^{12}$$

[12] It is perhaps of interest to establish equation (126) directly. We have (cf. eq. [55])

$$\beta H(\beta) = \frac{2}{\pi}\int_0^\infty e^{-(x/\beta)^{3/2}}x\sin x\,dx\,. \quad (1')$$

Putting $x = \beta y$ in the right-hand side of this equation, we can write

$$\beta H(\beta) = \beta^2\int_0^\infty \Phi(y)\sin\beta y\,dy\,, \quad (2')$$

where

$$\Phi(y) = \frac{2}{\pi}e^{-y^{3/2}}y\,. \quad (3')$$

Integrating equation (2') twice successively by parts, we obtain

$$\beta H(\beta) = -\int_0^\infty \Phi''(y)\sin\beta y\,dy\,. \quad (4')$$

[Footnote continued on following page]

ii) *A series expansion for* $\bar{\bar{\beta}}_{\mathbf{B}}(s)$ *for* $s \to \infty$.—A rapidly converging series for $\bar{\bar{\beta}}_{\mathbf{B}}(s)$ for $s \to \infty$ can be obtained in the following manner:

Differentiating equation (115) with respect to s, we find that

$$-\frac{d\bar{\bar{\beta}}_{\mathbf{B}}(s)}{ds} = \frac{15}{\pi}\int_0^\infty \frac{dz}{z^{3/2}} J_{3/2}(z)\, e^{-s^3 z^{3/2}}; \tag{127}$$

or, substituting for $J_{3/2}$, we have

$$-\frac{d\bar{\bar{\beta}}_{\mathbf{B}}(s)}{ds} = \frac{15}{\pi}\left(\frac{2}{\pi}\right)^{1/2}\int_0^\infty e^{-s^3 z^{3/2}} \frac{1}{z^3}(\sin z - z\cos z)\, dz\,. \tag{128}$$

Replacing sin z and cos z in the foregoing equation by their respective series expansions and inverting the order of the integration and the summation, we obtain

$$-\frac{d\bar{\bar{\beta}}_{\mathbf{B}}(s)}{ds} = \frac{15}{\pi}\left(\frac{2}{\pi}\right)^{1/2}\sum_{n=1}^{\infty}(-)^{n+1}\frac{2n}{(2n+1)!}\int_0^\infty e^{-s^3 z^{3/2}} z^{2n-2} dz\,. \tag{129}$$

If we now introduce the variable $t = s^3 z^{3/2}$, equation (129) becomes

$$-\frac{d\bar{\bar{\beta}}_{\mathbf{B}}(s)}{ds} = \frac{10}{\pi}\left(\frac{2}{\pi}\right)^{1/2}\sum_{n=1}^{\infty}(-)^{n+1}\frac{2n}{(2n+1)!}\frac{1}{s^{4n-2}}\int_0^\infty e^{-t} t^{(4n-5)/3} dt\,. \tag{130}$$

Hence,

$$-\frac{d\bar{\bar{\beta}}_{\mathbf{B}}(s)}{ds} = \frac{10}{\pi}\left(\frac{2}{\pi}\right)^{1/2}\sum_{n=1}^{\infty}(-)^{n+1}\frac{2n}{(2n+1)!}\Gamma\left(\frac{4n-2}{3}\right)\frac{1}{s^{4n-2}}. \tag{131}$$

Now multiplying both sides of equation (4′) by $\sin \beta z/\beta z$ (where z is some positive constant) and integrating over β from 0 to ∞, we find that

$$\int_0^\infty \beta H(\beta)\frac{\sin \beta z}{\beta z} d\beta = -\int_0^\infty \Phi'' \frac{1}{4z}\log\left(\frac{y+z}{y-z}\right)^2 dy\,. \tag{5′}$$

Passing now to the limit $z = 0$, we obtain

$$\int_0^\infty \beta H(\beta) d\beta = -\int_0^\infty \Phi''(y)\frac{dy}{y}\,. \tag{6′}$$

But, according to our definition of $\Phi(y)$ (eq. [3′]),

$$\Phi''(y) = -\frac{3}{2\pi}(5y^{1/2} - 3y^2)e^{-y^2/2}\,. \tag{7′}$$

Thus,

$$\int_0^\infty \beta H(\beta) d\beta = \frac{3}{2\pi}\int_0^\infty (5y^{1/2} - 3y^2)e^{-y^2/2}\frac{dy}{y}\,. \tag{8′}$$

The integrals which occur on the right-hand side of this equation can be reduced to Γ-function integrals by the substitution $t = y^2/2$. In this manner we find that

$$\left.\begin{aligned}\int_0^\infty \beta H(\beta) d\beta &= \frac{1}{\pi}\int_0^\infty (5t^{1/2} - 3t^{1/3})e^{-t}\frac{dt}{t}\\ &= \frac{1}{\pi}[5\Gamma(1/3) - 3\Gamma(4/3)]\\ &= \frac{4}{\pi}\Gamma(1/3)\,,\end{aligned}\right\} \tag{9′}$$

which is the required result.

Integrating this series, term by term, and remembering that $\overline{\overline{\beta}}_{\mathbf{B}}(s)$ must tend to 0 as $s \to \infty$, we obtain the following expansion for $\overline{\overline{\beta}}_{\mathbf{B}}(s)$:

$$\overline{\overline{\beta}}_{\mathbf{B}}(s) = \frac{10}{\pi}\left(\frac{2}{\pi}\right)^{1/2}\sum_{n=1}^{\infty}(-)^{n+1}\frac{2n}{(4n-3)\,(2n+1)\,!}\,\Gamma\left(\frac{4n-2}{3}\right)\frac{1}{s^{4n-3}}. \quad (132)$$

The dominant term of this series is

$$\overline{\overline{\beta}}_{\mathbf{B}}(s) = \frac{10}{3\pi}\left(\frac{2}{\pi}\right)^{1/2}\Gamma\left(\frac{2}{3}\right)\frac{1}{s}+O(s^{-5}) \qquad (s\to\infty), \quad (133)$$

or, numerically,

$$\overline{\overline{\beta}}_{\mathbf{B}}(s) \to \frac{1.14637}{s} \qquad (s\to\infty). \quad (134)$$

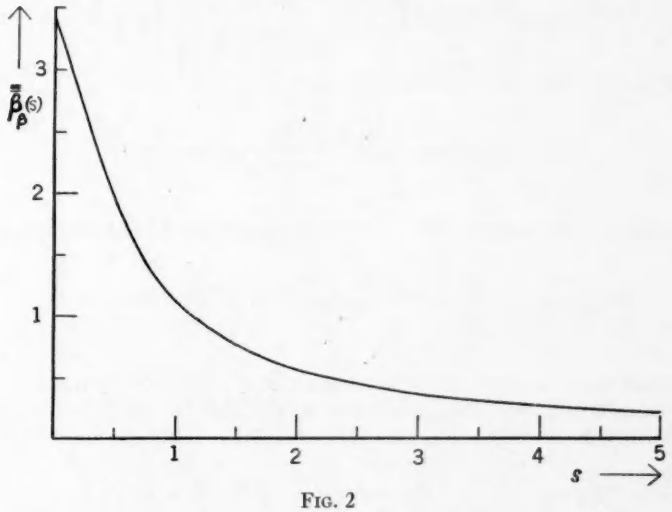

FIG. 2

This behavior of $\overline{\overline{\beta}}_{\mathbf{B}}(s)$ for $s \to \infty$ is, of course, to be expected on the basis of our earlier result (97).

In a later paper we shall undertake a full numerical discussion of the various formulae obtained in this paper: but in the meantime we may refer to Figure 2, in which the run of the function $\overline{\overline{\beta}}_{\mathbf{B}}(s)$ is illustrated.

8. *The average value of* $\mathbf{F}_1$ *in the direction of* $\mathbf{r}_1$.—In §§ 6 and 7 we have considered in some detail the various functions which arise from a discussion of the first moment of $\boldsymbol{F}_1$ in the direction of $\boldsymbol{F}_0$. We shall now consider certain other functions of comparable interest which result from a similar discussion of the first moment of $\boldsymbol{F}_1$ in the direction of $\boldsymbol{r}_1$. Since the ζ-axis of our co-ordinate system is in the direction of $\boldsymbol{r}_1$ (see Fig. 1), we have (cf. eq. [66])

$$\overline{F}_{1,\,r_1} = -\frac{2i}{\pi\beta H(\beta)}\left(\frac{\pi}{2}\right)^{1/2}\sum_{n=0}^{\infty}(-i)^n P_n(\mu)\int_0^{\infty} e^{-(x/\beta)^{1/2}}x^{3/2}J_{n+1/2}(x) \times [nC_{n-1}+(n+1)\,D_{n+1}]\,dx\,. \quad (135)$$

As in the case of $\overline{F}_{1,\,\boldsymbol{F}_0}$, greatest interest is attached to the foregoing equation only after it has been further averaged over all directions of $\boldsymbol{F}_0$ (keeping $\boldsymbol{r}_1$ and $|\boldsymbol{F}_0|$, how-

ever, fixed). When this further averaging process is carried out, it is seen that the only term in equation (135) which survives is that with $n = 0$, and we are left with

$$\bar{\bar{F}}_{1,\,r_1} = -\frac{2i}{\pi\beta H(\beta)}\left(\frac{\pi}{2}\right)^{1/2}\int_0^\infty e^{-(x/\beta)^{3/2}} x^{3/2} J_{1/2}(x)\, D_1 dx\,, \tag{136}$$

where, according to equation (69),

$$D_1 = iQ_H\,\frac{5}{4}\left(\frac{x}{\beta}\right)^{1/2}\int_0^\infty dz\,\xi^{1/2}\,\frac{\tilde{z}^{1/2}}{z^{3/2}}\,J_{3/2}(z)\,. \tag{137}$$

Combining equations (136) and (137) and expressing $\bar{\bar{F}}_{1,\,r_1}$ in units of Q_H, we have

$$\bar{\bar{\beta}}_{1,\,s} = \frac{5}{2\pi\beta^{3/2}H(\beta)}\int_0^\infty e^{-(x/\beta)^{3/2}} x^{3/2}\sin x\,\mathcal{R}\left(\frac{x}{s^2\beta}\right)dx\,, \tag{138}$$

where, for the sake of brevity, we have written

$$\mathcal{R}(y) = \int_0^\infty dz\,\xi^{1/2}\,\frac{\tilde{z}^{1/2}}{z^{3/2}}\,J_{3/2}(z)\,. \tag{139}$$

Now, according to the scheme (31) and (32), equation (139) has explicitly the form

$$\mathcal{R}(y) = \frac{1}{y^{1/2}}\int_0^y \frac{1}{z^{1/2}}\,J_{3/2}(z)\,dz + y\int_y^\infty \frac{1}{z^2}\,J_{3/2}(z)\,dz\,. \tag{140}$$

It is seen that, of the two integrals which occur in the foregoing equation, the first can be directly evaluated (cf. eq. [84]), while the second can be related quite simply to the function $\mathcal{Q}(y)$ introduced in § 6 (cf. eqs. [85] and [90]). Thus,

$$\mathcal{R}(y) = \left(\frac{2}{\pi y}\right)^{1/2} - \frac{1}{y}\,J_{1/2}(y) + 2y\left[\tfrac{2}{5} - \mathcal{Q}(y)\right]; \tag{141}$$

or, substituting for $\mathcal{Q}(y)$ from equation (88), we have

$$\mathcal{R}(y) = \left(\frac{2}{\pi y}\right)^{1/2} + \tfrac{2}{5}J_{3/2}(y) + \left(\tfrac{4}{5}y - \frac{1}{y}\right)J_{1/2}(y) + \tfrac{8}{5}y\left[\tfrac{1}{2} - \mathcal{F}(y)\right], \tag{142}$$

or, more explicitly,

$$\mathcal{R}(y) = \left(\frac{2}{\pi y}\right)^{1/2}\left[1 - \frac{3}{5}\,\frac{\sin y}{y} - \tfrac{2}{5}\cos y + \tfrac{4}{5}y\sin y\right] + \tfrac{8}{5}y\left[\tfrac{1}{2} - \mathcal{F}(y)\right]. \tag{143}$$

From equation (143) the behavior of $\mathcal{R}(y)$ for $y \to 0$ and $y \to \infty$ can be readily deduced. We find that

$$\mathcal{R}(y) = \tfrac{4}{5}y + O(y^{3/2}) \qquad (y \to 0) \tag{144}$$

and

$$\mathcal{R}(y) = \left(\frac{2}{\pi}\right)^{1/2} y^{-1/2} + O(y^{-5/2}) \qquad (y \to \infty)\,. \tag{145}$$

The asymptotic relations (144) and (145) for $\mathcal{R}(y)$ enables us to derive the behavior of $\bar{\bar{\beta}}_{1,\,s}$ for $s \to 0$ and $s \to \infty$. Thus, according to equations (138) and (145),

$$\bar{\bar{\beta}}_{1,\,s} \to \frac{5}{2\pi\beta H(\beta)} \left(\frac{2}{\pi}\right)^{1/2} s \int_0^\infty e^{-(x/\beta)^{3/2}} x \sin x\,dx \quad (s \to 0), \tag{146}$$

or, remembering our definition of $H(\beta)$,

$$\bar{\bar{\beta}}_{1,\,s} \to \frac{5}{4} \left(\frac{2}{\pi}\right)^{1/2} s \qquad (s \to 0). \tag{147}$$

In other words, for short separations between two points, there is, on the average, a repulsive force (proportional to the distance) operating on one relative to the other. On the other hand, for $s \to \infty$, we have (cf. eqs. [138] and [144])

$$\bar{\bar{\beta}}_{1,\,s} \to \frac{2}{\pi\beta^{5/2} H(\beta)} \frac{1}{s^2} \int_0^\infty e^{-(x/\beta)^{3/2}} x^{5/2} \sin x\,dx \quad (s \to \infty). \tag{148}$$

Since, however,

$$\frac{d}{d\beta}[\beta H(\beta)] = \frac{3}{\pi\beta^{5/2}} \int_0^\infty e^{-(x/\beta)^{3/2}} x^{5/2} \sin x\,dx, \tag{149}$$

we can re-write equation (148) in the form

$$\bar{\bar{\beta}}_{1,\,s} \to \frac{2}{3s^2} \frac{1}{H(\beta)} \frac{d}{d\beta}[\beta H(\beta)] \qquad (s \to \infty), \tag{150}$$

or, somewhat differently,

$$\bar{\bar{\beta}}_{1,\,s} \to \frac{2}{3s^2} \left(1 + \beta \frac{d \log H}{d\beta}\right) \qquad (s \to \infty). \tag{151}$$

According to this equation,

$$\bar{\bar{\beta}}_{1,\,s} \to \frac{2}{s^2} \quad (\beta \to 0) \quad \text{and} \quad \bar{\bar{\beta}}_{1,\,s} \to -\frac{1}{s^2} \quad (\beta \to \infty). \tag{152}$$

In other words, for large s, the sign of $\bar{\bar{\beta}}_{1,\,s}$ depends on the magnitude of β. In this respect $\bar{\bar{\beta}}_{1,\,s}$ differs from $\bar{\bar{\beta}}_{1,\,\mathfrak{B}}$, which is always positive and is, moreover, a monotonic decreasing function of β. An even more fundamental difference in the character of the functions $\bar{\bar{\beta}}_{1,\,s}$ and $\bar{\bar{\beta}}_{1,\,\mathfrak{B}}$ is revealed when we average $\bar{\bar{\beta}}_{1,\,s}$ over all β to obtain a quantity similar to $\bar{\bar{\beta}}_{\mathfrak{B}}(s)$ considered in § 7; for, as we shall now show,

$$\int_0^\infty \bar{\bar{\beta}}_{1,\,s} H(\beta)\,d\beta \equiv 0. \tag{153}$$

To prove this, write $x = \beta y$ in equation (138) and express $\bar{\bar{\beta}}_{1,\,s} H(\beta)$ in the form

$$\bar{\bar{\beta}}_{1,\,s} H(\beta) = \beta \int_0^\infty \Phi(y) \sin \beta y\,dy, \tag{154}$$

where

$$\Phi(y) = \frac{5}{2\pi} e^{-y^{3/2}} y^{3/2} \mathcal{R}\left(\frac{y}{s^2}\right). \tag{155}$$

Integrating equation (154) by parts, we have

$$\overline{\overline{\beta}}_1, {}_sH(\beta) = \int_0^\infty \Phi'(y) \cos \beta y \, dy \,. \tag{156}$$

Multiplying both sides of this equation by $\sin \beta z / \beta z$ (where z is some positive constant) and integrating over β from 0 to ∞, we obtain

$$\int_0^\infty \overline{\overline{\beta}}_1, {}_sH(\beta) \frac{\sin \beta z}{\beta z} \, d\beta = \int_0^\infty \int_0^\infty \Phi'(y) \frac{\cos \beta y \sin \beta z}{\beta z} \, d\beta dy \,. \tag{157}$$

On the other hand, since

$$\left.\begin{aligned} \int_0^\infty \frac{\cos \beta y \sin \beta z}{\beta} \, d\beta &= \frac{\pi}{2} \quad \text{if} \quad z > y \\ &= 0 \quad \text{if} \quad z < y \,, \end{aligned}\right\} \tag{158}$$

equation (157) becomes

$$\left.\begin{aligned} \int_0^\infty \overline{\overline{\beta}}_1, {}_sH(\beta) \frac{\sin \beta z}{\beta z} \, d\beta &= \frac{\pi}{2z} \int_0^z \Phi'(y) \, dy \\ &= \frac{\pi}{2} \frac{\Phi(z)}{z} \,, \end{aligned}\right\} \tag{159}$$

a formula which is valid for any positive finite z. Passing now to the limit $z = 0$, we find

$$\int_0^\infty \overline{\overline{\beta}}_1, {}_sH(\beta) \, d\beta = \frac{\pi}{2} \operatorname*{limit}_{z \to 0} \left[\frac{\Phi(z)}{z}\right]. \tag{160}$$

According to our definition of Φ (eq. [155]), the quantity on the right-hand side vanishes. Hence,

$$\overline{\overline{\beta}}_1, {}_s \equiv 0 \,, \tag{161}$$

which was the result to be proved.

THE STATISTICS OF THE GRAVITATIONAL FIELD ARISING FROM A RANDOM DISTRIBUTION OF STARS

IV. THE STOCHASTIC VARIATION OF THE FORCE ACTING ON A STAR

S. CHANDRASEKHAR
Yerkes Observatory
Received October 9, 1943

ABSTRACT

In this paper the theory of the stochastic variation of the force acting on a star is considered, and the solution to the formal problem is obtained in terms of the average force per unit mass $\mathbf{F}_t$ acting at time t, given that a force of intensity $\mathbf{F}_0$ acted at time $t = 0$. Various related quantities are also considered, and in particular an explicit formula for the correlation coefficient $R(\mathbf{F}_0, t)$ is derived.

1. *Introduction.*—A basic problem in statistical stellar dynamics is the characterization of the entire stochastic variation of the gravitational force acting on a star. And, as we have already explained in the introductory section to the preceding paper,[1] this requires the specification of the average force per unit mass $\mathbf{F}_t$ acting on a star at time t, given that a force of intensity $\mathbf{F}_0$ acted at time $t = 0$. In other words, the essential physical quantity which is needed concerns the correlation in the forces acting on a star at two different instants of time. In this paper we propose to present the formal parts of this theory. In a later paper we shall undertake a fuller discussion of the various formulae derived and also outline the applications of the theory developed here.

2. *The first moments of* $\mathbf{F}_t$.—As in III, § 2, the solution to the formal problem soon reduces to one of evaluating the characteristic function $C(\boldsymbol{\rho}, \boldsymbol{\sigma})$, associated with the distribution function $W(\mathbf{F}_0, \mathbf{F}_t)$ governing the probability that forces of intensities $\mathbf{F}_0$ and $\mathbf{F}_t$ will act, respectively, at times $t = 0$ and $t = t$. Similar to III, equation (7), we now have

$$C(\boldsymbol{\rho}, \boldsymbol{\sigma}) = N\int_{-\infty}^{+\infty}\int_{-\infty}^{+\infty}\left[1 - e^{iGM\left\{\frac{\mathbf{r}\cdot\boldsymbol{\rho}}{|\mathbf{r}|^3}+\frac{(\mathbf{r}+\mathbf{V}t)\cdot\boldsymbol{\sigma}}{|\mathbf{r}+\mathbf{V}t|^3}\right\}}\right]\chi(\mathbf{V})\,d\mathbf{r}d\mathbf{V}\,, \tag{1}$$

where $\chi(\mathbf{V})$ denotes the probability distribution of the *relative velocity* $\mathbf{V}$. In writing equation (1) we have assumed (as in III) that all the stars have the same mass M. (The generalization necessary to allow for a distribution over the masses is straightforward and will be indicated later.) The foregoing equation can be re-written in the form (cf. III, eq. [9])

$$\left.\begin{aligned} C(\boldsymbol{\rho}, \boldsymbol{\sigma}) &= \tfrac{4}{15}(2\pi GM)^{3/2}N|\boldsymbol{\rho}|^{1/2} \\ &\quad + N\int_{-\infty}^{+\infty}\int_{-\infty}^{+\infty}e^{iGM\mathbf{r}\cdot\boldsymbol{\rho}/|\mathbf{r}|^3}\left[1 - e^{iGM(\mathbf{r}+\mathbf{V}t)\cdot\boldsymbol{\sigma}/|\mathbf{r}+\mathbf{V}t|^3}\right]\chi(\mathbf{V})\,d\mathbf{r}d\mathbf{V}\,; \end{aligned}\right\} \tag{2}$$

and, since we are interested only in the first moments of $\mathbf{F}_t$, it would be sufficient to examine the behavior of $\operatorname{grad}_{\boldsymbol{\sigma}} C(\boldsymbol{\rho}, \boldsymbol{\sigma})$ for $|\boldsymbol{\sigma}| \to 0$. Accordingly, we express $C(\boldsymbol{\rho}, \boldsymbol{\sigma})$ in the form

$$C(\boldsymbol{\rho}, \boldsymbol{\sigma}) = \tfrac{4}{15}(2\pi GM)^{3/2}N|\boldsymbol{\rho}|^{1/2} + \mathfrak{D}(\boldsymbol{\rho}, \boldsymbol{\sigma}) + O(|\boldsymbol{\sigma}|^2) \tag{3}$$

[1] P. 25. This paper will be referred to as III. The earlier papers, *Ap. J.*, **95**, 489, 1942, and **97**, 1, 1943, will be referred to as I and II, respectively.

and verify that

$$\mathfrak{D}(\boldsymbol{\rho}, \boldsymbol{\sigma}) = \int_{-\infty}^{+\infty} D(\boldsymbol{\rho}, \boldsymbol{\sigma}; \boldsymbol{V}t)\, \chi(\boldsymbol{V})\, d\boldsymbol{V}\,, \tag{4}$$

where

$$D(\boldsymbol{\rho}, \boldsymbol{\sigma}; \boldsymbol{V}t) = -iGMN \int_{-\infty}^{+\infty} e^{iGM\boldsymbol{r}\cdot\boldsymbol{\rho}/|\boldsymbol{r}|^3} \frac{\boldsymbol{\sigma}\cdot(\boldsymbol{r}+\boldsymbol{V}t)}{|\boldsymbol{r}+\boldsymbol{V}t|^3}\, d\boldsymbol{r}\,. \tag{5}$$

It is seen that our present definition of $D(\boldsymbol{\rho}, \boldsymbol{\sigma}; \boldsymbol{V}t)$ agrees with our earlier definition of $D(\boldsymbol{\rho}, \boldsymbol{\sigma})$ in III (eq. [12]) with $+\boldsymbol{V}t$ replacing $-\boldsymbol{r}_1$. Hence (cf. III, eqs. [38] and [41]),

$$D(\boldsymbol{\rho}, \boldsymbol{\sigma}; \boldsymbol{V}t) = -\sigma_3 \sum_{l=0}^{\infty} A_l(|\boldsymbol{\rho}|;\, z_1) P_l(\mu) - \sigma_1 \sum_{l=1}^{\infty} B_l(|\boldsymbol{\rho}|;\, z_1) P_l^1(\mu)\,, \tag{6}$$

where σ_3 and σ_1 are the components of $\boldsymbol{\sigma}$ in a Cartesian system of co-ordinates in which the z-axis is in the direction of $\boldsymbol{\rho}$ and the xz-plane contains the vector $\boldsymbol{V}$ and where

$$\mu = \cos\vartheta\,; \qquad \vartheta = \sphericalangle(\boldsymbol{\rho}, \boldsymbol{V})\,, \tag{7}$$

$$\left.\begin{aligned} A_l = (-i)^l 2^{1/2}\pi^{3/2}(GM)^{3/2} N |\boldsymbol{\rho}|^{1/2} \int_0^{\infty} dz\, \xi^{l/2} \frac{\bar{z}^{1/2}}{z^{3/2}} \Big[&-\frac{3l(l-1)}{(2l+1)(2l-1)} J_{l-3/2} \\ &+ \frac{2l(l+1)}{(2l+3)(2l-1)} J_{l+1/2} - \frac{3(l+2)(l+1)}{(2l+3)(2l+1)} J_{l+5/2}\Big]\,, \end{aligned}\right\} \tag{8}$$

and

$$\left.\begin{aligned} B_l = (-i)^l 2^{1/2}\pi^{3/2}(GM)^{3/2} N |\boldsymbol{\rho}|^{1/2} \int_0^{\infty} dz\, \xi^{l/2} \frac{\bar{z}^{1/2}}{z^{3/2}} \Big[&-\frac{3(l-1)}{(2l+1)(2l-1)} J_{l-3/2} \\ &+ \frac{3}{(2l+3)(2l-1)} J_{l+1/2} + \frac{3(l+2)}{(2l+1)(2l+3)} J_{l+5/2}\Big]\,. \end{aligned}\right\} \tag{9}$$ [2]

Further, in the foregoing equations (cf. III, eq. [29])

$$z_1 = \frac{GM|\boldsymbol{\rho}|}{|\boldsymbol{V}|^2 t^2}\,. \tag{10}$$

And, finally, we may also recall that the integrals defining A_l and B_l should be broken at $z = z_1$ according to the scheme III, equations (31) and (32).

To evaluate $\mathfrak{D}(\boldsymbol{\rho}, \boldsymbol{\sigma})$, we have first to refer the solution (6) to a system of co-ordinates which is independent of the direction of $\boldsymbol{V}$. Letting the z-axis still point in the direction of $\boldsymbol{\rho}$, we can write

$$D(\boldsymbol{\rho}, \boldsymbol{\sigma}; \boldsymbol{V}t) = -\sigma_3 \sum_{l=0}^{\infty} A_l P_l(\mu) - (\sigma_1 \cos\varphi + \sigma_2 \sin\varphi) \sum_{l=1}^{\infty} B_l P_l^1(\mu)\,, \tag{11}$$

where φ denotes the azimuth of the meridian plane containing the vector $\boldsymbol{V}$.

Now, let $\boldsymbol{u}$ and $\boldsymbol{v}$ denote, respectively, the velocities of a typical field star and the star under consideration in an appropriately chosen local standard of rest. Then

$$\boldsymbol{V} = \boldsymbol{u} - \boldsymbol{v}\,. \tag{12}$$

[2] It will be noticed that our present definitions of A_l and B_l agree with those given in III, eqs. [39] and [40], except that $-i$ now replaces i. This difference can be traced to the circumstance that $\boldsymbol{V}$ and $\boldsymbol{r}_1$ occur with opposite signs in the relevant equations.

It would be natural to suppose that the distribution of the "peculiar" velocities $\boldsymbol{u}$ is spherical (cf. II, eqs. [58] and [59]). While it would be feasible to work with a general spherical distribution of the velocities $\boldsymbol{u}$, in the present investigation we shall assume, for the sake of simplicity, that the distribution of the velocities $\boldsymbol{u}$ is actually Gaussian. And it is evident that a Gaussian distribution of the velocities $\boldsymbol{u}$ implies that $\chi(\boldsymbol{V})$ has the form

$$\chi(\boldsymbol{V}) = \frac{j^3}{\pi^{3/2}} e^{-j^2|\boldsymbol{V}+\boldsymbol{v}|^2}, \tag{13}$$

where j is a certain parameter related to the mean-square residual velocities of the stars. Using the foregoing form for $\chi(\boldsymbol{V})$ in equation (4) and changing to polar co-ordinates, we have

$$\left.\begin{aligned}\mathfrak{D}(\boldsymbol{\rho}, \boldsymbol{\sigma}) = \frac{j^3}{\pi^{3/2}} \int_0^{\infty}\int_{-1}^{+1}\int_0^{2\pi} e^{-j^2(|\boldsymbol{V}|^2+|\boldsymbol{v}|^2+2|\boldsymbol{V}||\boldsymbol{v}|\cos\Theta)} \\ \times D(\boldsymbol{\rho}, \boldsymbol{\sigma}; \boldsymbol{Vt})\,|\boldsymbol{V}|^2 d|\boldsymbol{V}|\,d\mu\,d\varphi,\end{aligned}\right\} \tag{14}$$

where Θ denotes the angle between the directions of $\boldsymbol{v}$ and $\boldsymbol{V}$. If the xz-plane of our co-ordinate system is now assumed to contain the vector $\boldsymbol{v}$, then

$$\cos\Theta = \cos\vartheta\cos\vartheta_1 + \sin\vartheta\sin\vartheta_1\cos\varphi, \tag{15}$$

where

$$\vartheta = \sphericalangle(\boldsymbol{\rho}, \boldsymbol{V}); \qquad \vartheta_1 = \sphericalangle(\boldsymbol{\rho}, \boldsymbol{v}). \tag{16}$$

Writing

$$j|\boldsymbol{V}| = \lambda \text{ and } j|\boldsymbol{v}| = \nu, \tag{17}$$

we find equation (16) taking the form

$$\left.\begin{aligned}\mathfrak{D}(\boldsymbol{\rho}, \boldsymbol{\sigma}) = -\frac{1}{\pi^{3/2}} \int_0^{\infty}\int_{-1}^{+1}\int_0^{2\pi} d\lambda\,d\mu\,d\varphi\,\lambda^2 e^{-(\lambda^2+\nu^2+2\lambda\nu\cos\Theta)} \\ \times\left[\sigma_3\sum_{l=0}^{\infty} A_l P_l(\mu) + (\sigma_1\cos\varphi + \sigma_2\sin\varphi)\sum_{l=1}^{\infty} B_l P_l^1(\mu)\right],\end{aligned}\right\} \tag{18}$$

where we have further substituted for $D(\boldsymbol{\rho}, \boldsymbol{\sigma}; \boldsymbol{Vt})$ from equation (11). The integrations over μ and φ in equation (18) can be performed by first expanding $\exp(-2\lambda\nu\cos\Theta)$ in tesseral harmonics. We have[3]

$$\left.\begin{aligned}e^{-2\lambda\nu\cos\Theta} = \left(\frac{\pi}{4\lambda\nu}\right)^{1/2}\sum_{m=0}^{\infty}(-1)^m(2m+1)\,I_{m+1/2}(2\lambda\nu) \\ \times\left\{P_m(\mu)P_m(\mu_1) + 2\sum_{n=1}^{m}\frac{(m-n)!}{(m+n)!}P_n^m(\mu)P_n^m(\mu_1)\cos m\varphi\right\},\end{aligned}\right\} \tag{19}$$

where the I's are the Bessel functions for purely imaginary arguments.[4] Introducing the foregoing expansion into equation (18) and using the orthogonality properties of the Legendre functions, we find that $\mathfrak{D}(\boldsymbol{\rho}, \boldsymbol{\sigma})$ reduces to

$$\left.\begin{aligned}\mathfrak{D}(\boldsymbol{\rho}, \boldsymbol{\sigma}) = -\int_0^{\infty} d\lambda\,\frac{4}{\pi^{1/2}}\,e^{-(\lambda^2+\nu^2)}\lambda^2 \\ \times\left(\frac{\pi}{4\lambda\nu}\right)^{1/2}\left\{\sigma_3\sum_{l=0}^{\infty}(-1)^l I_{l+1/2}A_l P_l(\mu_1) + \sigma_1\sum_{l=1}^{\infty}(-1)^l I_{l+1/2}B_l P_l^1(\mu_1)\right\}.\end{aligned}\right\} \tag{20}$$

[3] See, e.g., G. N. Watson, *Theory of Bessel Functions*, p. 369, Cambridge, England, 1922.

[4] For the definition of these functions see *ibid.*, pp. 77–80.

We can thus express $\mathfrak{D}(\boldsymbol{\rho}, \boldsymbol{\sigma})$ in the form

$$\mathfrak{D}(\boldsymbol{\rho}, \boldsymbol{\sigma}) = -\sigma_3 \sum_{l=0}^{\infty} \mathfrak{A}_l(|\boldsymbol{\rho}|; \nu; \tau) P_l(\mu_1) - \sigma_1 \sum_{l=1}^{\infty} \mathfrak{B}_l(|\boldsymbol{\rho}|; \nu; \tau) P_l^1(\mu_1) , \quad (21)$$

where we have introduced the quantities $\mathfrak{A}_l$ and $\mathfrak{B}_l$, defined by

$$\mathfrak{A}_l = (-1)^l \frac{4}{\pi^{1/2}} \int_0^{\infty} e^{-(\lambda^2+\nu^2)} \lambda^2 \left(\frac{\pi}{4\lambda\nu}\right)^{1/2} I_{l+1/2}(2\lambda\nu) A_l(|\boldsymbol{\rho}|; \lambda\tau) \, d\lambda \quad (22)$$

and

$$\mathfrak{B}_l = (-1)^l \frac{4}{\pi^{1/2}} \int_0^{\infty} e^{-(\lambda^2+\nu^2)} \lambda^2 \left(\frac{\pi}{4\lambda\nu}\right)^{1/2} I_{l+1/2}(2\lambda\nu) B_l(|\boldsymbol{\rho}|; \lambda\tau) \, d\lambda , \quad (23)$$

where we have used τ to denote the time measured in the unit

$$t_0 = jl ; \qquad t = t_0 \tau , \quad (24)$$

l denoting the unit of length introduced in III, equation (72), so that (cf. III, eq. [73])

$$z_1 = \frac{x}{\lambda^2 \tau^2 \beta} . \quad (25)$$

It is now seen that $\mathfrak{D}(\boldsymbol{\rho}, \boldsymbol{\sigma})$ has exactly the same form as $D(\boldsymbol{\rho}, \boldsymbol{\sigma})$ in the theory of spatial correlations (cf. eq. [21] with III, eq. [38]). We can therefore write down at once the expressions for all the first moments of $\boldsymbol{F}_t$. Thus, choosing a co-ordinate system in which the ζ-axis is in the direction of $\boldsymbol{v}$ (i.e., the direction of motion) and the $\xi\zeta$-plane contains the vector $\boldsymbol{F}_0$ (see III, Fig. 1), we have (cf. III, eqs. [60], [65], and [66])

$$\left.\begin{aligned} \overline{F}_{t,\xi} = -\frac{2i}{\pi\beta H(\beta)} \left(\frac{\pi}{2}\right)^{1/2} \sum_{n=1}^{\infty} (-i)^n P_n^1(\mu) \int_0^{\infty} e^{-(x/\beta)^{3/2}} x^{3/2} J_{n+1/2}(x) \\ \times [\mathfrak{C}_{n-1} - \mathfrak{D}_{n+1}] \, dx , \end{aligned}\right\} \quad (26)$$

$$\overline{F}_{t,\eta} = 0 , \quad (27)$$

and

$$\left.\begin{aligned} \overline{F}_{t,\zeta} = -\frac{2i}{\pi\beta H(\beta)} \left(\frac{\pi}{2}\right)^{1/2} \sum_{n=0}^{\infty} (-i)^n P_n(\mu) \int_0^{\infty} e^{-(x/\beta)^{3/2}} x^{3/2} J_{n+1/2}(x) \\ \times [n\mathfrak{C}_{n-1} + (n+1)\mathfrak{D}_{n+1}] \, dx , \end{aligned}\right\} \quad (28)$$

where

$$\mathfrak{C}_l = \frac{1}{2l+1}\{\mathfrak{A}_l - l\mathfrak{B}_l\} \quad \text{and} \quad \mathfrak{D}_l = \frac{1}{2l+1}\{\mathfrak{A}_l + (l+1)\mathfrak{B}_l\} \quad (29)$$

and

$$\mu = \cos\vartheta ; \qquad \vartheta = \measuredangle(\boldsymbol{v}, \boldsymbol{F}_0) . \quad (30)$$

Combining equations (8), (9), (22), and (23), we find that the formulae defining $\mathfrak{C}_l$ and $\mathfrak{D}_l$ are explicitly (cf. III, eqs. [68] and [69])

$$\left.\begin{aligned} \mathfrak{C}_l = i^l \frac{15 Q_H}{8(2l+3)(2l+1)} \left(\frac{x}{\beta}\right)^{1/2} \int_0^{\infty} d\lambda \frac{4}{\pi^{1/2}} e^{-(\lambda^2+\nu^2)} \lambda^2 \left(\frac{\pi}{4\lambda\nu}\right)^{1/2} I_{l+1/2}(2\lambda\nu) \\ \times \int_0^{\infty} dz \, \xi^{l/2} \frac{\tilde{z}^{1/2}}{z^{3/2}} \{l J_{l+1/} - 3(l+2) J_{l+5/2}\} \end{aligned}\right\} \quad (31)$$

and

$$\left.\begin{aligned}\mathfrak{D}_l = i^l \frac{15 Q_H}{8(2l-1)(2l+1)}\left(\frac{x}{\beta}\right)^{1/2}\int_0^\infty d\lambda\,\frac{4}{\pi^{1/2}}\,e^{-(\lambda^2+\nu^2)}\lambda^2\left(\frac{\pi}{4\lambda\nu}\right)^{1/2} I_{l+1/2}(2\lambda\nu)\\ \times\int_0^\infty dz\,\xi^{l/2}\,\frac{\bar{z}^{1/2}}{z^{3/2}}\left\{-3(l-1)J_{l-3/2}+(l+1)J_{l+1/2}\right\}.\end{aligned}\right\}\quad(32)$$

With this we have formally solved the problem.

It is of interest to note that, since

$$I_{l+1/2}(2\lambda\nu)\to\frac{1}{\Gamma(l+\frac{3}{2})}(\lambda\nu)^{l+1/2}\qquad(\nu\to 0),\quad(33)$$

it follows that

$$\left(\frac{\pi}{4\lambda\nu}\right)^{1/2} I_{l+1/2}(2\lambda\nu)\to\frac{\pi^{1/2}}{2\Gamma(l+\frac{3}{2})}(\lambda\nu)^{l}\qquad(\nu\to 0).\quad(34)$$

Hence, for $\nu = 0$ all the functions $\mathfrak{C}_l$ and $\mathfrak{D}_l$ except $\mathfrak{C}_0$ vanish identically. This implies (cf. § 3 below) that for $|\boldsymbol{v}| = 0$ the only nonvanishing moment of $\boldsymbol{F}_t$ is in the direction of $\boldsymbol{F}_0$. In other words, the problem of the stochastic variation of the force acting on a "fixed" point in a system containing stars in random motion is exceptionally simple.

3. *The first moment of* $\mathbf{F}_t$ *in the direction of* $\mathbf{F}_0$ *and its averages.*—A quantity of considerable interest is the average value of $\boldsymbol{F}_t$ in the direction of $\boldsymbol{F}_0$. Analogous to III, equation (76), we now have

$$\left.\begin{aligned}\overline{F}_{t,\,\boldsymbol{F}_0} = -\frac{2i}{\pi\beta H(\beta)}\left(\frac{\pi}{2}\right)^{1/2}\Bigg\{\sum_{n=1}^\infty(-i)^n P_1^1(\mu)P_n^1(\mu)\int_0^\infty e^{-(x/\beta)^2/2}x^{3/2}J_{n+1/2}(x)\\ \times[\mathfrak{C}_{n-1}-\mathfrak{D}_{n+1}]\,dx+\sum_{n=0}^\infty(-i)^n P_1(\mu)P_n(\mu)\int_0^\infty e^{-(x/\beta)^2/2}x^{3/2}J_{n+1/2}(x)\\ \times[n\mathfrak{C}_{n-1}+(n+1)\mathfrak{D}_{n+1}]\,dx\Bigg\}.\end{aligned}\right\}\quad(35)$$

Again, as in the theory of spatial correlations, greatest interest is attached to $\overline{F}_{t,\,\boldsymbol{F}_0}$ only after it has been further averaged over all mutual orientations of the vectors $\boldsymbol{F}_0$ and $\boldsymbol{v}$. When this additional averaging process is carried out, we are left with

$$\overline{\overline{F}}_{t,\,\boldsymbol{F}_0} = -\frac{2}{\pi\beta H(\beta)}\left(\frac{\pi}{2}\right)^{1/2}\int_0^\infty e^{-(x/\beta)^2/2}x^{3/2}J_{3/2}(x)\,\mathfrak{C}_0\,dx,\quad(36)$$

where, according to equation (31),

$$\mathfrak{C}_0 = -Q_H\,\frac{15}{4}\left(\frac{x}{\beta}\right)^{1/2}\int_0^\infty d\lambda\,\frac{4}{\pi^{1/2}}\,e^{-(\lambda^2+\nu^2)}\lambda^2\left(\frac{\pi}{4\lambda\nu}\right)^{1/2} I_{1/2}(2\lambda\nu)\int_0^\infty dz\,\frac{\bar{z}^{1/2}}{z^{3/2}}J_{5/2}(z).\quad(37)$$

Combining equations (36) and (37) and expressing $\overline{\overline{F}}_{t,\,\boldsymbol{F}_0}$ in units of Q_H and t in units of t_0 (eq. [24]), we can write

$$\overline{\overline{\beta}}_{\tau,\,\mathbf{B}} = \frac{15}{2\pi\beta^{3/2}H(\beta)}\int_0^\infty e^{-(x/\beta)^2/2}x^{3/2}\left(\frac{\sin x}{x}-\cos x\right)\overline{\mathcal{Q}}\left(\frac{x}{\tau^2\beta};\,\nu\right)dx,\quad(38)$$

where

$$\overline{\mathcal{Q}}(y;\nu) = \int_0^\infty d\lambda \, \frac{4}{\pi^{1/2}} \, e^{-(\lambda^2+\nu^2)} \lambda^2 \left(\frac{\pi}{4\lambda\nu}\right)^{1/2} I_{1/2}(2\lambda\nu) \, \mathcal{Q}\left(\frac{y}{\lambda^2}\right), \tag{39}$$

the function $\mathcal{Q}(x)$ being defined as in III, equation (80). Since

$$I_{1/2}(2\lambda\nu) = \frac{1}{(4\pi\lambda\nu)^{1/2}} \, (e^{2\lambda\nu} - e^{-2\lambda\nu}) \, , \tag{40}$$

we can re-write equation (39) more explicitly in the form

$$\overline{\mathcal{Q}}(y;\nu) = \int_0^\infty d\lambda \, \frac{4}{\pi^{1/2}} \, e^{-(\lambda^2+\nu^2)} \lambda^2 \left[\frac{1}{2\lambda\nu} \sinh 2\lambda\nu\right] \tfrac{1}{2} \int_0^{y/\lambda^2} \frac{dz}{z^2} \, J_{3/2}(z) \, , \tag{41}$$

where we have further substituted for $\mathcal{Q}(y/\lambda^2)$ according to III, equation (85).

Now, the correlation coefficient $R(\boldsymbol{\beta}, \tau)$ is related to $\overline{\overline{\beta}}_{\tau, \boldsymbol{\beta}}$ very simply. Thus,

$$R(\boldsymbol{\beta}, \tau) = \frac{\overline{\boldsymbol{\beta} \cdot \boldsymbol{\beta}_\tau}}{|\boldsymbol{\beta}^2|} = \frac{1}{\beta} \, \overline{\overline{\beta}}_{\tau, \boldsymbol{\beta}} \, . \tag{42}$$

Hence,

$$R(\boldsymbol{\beta}, \tau) = \frac{15}{2\pi\beta^{5/2} H(\beta)} \int_0^\infty e^{-(x/\beta)^{3/2}} x^{3/2} \left(\frac{\sin x}{x} - \cos x\right) \overline{\mathcal{Q}}\left(\frac{x}{\tau^2\beta}; \nu\right) dx \, . \tag{43}$$

It is evident that (cf. III, eqs. [95] and [97])

$$R(\boldsymbol{\beta}, \tau) \to 1 \qquad \text{as} \quad \tau \to 0 \, , \tag{44}$$

while

$$R(\boldsymbol{\beta}, \tau) \propto \tau^{-1} \qquad \text{as} \quad \tau \to \infty \, . \tag{45}$$

According to equation (45), the correlation coefficient $R(\boldsymbol{\beta}, \tau)$ decreases relatively rather slowly for $\tau \to \infty$. In this respect the stochastic process we are considering is strikingly in contrast with processes of the usual Markoff type, in which the correlations are expected to decrease exponentially with the time.

As in III, § 7, we can also consider the result of further averaging $\overline{\overline{\beta}}_{\tau, \boldsymbol{\beta}}$ over all initial values of β weighted according to the Holtsmark function, $H(\beta)$. Analogous to III, equation (111), we now have

$$\overline{\overline{\beta}}_{\boldsymbol{\beta}}(\tau, \nu) = \frac{15}{\pi} \int_0^\infty e^{-y^{3/2}} \overline{\mathcal{Q}}\left(\frac{z}{\tau^2}; \nu\right) \frac{dy}{y^{1/2}} . \tag{46}$$

The appropriate asymptotic expansions for $\overline{\overline{\beta}}_{\boldsymbol{\beta}}(\tau, \nu)$ can be readily written down from the corresponding expansions for $\overline{\overline{\beta}}_{\boldsymbol{\beta}}(s)$ given in III, § 7.

4. *The average value of* $\mathbf{F}_t$ *in the direction of* $\mathbf{v}$.—The average value, $\overline{F}_{t, v}$ of $\boldsymbol{F}_t$ in the direction of $\boldsymbol{v}$ is, according to our choice of the co-ordinate system, the same as $\overline{F}_{t, \zeta}$, and this is given by equation (28). And, as in the case of $\overline{F}_{t, \boldsymbol{F}_0}$, the quantity of greatest physical interest is that which results from further averaging $\overline{F}_{t, v}$ over all mutual orientations of the vectors $\boldsymbol{F}_0$ and $\boldsymbol{v}$. Analogous to III, equation (138), we now have

$$\overline{\overline{\beta}}_{\tau, v} = \frac{5}{2\pi\beta^{3/2} H(\beta)} \int_0^\infty e^{-(x/\beta)^{3/2}} x^{3/2} \sin x \, \overline{\mathcal{R}}\left(\frac{x}{\tau^2\beta}; \nu\right) dx \, , \tag{47}$$

where

$$\overline{\mathcal{R}}(y;\nu) = \int_0^\infty d\lambda \, \frac{4}{\pi^{1/2}} \, e^{-(\lambda^2+\nu^2)} \lambda^2 \left(\frac{\pi}{4\lambda\nu}\right)^{1/2} I_{3/2}(2\lambda\nu) \, \mathcal{R}\left(\frac{y}{\lambda^2}\right), \tag{48}$$

the function $\mathcal{R}(x)$ being defined as in III, equation (139). Since

$$I_{3/2}(2\lambda\nu) = \frac{1}{(4\pi\lambda\nu)^{1/2}} \left[e^{2\lambda\nu}\left(1 - \frac{1}{2\lambda\nu}\right) + e^{-2\lambda\nu}\left(1 + \frac{1}{2\lambda\nu}\right)\right], \tag{49}$$

we can re-write equation (48) more conveniently in the form

$$\overline{\mathcal{R}}(y;\nu) = \int_0^\infty d\lambda \, \frac{4}{\pi^{1/2}} \, e^{-(\lambda^2+\nu^2)} \lambda^2 \, \frac{1}{(2\lambda\nu)^2} (2\lambda\nu \cosh 2\lambda\nu - \sinh 2\lambda\nu) \, \mathcal{R}\left(\frac{y}{\lambda^2}\right). \tag{50}$$

Again, the relevant asymptotic expansions for $\overline{\beta}_{r,\,\nu}$ can be derived from those given for $\overline{\beta}_{1,\,s}$ in III, § 8.

This completes the formal parts of the theory of the stochastic variation of the force acting on a star. In later papers we shall return to fuller discussions of the various implications of this theory to the problems of stellar dynamics.

ON THE STABILITY OF BINARY SYSTEMS

S. CHANDRASEKHAR
Yerkes Observatory
Received October 5, 1943

ABSTRACT

In this paper the theory of spatial correlations developed in an earlier paper is applied to the discussion of the stability of binary stars, and a formula for estimating the time of dissolution, τ, of a binary is derived. It is found that

$$\tau \simeq \frac{(M_1 + M_2)^{1/2}}{4\pi G^{1/2} M N a^{3/2}},$$

where M_1 and M_2 denote the masses of the two components of the binary system, M an average mass of the field stars, N the number of stars per unit volume, and a the semimajor axis of the relative orbit. According to the foregoing formula, the time of dissolution of binaries with semimajor axes in the range of 10^3–10^4 astronomical units can be estimated to lie in the interval 7×10^{10} to 2×10^9 years. Since there is evidence that the distribution of energies of the binary systems does not conform to Boltzmann's law (Ambarzumian), the present theory would lead one to conclude that the statistics of binary stars lends further weight to the adoption of a time scale in the neighborhood of 3×10^9 years. Some additional remarks on the related problems of the common proper-motion stars and on cometary orbits which are very close to the parabolic limit are also made.

1. *Introduction.*—As Jeans[1] has emphasized on various occasions, the statistics of binary stars should provide an important basis for drawing conclusions concerning the time scale appropriate for the Galaxy. In Jeans's own considerations relating to this problem, stress is laid on a comparison of the observed frequencies of occurrence of the different periods and eccentricities with those predicted under conditions of thermal equilibrium. Thus, under conditions of thermal equilibrium[2] the number of binaries with eccentricity less than e will be proportional to e^2; and, according to Jeans, the agreement of the data of observations with this e^2-law is "far too good to be accidental." On the strength principally of this evidence[3] Jeans concludes that the time scale of the Galaxy must be long enough to allow for the establishment of conditions approaching those of equipartition among the parameters of a binary. However, an important lacuna in Jeans's argument, and one which appears to vitiate his principal conclusions, was first pointed out by Ambarzumian,[4] who showed that the e^2-law can be derived under conditions far more general than those contemplated under thermal equilibrium. Indeed, Ambarzumian proved that *for any arbitrary distribution in the phase space of the binary which is a function of the energy* E *of the binary system only, the number of systems with eccentricity less than* e *will be proportional to* e^2. In other words, the validity of the e^2-law is a necessary but not a sufficient condition for the existence of thermal equilibrium. Accordingly, the agreement of the known statistics of binary systems with the e^2-law can be regarded as evidence only for supposing that the distribution function in the phase space has the form $f(E)$; it cannot be regarded as evidence for the special form of the distribution function, namely, $\exp(-E/\theta)$, demanded when conditions of thermal equilibrium obtain, and neither does it provide evidence for supposing that conditions approximating equipartition among the parameters of the binary have been established.

[1] *M.N.*, **79**, 100 and 408, 1919; *Astronomy and Cosmogony*, pp. 323–326, Cambridge, England, 1929; *Nature*, **136**, 432, 1935.

[2] As we shall presently indicate, the result we are about to quote is actually valid under conditions far more general than those of thermal equilibrium.

[3] See, e.g., *Nature*, **136**, 432, 1935.

[4] *Russian Astr. J.*, **14**, 207, 1937. See also *Nature*, **137**, 537, 1936.

On the other hand, as Ambarzumian has shown, there exist other features of the known statistics (e.g., the distribution of energies as inferred from the distribution of the semi-major axis) which quite definitely contradict the assumption that conditions even remotely resembling those of thermal equilibrium have been attained.[5] We may therefore conclude with Ambarzumian that the time scale of the Galaxy *cannot* be so long that Boltzmann's law describes the distribution in the phase space of the binary. It is now clear that, in order that we may go beyond this point and draw specific conclusions concerning the time scale itself, it is necessary that we make some estimate of the effectiveness of the tidal forces, due to the neighboring stars, in modifying the orbital elements of a binary. It is in the details of the estimation of these latter effects that Ambarzumian's considerations appear to lose rigor. Thus, he uses the two-body approximation of stellar encounters to evaluate the *tidal* effects of the near-by stars. But it is apparent that the essentially characteristic features of the problem are ignored if an attempt is made to evaluate the *differential* effects of the neighboring stars on the components of a binary along the conventional lines of treating stellar encounters as a series of independent two-body problems. However, it appears that the theory of spatial correlations developed in an earlier paper[6] provides an adequate basis for incorporating in the dynamics of binary systems the fluctuating gravitational field always present on account of the continually changing complexion of the local stellar distribution. It is the object of this paper to take a first step in this direction.

2. *On the rate of dissolution of a binary.*—As we have already indicated in § 1, the orbital elements of a binary system will be subject to changes on account of the differential effect of the neighboring stars on the two components of the system. Thus, for any given separation between the two stars, there exists a definite distribution function, $W(\boldsymbol{F}_0, \boldsymbol{F}_1)$, governing the probability that forces of intensities $\boldsymbol{F}_0$ and $\boldsymbol{F}_1$, respectively, will act simultaneously on the two components of the system. In other words, a differential acceleration governed by a definite probability law will operate on the system, which will tend to accelerate one star relative to the other. Thus,

$$\Delta\boldsymbol{F} = \boldsymbol{F}_0 - \boldsymbol{F}_1 \tag{1}$$

represents the amount by which the star "0" will be accelerated relative to the star "1." More particularly, the component

$$\Delta F_{||} = (\boldsymbol{F}_0 - \boldsymbol{F}_1) \cdot \mathbf{1}_{\boldsymbol{F}_0}, \tag{2}$$

where $\mathbf{1}_{\boldsymbol{F}_0}$ is a unit vector parallel to the direction of $\boldsymbol{F}_0$, represents the amount by which the star "0" will be *systematically* accelerated relative to the star "1." It is clear that it is this systematic acceleration of one star relative to the other which will chiefly be responsible for such changes in the orbital elements as may be effected. For a component of $\Delta\boldsymbol{F}$ in a direction at right angles to the direction of $\boldsymbol{F}_0$ represents a differential acceleration of the star "0" relative to the star "1," which (in contrast to $\Delta F_{||}$) is of a *random* character. Accordingly, the average net increase in the velocity of the star "0" relative to the star "1" during a time Δt long, compared to the periods of the elementary fluctuations in $\boldsymbol{F}$, will be given by

$$\overline{\Delta v}_{0,1} = \overline{\Delta F}_{||}\Delta t\,. \tag{3}$$

Now, if the relative orbit is an eccentric one, we should allow for the fact that, on account of the changing separation between the two stars, the parameter in the distribution function $W(\boldsymbol{F}_0, \boldsymbol{F}_1)$ will also change. However, in this paper we shall restrict ourselves to

[5] In spite of the conclusiveness of Ambarzumian's arguments it is unfortunate that his very significant discussion of this problem has so far remained ignored. (See, e.g., H. N. Russell, *Science*, 92, 19, 1940.)

[6] See p. 25 in this issue. This paper will be referred to as III.

the case of circular orbits, so that the separation remains constant. Under these conditions equation (3) can be written alternatively in the form

$$\overline{\Delta v}_{0,1} = \Delta t \int_{-\infty}^{+\infty}\int_{-\infty}^{+\infty} (\boldsymbol{F}_0 - \boldsymbol{F}_1) \cdot \mathbf{1}_{\boldsymbol{F}_0} W(\boldsymbol{F}_0, \boldsymbol{F}_1)\, d\boldsymbol{F}_0 d\boldsymbol{F}\ , \tag{4}$$

or, in the notation of III, equation (99),

$$\overline{\Delta v}_{0,1} = (\overline{|\boldsymbol{F}_0|} - \overline{\overline{\overline{F}}}_{1,\boldsymbol{F}_0})\,\Delta t\ . \tag{5}$$

If we measure $|\boldsymbol{F}|$ in units of

$$Q_H = (\tfrac{4}{15})^{2/3} 2\pi G M N^{2/3} \tag{6}$$

(where M denotes a certain average mass for the field stars and N the number of stars per unit volume), equation (5) can be expressed as (cf. III, eqs. [100] and [126])

$$\overline{\Delta v}_{0,1} = Q_H \left[\frac{4}{\pi}\Gamma(\tfrac{1}{3}) - \overline{\overline{\overline{\beta}}}_{\boldsymbol{\beta}}(s)\right]\Delta t\ . \tag{7}$$

In equation (7) s denotes the constant separation between the two stars expressed in units of (III, eq. [72])

$$l = \frac{15^{1/3}}{4^{1/3}(2\pi)^{1/2}} N^{-1/3}\ . \tag{8}$$

As we shall presently verify (in § 3, below), the case of greatest practical interest arises when the separation between the two components of the binary system is a small fraction of the average distance between the stars. We may then use the asymptotic expansion (III, eq. [123]):

$$\overline{\overline{\overline{\beta}}}_{\boldsymbol{\beta}}(s) = \frac{4}{\pi}\Gamma(\tfrac{1}{3}) - \frac{15}{4}\left(\frac{2}{\pi}\right)^{1/2} s + O(s^4)\ . \tag{9}$$

For values of $s < \frac{1}{2}$ we can therefore replace equation (7) to a sufficient approximation by

$$\overline{\Delta v}_{0,1} = \frac{15}{4}\left(\frac{2}{\pi}\right)^{1/2} Q_H s \Delta t\ . \tag{10}$$

If a denotes the separation between the two stars,

$$a = sl\ . \tag{11}$$

Accordingly, equations (7), (8), (10), and (11) can be combined to give

$$\overline{\Delta v}_{0,1} = 4\pi G M N a \Delta t\ . \tag{12}$$

The foregoing equation for $\overline{\Delta v}_{0,1}$ may be regarded as the fundamental formula of the present theory.

Now the mean square velocity of a star in its relative binary orbit is given by

$$\overline{V^2} = \frac{G(M_1+M_2)}{a}\ , \tag{13}$$

where M_1 and M_2 denote the masses of the two components and a the semimajor axis of the orbit. We may therefore *define* the time of dissolution τ of a binary by the equation

$$\overline{\Delta v}_{0,1} = \sqrt{\frac{G(M_1+M_2)}{a}}\ . \tag{14}$$

Using equation (12) for $\overline{\Delta v}_{0,1}$, we have

$$\tau \simeq \frac{(M_1+M_2)^{1/2}}{4\pi G^{1/2} M N a^{3/2}}. \tag{15}$$

Comparing this formula with the one given by Ambarzumian,[7] we notice that the two are of altogether different forms. In particular, we may draw attention to the fact that, while Ambarzumian's formula contains the mean velocity of the stars as a factor, equation (14) contains no term in the velocities.

3. *Numerical applications.*—Expressing the mass in solar units, N as numbers per cubic parsec, and the separation a in astronomical units, the formula (15) for the time of dissolution of a binary reduces to

$$\tau = 1.11 \times 10^{14} \frac{(M_1+M_2)^{1/2}}{M N a^{3/2}} \text{ years}. \tag{16}$$

In the neighborhood of the sun

$$N = 0.1 \quad \text{and} \quad M = 0.5\,; \tag{17}$$

and, setting

$$M_1+M_2 = 1\,, \tag{18}$$

equation (16) becomes

$$\tau = 2.22 \times 10^{15} a^{-3/2} \text{ years}. \tag{19}$$

Table 1 is derived from this formula.

Since the average distance between the stars is of the order of 3 parsecs, a separation of 60,000 astronomical units still corresponds to only a tenth of the average distance between the stars. This fully justifies the use of the expansion (9) in equation (7).

TABLE 1

THE TIME OF DISSOLUTION OF BINARIES

(N = 0.1 Stars/(Parsec)^3; $M = 0.5\odot$; $M_1 + M_2 = \odot$)

a (Astronomical Units)	τ (Years)	a (Astronomical Units)	τ (Years)
1000	7.0×10^{10}	10,000	2.2×10^{9}
2000	2.5×10^{10}	20,000	7.8×10^{8}
4000	8.8×10^{9}	40,000	2.8×10^{8}
6000	4.8×10^{9}	60,000	1.5×10^{8}

From Table 1 it is apparent that the time of dissolution of binaries with semimajor axes between 10^3 and 10^4 astronomical units lies in the range of 7×10^{10} to 2×10^9 years. And, since, according to Ambarzumian, we can infer from the distribution of the semimajor axis of binaries that conditions of equipartition have not been attained in the Galaxy, we may conclude that the time scale cannot exceed 3×10^9 years by any very large factor. In other words, "the data of double star astronomy do not support the long time scale hypothesis" (Ambarzumian).

4. *On common proper-motion stars.*—The existence of common proper-motion stars with relatively wide separations has been known for some time. Thus, in a recent paper, Kuiper[8] lists three pairs of common proper-motion stars with separations exceeding 10^4 astronomical units. According to Table 1, the time of dissolution of binaries with such separations is appreciably less than 3×10^9 years, and the question now arises as to how justifiable it is to class such common proper-motion stars among the binaries.

[7] *Russian Astr. J.*, **14**, 207, 1937. The formula for the time of dissolution is given on p. 216 (eq. [14]).

[8] *Ap. J.*, **95**, 201, 1942 (see particularly Table 5 in this paper).

To take a specific case, consider the pair $-32°$ 16135 A and $-31°$ 17815 for which Kuiper estimates a separation of 3.3×10^4 astronomical units. Now a binary with this separation will be disrupted in a time of the order of 4×10^8 years. What this means is simply this: In a time of this duration one of the components will be accelerated relative to the other by an amount which would make the kinetic energy of motion exceed the binding energy. Accordingly, we shall not be justified in regarding them *dynamically* as binaries. But this does *not* imply that the two stars will have widely different space motions in a chosen local standard of rest; for this to happen, we shall have to wait for a time of the order of the time of relaxation of the system, which is of an altogether different order of magnitude. It appears, therefore, that we cannot strictly regard common proper-motion stars with separations exceeding 10^4 astronomical units as binaries: they are more appropriately regarded as the residue of disrupted binaries. In other words, they are what they are: common proper-motion stars!

5. *On cometary orbits which are very close to the parabolic limit.*—It has been known that cometary orbits with eccentricities extremely near unity exist. Thus, Van Biesbroeck[9] finds that the comet Delavan ($1913f = 1914V$) had an eccentricity of 0.9999781 when it *entered* the outermost parts of the solar system. This implies that the semimajor axis of the orbit is in the neighborhood of 10^5 astronomical units, at which distance the tidal disturbances due to the near-by stars must be appreciable (see Table 1). Indeed, the very existence of such orbits (if fully substantiated) presents some exceedingly delicate considerations. It should, however, be borne in mind that comets such as comet Delavan do not remain *all* the time at distances of the order of 10^5 astronomical units from the sun, though they would, for an appreciable fraction of their periods ($\sim 2.4 \times 10^7$ years). It will therefore be of very great interest to see if cometary orbits as close to the parabolic limit as the orbit of comet Delavan will *leave* the solar system with eccentricities appreciably different from those with which they entered the system; to settle this question, the orbits would have to be integrated *forward* instead of backward, as has been customary.

[9] *Yerkes Obs. Pub.*, **5**, Part II, 34, 1927. The writer is greatly indebted to Professor Van Biesbroeck for discussions on these and related matters.

THE CONTINUOUS ABSORPTION COEFFICIENT OF THE NEGATIVE HYDROGEN ION

LOUIS R. HENRICH
Yerkes Observatory
Received November 10, 1943

ABSTRACT

An eleventh-order Hylleraas type of wave function for the negative hydrogen ion has been determined by the Ritz method, giving for the lowest state an energy of -0.52756 atomic units. The continuous absorption coefficient has also been computed, using this new wave function. The absorption-curve is found to have its maximum at 7500 A. A calculation of the color-temperature–effective-temperature relation from 4100 A to 6500 A showed that the discrepancy between theory and observation is considerably reduced.

1. *Introduction.*—The attempt to find the source of the continuous opacity in stellar atmospheres and the reconciliation of theory with observation have resulted in many investigations. The suggestion by Wildt[1] that the negative hydrogen ion was an important source of opacity has in turn led to investigations of this ion and its continuous absorption coefficient by, among others, Massey and Bates[2] and Williamson.[3, 4] However, there still remained discrepancies between theory and observation, especially in the visual region of the spectrum, at the completion of Williamson's investigation.

It has recently been shown by S. Chandrasekhar and M. K. Krogdahl[5] that the continuous absorption coefficient of the negative hydrogen ion in the spectral region of primary astrophysical interest (namely, in the wave lengths to the red of 4500 A) depends on the wave function of the ground state of the ion at distances of the order of five times the Bohr radius. They have pointed out that the wave functions of the negative hydrogen ion now in use do not provide the necessary accuracy at these distances. For, using the formula for the charge distribution as given by Williamson,[3] they find that the series for the mean-square radius, in terms of the distance from the center, is not sufficiently convergent. Hence, the wave function at the larger distances would not be sufficiently accurate. In addition, they have indicated how the over-all accuracy of a derived absorption-curve can be tested in terms of the sum rules adapted for the case under consideration. They point out that these rules were not satisfied very well by the sixth-order wave function developed by Williamson. It is, of course, to be expected that the third-order wave function is no better off in these respects.

It was hoped that a higher-order Hylleraas type of wave function for the negative hydrogen ion would remove some or all of these objections to the earlier wave functions.

2. *The wave function for the ground state of* H^-.—Following Hylleraas' investigations[6] on two electron systems, we seek a wave function of the form

$$\psi = e^{-\alpha\sigma} \sum c_{a,b,c} (2\alpha)^{a+b+c} \sigma^a \tau^b v^c , \tag{1}$$

where

$$\sigma = r_1 + r_2 , \qquad \tau = r_2 - r_1 , \qquad v = r_{12} , \tag{2}$$

(r_1, r_2, and r_{12} denoting the distances of the two electrons from the nucleus and each other, respectively), and adjust the constants introduced, namely, α and $c_{a,b,c}$, in such

[1] *Ap. J.*, **89**, 295, 1939.
[2] *Ap. J.*, **91**, 202, 1940.
[3] *Ap. J.*, **96**, 438, 1942.
[4] *Ibid.*, **97**, 51, 1943.
[5] *Ap. J.*, **98**, 205, 1943.
[6] For a general account of these and related researches see Bethe, *Handb. d. Phys.*, XXIV, Part I, 353, Berlin, 1933.

a way that the energy E is minimized in accordance with the Ritz principle. In our subsequent work we shall find it convenient to measure the various quantities in Hartree's atomic units as in Bethe's article.[6] If we now let

$$s = 2a\sigma\,, \qquad t = 2a\tau\,, \qquad u = 2av\,, \tag{3}$$

we can re-write equation (1) in the form

$$\varphi(s, t, u) = e^{-s/2}\Sigma c_{a,b,c}\, s^a t^b u^c\,. \tag{4}$$

For the energy we then have (cf. Bethe, *op. cit.*, p. 357, eqs. [17.23] and [17.24])

$$E = \frac{(2a)^2 M - (2a) L}{N}\,, \tag{5}$$

where

$$L = \int_0^\infty ds \int_0^s du \int_0^u dt\,(4Zsu - s^2 + t^2)\,\varphi^2\,, \tag{6}$$

$$\left.\begin{aligned} M = \int_0^\infty ds \int_0^s du \int_0^u dt \Big\{ u(s^2 - t^2)\left[\left(\frac{\partial\varphi}{\partial s}\right)^2 + \left(\frac{\partial\varphi}{\partial t}\right)^2 + \left(\frac{\partial\varphi}{\partial u}\right)^2\right] \\ + 2s(u^2 - t^2)\frac{\partial\varphi}{\partial s}\frac{\partial\varphi}{\partial u} + 2t(s^2 - u^2)\frac{\partial\varphi}{\partial t}\frac{\partial\varphi}{\partial u}\Big\}\,, \end{aligned}\right\} \tag{7}$$

and

$$N = \int_0^\infty ds \int_0^s du \int_0^u dtu\,(s^2 - t^2)\,\varphi^2\,. \tag{8}$$

Since the wave function includes only even powers of t, all these integrals can readily be evaluated for any given form of φ in terms of the elementary integral

$$2\pi^2 \int_0^\infty ds \int_0^s du \int_0^u dt\, e^{-s} s^l t^m u^n = 2\pi^2 \left[\frac{(l+m+n+2)!}{(m+1)\,(m+n+2)}\right]. \tag{9}$$

With any given wave function, φ, it is possible to develop a series in r to represent the charge distribution. And, in accordance with the criterion developed by Chandrasekhar and Mrs. Krogdahl,[5] we wish to have such a wave function that, when the mean-square radius of the ion as a function of the contribution from various powers of r is determined, the contribution from the higher powers of r is negligible—i.e., that we have a convergent series. The actual development of this series in r is rather tedious when high powers of s, t, or u are included in the wave function. However, the mean-square radius, $\overline{r^2}$, can be expressed as

$$\overline{r^2} = \frac{R^2}{2\,(2a)^2 N}\,, \tag{10}$$

where R^2 stands for the integral

$$R^2 = \frac{1}{2}\int_0^\infty ds \int_0^s du \int_0^u dtu\,(s^2 + t^2)\,(s^2 - t^2)\,\varphi^2\,; \tag{11}$$

and it is a relatively simple matter to evaluate the contribution to the integral R^2 by any specific term in φ^2. In particular, we can determine in this manner the contribution to $\overline{r^2}$ by the term in the *highest* power of r in the formula for the charge distribution.

In the choice of the terms in the wave function (1), we shall therefore be guided by (1) the minimizing of the energy and (2) the contribution to the R^2 integral.

The general procedure for determining the constants is to solve a determinant of the form (cf. Bethe, *op. cit.*, pp. 357, 358)

$$\left|\,(2a)^2 \frac{\partial^2 M}{\partial c_{a,b,c}\partial c_{a',b',c'}} - (2a)\frac{\partial^2 L}{\partial c_{a,b,c}\partial c_{a',b',c'}} - E\frac{\partial^2 N}{\partial c_{a,b,c}\partial c_{a',b',c'}}\,\right| = 0\,. \tag{12}$$

Before we go through a definitive solution of the minimal problem by solving a high-order determinant of the form (12), it would be useful to adopt a less elaborate procedure in making decisions as to the particular terms to be used in equation (4). For example, in deciding on the further terms to be used beyond those included in Williamson's sixth-order wave function, we may assume his values for the coefficients $c_0, c_1, c_2, \ldots, c_5$ for the terms u, t^2, s, s^2, u^2, add an extra term with an unknown coefficient c_6, and determine this one constant by a Ritz method involving only the solution of a second-order determinant. Having determined c_6 by this simplified procedure, we may next consider the improvement effected in the energy E and the increment in the R^2 integral. This will give an indication of the relative importance of the particular term added. In this manner, it was found that the terms in t^4 and t^6 are the most important beyond those used by Williamson. Using these seven terms, a definitive eighth-order wave function was first obtained. And next, starting from this eighth-order wave function, further terms were tested.

TABLE 1

THE RELATIVE IMPORTANCE OF THE VARIOUS TERMS IN EQUATION (4)

Term	Cumulative Addition			Addition of Single Terms		
	c_n	E	$\Delta(\frac{1}{2}R^2)$	c_n	E	$\Delta(\frac{1}{2}R^2)$
t^2u	$+6.8\cdot10^{-5}$	-0.527484	$+40$	$+6.8\cdot10^{-5}$	-0.527484	$+40$
t^2u^2	$1.5\cdot10^{-5}$	.527497	107	$+2.1\cdot10^{-5}$	.527505	+144
t^2u^3	$9.4\cdot10^{-7}$	.527505	86	$+2.2\cdot10^{-6}$	.527533	+197
t^2u^4	$+3.0\cdot10^{-8}$	-0.527508	$+40$	$+1.5\cdot10^{-7}$	.527542	+186
t^4u	.....	.....	.....	$+1.2\cdot10^{-6}$	.527488	+ 70
t^4u^2	.....	.....	.....	$+1.7\cdot10^{-7}$	.527503	+139
t^8	.....	.....	.....	$+2.4\cdot10^{-11}$	.527482	+ 3
u^3	.....	.....	.....	$+2.3\cdot10^{-5}$	.527488	+ 34
s^3	.....	.....	.....	$+2.0\cdot10^{-6}$	.527479	+ 5
t^2s	.....	.....	.....	$+4.4\cdot10^{-5}$	.527480	+ 31
su	.....	.....	.....	$-9.0\cdot10^{-5}$	-0.527484	− 17

$E_8 = -0.527482$; $\frac{1}{2}R_8^2 = 3166$

Now, in adding these additional terms, we may proceed in one of two ways: we may determine the effect of adding only one term at a time to the eighth-order wave function; or, having determined an additional constant, we may incorporate that term in the wave function and thus add a further term to the original function. In the latter method each successive term added will, therefore, represent a correction to a higher-order wave function.

The terms tested and their contribution, $\Delta R^2/2$ to $R^2/2$, as well as the value of E obtained on both the methods outlined, are shown in Table 1. The values of E and $R^2/2$ for the eighth-order wave function are given at the foot of the table. From an inspection of the two columns giving $\Delta R^2/2$, it is seen that the use of one high-order term alone, such as the t^2u^2 term, may give about the same effect in $R^2/2$ as the use of the particular term and a lower-order term, such as t^2u^2 and t^2u.

On the basis of this table it was decided to determine a wave function of the following type:

$$\varphi = e^{-s/2}\{c_0 + c_1u + c_2t^2 + c_3s + c_4s^2 + c_5u^2 + c_6t^4 + c_7t^6 + c_8t^4u^2 + c_9t^2u^2 + c_{10}t^2u^4\}. \quad (13)$$

When equation (13) is re-written in terms of the original unit of distance, it becomes

$$\psi = e^{-\alpha\sigma}\{c_0 + \beta v + \gamma\tau^2 + \delta\sigma + \epsilon\sigma^2 + \zeta v^2 + \chi_6\tau^4 + \chi_7\tau^6 + \chi_8\tau^4v^2 + \chi_9\tau^2v^2 + \chi_{10}\tau^2v^4\}, \quad (14)$$

where

$$\left.\begin{aligned} \beta &= (2a)\,c_1\,, & \chi_6 &= (2a)^4 c_6\,,\\ \gamma &= (2a)^2 c_2\,, & \chi_7 &= (2a)^6 c_7\,,\\ \delta &= (2a)\,c_3\,, & \chi_8 &= (2a)^6 c_8\,,\\ \epsilon &= (2a)^2 c_4\,, & \chi_9 &= (2a)^4 c_9\,,\\ \zeta &= (2a)^2 c_5\,, & \chi_{10} &= (2a)^6 c_{10}\,. \end{aligned}\right\} \tag{15}$$

The expressions for $L/2$, $M/2$, $N/2$, and $R^2/2$ needed in the determination of the wave function may be written in the forms

$$\left.\begin{aligned} \tfrac{1}{2}M &= \Sigma m_{jk} c_j c_k\,, & \tfrac{1}{2}L &= \Sigma l_{jk} c_j c_k\,,\\ \tfrac{1}{2}N &= \Sigma n_{jk} c_j c_k\,, & \tfrac{1}{2}R^2 &= \Sigma r_{jk} c_j c_k\,, \end{aligned}\right\} \tag{16}$$

etc., where the coefficients m_{jk}, l_{jk}, etc., are determined by integrals of type (10). The values of these quantities are given in Tables 2–5. And, finally, values of the constants

TABLE 2

THE COEFFICIENTS IN THE SERIES $\frac{1}{2}M = \Sigma m_{jk} c_j c_k$

	c_0	c_1	c_2	c_3	c_4	c_5	c_6	c_7	c_8	c_9	c_{10}
c_0	4	25	48	32	144	96	1,152	57,600	69,120	1,536	80,640
c_1	...	64	292	135	800	700	9,768	616,320	777,240	14,168	1,040,256
c_2	...	...	960	288	1920	1920	94,464	7,603,200	8,939,520	115,200	10,521,600
c_3	...	...	...	88	1056	672	9,216	576,000	714,280	13,056	913,920
c_4	...	...	...	...	4032	4992	80,640	6,220,800	7,925,600	119,808	10,859,520
c_5	...	...	...	...	...	2496	87,552	6,912,000	8,985,600	132,864	12,902,400
c_6	...	...	...	...	...	...	4,262,400	1,074,124,800	$1.197159\cdot10^9$	9,400,320	1,302,497,280
c_7	...	...	...	...	...	...	...	97,542,144,000	$2.097156\cdot10^{11}$	$11.252737\cdot10^8$	$2.187731\cdot10^{11}$
c_8	...	...	...	...	...	...	...	...	$11.929560\cdot10^{10}$	$13.633229\cdot10^8$	$2.699241\cdot10^{11}$
c_9	...	...	...	...	...	...	...	...	...	5,998,080	$1.705329\cdot10^9$
c_{10}	...	...	...	...	...	...	...	...	...	...	$1.747398\cdot10^{11}$

TABLE 3

THE COEFFICIENTS IN THE SERIES $\frac{1}{2}L = \Sigma l_{jk} c_j c_k$

	c_0	c_1	c_2	c_3	c_4	c_5	c_6	c_7	c_8	c_9	c_{10}
c_0	11	88	156	110	660	436	3,984	205,920	283,680	6,448	458,976
c_1	...	218	928	528	3,696	2,592	31,680	2,050,560	2,824,704	51,264	4,569,600
c_2	...	...	1992	1092	8,736	6,448	205,920	17,660,160	22,475,520	283,680	30,958,848
c_3	...	...	...	330	4,620	3,052	35,856	2,265,120	3,120,480	58,032	5,048,736
c_4	...	...	...	...	18,480	24,416	358,560	27,181,440	37,445,760	580,320	60,584,832
c_5	...	...	...	...	...	9,000	283,680	22,475,520	30,958,848	458,976	50,077,440
c_6	...	...	...	...	...	...	8,830,080	2,257,113,600	2,739,340,800	22,475,520	3,486,067,200
c_7	...	...	...	...	...	...	...	$20.070167\cdot10^{10}$	$47.194723\cdot10^{10}$	2,739,340,800	$57.276012\cdot10^{10}$
c_8	...	...	...	...	...	...	...	...	$28.638006\cdot10^{10}$	3,486,067,200	$72.885797\cdot10^{10}$
c_9	...	...	...	...	...	...	...	...	...	15,479,424	$4.801421\cdot10^9$
c_{10}	...	...	...	...	...	...	...	...	...	...	$5.018979\cdot10^{11}$

TABLE 4

THE COEFFICIENTS IN THE SERIES $\frac{1}{2}N = \Sigma n_{jk} c_j c_k$

	c_0	c_1	c_2	c_3	c_4	c_5	c_6	c_7	c_8	c_9	c_{10}
c_0	16	140	192	192	1,344	768	4,608	230,400	368,640	9,216	752,640
c_1	...	384	1232	980	7,840	5,040	38,880	2,407,680	3,877,632	78,624	7,983,360
c_2	...	...	2304	1536	13,824	9,216	230,400	19,353,600	27,648,000	368,640	44,789,760
c_3	...	...	...	672	10,752	6,144	46,080	2,764,800	4,423,680	92,160	9,031,680
c_4	...	...	...	...	48,384	55,296	506,880	35,942,400	57,507,840	1,013,760	117,411,840
c_5	...	...	...	...	...	19,200	368,640	27,648,000	44,789,760	752,640	92,897,280
c_6	...	...	...	...	...	...	9,676,800	2,438,553,600	$3.251405\cdot10^9$	27,648,000	4,683,571,200
c_7	...	...	...	...	...	...	...	$21.459272\cdot10^{10}$	$5.462360\cdot10^{11}$	$3.251405\cdot10^9$	$7.326499\cdot10^{11}$
c_8	...	...	...	...	...	...	...	...	$3.663250\cdot10^{11}$	4,683,571,200	$10.627450\cdot10^{11}$
c_9	...	...	...	...	...	...	...	...	...	22,394,880	$7.664026\cdot10^9$
c_{10}	...	...	...	...	...	...	...	...	...	...	$8.767646\cdot10^{11}$

TABLE 5

THE COEFFICIENTS IN THE SERIES $\frac{1}{2}R^2 = \Sigma r_{jk} c_j c_k$

	c_0	c_1	c_2	c_3	c_4	c_5	c_6	c_7	c_8	c_9	c_{10}
c_0	768	9,072	18,432	12,288	110,592	64,512	737,280	55,296,000	85,155,840	1,382,400	162,201,600
c_1		32,256	149,760	81,648	816,480	532,224	7,539,840	679,311,360	$1.051675 \cdot 10^9$	14,256,000	$2.016368 \cdot 10^9$
c_2			368,640	184,320	2,027,520	1,382,400	55,296,000	$6.502810 \cdot 10^9$	$9.057485 \cdot 10^9$	85,155,840	$14.089420 \cdot 10^9$
c_3				55,296	1,105,920	645,120	8,847,360	774,144,000	1,192,181,760	16,588,800	2,270,822,400
c_4					6,082,560	7,096,320	115,015,680	$11.612160 \cdot 10^9$	$17.882727 \cdot 10^9$	215,654,400	$34.062336 \cdot 10^9$
c_5						2,488,320	85,155,840	$9.057485 \cdot 10^9$	$14.089420 \cdot 10^9$	162,201,600	$27.172454 \cdot 10^9$
c_6							$3.251405 \cdot 10^9$	$10.924720 \cdot 10^{11}$	$14.306180 \cdot 10^{11}$	$9.057485 \cdot 10^9$	$20.065813 \cdot 10^{11}$
c_7								$12.360541 \cdot 10^{13}$	$31.041811 \cdot 10^{13}$	$14.306180 \cdot 10^{11}$	$40.858453 \cdot 10^{13}$
c_8									$20.429227 \cdot 10^{13}$	$20.065813 \cdot 10^{11}$	$5.764908 \cdot 10^{14}$
c_9										$7.044710 \cdot 10^9$	$31.473601 \cdot 10^{11}$
c_{10}											$4.552799 \cdot 10^{14}$

obtained in the solution of the eleventh-order wave function are given in Table 6.

To normalize ψ we have the relation

$$1 = \mathfrak{N}^2 \int \psi^2 d\tau = \mathfrak{N}^2 \frac{2\pi^2}{(2\alpha)^6} N . \tag{17}$$

With the values of (2α) and N given in Table 6, we find that $\mathfrak{N} = 0.0728887$.

TABLE 6

THE CONSTANTS OF THE ELEVENTH-ORDER WAVE FUNCTION (EQ. [14]) FOR THE GROUND STATE OF THE NEGATIVE HYDROGEN ION

$E = -$	0.527559	$\frac{1}{2}L =$	28.58433
$(2\alpha) =$	1.41547	$\frac{1}{2}N =$	38.34660
$\frac{1}{2}M =$	10.09713	$\frac{1}{2}R^2 =$	3530.166

$\overline{r^2} = 22.97$

Term	Coefficients	
1	$c_0 = +1$	
u	$c_1 = +1.955378 \cdot 10^{-1}$	$\beta = +2.76778 \cdot 10^{-1}$
t^2	$c_2 = +3.221812 \cdot 10^{-2}$	$\gamma = +6.45509 \cdot 10^{-2}$
s	$c_3 = -1.114171 \cdot 10^{-1}$	$\delta = -1.57708 \cdot 10^{-1}$
s^2	$c_4 = +0.366057 \cdot 10^{-2}$	$\epsilon = +0.73342 \cdot 10^{-2}$
u^2	$c_5 = -0.545059 \cdot 10^{-2}$	$\zeta = -1.09206 \cdot 10^{-2}$
t^4	$c_6 = +1.082316 \cdot 10^{-4}$	$\chi_6 = +4.34469 \cdot 10^{-4}$
t^6	$c_7 = +0.539262 \cdot 10^{-6}$	$\chi_7 = +4.33717 \cdot 10^{-6}$
t^4u^2	$c_8 = +0.091038 \cdot 10^{-6}$	$\chi_8 = +0.73220 \cdot 10^{-6}$
t^2u^2	$c_9 = +0.090642 \cdot 10^{-4}$	$\chi_9 = +0.36386 \cdot 10^{-4}$
t^2u^4	$c_{10} = +0.136776 \cdot 10^{-6}$	$\chi_{10} = +1.10006 \cdot 10^{-6}$

The energy of H^- and He, as given by various approximate wave functions, is shown in Table 7. It will be noticed that the convergence is much slower in the case of H^- than

TABLE 7

A COMPARISON OF THE DIFFERENT APPROXIMATIONS DERIVED BY THE RITZ METHOD FOR THE WAVE FUNCTIONS FOR THE GROUND STATE OF THE NEGATIVE HYDROGEN ION AND HELIUM

ORDER	ψ	H^-			He		
		E	ΔE	$\frac{\Delta E}{E}$	E	ΔE	$\frac{\Delta E}{E}$
First	$e^{-\alpha\sigma}$	−0.473			−2.84765		
Second	$e^{-\alpha\sigma}(1+\beta v)$	.509	−0.036	0.0707	2.8912	−0.0436	0.0151
Third	$e^{-\alpha\sigma}(1+\beta v+\gamma\tau^2)$	.5253*	.0163	.0310	2.90244†	.0112	.0039
Sixth	$e^{-\alpha\sigma}(1+\beta v+\ldots+\zeta v^2)$	.52646‡	.00116	.0022	−2.90324†	−0.00080	0.0003
Eleventh	$e^{-\alpha\sigma}(1+\beta v+\ldots+\chi_{10}\tau^2v^4)$	−0.52756§	−0.00110	0.0021			
Experimental					−2.90368		

* Bethe, Hylleraas. † Hylleraas. ‡ Williamson. § This paper.

in the case of He. It is in terms of this relatively slow convergence for H^-, as compared to He, that we have to explain the discrepancy between the value of the electron affinity as estimated by Hylleraas[7] (namely, 0.02642) and the value 0.02756 (= 0.7466 electron volts) as given by our present calculations. This increase in the electron affinity over

[7] *Zs. f. Phys.*, **60**, 624, 1930; also **63**, 291, 1930.

Hylleraas' extrapolated value (and also the value 0.02646, as given by Williamson's sixth-order wave function) amounts to as much as 4 per cent.

3. *The matrix elements for the transition probability and the continuous absorption coefficient.*—The procedure in calculating the absorption coefficient is the same as that followed in Williamson's paper.[3] As has usually been done heretofore, it was assumed that, after the absorption takes place, the system can be treated as an outgoing electron represented by a plane wave function and a hydrogen atom in the ground state.[8] If the z-axis is taken in the direction of emission of the photoelectron, the only nonvanishing matrix element will be μ_z, where

$$\left.\begin{aligned}\mu_z = \frac{\mathfrak{N}}{\sqrt{2\pi}} \int\int\int\int\int\int \psi\,(z_1+z_2)\,(e^{ikz_1-r_2}+e^{ikz_2-r_1})\,r_1^2 r_2^2 \sin\theta_1 \sin\theta_2 \\ \times d\theta_1 d\theta_2 d\phi_1 d\phi_2 dr_1 dr_2\,,\end{aligned}\right\} \quad (18)$$

(k being the momentum). For the form of ψ we have assumed (cf. eq. [1]) the matrix element μ_z can be expressed in the form

$$\mu_z = \sum_{a,b,c} c_{a,b,c}\,(2\alpha)^{a+b+c}\,\mu_z\,(\sigma^a \tau^b \upsilon^c)\,, \quad (19)$$

where $\mu_z(\sigma^a\tau^b\upsilon^c)$ denotes the contribution to the integral (18) by the term involving $\sigma^a\tau^b\upsilon^c$ in ψ. The first six terms of series (19) have already been evaluated by Williamson.[3] The evaluation of the remaining terms is further simplified by the fact that our additional terms in ψ are even in r_{12}. Since

$$\upsilon^2 = r_{12}^2 = r_1^2 + r_2^2 - 2r_1 r_2 \cos\Theta\,, \quad (20)$$

where

$$\cos\Theta = \cos\theta_1 \cos\theta_2 + \sin\theta_1 \sin\theta_2 \cos(\phi_2 - \phi_1)\,, \quad (20')$$

the additional terms contain only even powers of cos Θ. For convenience we may, therefore, first consider the result of the integration over the angles θ_1, θ_2, ϕ_1, and ϕ_2 of a term $\cos^n\Theta$ in equation (18). Thus, denoting by $I(\cos^n\Theta)$ the integral

$$\left.\begin{aligned}I(\cos^n\Theta) = \int_0^{\pi}\int_0^{\pi}\int_0^{\pi}\int_0^{2\pi}\int_0^{2\pi} \cos^n\Theta\,(z_1+z_2)\,(e^{ikz_1-r_2}+e^{ikz_2-r_1}) \\ \times \sin\theta_1 \sin\theta_2 d\theta_1 d\theta_2 d\phi_1 d\phi_2\,,\end{aligned}\right\} \quad (20'')$$

we have

$$\left.\begin{aligned}I(1) &= \int_0^{\pi}\int_0^{\pi}\int_0^{\pi}\int_0^{2\pi}\int_0^{2\pi} 1\cdot(z_1+z_2)\,(e^{ikz_1-r_2}+e^{ikz_2-r_1}) \sin\theta_1 \sin\theta_2 d\theta_1 d\theta_2 d\phi_1 d\phi_2 \\ &= 4\pi^2 \int_0^{\pi}\int_0^{\pi} (r_1\cos\theta_1 + r_2\cos\theta_2)\,(e^{ikr_1\cos\theta_1 - r_2} + e^{ikr_2\cos\theta_2 - r_1}) \sin\theta_1 \sin\theta_2 d\theta_1 d\theta_2 \\ &= 8\pi^2 \left\{ r_1 e^{-r_2} \int_0^{\pi} \cos\theta_1 \sin\theta_1 e^{ikr_1\cos\theta_1} d\theta_1 + r_2 e^{-r_1} \int_0^{\pi} \cos\theta_2 \sin\theta_2 e^{ikr_2\cos\theta_2} d\theta_2 \right\};\end{aligned}\right\} \quad (21)$$

and, remembering that the expression on the right-hand side is symmetrical in r_1 and r_2 and that all product functions will also be symmetrical, we may write

$$I(1) = 16\pi^2 r_1 e^{-r_2} \int_0^{\pi} \cos\theta_1 \sin\theta_1 e^{ikr_1\cos\theta_1} d\theta_1 \quad (22)$$

[8] For the discussion of this approximation see Massey and Bates, *loc. cit.*; also Chandrasekhar and Krogdahl, *loc. cit.*, § 5.

or

$$I(1) = 32\pi^2 i \frac{r_1 e^{-r_2}}{(kr_1)^2}(\sin kr_1 - kr_1 \cos kr_1) = 2qe^{-r_2} r_1^{1/2} J_{3/2}(kr_1) , \quad (23)$$

where

$$q = 16\pi^2 i \left(\frac{\pi}{2k}\right)^{1/2}, \quad (24)$$

and

$$J_{3/2}(kr_1) = \left(\frac{2}{\pi k r_1}\right)^{1/2} \left(\frac{\sin kr_1}{kr_1} - \cos kr_1\right). \quad (25)$$

Similarly,

$$I(\cos\Theta) = 2qe^{-r_2} r_1^{1/2} J_{3/2}(kr_1) \cdot \frac{r_1^{-1} r_2}{3} \quad (26)$$

and

$$I(\cos^2\Theta) = 2qe^{-r_2} r_1^{1/2} J_{3/2}(kr_1) \cdot \tfrac{1}{3} . \quad (27)$$

In terms of these integrals the remaining terms in the matrix element can be evaluated. Thus, for the term involving $\tau^2 v^2$ we have

$$\left.\begin{aligned} \mu_z(\tau^2 v^2) &= \frac{\mathfrak{N}}{\sqrt{2\pi}} 2q \int_0^\infty \int_0^\infty e^{-(a+1)r_2 - ar_1} (r_2 - r_1)^2 \left[(r_1^2 + r_2^2) - 2r_1 r_2 \frac{r_1^{-1} r_2}{3} \right] \\ &\qquad \times r_1^{1/2} J_{3/2}(kr_1)\, r_1^2 r_2^2 dr_1 dr_2 \\ &= \frac{\mathfrak{N}}{\sqrt{2\pi}} 2q \int_0^\infty \int_0^\infty e^{-r_2/\sigma - ar_1} r_1^2 r_2^2 \\ &\qquad \times \{ r_1^4 - 2r_1^3 r_2 + \tfrac{4}{3} r_1^2 r_2^2 - \tfrac{2}{3} r_1 r_2^3 + \tfrac{1}{3} r_2^4 \}\, r_1^{1/2} J_{3/2}(kr_1)\, dr_1 dr_2 , \end{aligned}\right\} \quad (28)$$

where

$$\sigma = (a+1)^{-1} . \quad (29)$$

Using the relations

$$\int_0^\infty e^{-r_2/\sigma} r_2^n dr_2 = \sigma^{n+1} n! \quad (30)$$

and

$$\left.\begin{aligned} &\int_0^\infty e^{-ar_1} r_1^m r_1^{1/2} J_{3/2}(kr_1)\, dr_1 \\ &\quad = -\left(\frac{2}{\pi k}\right)^{1/2} (m-1)!\, \rho^m k^{-1} \{ m\rho k \cos(m+1)\xi_1 - \sin m\xi_1 \} = \Im_m , \end{aligned}\right\} \quad (31)$$

say, where

$$\rho = (a^2 + k^2)^{-1/2}; \qquad \xi_1 = \tan^{-1}\frac{k}{a}, \quad (32)$$

the result of the integrations over r_1 and r_2 in equation (28) can be written down immediately. Thus, we have

$$\mu_z(\tau^2 v^2) = \frac{\mathfrak{N}}{\sqrt{2\pi}} 2q \{ 2!\sigma^3 \Im_6 - 2 \cdot 3!\sigma^4 \Im_5 + \tfrac{4}{3} 4!\sigma^5 \Im_4 - \tfrac{2}{3} 5!\sigma^6 \Im_3 + \tfrac{1}{3} 6!\sigma^7 \Im_2 \} . \quad (33)$$

Similarly,

$$\left.\begin{aligned}\mu_z(\tau^4v^2) = 2q\frac{\mathfrak{N}}{\sqrt{2\pi}}\{&2!\sigma^3\mathfrak{I}_8 - 4\cdot 3!\sigma^4\mathfrak{I}_7 + \tfrac{19}{3}4!\sigma^5\mathfrak{I}_6 - \tfrac{16}{3}5!\sigma^6\mathfrak{I}_5\\ &+ 3\cdot 6!\sigma^7\mathfrak{I}_4 - \tfrac{4}{3}7!\sigma^8\mathfrak{I}_3 + \tfrac{1}{3}8!\sigma^9\mathfrak{I}_2\},\end{aligned}\right\} \quad (34)$$

$$\left.\begin{aligned}\mu_z(\tau^2v^4) = 2q\frac{\mathfrak{N}}{\sqrt{2\pi}}\{&2!\sigma^3\mathfrak{I}_8 - 2\cdot 3!\sigma^4\mathfrak{I}_7 + \tfrac{1}{3}4!\sigma^5\mathfrak{I}_6 - \tfrac{16}{3}5!\sigma^6\mathfrak{I}_5\\ &+ 3\cdot 6!\sigma^7\mathfrak{I}_4 - \tfrac{2}{3}7!\sigma^8\mathfrak{I}_3 + \tfrac{1}{3}8!\sigma^9\mathfrak{I}_2\},\end{aligned}\right\} \quad (35)$$

$$\mu_z(\tau^4) = 2q\frac{\mathfrak{N}}{\sqrt{2\pi}}\{2!\sigma^3\mathfrak{I}_6 - 4\cdot 3!\sigma^4\mathfrak{I}_5 + 6\cdot 4!\sigma^5\mathfrak{I}_4 - 4\cdot 5!\sigma^6\mathfrak{I}_3 + 6!\sigma^7\mathfrak{I}_2\}, \quad (36)$$

and

$$\left.\begin{aligned}\mu_z(\tau^6) = 2q\frac{\mathfrak{N}}{\sqrt{2\pi}}\{&2!\sigma^3\mathfrak{I}_8 - 6\cdot 3!\sigma^4\mathfrak{I}_7 + 15\cdot 4!\sigma^5\mathfrak{I}_6 - 20\cdot 5!\sigma^6\mathfrak{I}_5\\ &+ 15\cdot 6!\sigma^7\mathfrak{I}_4 - 6\cdot 7!\sigma^8\mathfrak{I}_3 + 8!\sigma^9\mathfrak{I}_2\}.\end{aligned}\right\} \quad (37)$$

Collecting all the foregoing terms and combining with those already given by Williamson (eq. [50] of n. 3 above), and after some minor rearranging of the terms, we obtain

$$\left.\begin{aligned}\mu_z = -(2048\pi^3)^{1/2}\mathfrak{N}\sigma^3k^{-2}i\{&5040\mathfrak{L}_8[\chi_7+\chi_8+\chi_{10}] - 720\mathfrak{L}_7[\sigma(18\chi_7\\ &+12\chi_8+6\chi_{10})] + 120\mathfrak{L}_6[(\chi_6+\chi_9)+\sigma^2(180\chi_7+76\chi_8+44\chi_{10})]\\ &-24\mathfrak{L}_5[\sigma(12\chi_6+6\chi_9)+\sigma^3(1200\chi_7+320\chi_8+320\chi_{10})]\\ &+6\mathfrak{L}_4[(\gamma+\epsilon+\zeta)+\sigma^2(72\chi_6+16\chi_9)+\sigma^4(5400\chi_7+1080\chi_8\\ &+1080\chi_{10})] - 2\mathfrak{L}_3[-(\beta+\delta)+\sigma(6\gamma-6\epsilon)+\sigma^3(240\chi_6+40\chi_9)\\ &+\sigma^5(15{,}120\chi_7+3360\chi_8+1680\chi_{10})] + \mathfrak{L}_2[1+\sigma 3\delta+\sigma^2(12\gamma\\ &+12\epsilon+4\zeta)+\sigma^4(360\chi_6+120\chi_9)+\sigma^6(20{,}160\chi_7+6720\chi_8\\ &+6720\chi_{10})] - 2\beta[\sigma\mathfrak{R}_2+6\sigma^2\mathfrak{R}_1+12\sigma^3k\rho_4\cos\xi_2 - 12\sigma^4a\\ &\times(\xi_1-\xi_2)]\},\end{aligned}\right\} \quad (38)$$

where we have introduced the functions $\mathfrak{L}_m$ and $\mathfrak{R}_m$ defined by

$$\left.\begin{aligned}\mathfrak{L}_m &= \rho^m\{m\rho k\cos(m+1)\xi_1 - \sin m\xi_1\}\\ &= -\left(\frac{\pi k}{2}\right)^{1/2}\frac{1}{(m-1)!}k\mathfrak{I}_m,\end{aligned}\right\} \quad (39)$$

and

$$\mathfrak{R}_m = \rho_4^m\{\rho_4 k\cos(m+1)\xi_2 - \sin m\xi_2\}, \quad (40)$$

where

$$\rho_4 = [(2a+1)^2+k]^{-1/2}; \qquad \xi_2 = \tan^{-1}\frac{k}{2a+1}. \quad (41)$$

The absorption cross-section per atom, k_ν, is given by

$$k_\nu = \frac{32\pi^4m^2e^2}{3h^3c}\nu v|\mu_z|^2, \quad (42)$$

where ν is the frequency and v the velocity of the photoelectron.

We have calculated μ_x in atomic units. The absorption cross-section in square centimeters per H^- ion on substituting numerical values for the constants is given by

$$\left.\begin{aligned} k_\nu = 10^{-17}\frac{\nu_{at}}{k^3}(1.1644)\{&3.10939\cdot10^{-2}\mathfrak{L}_8 - 3.94021\cdot10^{-2}\mathfrak{L}_7 \\ &+ 9.29071\cdot10^{-2}\mathfrak{L}_6 - 1.04245\cdot10^{-1}\mathfrak{L}_5 + 4.49261\cdot10^{-1}\mathfrak{L}_4 \\ &- 2.15996\cdot10^{-1}\mathfrak{L}_3 + 1.02668\mathfrak{L}_2 - 3.24146\cdot10^{-1}\mathfrak{K}_2 - 1.13886\mathfrak{K}_1 \\ &- 1.33377\rho_4 k\cos\xi_2 + 9.64738\cdot10^{-3}(\xi_1^\circ - \xi_2^\circ)\}^2 . \end{aligned}\right\} \quad (43)$$

Using this formula, we obtain the values of k_λ given in Table 8. This absorption coefficient has a maximum at about 7500 A, compared with the previous maximum at 4750 A, and at the maximum k_λ is about 30 per cent higher than Williamson's maximum value. We shall now apply the sum-rule tests to our present absorption-curve.

TABLE 8

THE CONTINUOUS ABSORPTION COEFFICIENT OF NEGATIVE HYDROGEN ION FOR DIFFERENT WAVE LENGTHS

λ (In Angstrom Units)	$\kappa_\lambda \cdot 10^{17}$ Cm^2	λ (In Angstrom Units)	$\kappa_\lambda \cdot 10^{17}$ Cm^2	λ (In Angstrom Units)	$\kappa_\lambda \cdot 10^{17}$ Cm^2	λ (In Angstrom Units)	$\kappa_\lambda \cdot 10^{17}$ Cm^2
1000.....	0.2784	4500....	2.805	7000....	3.942	10,000....	3.179
2000.....	0.9604	5000....	3.147	7500....	3.963	12,000....	1.998
2500.....	1.322	5500....	3.443	8000....	3.915	14,000....	0.8510
3000.....	1.686	6000....	3.680	8500....	3.804	16,000....	0.0807
3500.....	2.058	6500....	3.849	9000....	3.638	16,533....	0.0000
4000.....	2.436			9500....	3.427		

According to Chandrasekhar and Mrs. Krogdahl,[5] we should have

$$\overline{r^2} = 3.716a^2\int_0^{x_0}\frac{k_x}{x}\,dx\,; \qquad 2 = 1.1303\int_0^{x_0}\frac{k_x}{x^2}\,dx\,, \quad (44)$$

where a^2 denotes the square of the Bohr radius, x the wave length in units of 1000 A, and k_x the absorption coefficient in units of 10^{-17} cm^2. Using the data given in Table 8, we find that

$$3.716\int_0^{x_0}\frac{k_x}{x}\,dx = 20.77\,; \qquad 1.1303\int_0^{x}\frac{k_x}{x^2}\,dx = 1.72\,. \quad (45)$$

These values should be compared with the theoretically predicted values, namely, 22.97 (cf. Table 6) and 2. The agreement is not as good as one might have hoped. However, it appears that we must attribute the present discrepancy to errors in the absorption coefficient to the violet of 4000 A. Now, as Chandrasekhar and Mrs. Krogdahl have pointed out, the absorption coefficient of H^- in the spectral region to the red of 4500 A is predominantly governed by the wave function of the ground state of H^- at distances of the order of four or five times the Bohr radius, and at these distances the representation of the outgoing electron by plane waves must be adequate. On this basis it would seem that our present values for the absorption coefficient must be trustworthy, at least in the region λλ 4500–8000 A (i.e., in the region of primary astrophysical interest). For, judged by the criterion of the R^2 integral (§ 2), the highest power of r in the formula for the charge distribution contributes to the total value by an amount not exceeding

10 per cent; and, moreover, the coefficients of these terms do not contribute appreciably to the matrix element μ_z.[9] In addition, it is seen from Table 1 that the contribution of the higher-order term t^8 would be extremely small. It would appear, then, that it is only in the violet ($\lambda < 4000$ A) that our absorption coefficients are probably in error, and this could perhaps be attributed to the failure of the plane-wave representation for the relatively fast outgoing electrons.

4. *The relation between effective temperature and color temperature.*—The disagreement between the theory and the observations of the relation between these two temperatures has been the source of this and similar investigations. Consequently, although a complete study of this relation will not be undertaken in this paper, calculations of the reciprocal color temperature were made for two values of the reciprocal effective temperature: $\Theta_e = 5040/T = 0.5$ and $\Theta_e = 0.8$ at the wave lengths 4100 A and 6500 A and for an electron pressure of $p_e = 10^3$ bar.

Since for $\Theta_e = 0.5$ the principal contribution to the continuous absorption arises from the hydrogen atom (see Williamson, n. 4 above, Table 2), it was not necessary to compute the Rosseland mean due to H^- for this temperature. However, it was necessary to do so for $\Theta_e = 0.8$. The Rosseland mean absorption due to H^- was increased by about 25 per cent for this temperature.

The relation between the reciprocal color temperature, Θ_c, and the effective temperature was not changed for $\Theta_e = 0.5$. It was found that $\Theta_c = \Theta_e - 0.16 = 0.34$, in agreement with Williamson's calculations. However, for $\Theta_e = 0.8$, it was found that $\Theta_c = \Theta_e - 0.06 = 0.74$, as compared with Williamson's value of 0.85. This improves considerably the relation between the two temperatures, although it does not remove entirely the discrepancy when $p_e = 10^3$ bar.

The origin of this improvement in the relation between predictions of the theory and the observations is, of course, obvious. It has been known for a long time[1] that to predict the correct color-effective temperature relations, the absorption coefficient must have its maximum at about 7500 A, and this is exactly where the maximum of our present absorption-curve lies.

A complete investigation to determine the full effects of the new absorption coefficient will be undertaken in a later paper.

I wish to thank Dr. Chandrasekhar, at whose suggestion the present investigation was undertaken.

[9] In this respect the present situation is different from that resulting from the computation of the absorption coefficients with the third-order (Massey and Bates) and the sixth-order (Williamson) wave functions for H^-.

THE ULTRAVIOLET SPECTRUM OF VV CEPHEI*

OTTO STRUVE
McDonald and Yerkes Observatories
Received August 15, 1943

ABSTRACT

The ultraviolet spectrum of VV Cephei shows many emission lines of *Fe* II, *Cr* II, *Mn* II, *Ti* II, *Ni* II, *V* II, and *Fe* I, some of which are flanked on their red sides by fairly narrow absorption lines. The appearance of these lines is qualitatively similar to that of the *H* lines. The continuous spectrum shows little or no jump at the Balmer limit, showing that an appreciable portion of it, on the violet side of λ 3647, is produced by the emitting shell. Nevertheless, it is probable that the ultraviolet absorption features are produced largely in front of the blue component of the binary system. Since approximately one-quarter of a revolution has passed since mid-eclipse, it would appear that the shell envelops the entire system, as, indeed, had already been suggested by Goedicke. Attention is called to a strong absorption line at λ 3384, which is probably the ultimate line of *Ti* II and is present also in interstellar space.

The interesting spectrum of VV Cephei[1] has been described by McLaughlin[2] for the ordinary photographic region and by Christie[3] for the near ultraviolet region. Christie also found that the radial velocities vary in a period of about twenty years;[4] and Gaposchkin[5] established that the star is an eclipsing binary, consisting of an M-type supergiant whose diameter is 2400 times that of the sun and of a smaller blue star whose spectral type may be B. The spectroscopic phenomena, especially during the last eclipse of 1936–1937, have been discussed by Goedicke.[6] As a result of his work we have an excellent picture of this interesting binary system, whose combined spectrum is probably a representative of Merrill's group of "symbiotic" spectra. In the visual region the light of the M star predominates, while in the violet and ultraviolet regions the blue star is much stronger. Goedicke finds, from the degree of blurring in the absorption lines of the M-type star by the continuous spectrum of the blue star, that the two companions are equally bright near λ 4100. At λ 3900 the blue star is nearly twice as bright at the M star; yet, the evidence for classifying the blue star as belonging to type B rests solely upon the evidence from its continuous spectrum. Goedicke has shown that the absorption lines of *H* do not belong to the B star but originate in a tenuous atmosphere surrounding the system.

The character of the spectrum in the ultraviolet region, especially on the violet side of the Balmer limit, should be of considerable interest. Of several plates taken with the Cassegrain quartz spectograph of the McDonald Observatory, the best were those of July 6, 8^h37^m U.T. and July 9, 10^h15^m U.T., 1943. These plates were measured simultaneously in a measuring engine which shows the two plates side by side. The results are given in Table 1, where the wave lengths have all been corrected for the velocity of the earth but have not been corrected for the velocity of the star. The appearance of the spectrum to the red of λ 3647 resembles the spectra reproduced by Christie[3] and taken at Mount Wilson in 1933 and 1934, that is, two or three years prior to the beginning of the last eclipse. The *H* absorption lines are strong and sharp. They are easily visible to *H* 29. These lines are almost completely devoid of wings and must originate in a shell,

* *Contributions from the McDonald Observatory, University of Texas*, No. 79.

[1] HD 208816, $\alpha = 21^h53^m8$, $\delta = +63° 9'$, 1900.

[2] *Ap. J.*, **79**, 380, 1934.

[3] *Pub. A.S.P.*, **50**, 52, 1938.

[4] *Ibid.*, **45**, 258, 1933.

[5] *Harvard Circ.*, No. 421, 1937.

[6] *Pub. Obs. U. of Michigan*, **8**, No. 1, 1939; *Observatory*, **62**, 197, 1939; *Ap. J.*, **95**, 319, 1942.

as Goedicke has already concluded from his radial-velocity measurements. But the bottoms of these lines are not particularly deep: they look as though they were covered with a film of continuous light. Since this cannot be the light of the M star, we must conclude that the background is produced by the blending of the strong *H* emission lines. Although it is true that several narrow metallic absorption lines cut into the stronger portions of the *H* emissions,[7] thus showing that the emissions are not produced *above* the absorbing layer or by a source which is geometrically displaced from the absorbing layer, the conditions are definitely not similar to those in Pleione or 48 Librae, where the line background is almost clear film. I believe that this is entirely in accord with our ideas concerning the depths of the *H* lines in Pleione and 48 Librae. In these stars re-emission within the shell could be neglected. In VV Cephei this cannot be done, because the motions within the shell are almost certainly more complicated than axial rotation.

The absorption components of the *H* lines show irregular intensities near the Balmer limit. For example, *H* 22 is abnormally weak; probably *H* 26 and *H* 27 are also too weak. It is probable that, while the absorption intensities of these higher *H* lines are not greatly disturbed by the violet emission components of their *H* neighbors, they are disturbed by the violet emission components of metallic lines. Thus, *H* 22 must be weakened by the emission of *Cr* II 3678 and *H* 26 by the emission of *V* II 3669. It is not possible to say whether this observation would justify the conclusion that the emission lines of the metals are produced at a greater distance above the *B* star than the absorption lines of *H*. We know from the work of McLaughlin and Goedicke that the emission lines of *H* disappear during eclipse, while those of *Fe* II and [*Fe* II] are not affected. Hence, it does seem certain that the metallic emission does not originate below the *H* absorption.

The *H* lines have the appearance of reversed P Cygni lines. But the analogy is probably spurious: the velocities from the emission lines are strongly negative, while those from the absorption lines are somewhat larger than the velocity of the system, as determined by Goedicke, namely, − 19 km/sec.

Table 1 shows a considerable number of emission lines, most of which are fairly reliably identified with permitted lines of *Fe* I, *Fe* II, *Cr* II, *Ti* II, *Ni* II, *Mn* II, and *V* II. Among these elements *Mn* II is particularly strong. There is good evidence that a few forbidden lines of [*Fe* II] are present, but all but one are complicated by blends. Previous work had revealed the presence of *Fe* II, [*Fe* II], [*S* II], and [*Cr* II?] 3993. The new measurements show that the character of the metallic emission spectrum is not unlike that of HD 190073,[8] B 1985,[9] and WY Geminorum.[9] A direct comparison of VV Cygni with α Cygni shows that all the stronger emission lines of the former coincide with strong absorption lines of the latter, though *Mn* II and *Cr* II appear to be relatively stronger in VV Cephei. The only very conspicuous departure is in the case of λ 3438.98, which is very strong in VV Cephei and corresponds to a weak *Mn* II line in λ Cygni. The identification in VV Cephei must be incomplete.[10]

Of great interest is the fact that many emission lines in VV Cephei are flanked on their red sides by faint absorption lines. This feature gives them an appearance quite similar to that of the *H* and *Ca* II lines. In some cases I have measured only absorption lines, without corresponding emission lines. Some of them may be spurious: it is some-

[7] This was pointed out by McLaughlin in the case of *Ca* II H, which cuts into the violet emission of $H\epsilon$. There are several other similar cases.

[8] *Pub. A.S.P.*, **54**, 11, 1942.

[9] *Ap. J.*, **93**, 455, 1941.

[10] Since this was written, Swings has very kindly informed me that several hitherto unidentified emission lines in peculiar stellar spectra are due to [*Ni* II]. The strongest line in his list is λ 3439.1, and there can be no doubt that in VV Cephei this line of [*Ni* II] is largely responsible for the observed line. Other [*Ni* II] lines in VV Cephei are λ 3626.6 and λ 3559.4.

TABLE 1

ULTRAVIOLET EMISSION AND ABSORPTION LINES IN VV CEPHEI

λ	Int.	Identification
3277.03	3e	*Fe* II 77.35 (9)
3281.05	1e	*Fe* II 81.29 (7)
3302.88	0e	*Fe* II 02.86 (4) *Fe* II 03.47 (4)
3310.33	1a	*Cr* II 10.65 (35)
3312.51	1a	*Cr* II 12.18 (40) *Cr* II 11.93 (40)
3324.37	0a	(*Cr* II 24.35 (50))
3338.82	1e	(*Cr* II 39.80 (50))
3340.45	0e	*Ti* II 41.87 (300)
3347.09	3e	*Ti* II 49.03 (800)
3348.44	1e	
3351.14	0e	(*Cr* II 53.12 (20))
3352.38	2e	
3357.89	2e	*Cr* II 58.50 (75)
3359.64	3e	*Ti* II 61.21 (600)
3365.02	1e	(*Ti* II 66.18 (50))
3367.19	3e	*Cr* II 68.05 (150)
3368.12	1a	
3372.19	1e	*Ti* II 72.80 (400)
3372.60	1a	
3374.50	1a	*Ni* II 73.98 (4)
3375.72	0e	[*Fe* II] 76.2
3379.15	1e	*Ti* II 80.28 (150)
3380.48	1a	
3382.02	3e	*Ti* II 83.76 (300)
3383.59	6a	
3386.91	1e	(*Ti* II 87.84 (125); [*Fe* II] 87.1)
3393.97	1en	*Ti* II 94.57 (200)
3395.32	1a	
3399.44	1a	(*Cr* II 99.54 (18))
3401.32	1en	*Ti* II 02.42 (90)
3402.68	4e	*Cr* II 03.35 (100)
3403.46	2a	
3406.11	1e	*Ni* II 07.30 (8)
3408.10	6e	*Cr* II 08.78 (150)
3408.84	2a	
3415.56	1en	*Fe* II 16.02 (5)
3420.03	2e	*Cr* II 21.20 (75)
3422.03	6e	*Cr* II 22.76 (125)
3422.82	1a	
3425.20	1e	*Fe* II 25.58 (3)
3432.55	5e	*Cr* II 33.30 (75)
3433.57	2a	
3455.08	1en	*Fe* II 36.11 (5)
3438.75	5e	*Mn* II 38.98 (20)
3441.05	4e	*Mn* II 41.98 (100)
3443.64	1e	*Ti* II 44 31 (150)
3445.33	1an	
3447.14	0e	(*Fe* II 48.43 (1))
3453.21	1e	(*Ni* II 54.16 (5); [*Fe* II] 52.3)
3456.00	2en	(*Fe* II 56.93 (5); [*Fe* II] 55.1)
3459.53	7e	*Mn* II 60.31 (75)
3460.54	3e	*Ti* II 61.50 (125)
3461.52	1a	
3463.32	0e	*Ti* II 65.56 (60)
3465.43	1a	
3468.13	2e	*Fe* II 68.68 (8)
3468.72	0a	
3470.85	1e	*Cr* II 72.07 (25)
3471.75	2a	
3473.16	2e	*Mn* II 74.04 (50) *Mn* II 74.12 (40)
3475.58	1e	*Ti* II 77.18 (100)
3482.21	4e	*Mn* II 82.90 (40)
3487.50	3en	*Mn* II 88.68 (40)
3489.17	1a	
3490.87	1a	*Ti* II 91.05 (70)
3492.41	1e	*Fe* II 93.47 (10)
3493.25	1a	
3494.53	3e	*Mn* II 95.83 (40)
3496.63	2e	*Mn* II 97.54 (25) *Mn* II 96.81 (20)
3503.70	2en	*Ti* II 04.89 [*Fe* II] 04.0
3504.98	1a	[*Fe* II] 04.5
3507.65	1a	(*Fe* II 07.39 (3))
3513.00	1e	*Ni* II 13.93 (8)
3513.96	2a	
3517.10	0a	*V* II 17.30 (800)
3534.50	1e	*Ti* II 35.41 (125)
3544.35	0e	*V* II 45.19 (1000)
3559.35	1e	(*Cr* I 60.91 (1))
3566.27	0a	*Fe* II 66.15 (3)
3568.62	0e	*Fe* I 70.10 (300)
3569.71	1a	
3575.80	1e	*Ni* II 76.76 (3)
3576.06	0a	
3580.16	0e	*Fe* I 81.19 (1000)
3581.14	1a	
3584.52	3e	*Cr* II 85.31 (60)
3585.38	1a	
3589.46	1a	*V* II 89.74 (1000)
3600.03	1e	
3602.82	2e	*Cr* II 03.80 (40)
3603.74	2a	
3606.05	1an	*Fe* I 05.46 (300)
3607.78	1e	*Fe* I 08.86 (500)
3612.28	1e	*Cr* II 13.21 (20)
3614.39	1e	*Fe* II 14.87 (5)
3616.88	1e	*Fe* I 18.77 (400)
3620.15	2e	*Fe* II 21.27 (6)
3622.50	2e	*Ti* II 24.83 (125)
3624.64	2a	
3626.63	3en	([*Fe* II] 25.8)
3627.91	2a	(*Ti* II 27.71 (12))
3630.54	3en	*Cr* II 31.49 (50)
3631.70	1a	*Cr* II 31.72 (40)
3640.61	0e	*Ti* II 41.33 (150)
3641.26	1a	
3659.61	0a	*Ti* II 59.76 (150)
3663.43	1a	*H* 29 63.40
3664.80	3a	*H* 28 64.68

TABLE 1—*Continued*

λ	Int.	Identification	λ	Int.	Identification
3666.05.....	0a	*H* 27 66.10	3714.23.....	2e	*Cr* II 15.19 (20)
3667.47.....	1a	*H* 26 67.68	3715.51.....	1a	*Cr* II 15.45 (20)
3669.33.....	2a	*H* 25 69.47	3719.69.....	1a	*Fe* I 19 93 (1000)
3671.34.....	4a	*H* 24 71.48	3720.75.....	7e	*H* 14 21.95 (6)
3673.68.....	4a	*H* 23 73.76	3722.04.....	7a	
3676.21.....	3a	*H* 22 76.36	3724.18.....	1a	
3677.70.....	1a	*Cr* II 77.86 (50) *Cr* II 77.69 (40)	3727.80.....	2a	*Fe* I 27.62 (200)
			3730.53.....	1a	
3679.35.....	6a	*H* 21 79.35.	3733.16.....	8e	*H* 13 34.37 (8)
3679.99.....	3a		3734.37.....	10a	
3682.72.....	5a	*H* 20 82.81	3737.87.....	3an	*Fe* I 37.13 (1000)
3685.06.....	0a	*Ti* II 85.19 (700)	3742.75.....	3a	*Ti* II 41.64 (200)
3686.75.....	6a	*H* 19 86.83	3745.62.....	3a	*Fe* I 45.56 (500)
3691.60.....	6a	*H* 18 91.56 (2)	3748.12.....	8e	*H* 12 50.15 (10)
3695.90.....	4e	*H* 17 97.15 (3)	3749.95.....	9a	
3696.97.....	6a		3748.29*....	1a	*Fe* II 48.49 (8)
3700.07.....	1a	*Fe* I 01.09 (300)	3753.31.....	1a	*Cr* II 54.59 (20)
3702.71.....	8e	*H* 16 03.86 (4)	3762.63.....	1an	*Ti* II 61.32 (300)
3703.68.....	7a		3766.18.....	1an	*Cr* II 65.62 (8) *Cr* II 66.65 (2)
3705.92.....	2a	(*Ca* II 06.03 (40))			
3708.83.....	1a	*Fe* I 07.82 (80) *Fe* I 07.92 (80)	3768.79.....	10e	*H* 11 70.63 (15)
			3770.55.....	10a	
3710.63.....	8e	*H* 15 11.98 (5)			
3711.80.....	6a				

*This absorption line is superposed over *H* emission.

times very difficult to decide whether one is concerned with an absorption line or with a space between two emission lines. The most conspicuous absorption line is at λ 3384, which can only be identified with *Ti* II 3383.76(300). This is the famous ultimate line of *Ti* II which is conspicuous in interstellar space ($a^4F_{1½} - {}^4G^0_{2½}$). The line is noticeably broadened in VV Cephei and is probably not all of interstellar origin. It is perhaps enhanced in the tenuous shell which gives rise to the forbidden lines of [*Fe* II], [*S* II], and [*Cr* II] and to the many permitted emission and absorption lines of other atoms. Since the other members of this multiplet of *Ti* II are present in emission and at least one of them, λ 3372.80(400), is weakly present in absorption, the enhancement of λ 3384 is not so great as it is in interstellar space. The excitation potential of the lower level of λ 3373 is 0.012 volt; that of λ 3384 is exactly zero. The lines λ 3349 and λ 3361 of the same multiplet are present in emission and probably in absorption, though I did not measure them for fear of confusing them with neighboring emission features. As Dunham has pointed out, in laboratory sources the line λ 3384 is not the strongest member of the multiplet. Hence its great strength in VV Cephei is abnormal. How much of this is contributed by interstellar absorption is not known, though if the distance is greater than 1000 parsecs, as Goedicke concludes from his discussion, it may be appreciable. But the observed intensity of λ 3384 is much greater than in any distant B-star heretofore observed at the McDonald Observatory.

The emission and absorption features on the violet side of λ 3647 are superposed over a continuous spectrum which shows no conspicuous discontinuity at the Balmer limit. Evidently, the continuous *H* emission fills in, to a large extent, the depression caused by continuous Balmer absorption in the shell or in the B star.

We conclude that, with the exception of the continuous spectrum, we have as yet not observed features belonging to the B star. Even the continuous spectrum is vitiated by continuous emission from the shell on the violet side of λ 3647. The absence of absorption lines belonging to the B star is not unusual and need not throw doubt upon

the interpretation given by Gaposchkin and by Goedicke. The ultraviolet lines of the B star may be too faint and too broad to show on the mottled spectrum of the shell.

Table 2 lists the radial velocities as determined from the various lines which I have measured. The remarkable violet displacement of the emission lines of *H* is a puzzle which has not, as yet, been solved. Although McLaughlin has shown that V/R varies between 4 and 0.8, values greatly in excess of 1 are apparently common at all phases.

TABLE 2

RADIAL VELOCITIES IN VV CEPHEI ON JULY 9, 1943

Atom	No. of Lines	Radial Velocity	Atom	No. of Lines	Radial Velocity
H emission	7	−115.4 km/sec	*Cr* II, *Ti* II, *Ni* II, *Mn* II, *V* II, *Fe* I, emission	45	−92.3
H absorption	19	− 6.6	*Cr* II, *Ti* II, *Ni* II, *Mn* II, *V* II, *Fe* I, *Fe* II, absorption	40	+ 3.1
Fe II emission	10	− 51.2			
[*Fe* II] emission	1	− 42.3			

It is extraordinary that the red components should be so effectively blotted out. The McDonald spectrograms show that the higher absorption members of the Balmer series, though fairly narrow, are not symmetrical. They have steep edges on their violet sides and shade off more gradually on their red sides. Some lines actually look double, with a faint red absorption component flanking the strong red component. There can be no doubt that these red components or wings absorb most of the light of the underlying red emission components. This is not inconsistent with McLaughlin's ideas on this subject, though the observations fail to show where in the shell the red absorption components originate. It is regrettable that we have no definite observations of V/R from maximum to minimum radial velocity of the M star. The Victoria observations by Harper cover this interval.

PLATE II

THE SPECTRUM OF VV CEPHEI

PLATE III

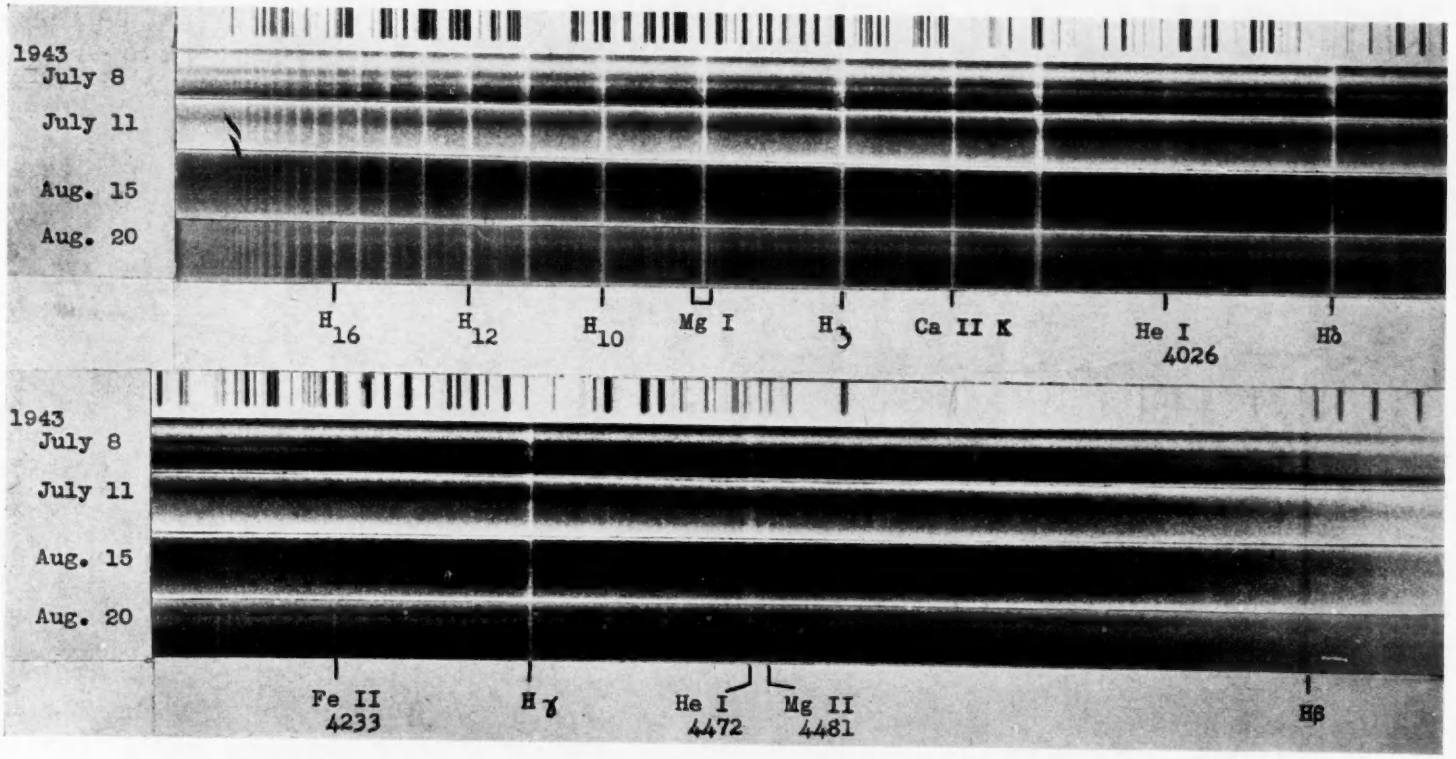

THE SPECTRUM OF HD 218393

RAPID CHANGES IN THE SPECTRUM OF HD 218393[1]

OTTO STRUVE
McDonald and Yerkes Observatories
Received September 15, 1943

ABSTRACT

Observations made in July, August, and September, 1943, at the McDonald Observatory show a series of changes in the spectrum which are very similar to those observed in AX Monocerotis. The *H* absorption lines become double at irregular intervals of 11–18 days, with the violet components always much weaker than the red components. On one occasion changes were observed in these components within an interval of 1 hour. *Hβ* and several other low *H* lines have P Cygni structure, but the higher members of the Balmer series show strong cores whose velocities vary in a somewhat regular manner between + 45 km/sec and −60 km/sec. Maximum occurred on July 22 and August 27, while minimum occurred on August 5 and September 3; but the rise toward maximum was slower than the decline, so that the period, if there is one, may be of the order of 30 days. There were variable α Cygni lines, which were strongest in the middle of July and again in the latter half of August. Their intensities changed from one day to the next. The *He* I lines are broad and very diffuse. Their velocities are always negative (from −22 to −180 km/sec). It is suggested that the star is a rapidly rotating main-sequence object of early B type with exceptionally powerful prominence activity. This prominence action would explain the surges affecting rotationally broadened *He* I and sharp *H* and would account for the formation of the shell of gas.

This star was classified at Harvard as A5p, while Merrill proposed Ave and Harper B9p. It is MWC 397 in the catalogue of Be stars by Merrill and Burwell.[2] Earlier descriptions have been given by Merrill,[3] by Harper,[4] and by Swings and Struve.[5] The *Henry Draper Catalogue* remarks: "The lines are very narrow and the intensities resemble those in the spectrum of α Cygni." The variability of the α Cygni lines and the large differences in the radial velocities obtained from different lines have already been commented upon by Merrill. The identification of the spectrum as that originating in an extended atmosphere, or shell, was made by Swings and Struve.

The general appearance of this spectrum (see Pl. III) resembles that of AX Monocerotis, in which very rapid transitions from double hydrogen absorption lines to single lines and from a strong α Cygni spectrum to complete absence of the usual metallic lines have been observed.[6] In order to find whether HD 218393 shows similar rapid fluctuations in spectrum, we obtained a series of plates in the summer of 1943, using the Cassegrain quartz spectrograph of the McDonald Observatory, equipped with a 500-mm camera. The linear dispersion at λ 3933 was 40 A/mm. The plates extend far into the ultraviolet region, where the dispersion is about 20 A/mm. They are somewhat overexposed between about λ 4100 and λ 4700. A chronological description of the plates follows:

July 6. The *H* absorption lines are strong and sharp and are visible to *H* 24 or *H* 25. The stronger lines have distinct violet components and are clearly double. The *He* I lines are exceedingly broad and diffuse; *Mg* II 4481 is not quite so broad and is weak. *Ni* II 3513 is fairly strong and moderately sharp. There are a few very faint, moderately narrow lines of *Fe* II, *Ti* II, and *Cr* II. *Ca* II is very strong. The emission at *Hβ* is strong, broad, and all on the red side

[1] *Contributions from the McDonald Observatory, University of Texas*, No. 80.

[2] $\alpha = 23^h2^m6$; $\delta = +49°40'$ [1900]; ptm. mag., 6.85.

[3] *Ap. J.*, **72**, 109, 1930; **78**, 109, 1933.

[4] *Pub. Dom. Ap. Obs. Victoria*, **7**, 94, 1937.

[5] *Ap. J.*, **91**, 590, 1940.

[6] *Ap. J.*, **98**, 212, 1943.

of the $H\beta$ absorption line. There is a faint red emission line at $H\gamma$. There is a faint suspicion of somewhat diffuse *Si* II. The great widths of *He* I and the intermediate widths of the relatively weak lines of *Mg* II and *Si* II stamp this spectrum as that of a shell with appreciable dilution and a large range in observed rotational velocities.

July 7. The strong *H* absorption components are weaker but are still visible to *H* 25. The violet components are much more conspicuous and are broader than on the preceding plate. The metallic lines have disappeared, except *Ni* II 3513. *Ca* II looks weaker but is still conspicuous. There may be some slight weakening in the *H* emission.

July 8. The stronger *H* components are conspicuous and sharp, while the violet components are more compact and less diffuse than on July 7. There is again a trace of *Ni* II and *Fe* II. The $H\beta$ emission is very narrow and much weaker than before.

July 9. The stronger *H* components are very intense and sharp but can be seen only to *H* 23 or *H* 24. The violet components are barely visible. *Fe* II is absent, and *Ni* II probably absent. *Ca* II is strong, and the $H\beta$ emission is stronger and broader.

July 11. The *H* lines are single and very strong and are visible to *H* 27. The stronger α Cygni lines are beginning to show, with *Ni* II 3513 fairly strong and *Fe* II weak and diffuse. The *Si* II lines are also weakly present, with the ultraviolet group slightly diffuse and the $\lambda\lambda$ 4128–4131 pair more so. There is no appreciable change in *Mg* II 4481. *Ca* II is strong. The $H\beta$ emission is not quite so strong as on July 9.

July 12. The α Cygni lines are now quite conspicuous, though they are much weaker than in an A2 supergiant. The ultraviolet group of *Si* II lines is fairly sharp, while the $\lambda\lambda$ 4128–4131 pair is distinctly diffuse. This resembles an observation in AX Monocerotis and suggests that the phenomenon has an important physical origin: the ultraviolet lines behave more nearly like lines originating in metastable levels than do the $\lambda\lambda$ 4128–4131 pair. Again, as in AX Monocerotis, the *Si* II 4128–4131 pair is less subject to broadening than is *Mg* II 4481. The α Cygni lines are sharper than on July 11. Bright $H\beta$ is strong and broad. It may be double with a weaker portion in the violet and a strong absorption line to the violet of this feature.

July 13. The α Cygni lines are still stronger, and *Fe* II is sharper than before, while *Ti* II remains slightly diffuse. The ultraviolet *Si* II are sharp, and the $\lambda\lambda$ 4128–4131 pair is diffuse. The *H* absorption lines are still single and very sharp. *Ca* II is very strong.

July 14. The strong *H* absorption components have faint violet extensions, showing that a new stage of double lines is forming. The α Cygni lines are much weaker, though some of the stronger *Fe* II lines are visible, while *Ni* II 3513 is very weak. The $H\beta$ emission is weaker and narrower. *Ca* II remains strong.

July 18. The α Cygni lines have reappeared with greater intensity than previously and almost resemble α Cygni, except for the broadening, which is greater in HD 218393, and for the usual dilution effects. There is a suspicion that the strongest *Fe* II lines are sharper than the other α Cygni lines. The *H* lines are still double, but the violet components are inconspicuous. The strong red *H* components and the *Ca* II lines are somewhat diffuse at the edges. Bright $H\beta$ is normal.

July 20. The α Cygni lines are somewhat weaker than on July 18. The violet components of the *H* lines have nearly disappeared, but the remaining components of *H* and the strong *Ca* II lines are fairly broad and diffuse at the edges. Bright $H\beta$ is strong and broad.

July 22. The α Cygni lines are very weak; and only the strongest *Fe* II, *Ti* II, *Ni* II, and *Mg* I lines are visible. The *H* lines perhaps have again very weak violet components; and the red components, together with the *Ca* II lines, are sharp. Bright $H\beta$ is strong and broad.

July 24. The α Cygni lines are weak but perhaps a little stronger than on July 22. The *H* lines are single and sharp. *Ca* II is strong, narrow, and sharp. Bright $H\beta$ is double with a weak component on the violet and a stronger and fairly narrow component on the red. It resembles the line observed on July 12. A rather diffuse and faint absorption line is on the violet side of the violet emission component. The *Si* II lines, though weak, consistently show the members of the ultraviolet group to be sharper than the λλ 4128–4131 pair.

July 28. The α Cygni lines are again weaker, and only the strongest of *Fe* II, *Ti* II, and *Mg* I are visible. The *H* absorption lines are narrow and single and perhaps weaker than on preceding dates. There seems to be some slight shading of the absorption toward the violet, but there are no violet components. Bright $H\beta$ is very weak and shows no structure.

July 29. The α Cygni lines are about the same. The violet shading of the *H* absorption cores is more conspicuous, but there are no violet components. The *He* I lines and *Mg* II 4481 are stronger and somewhat easier to measure than at any time this month. Bright $H\beta$ is weak and looks similar to that observed on July 24.

Aug. 5. The *H* absorption lines have strong violet components of considerable breadth. These are not completely separated from the stronger red cores. The violet $H\epsilon$ component is absent or very weak, although it should extend beyond the violet edge of *Ca* II H, which merges with the red core of $H\epsilon$. This phenomenon resembles that observed in AX Monocerotis, but the evidence in this case is much less convincing because *Ca* II is strong in HD 218393. The α Cygni lines are absent. Bright $H\beta$ is weak; but the cutoff on the red edges of the red *H* absorption cores is very sharp from $H\gamma$ to about *H* 11, showing that the red emission is actually present.

Aug. 6. The violet absorption components of the *H* lines have almost disappeared, except at $H\zeta$; and the red cores are sharp and strong. The α Cygni lines are absent, including *Ni* II 3513, which was visible on July 7 but had disappeared by July 9. Bright $H\beta$ is narrow and single.

Aug. 7. The strong *H* absorption cores show a very faint shading toward the violet, which extends over about 5 A from the cores. There may be a trace of the strongest α Cygni lines of *Fe* II and *Mg* I. Bright $H\beta$ is double with a strong red and a very weak violet component.

Aug. 8. The shading or doubling of the *H* absorption lines is still present. The α Cygni lines are absent, except *Ni* II 3513, which is present as a narrow absorption line. Bright $H\beta$ is now conspicuously double, with $R/V = 3$.

Aug. 9. The *H* cores are single and very sharp. A few of the stronger α Cygni lines are weakly present. Bright $H\beta$ is conspicuously double, with $R/V = 1.5$.

Aug. 13. The *H* cores are single and very sharp. The lines of *Fe* II, *Ti* II, and *Si* II are absent or vanishingly weak, while *Ni* II 3513 is fairly strong. Bright $H\beta$ is single, resembling a line of the P Cygni type.

Aug. 14. The *H* cores are single but may be shaded toward the violet. *Ni* II is strong; and there is a trace of *Fe* II and *Si* II, but not of *Ti* II. Bright $H\beta$ is unchanged.

Aug. 15. The *H* cores are single and very narrow. *Ni* II 3513 is very strong; but there is no evidence of the other α Cygni lines except for the *Ca* II lines, which are always present in great strength. Bright $H\beta$ is single and strong.

Aug. 20. There is no change in the *H* cores, but the α Cygni lines are present with great intensity. They are much stronger than on July 12 and 13 and slightly stronger

than on July 18, when they were last seen with considerable strength. On August 20 they were comparable in intensity to the lines of α Cygni. The strengthening involved *Ti* II, *Fe* II, *Cr* II, *Fe* I, and probably *Mg* II. On the other hand, *Ni* II 3513 is a little weaker than on August 15. The transformation of the spectrum from August 15 to August 20 is one of the most remarkable stellar variations on record. The bright $H\beta$ line is somewhat weaker than on August 15 and is double, with $R/V = 4$. The general strengthening of the α Cygni lines involved a noticeable increase in the intensity of *Ca* II.

Aug. 21. The α Cygni lines are very noticeably weaker and look more diffuse than on August 20. The *H* cores are also weaker and more diffuse than before. Bright $H\beta$ is weak, single, and diffuse.

Aug. 23. The α Cygni lines are somewhat stronger than on August 21 but much weaker than on August 20. The *H* cores have fairly conspicuous violet components. Bright $H\beta$ is diffuse and fairly strong.

Aug. 25. No appreciable change except that the violet components of *H* absorption cores have almost vanished. *Ca* II K is very strong, equaling $H\zeta$ in intensity.

Aug. 26. Almost no change. Bright $H\beta$ is double, with $R/V = 3$.

Aug. 27. Little change. *Ca* II K is very strong. The violet components of the *H* absorption components are a little stronger, and the duplicity of bright $H\beta$ is barely suspected.

Aug. 28. No change.

Aug. 29. The α Cygni lines are much weaker, but *Ca* II K is very strong. *H* bright. $H\beta$ is double and diffuse, with $R/V = 1.5$. The *Si* II lines again show the ultraviolet group sharp and the pair at $\lambda\lambda$ 4128–4131 somewhat diffuse.

Aug. 30. The α Cygni lines are very weak, and only a few of the strongest are visible. Bright $H\beta$ is single, strong, and diffuse.

Sept. 3. No change.

Sept. 4. The α Cygni lines are again a little stronger, though *Fe* II is weak, while *Fe* I is relatively stronger than is usual. *Mg* I is also prominent, and *Si* II 4128, 4131 is fairly strong, but the ultraviolet *Si* II lines are weak. The *H* cores are single and sharp. *Ca* II is of the usual intensity, and bright $H\beta$ is single and diffuse.

Sept. 5. The α Cygni lines have almost disappeared. Bright $H\beta$ is double, with $R/V = 1.5$. There is a very narrow absorption line between the emission components and a stronger and broader absorption line on the violet side of the violet emission component. The *H* cores are single and sharp.

Sept. 6. The α Cygni lines are invisible, except for faint traces of *Si* II. The *H* absorption cores have broad and indistinct violet wings, which may be partly due to the Stark-effect wings of the underlying stellar lines. The bright $H\beta$ is indistinct and faint but probably resembles in structure that of September 5.

Sept. 7. The violet components of the *H* cores are more distinct and no longer look like Stark-effect wings. At 4:14 U.T. the violet component of $H\zeta$ was very strong and sharp, obviously because of reinforcement from *He* I 3888. Its intensity was roughly one-half of that of the red component. At 5:14 U.T. the violet component was much weaker, although it was still visible. This change within 1 hour's time is the most rapid yet observed in this star. Apparently the strengthening of the line at 4:14 U.T. was due to increased prominence action rich in *He* I. The α Cygni lines are weakly present. *Ni* II 3513 is very weak. Bright $H\beta$ is probably double, with $R/V = 1.5$. The strengthening of the violet component of $H\zeta$ by *He* I is a phenomenon which was conspicuous in AX Monocerotis but is only occasionally observed in HD 218393.

Sept. 8. The α Cygni lines are slightly stronger. Four plates were obtained at 3^h51^m, 4^h04^m, 6^h50^m, and 11^h45^m. On the first three exposures the *H* cores are sharp

and single, in contrast to the two plates taken on the preceding night. On the fourth plate there is again a weak violet component at $H\zeta$ and probably at several other H lines. On the first plate bright $H\beta$ is double, with $R/V = 1.0$; but the narrow central absorption is exceedingly weak. On the other plates the duplicity is not clearly seen, but this may not represent a real change.

Sept. 12. The α Cygni lines are vanishingly weak. The H cores are single and strong. $H\beta$ is double, with $R/V = 0.7$. As usual, there is a fairly strong but diffuse absorption line on the violet side of the violet emission components. The two plates taken on this night clearly show a phenomenon which I had strongly suspected on many other plates: the strong absorption cores of $H\gamma$, $H\delta$, and sometimes $H\zeta$ are flanked on both sides by what looks like faint absorption components at distances of several angstrom units from the central cores. These components are probably identical with similar negative and positive H absorption components measured by J. S. Plaskett in several other peculiar stars. There can be no doubt that in HD 218393 they are caused by weak double emission lines, which in the case of $H\beta$ stand out as such above the intensity of the continuous spectrum but which in the case of $H\gamma$ and $H\delta$ look like narrow strips of continuous spectrum. It is also clear that the abnormal behavior of the radial velocities of $H\gamma$, $H\delta$, $H\epsilon$, and perhaps $H\zeta$, as compared to the higher members of the Balmer series, is caused by blending with emission components of appreciable intensity—even though these components cannot be seen as such.

Sept. 13. The α Cygni lines are very weak but may be a trace stronger than on September 12. The bright $H\beta$ line is conspicuously double, with $R/V = 0.5$. The reversal in the intensities of the bright components from the usual $R > V$ to $R < V$ is of interest, though it is apparently not correlated with other variations in the spectrum.

Sept. 14. No change except that the components of the bright $H\beta$ line give $R/V = 0.8$.

Sept. 15. No appreciable change, but the α Cygni lines are vanishingly weak. Bright $H\beta$ gives $R/V = 1.0$.

Table 1 gives the measured radial velocities for all the 51 plates. The spectrum is characterized by very rapid changes. The H lines are sometimes clearly double, with the weaker components always on the violet side. These components appear very suddenly and vanish within a few days. On some plates there may be a suspicion that the violet components are not separate lines but really represent the violet portions of broad Stark-effect wings of the underlying stellar lines. This is possible because the red wings are covered by the red emission lines of H. But this explanation can apply to only a few plates on which the violet components were seen to be very weak. There is no question about the reality of the outbursts, which again (as in the case of AX Monocerotis) suggests strong prominence activity. The principal absorption cores of the higher H lines show conspicuous and fairly smooth changes in radial velocity, and a very rough period of about 30 days is indicated with slow rise to maximum on July 22 and August 27 and rapid decline to minimum on August 5 and September 3. But it is quite probable that the variations do not have a real period and merely repeat themselves approximately every few weeks (see Fig. 1). The doubling of the H lines occurs at irregular intervals of 11–18 days. As far as we can tell from the limited amount of material now at our disposal, there is no direct relation between the tendency to show violet-displaced components and the radial velocity of the strong red components.

The α Cygni lines are variable in intensity and velocity, and there seems to be a correspondence between these variations and those of the H absorption lines. The *He* I lines are exceptionally broad and difficult to measure. The amazing violet displacement of

TABLE 1

Radial Velocities of HD 218393

Date	U.T.	*H* (λλ 3666–3835)	*Hζ*	*He*	*Hδ*	*Hγ*	*He* I	*Mg* II	*Ca* II	*Si* II	*Fe* II	*Mg* I	*Ni* II, *Ti* II *Cr* II, *Fe* I *V* II, *Sc* II *Mn* II
1943 July 6....	7:55	16 − 4 (10) 11 −150 (2n)	− 10 (10) −164 (3)	− 7 (8)	− 9 (9) −148 (1)	− 24 (8) −176 (2)	4 − 82 (1n)	.....	2 − 4 (8)	.....	.....	.....	3 −60 (1)
7....	9:16	17 0 (5) 9 −138 (1n)	− 10 (10) −162 (1n)	−10 (8)	− 5 (8) −126 (1)	− 39 (8)	1 −103 (1n)	.....	2 −21 (7)	.....	.....	.....	1 + 4 (1)
8....	10:28	17 + 2 (10) 6 −170 (2)	− 7 (10) −193 (2n)	−25 (9)	− 12 (10) −152 (1n)	− 12 (10) −229 (2)	2 −112 (1n)	−55 (1n)	2 −10 (8)	.....	.....	.....	1 0 (1)
9....	6:39	15 − 3 (10)	− 13 (10)	−10 (10)	− 18 (10)	− 35 (10)	2 −178 (1nn)	−26 (1nn)	2 −18 (8)	.....	.....	.....	.....
11....	8:30	18 0 (15)	− 16 (12)	− 5 (10)	− 15 (10)	− 28 (8)	2 −116 (2nn)	−47 (1n)	2 − 1 (9)	2 +16 (0n)	1 −14 (1n)	1 +13 (1n)	1 + 1 (2n)
12....	7:16	17 + 15 (10)	− 2 (12)	− 1 (10)	− 5 (10)	− 12 (8)	2 − 69 (2nn)	+10 (2n)	2 0 (10)	5 +12 (1n)	10 +10 (2)	3 +28 (2)	12 +21 (1n)
12....	7:58	19 + 13 (10)	+ 1 (10)	+11 (9)	− 5 (10)	− 24 (8)	1 − 38 (1nn)	−10 (1nn)	4 + 9 (10)	5 +18 (1)	7 +10 (2)	2 + 8 (2)	27 +12 (2)
13....	7:20	18 + 10 (10)	− 2 (10)	+ 5 (10)	− 12 (9)	− 31 (8)	2 − 64 (2nn)	−14 (1nn)	2 + 3 (9)	4 +33 (0n)	5 +15 (3)	2 +18 (1)	10 +13 (3)
13....	8:17	19 + 10 (10)	+ 1 (10)	+11 (10)	− 9 (9)	− 16 (8)	3 − 60 (1nn)	+47 (1nn)	4 +29 (9)	4 +28 (1)	6 0 (4)	3 + 7 (2)	14 + 9 (3)
14....	7:47	16 + 13 (10) 6 −103 (1)	+ 1 (10) −108 (1)	+ 2 (10)	− 5 (10) −102 (1)	− 9 (9) −146 (1)	3 − 64 (1nn)	−14 (1nn)	2 + 3 (9)	2 +30 (1n)	2 +25 (1)	2 +26 (1)	1 +28 (1)
14....	8:50	17 + 17 (6) 2 − 97 (1)	− 2 (10) −140 (1)	+17 (10)	+ 5 (9) −135 (1)	− 16 (8)	2 − 67 (2nn)	+ 6 (1nn)	2 − 3 (10)	3 +34 (1n)	2 +22 (1)	2 +39 (1)	.....
18....	8:55	13 + 34 (10) 1 −143 (2)	+ 9 (10) −173 (2)	+ 7 (10)	− 2 (8) −159 (1)	− 20 (7) −214 (2)	2 −105 (2nn)	+51 (1nn)	2 − 5 (10)	3 +56 (1n)	6 +41 (3)	2 +73 (2)	12 +48 (2)
20....	9:02	15 + 42 (10)	+ 18 (10)	+13 (10)	+ 14 (9)	− 20 (7)	2 − 82 (3nn)	+58 (2nn)	2 +12 (10)	2 +77 (1)	10 +54 (3)	2 +73 (1)	8 +49 (1)
22....	7:53	15 + 45 (10)	+ 27 (10)	+22 (10)	+ 28 (9)	− 13 (8)	.....	.....	2 + 6 (10)	.....	1 +62 (1)	2 +69 (1)	4 +24 (2)
24....	11:04	15 + 4 (10)	− 3 (10)	+10 (10)	− 2 (10)	− 17 (8)	2 − 82 (1nn)	+ 9 (1nn)	2 +15 (9)	2 +24 (1)	5 +14 (1)	2 +10 (1)	2 +12 (0)
28....	5:53	16 + 2 (10)	− 14 (10)	−14 (9)	− 6 (10)	− 21 (8)	2 −115 (2nn)	−16 (1nn)	2 −10 (9)	2 + 6 (1)	2 + 6 (2)	2 +18 (1)	2 − 8 (1)
29....	6:55	16 − 27 (10)	− 29 (10)	−21 (8)	− 30 (10)	− 33 (10)	2 −109 (3n)	−56 (2n)	2 −18 (9)	2 −21 (1)	2 −34 (1)	1 −16 (1)	2 −41 (1n)
Aug. 5....	7:37	11 − 62 (7) 3 −236 (2n)	− 59 (10) −264 (2n)	−62 (10)	− 47 (8) −214 (3)	− 56 (8) −193 (1)	2 −180 (3nn)	−41 (1nn)	1 −29 (6)	.....	.....	.....	.....
6....	8:40	13 − 35 (10) 2 −155 (1)	− 36 (10) −148 (1)	−31 (10)	− 41 (10)	− 52 (10)	2 − 95 (2nn)	.....	2 −13 (8)	.....	.....	.....	.....
7....	7:32	13 − 32 (10)	− 33 (10)	−28 (10)	− 31 (10)	− 37 (10)	2 − 58 (2nn)	+ 4 (1n)	2 −14 (7)	.....	1 − 5 (1)	.....	.....
7....	8:41	13 − 33 (10) 3 −236 (1)	− 31 (10) −202 (1)	−22 (10	− 31 (10) −185 (1)	− 42 (10) −205 (1)	2 −127 (2nn)	+12 (1n)	1 −23 (9)	.....	.....	.....	.....
8....	8:12	13 − 35 (10)	− 21 (10)	−28 (10)	− 25 (10)	− 31 (10)	2 −104 (2nn)	−54 (1nn)	2 −27 (9)	.....	.....	.....	1 −18 (1)
9....	9:44	13 − 25 (10)	− 31 (10)	−19 (10)	− 31 (10)	− 34 (10)	2 −102 (2nn)	−25 (1nn)	2 −23 (9)	.....	1 −31 (1)	.....	1 −11 (1)
13....	5:58	13 − 18 (10)	− 25 (12)	−23 (10)	− 29 (10)	− 38 (10)	2 − 44 (2nn)	−67 (1nn)	2 −16 (8)	.....	1 −56 (1)	.....	3 −36 (2)
14....	6:07	13 − 26 (10)	− 29 (12)	−26 (10)	− 29 (10)	− 43 (8)	2 − 93 (2nn)	−59 (1nn)	2 −23 (8)	.....	1 −46 (1)	.....	1 − 4 (1)
15....	6:58	13 − 21 (9)	− 32 (10)	−17 (8)	− 32 (10)	− 39 (9)	2 −134 (1nn)	.....	2 −11 (7)	.....	.....	.....	1 −12 (4)
20....	7:45	13 − 9 (10)	− 21 (10)	−22 (10)	− 23 (10)	− 36 (8)	2 − 90 (2nn)	+ 9 (3n)	2 −13 (9)	4 +15 (2)	14 + 5 (3)	3 + 6 (2)	29 +10 (2)
21....	5:35	13 + 2 (10)	− 4 (12)	−16 (8)	− 10 (7)	− 33 (6)	3 − 71 (2nn)	− 7 (1nn)	2 −10 (8)	3 +51 (1n)	5 +12 (3)	.....	7 +35 (1)
23....	9:27	13 + 2 (10)	− 13 (10) −220 (2)	−10 (10)	− 15 (9) −208 (2)	− 18 (9) −201 (3)	3 −122 (3nn)	+ 8 (2nn)	2 −10 (10)	4 +22 (2n)	8 + 4 (3)	2 +16 (2)	5 + 8 (1)
25....	4:28	13 + 15 (10)	+ 10 (10)	+14 (10)	− 7 (10)	− 18(8)	2 − 61 (2nn)	+20 (3nn)	2 + 1 (10)	4 +22 (1)	7 +15 (2)	2 +33 (2)	5 +20 (1)
26....	5:47	13 + 24 (10)	0 (10)	+11 (10)	+ 12 (9)	− 11 (6)	2 − 65 (3nn)	+33 (2nn)	2 +17 (10)	4 +42 (1nn)	8 +27 (2)	2 +33(2)	1 +27 (1)

TABLE 1—*Continued*

Date	U.T.	*H* (λλ 3666–3835)	*Hζ*	*He*	*Hδ*	*Hγ*	*He* I	*Mg* II	*Ca* II	*Si* II	*Fe* II	*Mg* I	*Ni* II, *Ti* II *Cr* II, *Fe* I *V* II, *Sc* II *Mn* II
1943 Aug. 27....	6:02	13 + 40 (12)	+ 21 (12)	+22 (10)	+ 15 (10)	0 (7)	2 − 75 (3nn)	0 (2nn)	2 +10 (12)	2 +54 (1)	8 +50 (3)	2 +71 (1)	3 +47 (1)
28....	5:49	13 + 33 (10)	+ 11 (12)	+38 (10)	+ 21 (10)	− 8 (7	2 −104 (2nn)	+16 (2nn)	2 +16 (10)	4 +64 (1n)	7 +68 (3)	2 +48 (1)	3 +78 (1)
29....	5:45	13 + 32 (10)	+ 14 (12)	.....	+ 21 (10)	− 12 (9)	2 − 62 (2nn)	+19 (2n)	1 + 9 (10)	2 +42 (1)	7 +58 (2)	2 +30 (1)	3 +59 (1)
30....	2:54	13 + 24 (10)	+ 6 (12)	.....	− 6 (10)	− 23 (9)	2 − 57 (2nn)	− 1 (2nn)	1 +15 (10)	2 +53 (1)	3 +35 (1)	1 +58 (1)	2 +47 (1)
Sept. 3....	5:28	6 − 32 (9)	− 28 (10)	.....	− 20 (10)	− 40 (10)	2 − 81 (2nn)	−51 (2n)	1 −20 (9)	.....	1 − 8 (1)	.....	2 − 4 (1)
4....	5:26	13 − 24 (10)	− 37 (10)	−25 (10)	− 34 (10)	− 32 (10)	2 − 86 (2nn)	−10 (1nn)	2 −16 (8)	2 + 6 (2)	3 −17 (1)	2 −26 (2)	4 + 7 (1)
5....	5:05	13 − 19 (8)	− 16 (10)	−25 (10)	− 21 (10)	− 33 (10)	2 −106 (2nn)	− 3 (1nn)	2 −22 (8)	.....	2 − 5 (1)	2 + 2 (1)	.....
5....	5:27	13 − 19 (9)	− 34 (10)	−22 (9)	− 24 (10)	− 21 (10)	2 −110 (1nn)	−80 (1nn)	2 −22 (8)	.....	1 − 5 (1)	.....	1 − 3 (1)
6....	2:52	13 − 15 (10)	− 22 (10)	−16 (10)	− 14 (10)	− 21 (8)	2 −139 (2nn)	−15 (1nn)	2 − 9 (9)	.....	.....	.....	1 −27 (1)
7....	4:14	13 − 15 (9) 2 *−157* (1)	− 25 (10) *−173* (5)	−14 (9)	− 28 (10) *−208* (1)	− 29 (10)	2 − 71 (2nn)	−20 (1nn)	2 −20 (8)	.....	2 +10 (1)	.....	.....
7....	5:14	13 − 13 (10) 3 *−152* (1)	− 20 (10) *−159* (2)	−23 (10)	− 31 (10)	− 29 (10) *−178* (1)	2 −127 (2nn)	−11 (1nn)	2 −15 (9)	2 + 7 (1)	1 +17 (2)	2 +15 (1)	.....
8....	3:51	13 − 14 (10)	− 28 (10)	−26 (10)	− 28 (10)	− 33 10)	2 − 53 (1nn)	+30 (1nn)	2 −20 (9)	3 − 2 (1)	1 +13 (2)	2 + 3 (1)	.....
8....	4:04	13 − 14 (10)	− 17 (10)	−17 (10)	− 15 (10)	− 26 (10)	2 − 52 (2nn)	+25 (2n)	2 −17 (9)	3 +14 (1)	5 +11 (2)	.....	.....
8....	6:50	13 − 19 (9)	− 28 (10)	−23 (10)	− 21 (10)	− 34 (10)	2 − 81 (2nn)	− 7 (2n)	2 −19 (9)	2 − 5 (1)	2 − 5 (1)	2 0 (1)	1 −50 (1)
8....	11:45	8 − 9 (9)	− 20 (10) *−236* (1)		− 8 (10)	− 11 (10)	− 30 (10)	2 −110 (2nn)	+33 (2n)	2 −11 (8)	.....	3 − 6 (1)	.....
12....	2:48	13 − 9 (10)	− 24 (10)	−12 (10)	− 9 (10)	− 23 (9)	2 − 43 (2nn)	+24 (2nn)	2 − 9 (8)	.....	1 + 8 (1)	.....	1 − 5 (0)
12....	5:51	13 − 3 (11)	− 24 (12)	−15 (10)	− 10 (10)	− 12 (9)	2 − 73 (2nn)	+19 (2n)	2 −17 (9)	1 +13 (0)	2 +35 (0)	2 +13 (0)	.....
13....	3:24	13 − 6 (11)	− 18 (12)	−16 (10)	− 6 (10)	− 12 (10)	2 − 22 (1nn)	+32 (1nn)	2 −11 (9)	1 + 1 (0)	2 +23 (1)	1 + 6 (0)	1 − 5 (0)
14....	3:39	13 − 16 (12)	− 27 (12)	−25 (10)	− 30 (10)	− 39 (10)	2 − 49 (2nn)	− 9 (1nn)	2 −19 (7)	2 + 3 (1)	2 −11 (0)	.....	1 −22 (0)
15....	3:02	13 − 12 (10)	− 22 (10)	− 1 (10)	− 13 (10)	− 24 (10)	2 − 68 (1nn)	−18 (1nn)	2 −16 (9)	.....	.....	.....	1 + 4 (0)

NOTE TO TABLE 1

In each column the radial velocity is followed by an estimate of the intensities of the following lines: λ 3835 for *H*, λ 4471 for *He* I, λ 3934 for *Ca* II, λ 4128 for *Si* II, λ 4233 for *Fe* II, λ3832 for *Mg* I, λ 3514 for *Ni* II (or λ 3742 for *Ti* II). Radial velocities which are based upon more than a single line are preceded by the numbers of lines used. The weaker components of the *H* lines are given in italics.

these lines, noticed previously, is confirmed and persists throughout the series of observations. There is no adequate explanation for this phenomenon, but it reminds one of the temporary doubling of the *He* I lines in AX Monocerotis. Perhaps we must assume that the violet components, which are occasionally observed in the *H* lines, are always present, with considerable intensity, in the *He* I lines.

The interpretation of the observations is at least as difficult as in the case of AX Monocerotis. We have here two stars whose spectra vary in much the same manner. Both are bright-line objects, consisting of a rapidly rotating early B star of moderate luminosity, surrounded by a tenuous shell whose spectrum normally shows only sharp *H* and *Ca* II lines. This shell is usually not expanding in HD 218393 and is usually slightly expanding in AX Monocerotis. In both stars the velocity of this shell is variable.

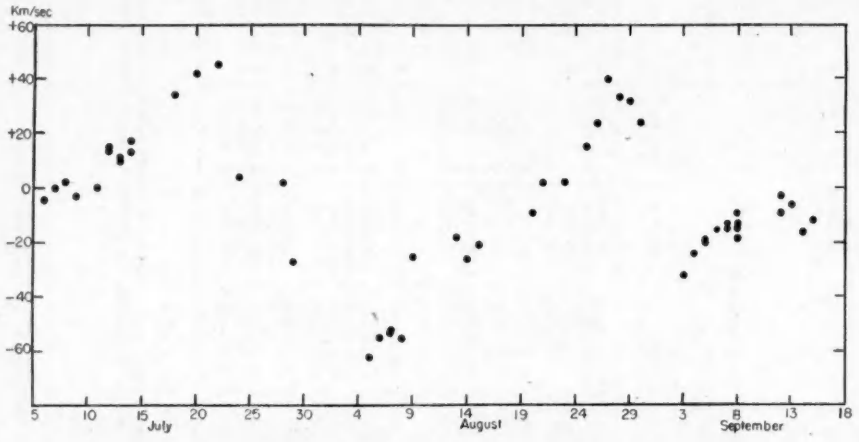

FIG. 1.—Velocity-curve of HD 218393 determined from the red cores of the higher members of the Balmer series (λλ 3666–3835).

In addition to this inner (?) shell there is an outer shell, which is also always present and gives rise to the P Cygni lines $H\beta$, $H\gamma$, and perhaps $H\delta$. These lines are quite conspicuous in AX Monocerotis; but they are also noticeable in HD 218393, where $H\beta$ is clearly of the P Cygni type, while $H\beta$, $H\gamma$, and $H\delta$ show in their radial velocities a tendency to be more negative than the higher members of Balmer series and do not show as large a range in velocity as the higher members. It would seem that the outer strata of the shell always tend to expand, as has already been suggested in the case of AX Monocerotis.[7] In both stars there are frequent and violent disturbances, in the form of rapidly expanding masses of gas. In AX Monocerotis these disturbances definitely reach throughout the entire thickness of the shell and affect the low-level *He* I lines. In HD 218393 this is less clearly indicated, but the violet displacement of the *He* I lines suggests that the same conditions may prevail in it.

Both stars have variable α Cygni lines. In AX Monocerotis these lines are affected by the explosive disturbances, while in HD 218393 they are not. But this is probably due to the fact that in HD 218393 the violet components of the *H* absorption lines are usually much weaker than in AX Monocerotis. As a rule, in both stars the α Cygni lines are not taking part in the expansion; and it is probably reasonable to associate them with the lower levels of the shell, where the *H* lines show little or no expansion (or a blending of the two, as in AX Monocerotis).

[7] *Ap. J.*, **95**, 134, 1942.

There can be no doubt that in both stars the strong and sharp *Ca* II lines belong to this α Cygni layer. In AX Monocerotis and probably also in HD 218393 the appearance of the α Cygni lines coincides with a strengthening of the *Ca* II lines. There must be a corresponding strengthening of undisplaced (or little-displaced) *H* lines, but this would be lost in the complexity of the structure of the *H* lines.

The cause of the variations in the intensities of the α Cygni lines remains obscure. In AX Monocerotis there were apparently marked changes in the ionization of the α Cygni shell, with *Ni* II alone present in certain stages, while in other stages *Ti* II was strong without any marked change in *Ni* II. I have noticed similar changes in HD 218393, and *Ni* II is also conspicuous in its α Cygni spectrum. This appears to be an interesting feature of most shell spectra.

The existence of surges from low atmospheric levels very strongly suggests that we are concerned with a phenomenon resembling prominence action. This action must, in both stars, be enormously more powerful than on the sun, and it is probable that it is the primary cause for the origin of the tenuous shells in these and other stars. The fact that the occurrence of shell spectra is nearly always associated with rapid rotation of the deeper strata—when these strata can be seen through the shells—suggests that prominence action is facilitated or enhanced by rapid rotation. But there remains the enigma that not all rapidly rotating stars show the effects of prominence action.

I am indebted to Messrs. C. A. Bauer and G. Münch for their help in securing many of the spectrograms used in this work.

RADIAL VELOCITIES OF THE FOUR STARS OF THE TRAPEZIUM IN ORION*

OTTO STRUVE AND JOHN TITUS[1]
McDonald and Yerkes Observatories
Received October 5, 1943

ABSTRACT

Seventy-six spectrograms of the stars HD 37020, 37021, 37022, and 37023 have been obtained at the McDonald Observatory. The measures indicate that HD 37021 = BM Orionis has the following elements: $P = 6.50$ days, $\gamma = +24.0$ km/sec, $K = 81$ km/sec, $e = 0.14$, $\omega = 194°$, $T =$ JD 2430787.86. The other three stars have relatively small ranges in velocity. The mean velocities of these four stars and of θ^2 Orionis = HD 37041 exceed the velocity of the Orion nebula by 15.0 km/sec. This may be due to a gravitational red shift or to a systematic motion of the four stars through the nebula.

All four stars of the Trapezium have been announced as spectroscopic binaries. Unfortunately, the spectra of these stars are among the most difficult to measure. Not only are their absorption lines diffuse and weak, but they are complicated by the emission lines of the Orion nebula. Hence, the precision of the measurements is low, and no period has been published for any of them. The faintest star of the group, HD 37021, or star B of the multiple object θ^1 Orionis, is the known variable BM Orionis. This fact adds to the interest of the group. The spectrograms used in this work were obtained at the McDonald Observatory with the Cassegrain quartz spectrograph, equipped with a 500-mm camera. The dispersion was 40 A/mm at λ 3933. The instrument possesses a slight advantage over other spectrographs used elsewhere for the Trapezium stars: it is efficient in the ultraviolet region, so that we were always able to measure *He* I 3820 and often other violet and ultraviolet lines which are not appreciably distorted by nebular emission lines. However, these lines were not sufficient, and we have also used the other *He* I lines, λλ 4009, 4026, 4120, 4144, 4388, 4472, and occasionally a few other lines.

The purpose of the investigation was to establish, as accurately as is possible, the mean velocities of the four stars in order to find whether they agree with the velocity of the Orion nebula. The individual measurements are listed in Table 1. Stars HD 37020 and HD 37023 were measured by both authors. Star HD 37021 was measured only by Struve, and star HD 37022 was measured only by Titus. The number of lines used for each entry, when greater than one, is given just preceding the radial velocity. The scatter between the two measures is large but is fully accounted for by the extreme difficulty of the settings. The observed scatter of the mean stellar velocities of the two observers is small for HD 37020 and HD 37023. Although these measurements do not disprove the possibility that these stars are binaries, it is safe to say that their ranges in velocity are small. The mean values of all plates for each star should, therefore, give a good approximation to the velocity of the system if they are really binaries. Titus' measures of HD 37022 also show a relatively small range. No attempt has been made to derive periods for these stars, and the task would probably be hopeless without a very large amount of additional material. But Struve's measures of HD 37021—the most difficult of the four spectra—not only confirm the large range in velocity discovered by Plaskett and Pearce[2]

* *Contributions from the McDonald Observatory, University of Texas*, No. 83.

[1] Dr. Titus left Yerkes Observatory on a leave of absence for war research before this paper was finished.

[2] *Pub. Dom. Ap. Obs.* Victoria, **6**, 34, 1931.

TABLE 1

RADIAL VELOCITIES IN KM/SEC

HD 37020

Date	U.T.	Stars (O. S.)	Star (J. T.)	*Ca* II (O. S.)	*Ca* II (J. T.)	Nebula (J. T.)
1943 Mar. 4	2:03	7 + 19	5 +15	+19	+ 4	3 +10
4	5:48	4 + 5	.....	.....	.....	.....
6	2:02	6 + 27	7 +23	− 2	.....	2 + 5
6	3:28	8 + 16	8 +17	+37	+28	4 +12
7	2:19	8 + 49	7 +40	−12	− 5	5 +14
8	2:28	9 + 41	6 +38	+25	+36	2 +17
9	1:33	8 + 43	7 +42	+37	.....	4 +23
10	1:29	7 + 46	6 +36	+ 8	.....	4 +15
13	4:24	6 + 30	7 +25	+ 6	− 5	3 +10
15	3:53	8 + 36	8 +43	+24	+ 7	4 +15
18	2:42	6 + 34	7 +40	− 3	− 2	5 +14
21	4:39	5 + 40	7 +40	.....	.....	5 +18
27	4:16	7 + 35	7 +52	+ 4	+ 1	5 +18
28	2:02	7 + 36	8 +36	−23	+ 1	3 +20
29	2:13	6 + 24	7 +21	+13	+ 8	3 − 1
Apr. 10	3:22	8 + 42	8 +38	+30	.....	4 +21
11	2:37	8 + 49	7 +49	− 6	+ 1	5 +23
12	3:29	8 + 70	8 +60	+34	+31	5 +21
13	2:40	8 + 21	6 +29	.....	.....	5 + 8
17	2:35	7 + 35	7 +37	.....	+ 2	3 +15
18	3:01	7 + 29	8 +27	−16	.....	5 + 3

HD 37021

Date	U.T.	Star (O. S.)	*Ca* II (O. S.)	Nebula (O. S.)	Phase	
1943 Mar. 4	1:31	4 − 72	.....	4 +22	0.00	
4	5:15	5 − 65	−12	4 +19	0.16	
5	2:34	5 − 9	+49	4 + 8	1.05	
6	1:43	4 + 2	.....	4 +14	2.01	
6	3:06	5 + 43	.....	4 +15	2.07	
7	1:49	4 +111	+25	4 +24	3.02	
8	2:00	3 + 88	.....	3 +32	4.02	
9	2:06	2 − 40	.....	4 +25	5.03	
9	2:35	3 + 42	+13	4 +23	5.05	
10	2:04	4 − 57	.....	4 +17	6.03	
10	2:40	5 − 45	+31	4 +18	6.05	
13	3:58	4 + 83	.....	4 +14	2.61	
13	5:06	3 +117	.....	4 +23	2.65	
14	4:40	5 + 88	+ 6	4 +14	3.63	
15	3:20	3 + 64	.....	4 +14	4.58	
18	3:54	4 − 22	.....	4 +19	1.10	
21	3:58	3 + 78	+16	4 + 8	4.11	
26	3:43	4 + 74	+37	4 +19	2.59	
27	3:36	4 + 93	.....	4 +23	3.59	
28	2:36	5 + 54	+44	4 +13	4.55	
29	2:55	5 − 54	− 8	4 +12	5.56	
Apr. 10	2:42	5 + 61	+46	4 +15	4.55	
12	2:50	5 − 68	+16	4 +14	0.06	

TABLE 1—*Continued*

HD 37022

Date	U.T.	Star (J. T.)	*Ca* II (J. T.)	Nebula (J. T.)		
1943 Mar. 6	2:18	6 + 14	− 9	−19		
7	1:22	7 + 41	.....	−13		
9	1:21	6 + 41	+34	+10		
10	1:20	8 + 30	+19	+19		
13	4:42	8 + 42	+19	+10		
28	3:22	6 + 23	+ 5	+ 2		
29	2:03	7 + 54	.....	− 9		
Apr. 10	3:56	5 + 39	+22	−24		
11	2:15	8 + 47	.....	+ 7		
12	3:58	5 + 51	.....	+ 4		
13	2:18	7 + 43	+16	+19		
17	2:20	8 + 31	.....	+ 8		
18	2:15	10 + 41	+33	− 2		
18	3:21	6 + 27	+44	− 3		

HD 37023

Date	U.T.	Star (O. S.)	Star (J. T.)	*Ca* II (O. S.)	*Ca* II (J. T.)	Nebula (J. T.)
1943 Mar. 4	2:04	6 + 32	6 +31	+25	.....	4 +28
6	2:12	7 + 34	6 +29	+40	+37	1 +36
6	3:38	6 + 49	5 +30	+31	+19	3 +21
7	2:32	7 + 36	6 +41	+34	+22	4 + 8
8	2:38	7 + 36	6 +31	+37	.....	3 +20
9	1:43	7 + 45	7 +42	+40	+31	3 +32
10	1:40	7 + 40	5 +30	+25	+16	3 +21
13	4:35	7 + 38	5 +24	+19	+22	4 + 8
15	4:10	7 + 38	6 +27	+16	+13	4 +18
18	3:06	7 + 41	7 +32	−14	.....	4 +15
21	4:58	7 + 48	7 +48	+13	.....	2 +18
28	3:10	7 + 42	6 +36	+ 7	+44	3 +14
29	2:29	7 + 40	7 +46	+14	+23	2 +23
Apr. 10	3:42	7 + 30	6 +18	+24	+ 6	4 +11
11	3:08	6 + 22	6 +15	+49	.....	5 +15
12	3:47	5 + 17	6 + 7	.....	.....	3 +30
13	3:13	6 + 27	5 +10	+16	.....	5 +9
18	2:32	7 + 33	7 +22	+32	+17	4 +11

at Victoria but establish beyond doubt that the period is approximately 6.50 days.[3] The phases in Table 1 were computed by setting the epoch of the first plate, JD 2430787.56, as zero. The velocity-curve is shown in Figure 1. In spite of the large scatter, the character of the curve is well established, and the elements derived from it by a graphical procedure are given in Table 2.

The variable star BM Orionis has been the subject of considerable controversy among astronomers. It has recently been regarded as an irregular variable, possibly of the kind

[3] At the Cincinnati meeting of the A.A.S., McLaughlin asked whether the period could be close to one day. Our observations do not exclude this, but the duration of the light minimum is reported to be 23.5 hours.

associated with nebulae.[4] But Hartwig[5] had announced in 1920 the value $P = 6.4754$ days, and there can now be little question that this period is identical with the one found spectroscopically. The photometric observations of this star are especially difficult, as has been shown by Parkhurst,[6] who was unable to find a variation in excess of a quarter of a magnitude on 103 photographs of the Orion nebula taken with the Yerkes 40-inch refractor. The last issue of the *Katalog und Ephemeriden Veränderlicher Sterne* by H. Schneller available to me (1940) lists BM Orionis as an Algol-type star with

$$\text{Minimum} = 2422717.342 + 6.47075E\,.$$

The light at maximum is given as 8.1 mag., and the depth of primary eclipse is 0.61 mag. The duration of this eclipse is 23.5 hours; there is no secondary minimum. Apparently no accurate light-curve has been published.

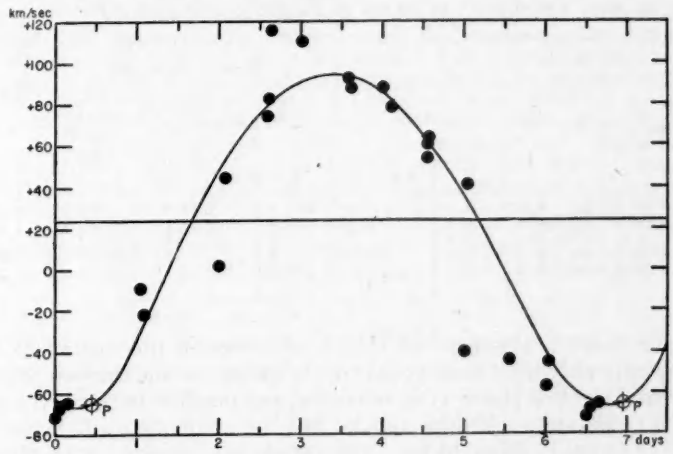

FIG. 1.—Velocity curve of HD 37021

TABLE 2

ORBITAL ELEMENTS OF HD 37021 = BM ORIONIS

$P = 6.50$ days	$T =$ JD 2430787.86 = phase 0.30 days
$\gamma = +24.0$ km/sec	$a \sin i = 7 \times 10^6$ km
$K = 81$ km/sec	$\dfrac{m_2^3}{(m_1 + m_2)^2} \sin^3 i = 0.35\odot$
$e = 0.14$	
$\omega = 194°$	

The summarized results of the radial velocity measurements are given in Table 3, where the star θ^2 Orionis = HD 37041 has been added from the recent orbit by Münch[7] and the earlier one by Struve.[8] The last column contains the stellar radial velocities of Moore's catalogue,[9] and the spectral types are those determined at Victoria.

The results shown in Table 3 are of great interest. The radial velocities of all five stars are greatly in excess of the radial velocities of the Orion nebula determined from

[4] C. and S. Gaposchkin, *Variable Stars*, pp. 30–31, 302–303, Cambridge, 1938.

[5] *Geschichte und Literatur der Veränderlichen Sterne*, **3**, 82, 1922.

[6] *Pop. Astr.*, **27**, 578, 1919; *Ap. J.*, **53**, 317, 1921.

[7] *Ap. J.*, **98**, 229, 1943. [8] *Ap. J.*, **60**, 159, 1924. [9] *Pub. Lick Obs.*, **18**, 46, 1932.

the same plates. The best available average velocity of the Orion nebula is +17.5 km/sec.[10] It is improbable that these stars are passing through the nebula and are not physically associated with it. The appearance of the Trapezium in the midst of a small hollow within the nebula would appear to rule this out. Hence it is possible that the systematic difference of

$$\text{Stars } \textit{minus} \text{ Nebula} = +15.0 \text{ km/sec}$$

should be interpreted as a gravitational red shift. The masses of the five stars are probably very large, and there is no reason why they should not have a red shift similar to those of the massive Trumpler stars in clusters,[11] which range from +5 to +15 km/sec.

TABLE 3

RADIAL VELOCITIES OF STARS IN TRAPEZIUM (θ^1 AND θ^2 ORIONIS)

STAR	DESIGNATION	SP.	MAG.	RADIAL VELOCITIES										
				Star			Nebula			Interstellar *Ca* II			Moore Star	
				V	P.E.	No.	*V*	P.E.	No.	*V*	P.E.	No.		
HD 37020	θ^1 Ori A	B2	6.8	+34.3	±1.9	21	+14.0	±1.0	20	+ 9.5	±2.1	18	+32	± 4
HD 37021	θ^1 Ori B	B2	7.9	+24.0	.....	23	+17.6	±0.8	23	+22.0	±3.1	12	−24	±18
HD 37022	θ^1 Ori C	O7*k*	5.4	+37.4	±2.0	14	+ 0.5	±2.3	14	+20.3	±2.9	9	+23.1	± 1.8
HD 37023	θ^1 Ori D	B0	6.8	+32.4	±1.5	18	+18.8	±1.3	18	+23.0	±1.7	17	+27	± 3
HD 37041	θ^2 Ori A	O9*k*	5.2	+34.5	±0.7	22	+17.6	.....	....	+18.9	±3.5	12	+36.8	

It is suggestive that the smallest red shift is observed in the case of HD 37021—the faintest and presumably least massive star of the group—while the two largest red shifts occur in the two brightest stars. It is, of course, not possible to prove the physical connection of the Orion stars with the nebula, but the component of the solar motion in the direction of Orion is about 18 km. The nebula is, therefore, approximately at rest with respect to the solar system, while the stars show a systematic velocity of recession from the solar system of the order of 15 km/sec. If this amount is interpreted as an effect of galactic rotation, the corresponding distance of the group of stars would be about 1000 parsecs, which is probably not consistent with the distance of the Orion nebula. It should also be noted that the interstellar *Ca* II lines of the five stars in Table 3 give an average value of about +20 km/sec. Subtracting the solar motion, we obtain a residual motion of only +2 km/sec to be attributed to galactic rotation. Twice this amount, or +4 km/sec, might be expected for the galactic-rotation component of the five stars. But it is difficult to account for anything like +15 km/sec. Hence, the only two alternatives are gravitational red shift or a systematic motion of the stars through the nebula.

[10] J. H. Moore, *Pub. Lick Obs.*, **18**, 213, 1932.

[11] *Pub. A.S.P.*, **47**, 254, 1935.

THE SPECTRUM OF SX CASSIOPEIAE*

OTTO STRUVE
Yerkes and McDonald Observatories
Received October 30, 1943

ABSTRACT

The velocity-curve of this eclipsing binary has been derived from 42 spectrograms obtained during three consecutive cycles in the summer of 1943. The curve is very unsymmetrical and leads to the following elements: $P = 36.567$ days, $\gamma = -9.7$ km/sec, $K = 50.0$ km/sec, $e = 0.50$, $\omega = 10°$, and $T =$ phase 32.0 days after principal eclipse. These elements are inconsistent with the light-curve by Dugan, which requires $e \cos \omega = 0$. Eclipses of the emission lines of *H*, *Ca* II, *Fe* II, and a few other elements suggest the existence of a stream of gas receding from the G-type component and flowing along the following side of the A-type component. This stream probably divides on the far side of the A star, a part expanding outward and giving rise to a negative displacement of the shell-absorption lines at secondary minimum and a part continuing to flow around the preceding side of the A star until it merges with the atmosphere of the G star. It is suggested that at principal minimum and at the two elongations the measured radial velocities of the absorption lines give the true radial velocity of the A star. Under this assumption the orbit of the A star is circular, with $\gamma = -8$ km/sec and $K = 27$ km/sec. The unsymmetrical appearance of the velocity-curve is caused by the streams of gas which in certain phases are seen projected upon the disk of the bright A star. The existence of a tenuous shell is confirmed by the dilution effect which causes the lines of *Mg* II 4481 and of *Si* II 4128 and 4131 to be abnormally weak. The remarkable variations in the velocity-curve, discovered by Joy at Mount Wilson, are probably caused by changes in the density of the gas within the streams. It is possible that irregular changes in the streams may also account for the large scatter in Dugan's photometric observations.

Recent studies of the spectral changes in β Lyrae,[1] WW Draconis,[2] and RW Tauri[3] have shown that the contours and intensities of the bright lines in these eclipsing variables can be explained in terms of a large shell or ring which surrounds one of the components (WW Dra and RW Tau) or the entire system (β Lyr). This represents an important advance in our knowledge of the formation of emission lines in stellar spectra and supplements, in a very satisfactory manner, information gathered from statistical and individual studies of Be and Ae stars. It is, therefore, desirable to investigate other eclipsing binaries with emission lines. Among these, SX Cassiopeiae plays an important part.

The variability of SX Cas was discovered by Mme L. Ceraski at Moscow in 1907. Numerous visual photometric observations have been made by Enebo, Luizet, Pračka, and others; these were used by Shapley, and later by Miss Fowler and Sitterly, for the derivation of the photometric elements of the orbit of this eclipsing binary. In 1927 Gerasimovič published a light-curve based on 905 estimates of the brightness on Harvard plates. The latest and most complete photometric study of SX Cas was made by Dugan[4] in 1933. His paper contains a complete bibliography and a summary of previous photometric and spectrographic observations. The final elements by Dugan give for the principal minimum:

$$\text{Pr. Min.} = \text{JD } 2417983.33 + 36.56757E.$$

The value of the period rests upon observations covering some twenty-five years, or 251 epochs; and, since Dugan states that the residuals from this formula are "surprisingly small," it is probable that the period is essentially constant and that its value is suffi-

* *Contributions from the McDonald Observatory, University of Texas*, No. 84.

[1] Struve, *Ap. J.*, **93**, 104, 1941.

[2] A. H. Joy, *Ap. J.*, **94**, 407, 1941.

[3] A. H. Joy, *Pub. A.S.P.*, **54**, 35, 1942.

[4] *Contr. Princeton U. Obs.*, No. 13, 1933.

ciently accurately known to predict the phases for 1943, or about twelve years after the close of Dugan's series.

Dugan gives the visual magnitude at maximum as 9.0, while Prager gives 9.8. The principal minimum has a depth of 0.99 mag., and the secondary minimum a depth of 0.32 mag. The eclipse is total, and the duration of eclipse is 3.74 days. There is no noticeable shift in the phase of the secondary minimum from $0.5P$, so that

$$e \cos \omega = 0.$$

Shapley and Luizet had previously suspected a small negative shift, of about one day, so that

$$e \cos \omega = -0.043.$$

The other relevant elements of the photometric orbit are:

$$L_1 = 0.46 \qquad r_f = 0.250$$

$$L_2 = 0.54 \qquad \frac{b}{r} = 0.85$$

$$\frac{J_1}{J_2} = 0.19 \qquad \frac{c}{r} = 0.79$$

$$i = 88° \qquad \rho_b = 0.0046$$

$$r_b = 0.118 \qquad \rho_f = 0.0005$$

The densities were computed on the assumption of equal masses. Dugan states that his 508 measures show a large amount of scatter, and systematic corrections amounting to as much as ± 0.08 mag. were added to groups of measures during primary minimum; somewhat larger corrections were also made at secondary minimum. Dugan considers these irregular variations to be real and attributes them to the brighter star.

The spectrum of the star has been observed by Adams and Joy,[5] but the details of their work have not been published. The spectrum shows only one component, A6s, except at primary eclipse, when the type is G6. The A-type star resembles α Cygni and is a supergiant from the Mount Wilson spectra. Dugan's values of ρ suggest that both stars are giants. Joy states that at primary minimum only the G6 spectrum is visible, without a trace of the A6 star for one day on each side of mid-eclipse. The A6 and G6 spectra are blended up to about two days before and after mid-eclipse. Beyond these limits Joy did not detect the spectrum of the late-type star. The H lines have bright fringes, and these emission features vary in intensity with the phase of the binary. There have been "remarkable variations in the amplitude and eccentricity" for which no satisfactory explanation could be found. The average semiamplitude of the velocity-curve is about $K = 50$ km/sec. On this basis Dugan computed that, if the masses are equal, they are $m_b = m_f = 1.9\odot$. The distance between the stars is 5×10^7 km, and the radii are $r_b = 5 \times 10^6$ km and $r_f = 1 \times 10^7$ km.

The behavior of the bright lines is especially intriguing. Hence the star was observed with the 82-inch McDonald telescope and a Cassegrain quartz spectrograph, giving a dispersion of 40 A/mm at λ 3933. In order to minimize, as much as possible, the effect of the irregular variations in velocity discovered at Mount Wilson, an effort was made to obtain the entire series of plates during one observing season. A total of 42 plates was secured between June 23 and September 14, 1943. They cover parts of three consecutive

[5] *Pub. A.S.P.*, **31**, 308, 1919; *Pop. Astr.*, **28**, 513, 1920; *Rept. Mt. W. Obs.*, 1922 and 1928–1929.

cycles and are shown in Figure 1 as they fall on Dugan's light-curve. One principal minimum was very completely observed, and I am especially indebted to Messrs. C. A. Bauer and G. Münch, who obtained these critical exposures for me, together with a number of spectrograms at other phases.

Table 1 contains a list of 27 star lines which were chosen for the determination of radial velocities. These lines were measured on almost all of the plates; only one or two

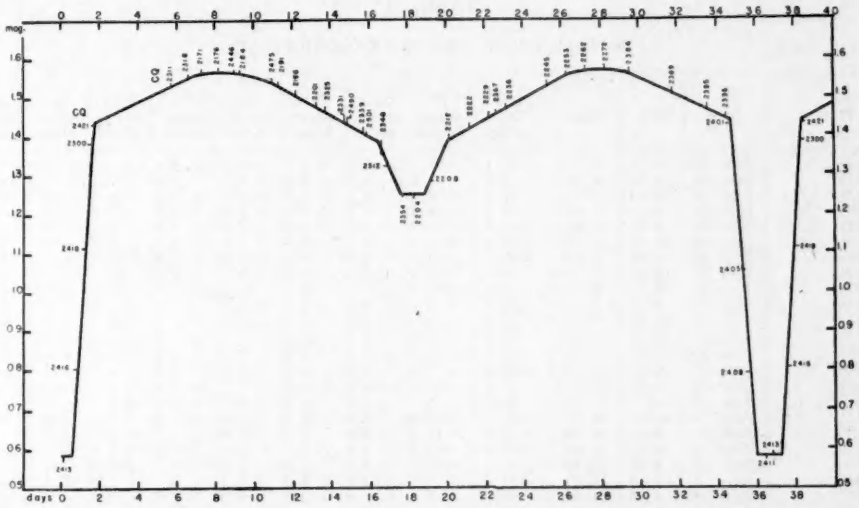

FIG. 1.—Distribution of the spectrographic observations on the light-curve

TABLE 1

LIST OF STAR LINES MEASURED IN SX CASSIOPEIAE

H		*Fe* II	*Ti* II	*Fe* I	*Ca* II	*Sr* II
H 10	3797.90	4178.85	3900.54	3820.44	3933.68	4077.71
H 9	3835.39	4233.17	3913.47	4045.81		
H 8	3889.05	4351.76	4395.04	4063.60	*Mg* I	*Ca* I
Hδ	4101.74	4549.47	4443.80	4071.74	3832.31	4226.73
Hγ	4340.46		4468.50	4307.91	3838.30	
			4501.27			
			4533.97			
			4571.98			

were too weak to allow the measurement of the lines in the extreme violet. Although the spectrum changes conspicuously during principal eclipse, and less conspicuously at other phases, all lines were measured, irrespective of the phase. As a consequence of this procedure, a few lines which became very faint at minimum were measured with difficulty; but it seemed best to retain them in order to make the material as homogeneous as possible. The line *Ca* I 4226 was faint and very broad except at principal minimum and at a few other phases. I believe that the feature measured outside of eclipse is a complicated blend and that the corresponding velocities are probably meaningless. But, since they contribute little to the means, they have also been retained throughout. The line *Sr* II 4077 was weak outside of eclipse, and the precision of measurement was correspondingly

low. All other lines were sharp, and a few were of excellent quality for radial-velocity work. The lines were chosen in such a way that there were not only many which normally belong to the A star but also a number which were greatly strengthened at primary eclipse. Table 2 lists the velocities for all lines and then gives in the remaining columns the differences (Element *minus* Mean). The phases were computed with Dugan's formula and start at mid-eclipse. Estimates by the observers show that primary eclipse actual-

TABLE 2

RADIAL VELOCITIES OF SX CASSIOPEIAE

Plate	Date	U.T.	Phase	Final Vel. (Km/Sec)	*H* minus Mean	*Fe* II minus Mean	*Ti* II minus Mean	*Ca* II minus Mean	*Fe* I minus Mean	*Mg* I minus Mean	*Ca* I minus Mean	*Sr* II minus Mean
CQ 2413	Aug. 28	10:36	0.12	−19.7	+15.5	−11.9	− 3.7	+ 7.5	+ 4.1	.....	− 1.9	−26.8
CQ 2416	Aug. 29	4:10	0.85	− 5.2	+ 5.3	− 9.5	+ 4.0	− 9.7	− 0.9	.....	+ 1.7	− 8.6
CQ 2418	Aug. 29	10:40	1.12	−22.5	+ 0.8	− 1.1	+ 1.9	− 8.1	+ 3.7	−11.3	+ 0.8	− 1.3
CQ 2300	July 24	9:59	1.67	−10.2	+ 4.4	− 5.8	+ 2.0	+ 8.0	+ 0.8	− 1.1	− 7.5	−16.2
CQ 2421	Aug. 30	4:09	1.85	− 7.5	+ 1.3	− 7.0	+ 4.0	− 1.4	+ 4.2	− 7.1	+ 0.4	− 2.7
CQ 2311	July 28	10:41	5.70	−33.8	+14.9	− 3.3	−14.0	+ 3.9	− 2.6	− 4.7	+40.7	+ 0.5
CQ 2318	July 29	8:08	6.59	−45.7	+10.2	− 2.2	− 9.0	+3.9	+ 3.8	−10.9	+17.4	+12.7
CQ 2171	June 23	10:27	7.26	−30.8	+15.3	− 3.2	− 5.5	+ 4.6	+ 0.7	−10.1	− 0.2	− 7.8
CQ 2176	June 24	9:25	8.21	−24.1	+10.1	−13.2	− 8.3	−14.2	+13.8	− 9.7	+25.2	+21.6
CQ 2446	Sept. 6	4:13	8.86	−28.4	+21.1	− 0.4	− 5.0	+ 5.9	−16.8	− 8.0	+ 8.1	−36.2
CQ 2184	June 25	10:24	9.25	−40.2	+ 9.9	− 4.9	−10.4	− 2.0	+ 1.7	−16.1	+69.9	+21.5
CQ 2475	Sept. 8	5:24	10.91	−41.5	+ 9.8	−12.7	−12.9	− 9.1	+ 8.7	− 1.0	+57.1	+16.0
CQ 2191	June 27	10:29	11.26	−25.3	− 1.8	+ 2.4	+ 6.4	+ 5.8	− 8.9	+11.9	+51.7	+19.7
CQ 2196	June 28	10:31	12.26	−30.0	+ 5.8	− 5.1	− 4.3	− 4.6	− 9.2	− 6.0	+45.9	+41.4
CQ 2201	June 29	9:58	13.24	−43.7	−12.7	−16.8	+ 9.8	.....	+26.4	(poor plate)		
CQ 2325	Aug. 5	10:43	13.70	−46.0	+ 6.2	+ 2.4	−15.0	+ 9.7	+ 4.2	+ 1.6	+42.9	− 3.7
CQ 2331	Aug. 6	10:03	14.67	−52.2	+13.6	− 6.3	−11.0	+ 9.6	+ 1.7	− 2.5	+58.6	−27.2
CQ 2490	Sept. 12	4:18	14.86	−60.7	+11.1	− 5.4	− 6.3	+12.3	− 7.3	− 1.0	+47.1	− 4.6
CQ 2339	Aug. 7	9:57	15.66	−33.2	+10.9	− 1.6	− 7.9	+12.0	+ 0.2	− 2.8	+21.9	−13.8
CQ 2501	Sept. 13	4:59	15.89	−43.7	+16.1	− 8.3	− 2.1	− 3.5	− 0.3	+ 9.4	−17.1	−25.7
CQ 2348	Aug. 8	9:38	16.65	−35.2	+ 8.1	+ 1.1	− 3.0	+ 4.7	− 3.3	+ 1.5	+ 6.0	−17.8
CQ 2512	Sept. 14	5:19	16.90	−34.0	+ 5.2	− 8.0	− 3.0	+ 0.3	− 2.8	− 0.1	+26.9	+16.6
CQ 2354	Aug. 9	10:53	17.70	−28.3	+ 2.1	− 2.3	− 3.8	+ 3.7	+ 4.4	− 2.4	+16.7	− 8.7
CQ 2204	July 4	10:35	18.26	−30.0	− 4.2	− 2.4	− 7.2	− 3.9	+ 9.4	−25.8	+21.7	− 1.3
CQ 2208	July 5	10:27	19.26	−27.6	+ 0.2	+ 2.4	− 2.2	− 0.1	+ 6.1	− 4.4	− 6.1	− 7.4
CQ 2212	July 6	9:58	20.24	−14.7	− 2.7	− 3.7	− 4.4	+ 2.4	+ 7.2	+ 5.1	+13.8	+ 0.6
CQ 2222	July 7	10:24	21.25	−24.9	− 0.8	+ 3.4	− 0.7	+ 6.5	+ 1.8	+ 0.1	−15.7	− 5.4
CQ 2229	July 8	10:30	22.26	−13.7	−11.6	− 2.4	+ 8.3	+13.7	+ 3.5	+ 1.9	−26.8	− 4.0
CQ 2367	Aug. 14	8:45	22.61	−14.9	+ 2.7	− 6.9	− 5.4	− 0.8	+10.7	+ 4.9	− 7.7	+ 3.3
CQ 2236	July 9	7:57	23.15	− 4.1	− 3.5	−21.3	+ 8.2	+ 4.4	− 5.3	+14.1	−14.1	0.0
CQ 2245	July 11	10:24	25.25	+ 7.8	−10.1	− 5.0	+ 5.8	− 1.4	+ 8.4	+26.4	−44.5	−25.2
CQ 2253	July 12	9:50	26.23	+16.9	− 7.1	+ 8.7	− 4.9	− 1.3	+ 7.2	+ 8.7	+20.9	+ 9.1
CQ 2262	July 13	10:25	27.25	+13.1	+28.4	− 4.8	0.0	+20.1	+ 4.6	+18.5	−60.3	+13.0
CQ 2272	July 14	10:32	28.26	+27.7	+26.4	− 7.0	− 8.6	− 2.9	+ 0.4	− 2.0	+ 3.9	− 8.2
CQ 2386	Aug. 21	7:10	29.55	+43.3	+13.7	− 6.3	− 1.3	−26.5	+ 3.2	− 1.1	− 6.5	+ 0.8
CQ 2389	Aug. 23	10:46	31.70	+54.1	− 3.3	− 8.7	− 1.2	−17.3	+ 5.5	+14.9	+10.4	+12.2
CQ 2395	Aug. 25	5:43	33.49	+10.8	+ 9.5	− 6.8	− 7.4	− 3.9	+ 4.2	+13.8	+ 0.3	− 4.3
CQ 2396	Aug. 26	4:37	34.44	+10.5	+ 9.0	− 2.9	− 4.6	− 6.5	+ 6.0	− 2.9	− 2.7	−13.3
CQ 2401	Aug. 26	10:53	34.70	+10.5	+10.3	− 8.2	− 2.6	− 1.0	+ 3.3	+ 0.8	−17.5	+ 2.2
CQ 2405	Aug. 27	4:33	35.44	+16.6	+12.0	− 9.0	+ 1.3	−21.9	− 4.2	−17.8	−16.1	−10.1
CQ 2408	Aug. 27	10:41	35.70	+ 0.2	+29.0	−11.6	− 8.0	+39.0	− 7.5	.....	−32.1	−28.8
CQ 2411	Aug. 28	4:15	36.43	− 8.6	+15.8	−11.0	− 3.6	+18.3	+ 3.1	.....	− 8.9	−30.7

ly did occur when it was scheduled to take place; but these observations were not numerous and accurate enough to prove whether mid-eclipse actually fell within an hour or so of zero phase, which would be required in order to interpret the spectrographic observations without ambiguity. We shall assume that this was the case.

A few of the spectrograms were measured twice. The agreement of these duplicate measures was usually of the order of ± 1.0 km/sec, so that a corresponding probable error of less than ± 0.5 km/sec may be inferred. The probable error from the residuals of the 27 lines is somewhat larger, but this is at least partly inherent in the behavior of the different groups of lines.

The observations are plotted in Figure 2. They show a well-pronounced, sharp, and somewhat unsymmetrical maximum at phase 32 days, and a broad, flat minimum near

phase 14 days. The best elements of the spectrographic orbit which I obtained after several adjustments, but without a least-squares solution, are the following:

$$P = 36.567 \text{ days (assumed)}$$

$$\gamma = -9.7 \text{ km/sec}$$

$$K = 50.0 \text{ km/sec}$$

$$\omega = 10°$$

$$e = 0.50$$

T = phase 32.0 days after Dugan's light-minimum

$$a \sin i = 2.2 \times 10^7 \text{ km}$$

$$\frac{m_2^3 \sin^3 i}{(m_1 + m_2)^2} = 0.31$$

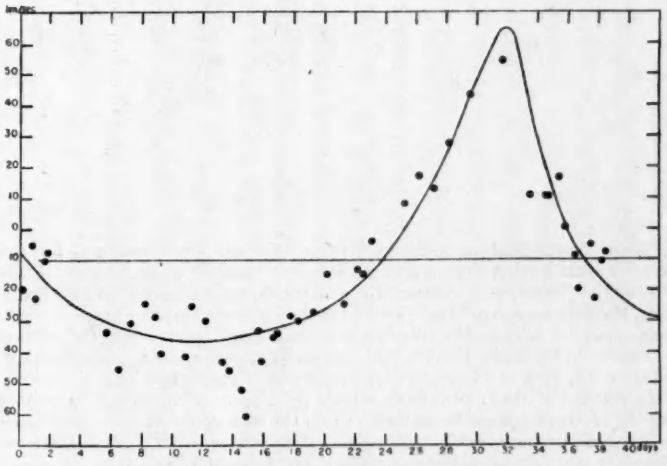

FIG. 2.—Observed velocity-curve of SX Cas

The velocity-curve shows a large amount of scatter, with departures as great as 20 or 25 km/sec. These departures are probably not systematic, in the sense that they appear to have no relation to the cycle during which the corresponding plates were obtained. It is very tempting to identify these large residuals with the irregular variations found at Mount Wilson or to relate them to the equally disturbing amount of scatter in Dugan's photometric measures. But it must be remembered that my exposures were long—usually 2 or $2\frac{1}{2}$ hours. The McDonald Observatory spectrograph is new; and, while it has not previously been suspected of any large instrumental errors, it has, in my opinion, not yet been tested sufficiently to be quite certain that the automatic temperature control is adequate. I am not wholly satisfied with the thermostatic arrangement; and, while I have no definite reason to suspect anything like the residuals we have encountered in the case of SX Cas, it will be necessary to make further tests before this possible instrumental source can be eliminated. I want to emphasize that with shorter exposures—of the order of 30 minutes—no perceptible errors of this kind were noticed. The slit was usually kept at the normal width of 0.05 mm, which is reduced in the camera to 0.025 mm. On

some exposures the slit was opened to 0.075 mm or, in one or two cases, to 0.10 mm. But care was always taken to bisect the star image exactly. I feel quite certain that there could have been no serious errors from faulty guiding. All other sources of instrumental errors, including flexure, focus, etc., have been investigated without revealing

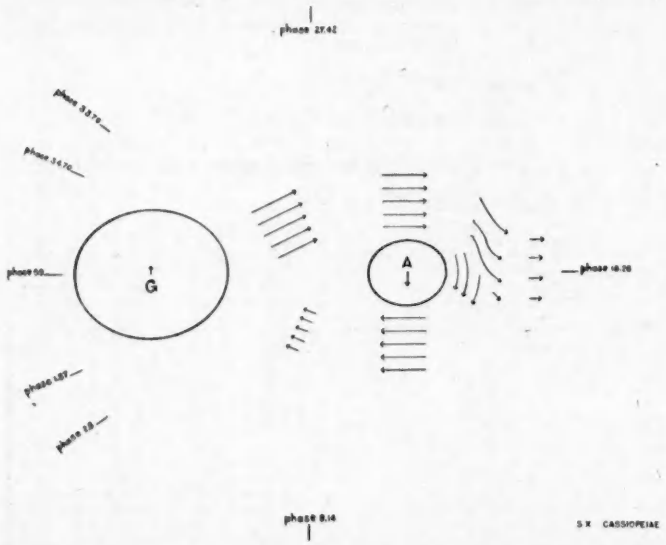

FIG. 3.—Schematic representation of the system of SX Cas. The drawing is not quite to scale, the distance between the stars having been made slightly less than given by Dugan. At phase 0.0 day we observe the center of the photometric eclipse. Beyond the G star there remain uneclipsed two streams of gas—one receding, the other approaching—which produce double emission lines of equal intensity. Immediately preceding partial eclipse, the receding stream is uneclipsed, while the approaching stream is covered by the G star. At the same time, a cool but rapid stream flowing from the G star to the A star is seen projected upon the disk of the latter, producing sharp absorption lines displaced toward the red. Immediately after the end of the photometric eclipse the approaching stream producing emission lines is uncovered and the receding stream is eclipsed. Upon the disk of the A star we now see projected a hot and slowly approaching stream which produces a shell spectrum with a small shift toward the violet. At phase 9.14 days the stars are at elongation. The shell-absorption lines show no relative shift, but the emission lines are produced from the stream at the far side of the A star, rushing away from the latter, and fill in the central *H* absorption lines. At phase 18.28 days the emission lines are double, but the absorption lines are displaced toward the violet. We infer that the stream of gas rushing around the following side of the A star divides into two streams, as in β Lyr. One part of the stream, presumably composed of the more distant or more rapid strata, expands outward, while the other part flows around the preceding side of the A star and ultimately returns to the G star. At phase 27.42 days conditions are similar to those observed at the first elongation: the velocity measured from the shell lines again equals the radial velocity of the A star, and the outrushing gases at secondary minimum cause undisplaced emission, which fills in the central hydrogen absorption lines. The arrows indicate the approximate directions of the motions of the stars and streams, but no attempt has been made to draw them to scale. Since the spectrum of the G star is only observed during totality and the slope of its velocity-curve during that interval is not sufficiently accurately determined, we have no knowledge about the relative masses. But analogy with the case of β Lyr suggests that the G star may be the more massive component of the system.

any explanation of the large residuals. Incidentally, all plates were taken with the telescope east of the piers. I also want to stress the fact that, while the residuals are larger than they usually are for a spectrum of the kind of SX Cas, these residuals in no way affect the general run of the velocity-curve with its large amplitude of 100 km/sec and its striking lack of symmetry. Close to 1000 radial velocities, measured from plates taken with this instrument, dispel any doubts of that nature.

PLATE IV

PLATE IV

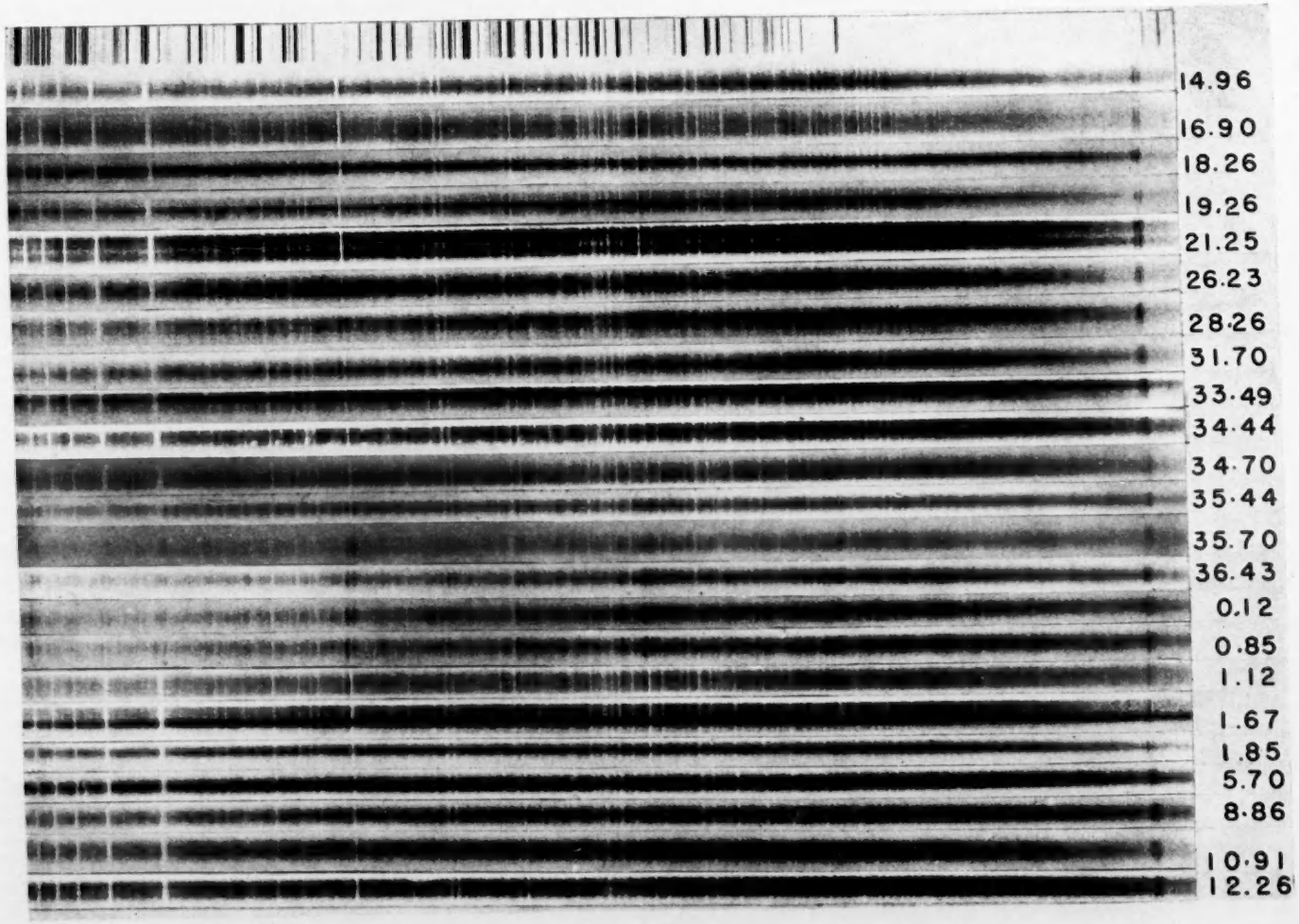

SPECTRA OF SX CASSIOPEIAE

UNIV. OF MICH.

Although the spectrographic elements give a reasonable interpretation of the observations of radial velocities, the remaining departures are of a systematic character, and it does not seem possible to improve the representation appreciably by altering the elements. Hence, I did not make a least-squares solution. It is better to recognize that the observations do not entirely satisfy the relations of the two-body problem. Thus, the velocities on the steep, descending branch are systematically too low. This could be corrected by one of the following procedures: (*a*) shifting ω and T toward larger values, (*b*) lowering the entire curve, (*c*) decreasing K, or (*d*) increasing e. But every one of these steps would result in making the agreement worse on the ascending branch, at maximum, or at minimum.

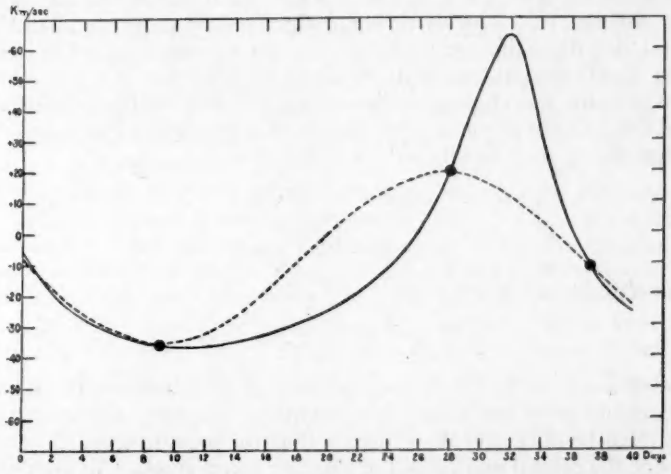

FIG. 4.—Reconstruction of the velocity-curve of the A star in SX Cas. The solid curve represents the observed radial velocities. In accordance with the model proposed in Fig. 3, we assume that near mid-eclipse of the A star by the G star and at the two elongations (phases 9.1 and 27.4 days) the observed velocity is equal to that of the A star. This would indicate a symmetrical velocity-curve ($e = 0.0$), in harmony with the photometric results, which require $e \cos \omega = 0$. The broken curve has been computed under these assumptions, with $\gamma = -8$ km/sec and $K = 27$ km/sec. The large negative departures of the observed curve from the true curve are attributed to an expanding stream of gas from the A star, as seen between phases 10 and 27 days. The effect reaches maximum near secondary minimum. The large positive departures between 30 and 34 days are attributed to a cool receding stream of gas which flows from the G star toward the following side of the A star.

There are, however, other, even more weighty, reasons for regarding the velocity-curve with suspicion. It is not that the large irregular departures cause it to be too uncertain. The principal difficulty is that the spectrographic elements are in violent disagreement with the photometric elements. The former give

$$e \cos \omega = +0.49,$$

while the latter give, for this quantity, zero or a small negative value. It is not possible to reconcile the results without casting doubt upon the interpretation of the velocity-curve. In fact, if we apply the well-known formula

$$e \cos \omega = \frac{\pi \left(t_2 - t_1 - \frac{P}{2} \right)}{P (1 + \operatorname{cosec}^2 i)},$$

we find, with $e \cos \omega = 0.49$, that the interval from principal minimum to secondary minimum should be

$$t_2 - t_1 = 29.7 \text{ days}$$

and that the interval from secondary minimum to principal minimum should be

$$t_1 - t_2 = 6.9 \text{ days.}$$

The theoretical formula for $t_2 - t_1$ is derived from the series expansion of $v - M$, the equation of center. This derivation neglects powers of e higher than the first and is only correct for small values of e. But we can derive $t_2 - t_1$, directly from the observed velocity-curve by remembering that $\gamma + Ke \cos \omega$ is the radial velocity at the times of eclipse, when $v + \omega = 90°$ or $270°$. The result is not significantly different from the one given by the formula. Anything like the asymmetry of the two minima in the light-curve, demanded by the spectrographic elements, is out of the question. On the other hand, it is not possible to alter the spectrographic elements appreciably without violating the velocity-curve, and this in spite of the large residuals. For example, if we take $e = 0.37$, $\omega = 21°$, $K = 47$ km/sec, $\gamma = -10$ km/sec, we still find

$$e \cos \omega = +0.35$$

and

$$t_2 - t_1 = 26.5 \text{ days.}$$

The photometric observations give

$$t_2 - t_1 = 18.28 \pm 0.5 \text{ days,}$$

where I have estimated the uncertainty of secondary minimum from Dugan's data. Yet, even the second set of spectroscopic elements violates the velocity-curve to such an extent that it must be rejected. We conclude that the measured radial velocities do not wholly represent the orbital motion of the brighter components. An appreciable portion of the measured velocities must come from some other type of motion—perhaps from a gaseous atmosphere which only in part belongs to the ordinary reversing layer of the A-type star. What I have in mind is some tenuous, absorbing cloud, resembling in character and astrophysical behavior the peculiar streams in the system of β Lyr. The dynamical properties of such a stream need, of course, not be similar to those in β Lyr. This hypothesis would probably provide an explanation of the peculiar variations in eccentricity and amplitude that have been observed at Mount Wilson by Adams and Joy. It will be recognized that this hypothesis is very revolutionary in character. If we cannot trust the velocity-curve of SX Cas for which the photometric observations provide the crucial test, how can we trust the velocity-curve of any other spectroscopic binary to give us an orbit which has a dynamical meaning? The answer is that the spectrum of SX Cas is peculiar and that we should never trust a peculiar spectrum to give us the radial velocity of the center of mass of the star. Astronomers used to believe that the so-called "B5 component" of β Lyr gave the velocity of the secondary component of that binary system. But the spectrum is not that of a normal B5 star, and it does not represent the motion of any star—only the motion of that section of a tenuous nebula which happens to be in the line of sight of the bright B8 star at the time of observation. In spite of this precedent, some astronomers may think it unreasonable to doubt the evidence in the case of SX Cas. But consider the alternative: The behavior of the bright lines, which we shall presently discuss, proves beyond doubt that the eclipse occurred very close to the time predicted by Dugan's elements. The error cannot have been in excess of 0.5 day. In addition, we have the supporting estimates of the magnitude by the spectrographic observers at McDonald. But Dugan's light-curve, and every other complete light-curve obtained over a period of twenty-five years, shows that secondary mini-

mum follows primary minimum after 18.3 days, with an uncertainty of perhaps less than 1 day. We can be certain, therefore, that in the summer of 1943 the secondary minimum occurred between phases 16.8 and 19.8 days. The radial velocities at these phases were approximately −33 and −26 km/sec—that is, not very far from the minimum of the velocity-curve at −36 km/sec. Anyone who would believe that an eclipse takes place near minimum radial velocity of a curve which has a large eccentricity and a small longitude of periastron is accepting a far more revolutionary idea than the one which I have proposed.

The considerations in the preceding paragraph show convincingly that not a small feature of the velocity-curve but a very substantial portion of all radial velocities must be due to the hypothetical stream. We can only be certain at this stage that the trend of the velocities in the vicinity of the two eclipses is in accordance with the true orbital elements. More information may be derived from a discussion of the spectrum.

Adams and Joy pointed out long ago that, outside of eclipse, the spectrum is that of an A6 star which resembles α Cyg. My spectrograms confirm this description, but they add some rather remarkable additional information. There can be no doubt that the spectrum is that of a very luminous A-type star, in the later subdivisions of that class. But if the spectrum resembles α Cyg, where are the strong lines of *Mg* II 4481 and of *Si* II 4128 and 4131? All three are present but are surprisingly weak. Thus, *Mg* II 4481 is weaker than *Ti* II 4468 or *Ti* II 4501 and is similar in intensity to *Ti* II 4488. In all normal supergiants of class A and even in some F-type supergiants, like ϵ Aurigae, the *Mg* II line is stronger than these *Ti* II lines. Moreover, *Mg* II 4481 is broader and more diffuse than the neighboring lines of *Ti* II and of *Fe* II. The conclusion is evident: We have before us —at certain phases—the spectrum of a shell whose dilution factor differs appreciably from 1. It is difficult to estimate the departure in the intensity of the *Mg* II line, but a factor of the order of 2 or 3 is indicated. The shell, or stream, is therefore a formation which extends above the height of a normal supergiant reversing layer but does not extend to a height where the dilution is extreme. Possibly, a height above the reversing layer of the order of 1 radius of the A star would be consistent with the observations. But this conclusion is quite uncertain, because we do not know whether the *Mg* II 4481 line originates in the stream or in the underlying A star. Only measures of the velocity can answer this. The line had not been included in the original list; but, after its importance became apparent, I made a new series of measurements, using it exclusively. The results are given in Table 3.

The *Mg* II line is quite faint, and on many plates it is so diffuse that no accurate settings are possible. The dispersion of the velocities is very large, and it is impossible to decide whether the *Mg* II line gives a curve different from those of the other lines. The maximum at phase 31.70 days is, however, well shown, and it is probable that in this particular stage the velocity of *Mg* II agrees with that from the other lines. It is possible that we are measuring a blend of *Mg* II 4481.33 with a faint line belonging to the shell.

The spectrum of SX Cas shows a number of bright lines which are greatly strengthened during the principal eclipse. Outside of eclipse, only $H\beta$, $H\gamma$, $H\delta$, $H\epsilon$, and $H\zeta$ are bright. During eclipse several other lines are bright, notably *Ca* II, *Fe* II, and *Sc* II 4247. There is no definite proof of the existence of forbidden [*Fe* II]. We infer that the emission lines are produced fairly close to the A star and not, as in VV Cephei, in an enormous envelope surrounding the entire system.

The emission lines are fairly broad at all times and are usually, but not always, divided into two components by a central absorption line of considerable intensity. The entire width of the emission lines is about 6 or 7 A for $H\delta$, and there seems to be no great difference in width from one phase to another or from one line to another. If the emission-line widths are interpreted as radial velocities of two streams of gas, they would correspond to values of the order of ± 220 km/sec.

During the principal eclipse the bright lines undergo a series of remarkable changes.

At phase 33.49 days we notice a gradual strengthening of the red component, at the expense of the violet. This process continues until phase 34.70, or possibly a little later, when the violet component is about three or four times weaker than the red component. Thereafter the two components become more nearly alike and reach equality at phase 36.4. At later phases the violet component is the stronger, and at phase 0.85 it is five or six times stronger than the red component. At this and at neighboring phases the violet component is perhaps twice as strong as the red component ever becomes prior to mid-eclipse. At phase 1.85 the violet component is still much stronger than the red component. My next plate, at phase 5.70, shows the two components of approximately the same intensity.

TABLE 3

RADIAL VELOCITIES FROM *Mg* II λ 4481

Phase	Vel. of *Mg* II (Km/Sec)	*Mg* II *minus* All Lines (Km/Sec)	Phase	Vel. of *Mg* II (Km/Sec)	*Mg* II *minus* All Lines (Km/Sec)
0.12	−37.5	−17.8	16.90	−32.7	+ 1.3
0.85	(+81.3)	(+86.5)	17.70	+ 6.9	+35.2
1.12	−29.6	− 7.1	18.26	.....	.....
1.67	+23.2	+33.4	19.26	+10.1	+37.7
1.85	+19.6	+27.1	20.24	+10.3	+25.0
5.70	+27.1	+60.9	21.25	+ 2.3	+27.2
6.59	− 0.7	+45.0	22.26	−10.3	+ 3.4
7.26	− 7.5	+23.3	22.61	−22.9	− 8.0
8.21	−12.0	+12.1	23.15	−26.1	−22.0
8.86	+10.0	+18.4	25.25	+18.7	+10.9
9.25	+ 0.9	+41.1	26.23	− 5.4	−22.3
10.91	−51.4	− 9.9	27.25	−14.0	−27.1
11.26	−35.6	−10.3	28.26	− 5.3	−33.0
12.26	+ 9.3	+39.3	29.55	+45.7	+ 2.4
13.24	+ 1.5	+45.2	31.70	+57.1	+ 3.0
13.70	−22.1	+23.9	33.49	+12.1	+ 1.3
14.67	−30.3	+21.9	34.44	−16.5	−27.0
14.86	−52.2	+ 8.5	34.70	− 4.3	−14.8
15.66	−14.3	+18.9	35.44	+40.9	+24.3
15.89	−28.5	+15.2	35.70	−49.3	−49.5
16.65	−38.5	− 3.3	36.43	+15.9	+24.5

This succession of changes indicates an eclipse of the emitting gases and is somewhat similar to that observed by Joy in RW Tau.[3] We have, however, in SX Cas no phase of total eclipse, but either a partial or an annular eclipse. Nor can we be certain that the emission lines originate from a rotating ring. The observations only show that about one day before the beginning of the photometric eclipse the G star begins to occult a mass of gas whose extreme velocity is −220 km/sec. This value refers to the violet edge of the violet component. If we allow for turbulent motions in the gas and for instrumental distortion of the emission-line contour, the corresponding stream velocity is of the order of −150 km/sec.

At about the beginning of total phase in the photometric eclipse, or perhaps a little earlier, the violet component is weakest; but it does not completely disappear and is, therefore, never totally eclipsed. A little before mid-eclipse the two components are equally strong. Thus, at the end of totality the violet component is strongest, but the red component is still visible. A little later the red component is completely gone and is therefore totally eclipsed by the G star.

It is, of course, tempting to think of the emitting gas as constituting a shell around the A star, which rotates in the direction of the orbital motion with $V_e = 150$ km/sec and shows the familiar rotation effect during its eclipse. But closer consideration renders

this hypothesis untenable. The radius of the A star is of the order of 10^7 km, according to Dugan. If it rotates in phase with the orbital motion, its equatorial velocity is

$$V_e = \frac{2\pi r}{P} = 20 \text{ km/sec}.$$

In all ordinary rotating shells the velocity of the shell decreases outward as r^{-1}. Even if the A star should not rotate synchronously with its orbital motion, the sharpness of its absorption lines conclusively shows that V_e cannot be much larger than 20 km/sec, and certainly cannot be anything like 150 km/sec. Moreover, it would seem quite doubtful that a stable rotating shell can exist around the A star, considering that the distance from its surface to the surface of the G star is only about twice the radius of the latter.

We must, I think, attribute the emission to a stream of gas which flows toward us at $V = -150$ km/sec and is eclipsed before principal photometric eclipse. Since this eclipse of the stream begins about one day earlier than the photometric eclipse, we attribute to the stream a height above the surface of the A star of the order of the latter's diameter. After photometric mid-eclipse we observe the eclipse of the opposite stream, whose velocity is one of recession.

The entire picture is very similar to that observed in β Lyr. Only here the smaller (and probably less massive) star is the bright A-type component, while in β Lyr the smaller and less massive star is the invisible F-type component.

The most interesting feature of SX Cas is the observation of an approaching shell at and near secondary eclipse. These motions are plausibly attributed to the turning-over of the shell stream due to conservation of angular momentum. Only a part of the stream is retained by the system and completes the entire circuit around the A star. The observations fit this hypothesis surprisingly well. The only discrepancy consists in the greater strength of the violet emission component after mid-eclipse over the red component before mid-eclipse. A priori, we should have expected the opposite trend, since fewer atoms participate in the approaching stream than in the receding stream.

We next investigate the behavior of the radial velocities at and near principal eclipse. The observations of the bright lines place mid-eclipse very near to the epoch predicted from Dugan's formula. Unless the bright lines are physically unsymmetrical with respect to primary eclipse, the point of mid-eclipse may come about 0.2 day earlier than phase 0.0 day. Disregarding this small departure, we find that the velocity-curve at phase 0.0 gives approximately -6 km/sec, while the observations during the eclipse run as shown in the accompanying table.

Phase	Velocity		Remarks
	All Lines	*Ca* I+*Sr* II	
34.44	+10.5	+ 2.5	
34.70	+10.5	+ 2.9	
35.44	+16.6	+ 3.5	
35.70	+ 0.2	−30.2	Trend of G component should predominate
36.43	− 8.6	−28.4	
0.12	−19.7	−34.1	
0.85	− 5.2	− 8.6	
1.12	−22.5	−22.7	
1.67	−10.2	−22.0	
1.85	− 7.5	− 8.7	

Allowing for the large amount of scatter, which we have found in the other parts of the curve as well, these observations give no clear indication of the velocity of the G

component, which, at least close to the total phase, should have a trend opposite to that of the velocity-curve of the A star. The three observations at phases 35.70, 36.43, and 0.12 show, however, approximately the same rate of descent as the rest of the observations. This result is very puzzling, since the photometric observations leave little doubt that the eclipse is actually total and since color observations by Gerasimovič support the generally accepted conclusion that the eclipsing star is considerably later in type than the eclipsed star. To strengthen the argument, we consider next the radial velocities of those lines that are greatly strengthened during the eclipse, namely *Fe* I, *Ca* I, and *Sr* II. The *Fe* I lines show little of interest; but those of *Ca* I and *Sr* II, which are strengthened during eclipse more than any of the others, do suggest the required trend: they are much more negative in velocity at phases 35.70, 36.43, and 0.12 than after mid-eclipse. We must conclude that at the phases considered the observed spectrum is a blend of a true star of a fairly late spectrum—probably G—and lines of another origin which resemble in character the shell lines of the A star and share with it the descent of the velocity-curve. The interpretation of this result is not quite clear. Since it is almost certain that Dugan's conclusion of a total eclipse during the deeper of the two minima is correct, the existence of lines at totality which share the velocity of the A star is very peculiar. But perhaps there are other streams of gas near the G star which our study has not otherwise revealed. The observations of the lines of *Ca* I and *Sr* II are not accurate enough to establish the mass ratio.

Even more puzzling is the great steepness of the velocity-curve between phases 32 and 2 days. If the velocity-curve gives us the correct velocity of the system at mid-eclipse, or -6 km/sec, we must assume that, since $e = 0$ from Dugan's work,

$$\gamma = -6 \text{ km/sec},$$

and the distortion of the velocity-curve at secondary minimum amounts to

$$\text{Observed } -\gamma = -24 \text{ km/sec}.$$

Since this is presumably a "blended" velocity, the actual expansion velocity of the gases at secondary minimum may be of the order of

$$V_{\text{exp}} = -50 \text{ km/sec}.$$

The question now is whether the maximum of the velocity-curve at about $+60$ km/sec represents a point on the real velocity-curve of the A star. If it does, then we cannot have $\gamma = -6$ unless the true velocity-curve has a much deeper minimum than that observed, namely, -36 km/sec. It is, of course, possible that the true range of the velocity-curve is much greater than 100 km/sec. It would have to be of the order of 140 km/sec in order to give -6 km/sec at phases 0.0 and 18.3 days, $+65$ km/sec at phase 27.5 days, and -75 km/sec at phase 9.1 days. But our proposed picture of SX Cas gives us no reason whatever to expect large deviations from the observed velocity-curve at phases 9.1 and 27.5 days. It is much more reasonable to suppose that at these two phases the velocities of the true curve are approximately as observed, namely, -35 and $+19$ km/sec. For an eccentricity of zero this would give $\gamma = -8$ km/sec, in good accordance with the observed value of -6 km/sec. We conclude that actually

$$2K = 54 \text{ km/sec}.$$

If this is correct, the descending branch of the velocity-curve is too steep. Near phases 32 and 33 days, in particular, we observe too large a velocity of recession in the absorption lines, while immediately after eclipse the velocity may be slightly too low. If this phenomenon were limited to the duration of the principal eclipse—that is, from phase 34.7 to phase 1.9 days—then we should have been entitled to suspect the presence of a large rotational effect. But in this case the explanation must be sought elsewhere.

The answer lies, I believe, in the fact that, even though the shell phenomena are most pronounced near secondary minimum, we almost certainly observe a shell spectrum between phase 31 days and mid-eclipse and again immediately after eclipse. There is no phase where *Mg* II 4481 is of normal intensity. We must conclude that before principal eclipse we see projected upon the disk of the A star a powerful stream of gas flowing from the G star toward the A star, while after eclipse we see a much slower stream flowing from the A star toward the G star. This observation is also in excellent harmony with my conclusions concerning the phenomena of β Lyr.

The bright *H* lines undergo conspicuous changes during the entire 36.56-day cycle. After the end of the eclipse these lines are clearly double, with shell-absorption lines between the bright components. The same is true just before eclipse. But at phases between 27 and 31 days the central absorption at $H\beta$ is almost invisible, while those of the other *H* lines appear greatly weakened, as though they were covered with emission. This phenomenon is most pronounced at phase 28.26 days, just preceding the observed maximum of the velocity-curve. If other proof were needed, this weakening of the central absorption at H, δ, ϵ, ζ, etc., and its disappearance at $H\gamma$, β would suffice to eliminate the hypothesis of a rotating shell. We attribute the phenomenon to the emission of gas expanding from the A star, in the general direction away from the G star—the same gas that gives rise to the violet shift of the absorption line at secondary minimum. A somewhat similar but less conspicuous stage of a single emission line at $H\beta$ occurs at phases of 7 and 8 days. At these phases the emission from the outward-moving atoms would again be undisplaced and would cover up the shell- and star-absorption lines. We should have expected that at the two stages, near phases 8 and 28 days, the emission lines would be somewhat narrower than at the two minima. I do not believe that such an effect is noticeable, and we must conclude that the internal motions within the streams of gas are quite complicated.

Another remarkable observational result is the persistent absence of the violet emission component of $H\gamma$ throughout the entire cycle except between phases 35.70 and 1.12, inclusive. Only in the second half of the eclipse does this component show. Yet the *H* absorption line and the red emission component behave in a perfectly normal manner. This suppression of the violet emission component, which is independent of the phase, is occasionally observed in other stars. It must be caused by the absorption of the emitting radiation by the absorbing atoms of the line *Ti* II 4337.9. Since *Ti* II is very strong in SX Cas, this explanation is entirely plausible. The laboratory intensity is 125, which compares favorably with the intensities of other *Ti* II lines which are strong absorption features in SX Cas (λ 4443.81 [125]; λ 4468.50 [150]; λ 4501.27 [100]). The fact that the *Ti* II line completely (or nearly completely) obliterates the emission shows that the *Ti* II absorption takes place in front of the emitting layer. This is reasonable at most phases, but not near phases of 8 and 28 days, where the violet component of the $H\gamma$ line must originate from turbulent motions in the emitting layer as seen when the two stars are in elongation. There is then no particular reason why the *Ti* II should originate in front of the emitting mass. Our plate at phase 28.26 days does, indeed, suggest that the *Ti* II absorption is less effective.

There remains the problem of the changes in the intensities of the absorption lines, other than those of *H*. Although the shell spectrum is visible at all phases, including those of the eclipse, the intensities of the lines undergo fairly marked variations. We have already commented upon the great strength of the shell-absorption lines near phase 18.3 days. This stage may be said to develop some five days after principal minimum and to last until about phase 21 days. It is characterized by the great intensity of *Fe* II absorption lines. After phase 21 days the *Ti* II lines become relatively stronger than the *Fe* II lines; and this is accompanied by a gradual strengthening of *Fe* I and especially of *Sr* II and *Ca* I. In other words, the spectral type becomes appreciably later than in the early phases and remains so, without much change from about phase 26 days until the begin-

ning of the eclipse at phase 34.44 days. During the eclipse the spectrum changes still further and displays an enormous increase in the intensity of *Ca* I and *Sr* II. We have already seen that during and near the total phase these lines belong to the later-type companion of the binary. The fact that the transition from a pure A-type shell spectrum to a later type occurs gradually, beginning at about that phase at which we presume the observed velocity-curve to fall above the true curve, implies that the receding current of gas which flows from the G star toward the A star and through which we observe the A star for some days prior to the beginning of the photometric eclipse has a later spectrum and presumably a lower temperature than the stream which we observe at secondary eclipse or prior to it. This state of affairs is opposite to that observed in β Lyr, where the stream starts at a higher temperature and where it flows out of the B8 star and returns at a cooler temperature after it has flown around the F star. But in SX Cas the roles of the hot and the cool stars are reversed. Hence, we observe precisely what we should expect.

It should be pointed out that the spectrum of the secondary cannot be seen at phases of between 29 and 32 days. If the observed velocity-curve were real, the separation should be of the order of 120 km/sec for equal masses. This is entirely sufficient to show double lines. Dugan's light-elements give $L_1 = 0.46$ for the G star and $L_2 = 0.54$ for the A star. If these values are reliable, the spectrum of the secondary might be expected in the visual region. In the photographic region it is probable that the A star is much brighter than the G star. But, aside from this, the velocity-curve is so badly distorted that the true range is probably too small to show the doubling of the lines at elongation.

The proposed hypothesis explains the majority of the observed effects. It is certainly far more acceptable than any attempt which would accept the observed velocity-curve as real, despite its contradictory character. A few observed facts remain unexplained, and one—the large negative velocity of the lines of *Ca* I and *Sr* II during totality—is unfavorable to it. From the theoretical point of view, the large velocity of the streams as found from the emission lines is perhaps surprising. But, whatever we may say about the rest of our hypothesis, this large velocity, of the order of 150 km/sec, is directly inferred from the widths of the emission lines.

Before I conclude this discussion I want to call attention to Carpenter's work on the spectrographic orbit of U Cephei.[6] We have in this case a velocity-curve which is quite similar to that which I have found for SX Cas, except for the scales in time and velocity. Carpenter finds that $e = 0.47$ and $\omega = 25°$. The photometric results, on the other hand, show that $e \cos \omega = 0$. The spectra of the two stars are also similar—A0 for the bright star and K0 for the fainter companion. It would be of interest to apply to U Cep the results obtained for SX Cas. J. Ellsworth[7] has attempted to reconcile Carpenter's spectrographic results with his own light-curve by adopting for the latter a value of $e \cos \omega = 0.204$. He rediscusses the spectrographic observations under the assumption that $e = 0.211$ and $\omega = 15°$. However, the velocity-curve obtained with these elements differs systematically from the observations, and there can be no doubt that Carpenter's values $e = 0.474$ and $\omega = 25.0°$ are more consistent with the observations. There is also some uncertainty concerning the interpretation of the secondary minimum in U Cep. Dugan[8] finds that $e = 0$. Moreover, Dugan states in a supplement to his *Finding List for Observers of Eclipsing Variables* that Joy and Rosenberg found no large eccentricity, the former presumably from spectrographic observations. Recent spectrograms of U Cep taken by me at the McDonald Observatory show that the early-type star, which incidentally shows nice helium lines, does not have a weakened line of *Mg* II 4481 and therefore probably does not have an extensive shell. But a final answer will only be possible after a new velocity-curve has been determined. It is possible that in U Cephei the streams of gas are too close to the surface of the star to show dilution effects.

[6] *Ap. J.*, 72, 205, 1930.

[7] *Pub. Obs. Lyon*, 2, Part I, 1936.

[8] *Contr. Princeton U. Obs.*, No. 5, 1920.

A NOTE ON THE SHELL SPECTRUM OF 48 LIBRAE (HD 142983)[1]

W. A. HILTNER[2]
McDonald Observatory and Observatory of the University of Michigan
Received September 20, 1943

ABSTRACT

A Coudé spectrogram shows all the shell lines of 48 Librae to be asymmetrical with sharp red edges shaded toward the violet. A difference in line profiles for various elements is observed.

In a recent paper Struve[3] called attention to the asymmetry of the lines in the shell spectrum of 48 Librae. His discussion of the observed asymmetrical lines was based largely on a Coudé spectrogram obtained at McDonald Observatory on May 16, 1943. This spectrogram was exposed only sufficiently heavily to show that the stronger lines possessed a pronounced asymmetry, while the profiles of the weaker lines were lost in the grain of the emulsion.

A second Coudé spectrogram, much more heavily exposed, was obtained by the author at McDonald Observatory on 103a-0 baked emulsion on June 2, 1943. The plate was calibrated with a V-slit on the Coudé spectrograph and was analyzed with the direct-intensity microphotometer of the Observatory of the University of Michigan. Tracings for the region λλ 4118–4593 are shown in Figure 1. The ordinates are intensities, with an intensity of 70 representing the continuous spectrum. The vertical lines correspond to millimeters on the spectrogram.

The shell lines, weak ones as well as strong ones, are asymmetrical, being shaded toward the violet and possessing a sharp red edge. The only notable exception is *Mg* II 4481. The hydrogen lines show strong Stark wings accompanied by sharp central cores which are asymmetrical in the same sense as the metallic shell lines. The cores of the hydrogen lines have very low residual intensity. However, the core of $H\delta$ may consist of two components, but $H\gamma$ shows no evidence of duplicity on the original spectrogram. The *He* I lines, λ 4144 and λ 4472, produced in the reversing layer, are extremely broad, with total breadths of approximately 15 A and 25 A, respectively. The asymmetrical lines suggest an expanding shell in which the velocity of expansion is not uniform throughout the shell.[4]

The mean profiles of *Ni* II, *Fe* II, *Fe* I, *Cr* II, *Ti* II, and *Mg* II are shown in Figure 2. All lines have been reduced to the same scale, in intensity as well as wave length. Nickel and magnesium are represented by only one line each, *Ni* II (λ 4067) and *Mg* II (λ 4481), while the profiles of *Fe* II, *Fe* I, *Cr* II, and *Ti* II are means of two or more lines of different intensities. No systematic variation in profile of lines of different intensities for any one element is observed. However, there is a pronounced difference in line profiles for the various elements. This is probably a consequence of stratification in the shell.[5] Struve,[6]

[1] *Contributions from the McDonald Observatory, University of Texas*, No. 82.

[2] Fellow of the National Research Council.

[3] *Ap. J.*, 98, 98, 1943.

[4] *Ibid.*, pp. 108–111.

[5] Struve, *Ap. J.*, 95, 140, 1942.

[6] *Ap. J.*, 98, 98, 112, 1943.

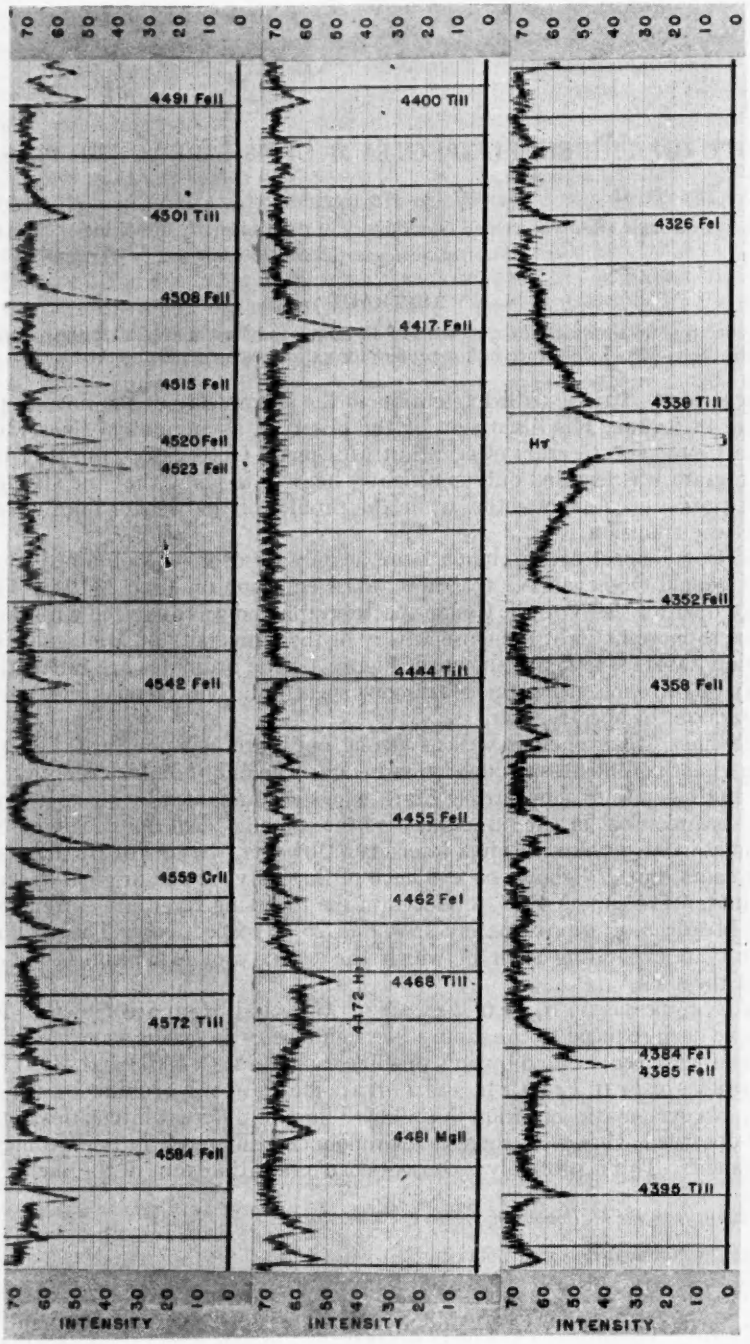

FIG. 1.—Intensity tracings of spectrogram of 48 Librae taken June 2, 1943

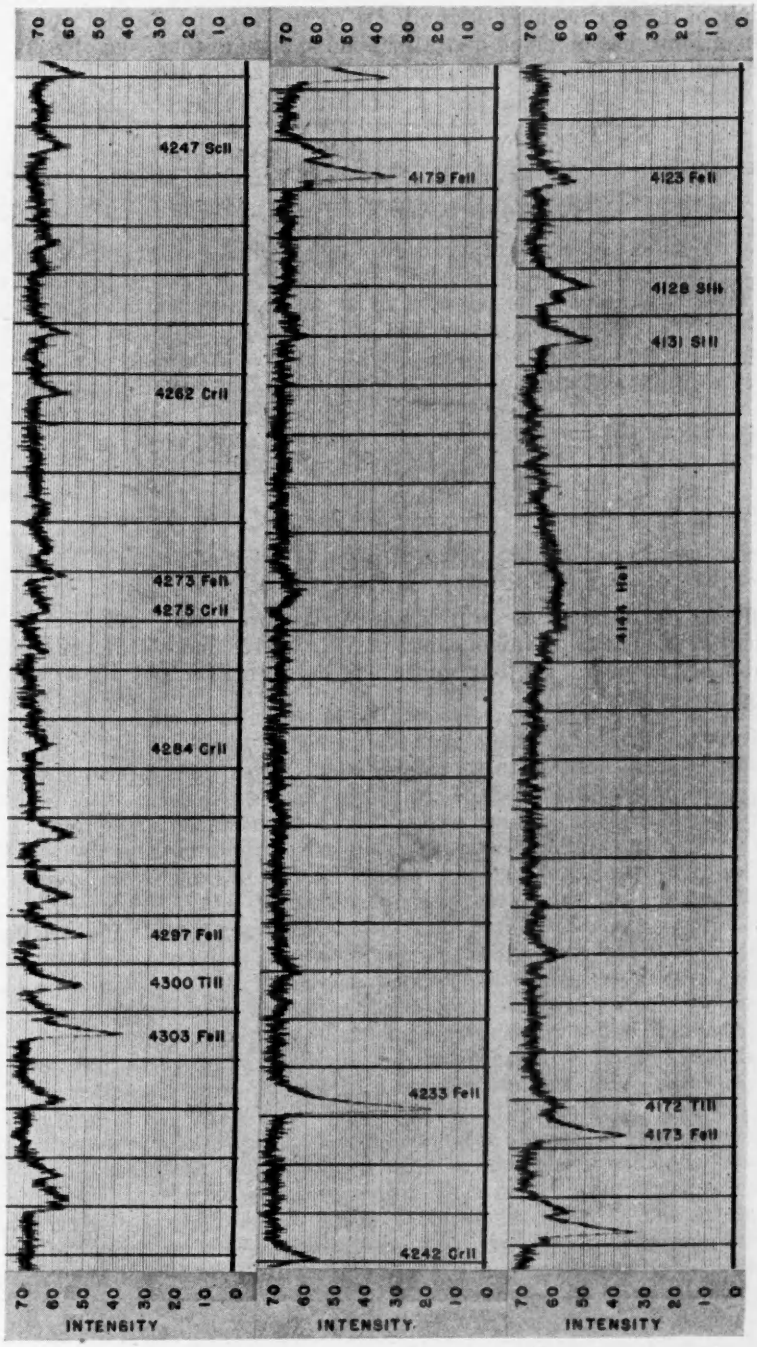

FIG. 1.—*Continued*

from a study of the relative intensities of *Fe* II, *Cr* II, *Ti* II, and *Ni* II lines on either side of the Balmer limit, has observed a stratification similar to that suggested by the profiles of the shell lines. The *Fe* I line (mean of λ 4326 and λ 4462) of Figure 2 has the

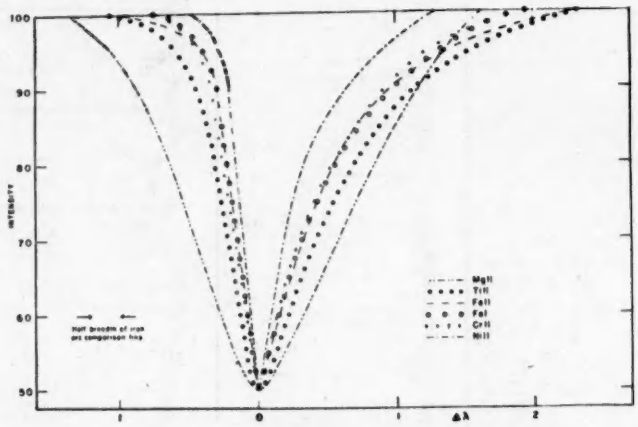

FIG. 2.—Profiles of shell lines in 48 Librae. Violet is to the right

same profile as *Fe* II and *Cr* II. *Ti* II is somewhat more broad, and *Ni* II (λ 4067) is sharper than *Fe* II. The two available lines of *Si* II, λ 4128 and λ 4131, are blends; their profiles probably lie near *Ti* II, but somewhere between *Ti* II and *Mg* II, which latter is only slightly asymmetrical.

RECENT PROGRESS IN ASTROPHYSICS

"THE VARIATIONS IN THE PROFILES OF STRONG FRAUNHOFER LINES ALONG A RADIUS OF THE SOLAR DISK" BY J. HOUTGAST

Houtgast's dissertation is one of the most important papers on solar spectroscopy that have appeared in the last few years. Prepared under the supervision of M. Minnaert, and submitted in June, 1942, to the University of Utrecht in candidacy for a doctorate, it presents an extensive and homogeneous body of data on center-limb variations of strong absorption lines in the solar spectrum. The analysis of this material provides perhaps the first observational evidence in astronomy for the importance of noncoherent scattering.

The first section in this review discusses the observational data obtained by Houtgast. In Section II Houtgast's theoretical interpretation of these data is summarized and evaluated.

I. OBSERVATIONAL DATA

Plates were taken from 1935 through 1938 with grating spectrographs both at the Heliophysical Institute at Utrecht and at the Institut für Sonnenphysik at Potsdam. Spectra were recorded from the center of the solar disk and at points 0.60, 0.80, 0.90, 0.95, and 0.98 of the solar radius from the center. On some of the later plates spectra were also taken in regions whose mid-points were 0.99 and $0.995R_\odot$ from the center.

Different observational techniques were used at Utrecht and at Potsdam. The Utrecht plates were made with second-order spectra, yielding a dispersion of 2 A/mm, except for the H and K lines, for which the first order was used. A platinum step-reducer, with five steps, was placed above the slit for calibration purposes. For each exposure one of a set of general reducers was used to give the same blackening for center and limb spectra with the same exposure time. In this way a single characteristic curve could be used for each series of spectra along a radius. The characteristic curve actually used in each case was checked for each exposure, however, except for those $0.98R_\odot$ or more from the center of the disk, since for these exposures the nonuniformity of the illumination along the slit prevented an accurate check. This lack of uniformity arose from the darkening toward the limb, combined with the curvature of the solar image and the length of the slit, the latter placed perpendicular to the radius. It should perhaps be noted that, since the general reducers gave the spectra the same blackening as those at $0.98R_\odot$ taken without a reducer, the spectra closer to the limb were made with longer exposures to give the same blackening. In principle, a different calibration-curve should have been used for these spectra; there are various other reasons, however, for not trusting too heavily these measurements so close to the limb.

A Moll microphotometer was used in reducing the spectra. Profiles were determined from at least four of the five steps produced with the step-reducer. These separate determinations, which "always agreed within 5 per cent," were averaged to give final profiles for each line at each distance from the center of the sun. The determination of the continuous spectrum and the correction for ghosts were carried through in the usual manner. Scattered light from other regions of the sun was shown to be negligible by a thermoelectric comparison of intensities within and beyond the limb. A color filter was placed above the slit to reduce scattered light within the spectrograph; no attempt was made to correct for the light actually scattered within the spectograph, however, or for the finite resolving-power of the spectograph. As a result, the Utrecht data do not apply to the cores of strong lines, except for the very wide H and K lines.

At Potsdam a monochromator was used with a grating spectrograph, giving a dispersion of 0.67 A/mm in the second order. As a result, intensity measurements in line centers were possible. The limb spectra beyond $0.90R_\odot$ were each taken twice with a radial slit—once with a long slit extending from the limb to $0.95R_\odot$ and once with a much shorter (3-mm) slit extending from the limb to $0.98R_\odot$. The first exposure was used to measure the profiles at points $0.95R_\odot$ and $0.98R_\odot$ from the center, while the second was used for the points closer to the limb and also at $0.98\ R_\odot$. No systematic difference in resultant line profile could be detected between these two procedures. In addition, each exposure was made twice—once with the monochromator passing a wavelength region of about 30 A and once with only 3–4 A admitted; the first exposure was necessary for measurements of the continuous background and the line wings, while the second was used for measuring the intensities in the line cores.

The Potsdam spectra were photographed with a miniature camera, using Afga Isopan F or Isopan SS film, with 36 spectra on each film. Standardization spectra, taken with a step-reducer and a small grating spectograph, were interspersed between the other spectra. Various exposure times were used; in each case the exposure times for the spectrum and for the standardization spectrum used in the reduction differed by a factor of less than 2. No change of characteristic curve with exposure time was ever observed, however. A Zeiss photometer, with a slit width corresponding to 0.02 A on the film, was used in reducing the Potsdam spectra.

The central intensities found were corrected for the instrumental curve of the spectrograph, determined from narrow lines, using the method of van de Hulst and Kremer.[1] The corrections ranged between 3 and 7 per cent of the continuous background. Intensities at other parts of the line profiles were not corrected for finite resolving-power.

A discussion of the possible sources of error and an intercomparison of the values found at Utrecht and Potsdam lead Houtgast to the conclusion that the errors "have but a very slight systematic influence on the centre-limb variation." One of the greatest sources of error is thought to be the steepness of slope of the inner wings of some Fraunhofer lines, where a small error in the distance from the center of the line leads to a large error in relative intensity. In addition, there is also some question as to the exact distance from the limb of the points denoted by $0.99R_\odot$ and $0.995R_\odot$.

In view of the many difficulties inherent in this type of work, Houtgast's data on center-limb variations, despite the many experimental precautions taken, cannot be relied upon too greatly without an elaborate and detailed confirmation. Different determinations of line profiles frequently disagree, and the present case is no exception. Houtgast compares his measurements with those of other workers;[2] and the agreement, while satisfactory in some instances, is not very good in others, with systematic differences appearing in the center-limb variations.

As an example of the discrepancies which may appear, Houtgast's results on the *Na* D lines may be compared with those of C. D. Shane,[3] obtained with an interferometer and therefore presumably very accurate. A comparison of the two sets of central intensities is given in Table 1.

The values listed for Houtgast with $r/R_\odot = 0.965$ were found by averaging the values for $r/R_\odot = 0.95$ and 0.98. Essentially the same values are found, however, if a smooth curve is drawn through the intensities at all values of $r/R_\odot$ and the value at 0.965 read from this curve. Table 1 shows that the errors, whatever their cause, do, in fact, have a systematic effect on the center-limb variations.

[1] H. C. v. d. Hulst, *B.A.N.*, **9**, 225, 1941, and P. Kremer, *B.A.N.*, **9**, 229, 1941.

[2] M. Minnaert, *Zs. f. Phys.*, **45**, 610, 1927; A. D. Thackeray, *M.N.*, **95**, 293, 1935; T. Royds and A. L. Narayan, *Kodaikanal Obs. Bull.*, **109**, 375, 1936; H. H. Plaskett, *M.N.*, **91**, 870, 1931; E. Cherrington, *Lick Obs. Bull.*, No. 477, 1935; G. Righini, *Pub. Arcetri*, **51**, 57, 1933, and *Mem. Soc. astr. ital.*, **7**, 191, 1933; C. W. Allen, *M.N.*, **100**, 10, 1939.

[3] *Lick Obs. Bull.*, No. 507, 1941.

Another example may be obtained from the intensities in the wings, as shown in Table 2. For the D_2 line Houtgast's values for the red and violet wings have been averaged, while for the D_1 line only the intensities for the violet wing have been used, since the red wing was not measured at the same distance from the line center, and, moreover, at the closest corresponding wave length is marked "disturbed by blends." It is again evident that the center-limb variations are systematically different in the two sets of data. In general, Shane's data suggest that the far wings of the D lines may become appreciably weaker near the limb than is indicated by Houtgast's observations on the same lines.

TABLE 1

RELATIVE CENTRAL INTENSITIES FOR THE D LINES

	D_1(λ 5895.9)		D_2(λ 5890.0)	
Position on solar disk	$r/R_\odot=0.00$	$r/R_\odot=0.965$	$r/R_\odot=0.00$	$r/R_\odot=0.965$
Houtgast (Potsdam)	0.053	0.044	0.028	0.040
Shane	0.058	0.080	0.052	0.070

TABLE 2

RELATIVE INTENSITIES IN THE WINGS OF THE D LINES

	$D_1(\Delta\lambda=0.40)$		$D_2(\Delta\lambda=0.80)$	
Position on solar disk	$r/R_\odot=0.00$	$r/R_\odot=0.965$	$r/R_\odot=0.00$	$r/R_\odot=0.965$
Houtgast (Potsdam)	0.768	0.787	0.878	0.875
Shane	0.740	0.797	0.850	0.892

It is, of course, not impossible that these differences may be real, arising from a variation of the solar spectrum with time. Houtgast took pains to photograph only those regions of the solar disk which were relatively undisturbed by sunspots and other evidences of local variability, but Shane does not state whether or not the regions photographed by him were free from apparent disturbances. It is to be hoped that further work may resolve the discrepancies between these different measurements.

TABLE 3

THE OBSERVED LINES

Fe		*Mg*		*Ca*	Ca^+	*Na*
3815.9A	4063.6A	3829.4A	5183.6A	4226.7A	3933.7A	5890.0A
3820.4	4071.8	3832.3	.....	.....	3968.5	5895.9
3859.9	4132.1	3838.3	.....	.....	8498.1	
4005.3	4143.0	5167.3	.....	.....	8542.1	
4045.8	.....	5172.7	.....	.....	8662.2	

The 23 lines measured by Houtgast make up seven multiplets, in addition to the *Ca* I line λ 4226.7. The list of the lines examined forms Table 3. For each line at each point on the solar disk the measured intensities at various points on the line profiles are listed. For some lines profiles are plotted. The greatest emphasis, however, is placed on

the intensities in the far wings (relative intensity greater than 0.80). Since theory suggests that in the far wings the relative intensity r is given by

$$r = \frac{1}{1 + \frac{c}{(\Delta\lambda)^2}},$$

the observations were combined to give values of c. These were found by plotting r against $r/(\Delta\lambda)^2$ and taking the slope of this curve for very large $\Delta\lambda$. This procedure has the great advantage that it minimizes the effect of random errors, although systematic errors may still remain. Blending of lines, especially in the ultraviolet, makes it impossible to determine this quantity for all of the lines investigated. Nevertheless, the values of c for each of 15 lines as a function of $r/R_\odot$ form the most important part of the observational material in Houtgast's paper. Equivalent widths are also given for all lines sufficiently undisturbed by blends.

II. INTERPRETATION OF THE OBSERVATIONS

The discussion of the observational material proceeds in three separate sections—for the central intensities, the inner wings, and the far wings, respectively. Early preliminary discussions[4] of some of the Utrecht observations are supplanted by this much more exhaustive treatment.

The analysis of the central intensities is quite standard, confirming what has previously been known. Theory predicts that in any given multiplet the central intensities should be almost entirely independent of most of the factors responsible for a variation of the continuous background both with frequency and with the angle of the emergent ray. Houtgast's results show that the center-limb variations of the relative central intensities simply reflect the center-limb variation of the continuous background. For a discussion of line cores, absolute intensities are much more relevant to the problem than intensities relative to the adjacent background. This fact has been noted before, not only for the solar spectrum but also for the M supergiant stars.[5]

Houtgast also derives from his results the values of s/k (or σ_ν/χ_ν), the ratio of the selective absorption to the selective scattering; in Eddington's notation this quantity is denoted by ϵ. As B. Strömgren has pointed out,[6] the selective absorption for a given line is probably due to the effect of electron captures in the upper level producing the line. Theoretical values of s/k based on this assumption have been derived by A. Unsöld.[7] In view of the uncertainties both in the theory and in the data, the agreement between the two sets of values is satisfactory, except for the Ca^+ lines, for which the high ionization potential and the known excess of ultraviolet energy in the solar spectrum may perhaps be responsible for the high observed central intensities. Houtgast's conclusion that lines in the same multiplet show radically different values of s/k, in disagreement with theory, is largely based on his data for the *Na* D lines; Table 1 shows that this conclusion is not based on incontrovertible evidence.

To interpret a line profile at some distance from the center of the line, a much more elaborate theory is necessary; Houtgast spends some time discussing the various necessary approximations and deriving general formulae for the emergent intensity as a function of angle of emergence. The usual Eddington-Milne approximation is used to obtain a solution of the equation of radiative transfer. The lines are assumed to be formed in a layer of arbitrary thickness τ_1, measured in terms of the optical depth in the

[4] M. Minnaert and J. Houtgast, *Zs. f. Ap.*, **12**, 81, 1936; J. Houtgast, *Zs. f. Ap.*, **16**, 43, 1938.

[5] L. Spitzer, Jr., *Ap. J.*, **90**, 517, 1939.

[6] *Zs. f. Ap.*, **10**, 237, 1935.

[7] *Physik der Sternatmosphären*, p. 307, eq. (74.8), Berlin: J. Springer, 1938.

continuous spectrum on each side of the line; this layer is assumed to overlie a purely absorbing photosphere. The quantity τ_1 may be varied to represent different concentrations of scattering atoms toward the surface. When τ_1 is zero, the equations reduce to those for the Schuster-Schwarzschild model of a purely scattering layer above the photosphere, while, when τ_1 is very large, the equations reduce to those of the Milne-Eddington model, where all quantities are constant with optical depth.

The general equations derived by Houtgast allow not only for selective scattering and absorption but also for selective extinction; i.e., the total monochromatic absorption coefficient is represented as the sum of four terms: χ, representing the general absorption; χ_ν, the selective scattering; σ_ν, the selective pure absorption; and λ_ν the selective extinction. All but the last of these quantities are accompanied by corresponding terms in the total emission. The notation used is essentially that of Unsöld.[7] In the Eddington-Strömgren notation[8] these three quantities are denoted by k_ν, $(1 - \epsilon)l_\nu$, and l_ν, respectively.

There follows a considerable discussion of noncoherent scattering. This phenomenon arises when the selectively scattered radiation is first captured in the usual way and is subsequently re-emitted with a slightly different frequency. In the limiting case of completely noncoherent scattering the distribution of the emitted radiation is proportional to the line-scattering coefficient and is independent of the frequency distribution of the radiation captured by the atoms. For a strong line the scattering coefficient at the line center is much greater than at points some distance from the line center, and the total energy scattered by a group of atoms will be essentially determined by the intensity at the line center. It is readily shown that for a point some distance from the line center the emission contains a term $l_\nu\overline{J(\tau)}$, where l_ν is the line-scattering coefficient and $\overline{J(\tau)}$ is a mean radiation intensity, averaged over l_ν; for a strong line, $\overline{J(\tau)}$ is essentially equal to $J_{\nu_0}(\tau)$, the intensity at the line center.

To relate this situation to the existing solutions for the equation of transfer, Houtgast makes some useful simplifications. The theory of coherent scattering indicates that the intensity $J_{\nu_0}(\tau)$ at the line center should be equal to the black-body radiation intensity B_ν for values of τ greater than a few tenths. As a result of the high scattering and absorption coefficients at the line center, $J_{\nu_0}(\tau)$ reaches its value for local thermodynamic equilibrium very rapidly with increasing depth, while for other frequencies a greater optical depth is necessary to shield the interior from the exterior and to provide the nearly isotropic radiation field which is a prerequisite for black-body radiation. On the other hand, at the very surface of the atmosphere J_{ν_0} is very small, since the emergent intensity in the line center is low. It is assumed by Houtgast that these values for $J_{\nu_0}(\tau)$, computed on the basis of coherent scattering, may be used in a first approximation for the effects produced by noncoherent scattering. It follows that for appreciable optical depths the re-emission of scattered radiation in the wings of the line will be $l_\nu B_\nu$, while at the very surface practically no scattered radiation will be emitted in the line wings. Thus, when noncoherent scattering is present, the scattering process at appreciable optical depths behaves as pure absorption, since the re-emission is determined by B_ν rather than by J_ν, while at the very surface the scattering coefficient may be treated rather as an extinction coefficient, with no subsequent re-emission. In this way the presence of noncoherent absorption should reveal itself in the line wings as an apparent pure absorption plus some extinction. Near the line center, on the other hand, J_ν becomes practically equal to J_{ν_0}, and the equations for coherent scattering should be applicable.

The foregoing argument assumes the presence of completely noncoherent scattering. When the noncoherency is due to the natural width of the lower atomic level of the transition producing the line, the scattered radiation emitted is not completely non-

[8] B. Strömgren, *Handb. d. Ap.*, **7**, 228, Berlin: J. Springer, 1936.

coherent but may be represented as the sum of two terms, one corresponding to coherent scattering, the other to completely noncoherent scattering. The relevant formulae, which had been derived previously[9, 10] are given in Houtgast's paper.

To test for the presence of noncoherent scattering, Houtgast therefore compares the observed intensities with what would be expected in turn for pure absorption, pure extinction, and pure scattering. For the far wings the values of c for each line are divided by the value found at the center of the solar disk and plotted in Figure 1 (Fig. 41 in Houtgast's paper) together with the theoretical curves. The values of β_0, the slope of the continuous spectrum with depth in the formula

$$B_\nu(\tau) = B_\nu(0)\{1 + \beta_0\tau\},$$

are taken from the measurements of limb darkening made by Abbot and his collaborators.[11] The values of τ_1 are less definite but represent likely values.

It is evident from this figure that coherent scattering does not adequately represent the observations, especially for the ultraviolet lines with a high value of β_0. In fact, if coherent scattering were the mechanism of line formation, c would vanish for the ultraviolet lines at some distance from the limb, and for points closer to the limb the wings would appear in emission, corresponding to negative values of c.

The intensities in the inner wings, at about 60 per cent of the continuous background, give essentially the same results. The intensities closer to the line center, in the neighborhood of 30 per cent of the continuous background, are shown in Figure 2 (Houtgast's Fig. 48). These conform more closely to the curve for pure coherent scattering and suggest, according to expectations, that coherent scattering may be a useful approximation so close to the line center.

While Houtgast's treatment is straightforward enough, it is perhaps not physically clear from his discussion why the wing intensities for the ultraviolet lines should provide such sensitive discrimination between noncoherent scattering, or pure absorption, on the one hand, and pure coherent scattering, on the other. It may be of interest to investigate more closely this effect, which may be shown to depend on the high value of β_0 in the ultraviolet.

For integrated radiation β_0 is determined by the condition that the average radiation intensity from all directions absorbed in a given volume is just equal to the average intensity emitted from the volume. For monochromatic radiation, however, this is no longer true. When β_0 is large for some frequency, $B_\nu(\tau)$ for that frequency increases rapidly with optical depth; and the intensity of radiation of that frequency reaching a given volume near the surface and absorbed there will be greater than the radiation of that frequency emitted from the same volume, the lost energy appearing in a different frequency. As a result of this phenomenon, a purely scattering atom, emitting all the radiation which it has captured in a particular frequency, will emit more radiation, for the same amount of absorption, than a purely absorbing atom, for which the emission is determined by Kirchhoff's law and hence depends on the local temperature. The presence of scattering atoms at the surface will therefore lead to an increase of the radiation emitted, as compared to the frequencies outside the line, where only pure absorption takes place, provided that the total net flux near the surface is much the same at both frequencies. In the far wings of a line this last condition will be satisfied; the wings of such a line, if formed by coherently scattering atoms, will therefore be seen in emission at points sufficiently close to the limb. When β_0 is 3/2, in the first approximation, the effects of scattering and absorption become roughly the same, since in either

[9] L. Spitzer, Jr., *M.N.*, **96**, 794, 1936.

[10] R. v. d. R. Woolley, *M.N.*, **98**, 624, 1938.

[11] C. G. Abbot, F. E. Fowle, and L. B. Aldrich, *Ann. Ap. Obs. Smithsonian Inst.*, **3**, 157, 1913; **4**, 221, 1922.

case each atom emits as much energy in a particular frequency as it absorbs. For smaller values of β_0, scattering increases the strength of a line near the limb in comparison with a line formed by pure absorption.

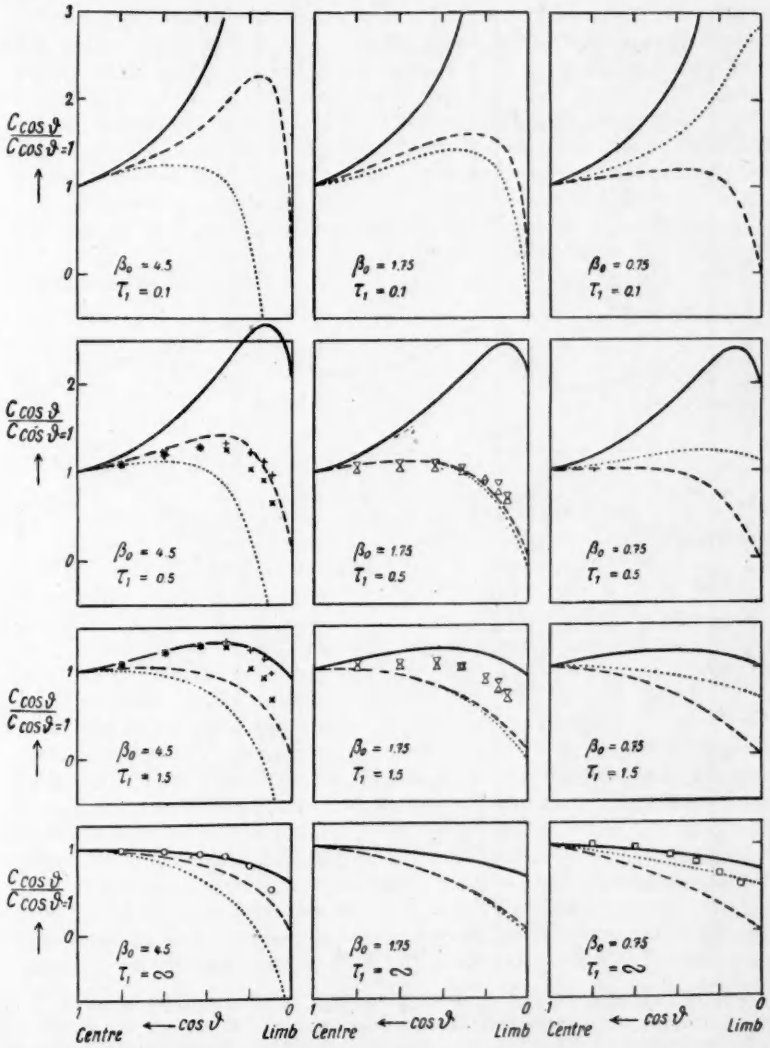
$\frac{C_{\cos\vartheta}}{C_{\cos\vartheta=1}}$
$\beta_0 = 4.5$ $\tau_1 = 0.1$
$\beta_0 = 1.75$ $\tau_1 = 0.1$
$\beta_0 = 0.75$ $\tau_1 = 0.1$
$\beta_0 = 4.5$ $\tau_1 = 0.5$
$\beta_0 = 1.75$ $\tau_1 = 0.5$
$\beta_0 = 0.75$ $\tau_1 = 0.5$
$\beta_0 = 4.5$ $\tau_1 = 1.5$
$\beta_0 = 1.75$ $\tau_1 = 1.5$
$\beta_0 = 0.75$ $\tau_1 = 1.5$
$\beta_0 = 4.5$ $\tau_1 = \infty$
$\beta_0 = 1.75$ $\tau_1 = \infty$
$\beta_0 = 0.75$ $\tau_1 = \infty$
Centre ← cos ϑ Limb

FIG. 1.—Computed center-limb variations of c: — — —, absorption; ....., coherent scattering; ——, extinction. Observations added: ○, K line of Ca^+; +, *Fe* multiplet at 4100 A; ×, *Ca* 4226.7; △, *Mg* b lines; ▽, *Na* D lines; □, infrared lines of Ca^+.

There is one serious criticism which must be made of Houtgast's analysis. He assumes, following Woolley,[10] that the first approximation for J_{ν_0}, derived without consideration of noncoherent scattering, may be used to determine the effect of this process on the intensity in the far wings. This assumption, while natural enough, may be true under some conditions but is not generally valid. The process of noncoherent scattering cannot directly alter the total net flux in a line; it simply transfers it from one frequency to

another. The net flux at the line center is lower than anywhere else. If J_{ν_0} in the absence of noncoherent scattering is such that the net flux in the line will apparently be increased (or decreased) when noncoherency is introduced, then actually J_{ν_0} will tend

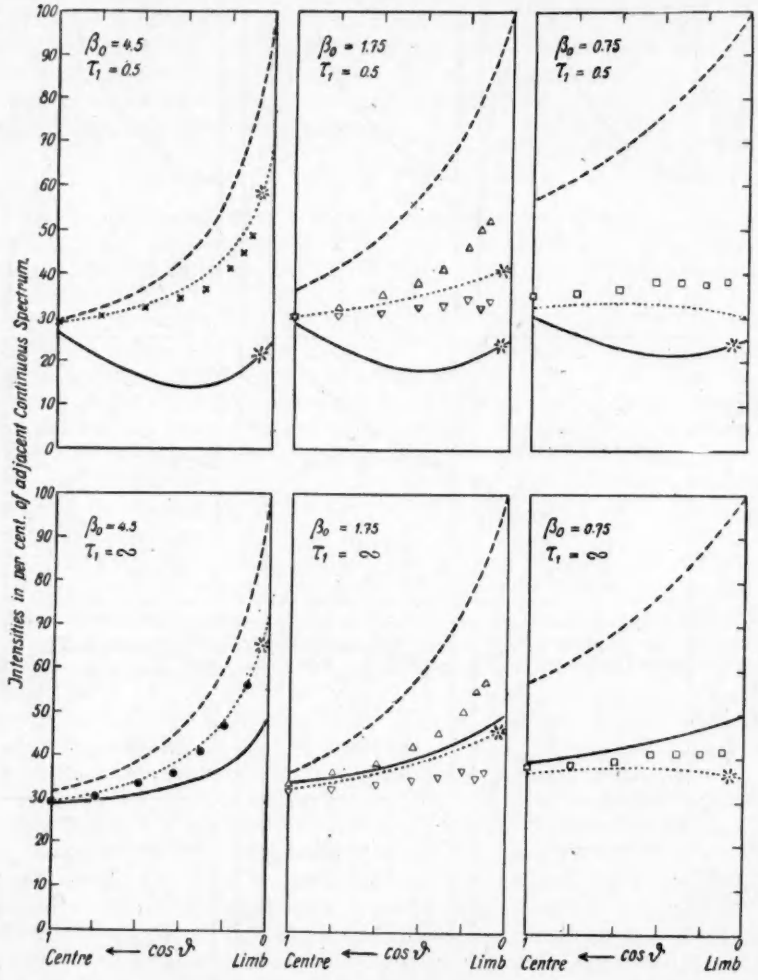
$\beta_0 = 4.5$ $\tau_1 = 0.5$
$\beta_0 = 1.75$ $\tau_1 = 0.5$
$\beta_0 = 0.75$ $\tau_1 = 0.5$
$\beta_0 = 4.5$ $\tau_1 = \infty$
$\beta_0 = 1.75$ $\tau_1 = \infty$
$\beta_0 = 0.75$ $\tau_1 = \infty$
Intensities in per cent. of adjacent Continuous Spectrum.
Centre ← cos ϑ Limb

FIG. 2.—Center-limb variations in the Fraunhofer lines. Theoretical curves: — — —, absorption; ....., coherent scattering; ——, extinction. Observations: ●, H and K line of Ca^+; ×, *Fe* multiplet and *Ca* 4226.7; △, *Mg* b lines; ▽, *Na* D lines; □, infrared lines of Ca^+. The theoretical curves, appropriate to a comparison with the observations, are marked with an asterisk (*) (extinction is only to be expected in a comparatively thin surface layer); the comparison concerns the center-limb variations; the heights of the various theoretical curves and of the observational points are, therefore, adapted as well as possible to each other.

to fall (or rise) to a lower (or higher) value when the scattering becomes noncoherent, so that the total drain on the flux at the center will be zero. If some additional, extraneous source of net flux appears, as J_{ν_0} falls below (or rises above) B_ν, then J_{ν_0} may remain almost equal to B_ν. As pointed out before,[9] this will be the case if the ratio of selective absorption to scattering (ϵ in Eddington's notation) is sufficiently high. But if the selective absorption is not very great, J_{ν_0} as a function of τ will be quite different

from that computed on the basis of coherent scattering. This same argument may, of course, be carried through analytically. The exact computation of J_{ν_0} when the scattering is noncoherent and when no selective absorption is present offers some difficulties, however.

It is probable that the selective absorption for most of the lines measured by Houtgast is sufficiently great to keep J_{ν_0} roughly equal to B_{ν} for an appreciable range in optical depth. Until this point has been examined more carefully, however, the exact interpretation of Houtgast's data and their apparent agreement with what would be expected from completely noncoherent scattering, acting as pure absorption, are both open to question. In any case, the disagreement between the theory of coherent scattering and the center-limb variations of the far wings is quite clear cut and seems to be considerably greater than could be accounted for even by very large systematic errors in the observed profiles. It may be concluded that Houtgast's work strongly suggests, although it does not quite prove, that noncoherent scattering is the dominant process involved in the formation of strong absorption lines.

LYMAN SPITZER, JR.

NEW YORK CITY
August 14, 1943

ASTROPHYSICAL RESEARCH IN FRANCE IN 1940–1942

Despite the very difficult present conditions in the occupied countries, our French colleagues (like those in Holland[1]) have succeeded in carrying on important astronomical research. This is illustrated by Volumes **4** and **5** of the *Annales d'astrophysique*, one copy of which has recently reached this country. These publications illustrate only part of the astrophysical activity in France, since other notes must have been published in the *Comptes rendus*, the *Bulletins de la Société astronomique de France*, the *Cahiers de physique*, the *Publications de l'observatoire de Lyon*, and other periodicals. Such activity is highly gratifying, since it provides reasonable hope that the scientific reconstruction in all countries after the war may be speedier than many of us had anticipated.

The annual reports of the Service d'Astrophysique du Centre National de la Recherche Scientifique for 1939–1940 (by H. Mineur) and for 1941 (by D. Chalonge[2]) mention that even the construction work at the new observatory in Haute Provence has progressed during the war. The buildings for the general services, the director's house, a big workshop (with the most essential tools), the water system, and three domes (of radius 11.50, 8, and 6.50 meters, respectively) have been completed; in October, 1942, work was being continued on the laboratories, a private house, a dormitory, and a road. The 120-inch reflector is installed but was not yet functioning in October, 1942. A Schmidt telescope of 25-cm aperture, working at $f/1.5$, is probably ready for use, as well as a specially built spectrograph intended for the continuation of the spectrophotometric program (down to magnitude 6, from λ 3100 to λ 6600 A).

Similarly, a good deal of construction and repair has been done—of course, at a very slow pace—at the Astrophysical Institute in Paris; also, a number of spectrographic and other instruments have been built.

The investigations mentioned in the annual reports concern: (*a*) the spectrum of the night sky with fast instruments, one of these having a much higher dispersion in the

[1] See *Ap. J.*, **98**, 235, 1943.

[2] In October, 1942, it was stated by D. Chalonge that H. Mineur was not in a position to write his annual report of the Service d'Astrophysique as he had done in all previous years. The implication of this remark is unfortunately too obvious and will be a source of deep anxiety to all friends of Dr. Mineur in this country.

ultraviolet than hitherto available (D. Barbier, Tcheng Mao-Lin, and others); (*b*) The spectrum of the aurora borealis (Dufay and Tcheng, and Bernard); (*c*) the investigation of the temperature of the stratosphere, as derived from the intensity distribution in the bands of ozone (Barbier and Chalonge) (this investigation has required extensive laboratory work); (*d*) various laboratory, solar, and stellar investigations related to the spectrophotometric program of Barbier, Chalonge, Déjardin, *et al.*: the continuous spectrum of the sun from λ 4500 to λ 3200 A; the color temperatures of dwarfs and giants of type G0; properties of coated mercury discharge tubes as standard sources; construction of a "black-body" standard for calibration of the sources used in stellar spectrophotometry; the continuous spectrum of hydrogen in the infrared; total intensities of the *H* and *Ca* II lines in early-type stars, etc.; (*e*) various investigations of the ozone molecule: especially[3] the demonstration that the glow which accompanies the thermal dissociation of ozone in ozonized air is emitted by nitrogen peroxide (NO_2) (Barbier, Chalonge, Masriera); (*f*) statistical investigations on Cepheid variables (Mineur); and (*g*) investigations on the equilibrium of clusters (Mineur, Mayot).

Only a few of these investigations are found in the volumes of the *Annales* received in this country. Two of the most important ("Continuous Radiation of Various Stars in the Region 3100–4600 A," by D. Barbier and D. Chalonge; "Measures of Total Intensities of the Lines of *H* and *Ca* II in Stellar Spectra," by D. Barbier, D. Chalonge, and N. Morguleff) have been reviewed recently.[4] The present review gives a summarized account of the other papers.

1. *René Bernard* (*Dept. of Physics, Lyons*), "*Atomic Nitrogen in the High Atmosphere*" (**4**,13–29).—The author shows that the auroral transition $^4S - {}^2P$ of [*N* I] (λ 3466.5) is absent in the night sky[5] but that it is present in the aurora. The author describes the results of his photometric measurements of the intensities of the [*O* I], [*N* I], and N_2 transitions at the base and the summit of the aurora: λ 3466.5 behaves in the aurora as do the green [*O* I] line and the $A \rightarrow X$ bands of N_2. The author tries to explain the "altitude effect" on the [*O* I], [*N* I], and $A \rightarrow X$ transitions by triple collisions: the dissociation of N_2 is considerable in the aurora, increasing with the height in the atmosphere.

From a long controversial discussion concerning the identification of the nebular transitions $^4S - {}^2D$ of [*N* I] (near λ 5200) in the aurora and the night sky, the author concludes that these lines are actually absent, in agreement with Nicolet's previously published results. Incidentally, in another paper not available here,[6] Dufay, Gauzit, and Tcheng Mao-Lin announce the observation of the λ 5200 line in the high atmosphere. Pending detailed information, the reviewer prefers to abstain from any comment concerning this problem.

2. *Tcheng Mao-Lin* (*Observatory of Lyons*), "*Spectrophotometric Study of the Minima of Algol*" (**4**, 97–117).—The author has reinvestigated the so-called "Tikhoff-Nordmann effect" by careful spectrophotometric measures near the principal minima of Algol. His monochromatic light-curves, which cover the region λλ 3951–6373 A, do not reveal any systematic shift in the times of minima, the dispersion of the instant of minimum being only from 1 to 3 minutes. This result agrees perfectly with Hall's recent photoelectric observations. Most probably the "Tikhoff-Nordmann effect" does not exist; or, if it does, it must be much smaller than was announced by Nordmann and others. The author gives an excellent historical review of the problem of the "Tikhoff-Nordmann effect."

3. *Tcheng Mao-Lin* (*Observatory of Lyons*), "*The Absorption Spectrum of γ Cassiopeiae from August to October, 1940*" (**4**, 118–35).—On the basis of objective-prism and slitless

[3] *C.R.*, **213**, 1010, 1941.

[4] J. Greenstein, *Ap. J.*, **97**, 445, 1943; O. Struve, *Ap. J.*, **98**, 231, 1943.

[5] Obtained independently by the McDonald observers (*Ap. J.*, **93**, 337, 1941).

[6] *Pub. Obs. Lyon*, **3**, 59, 1941, reference found in paper No. 8 by R. and L. Herman.

spectrograms of γ Cas the author has established a list of absorption lines in the region λλ 3890–5317 A. In agreement with observations made in this country, the lines of *H*, *He* I, and *Fe* III are found to be very intense. A large number of other elements are mentioned, some of which seem very doubtful to the reviewer on the basis of a comparison with the McDonald slit spectrograms, which are of much higher quality.

4. *D. Barbier, D. Chalonge, and E. Vigroux (Paris), "Spectrophotometric Investigation of the Lunar Eclipse of March 2–3, 1942"* (**5,** 1–22).—The results described in this paper are of a more or less provisional nature, the aim of the authors being to call the attention of the astronomers again to the important results concerning the high atmosphere which are likely to be obtained from a more thorough observational treatment of lunar eclipses. The essential telluric features are the bands of oxygen (B- and α-bands) and ozone (Chappuis system). The intensity distribution of the ozone bands across the eclipsed disk of the moon provides data on the distribution of ozone in the high atmosphere of the earth.

5. *D. Barbier and D. Chalonge (Paris), "Photometric Investigation of the Lunar Eclipse of March 2–3, 1942"* (**5,** 58–70).—The photometric study of lunar eclipses is of importance in relation to the high atmosphere of the earth,[7] the method consisting essentially in measuring the variation, during the course of an eclipse, of the luminosity of a small region of the lunar disk. The authors employed the photographic method of Fabry and Buisson with a yellow filter. They compared their results with those obtained by Danjon in 1921 and 1931, and by Rougier at the March, 1942, eclipse.

6. *J. Dubois (Observatory of Bordeaux), "The Electrometer Tubes,"* (**5,** 23–37).—This is a technical discussion of the utilization conditions of the Philips No. 4060 electrometer triod; the results may be readily applied to other electrometer tubes.

7. *E. Vigroux (Paris), "Source of Continuous Spectrum for Spectrophotometry in the Visual Region"* (**5,** 41–57).—The author has discussed all factors affecting the spectral intensity distribution of the continuous emission by a certain fluorescent screen excited by a mercury-vapor lamp and giving a fairly uniform photographic density between λ 4400 and λ 5500 (prism spectrograph, Agfa ISS plates). The intensity distribution is independent of the factors examined: aging of the tube, intensity of excitation, temperature, even composition of the exciting light. The source has been compared to the black body through the intermediary of a calibrated incandescent lamp with tungsten ribbon; it has been utilized for the photometry of the lunar eclipse of March 2–3, 1942. The emission may be obtained very homogeneously over the whole surface of a screen of 6 cm.[2] The fluorescent coating consists of a mixture of several mineral substances.

8. *R. and L. Herman, "Extension of the Lyman-Birge-Hopfield System of N_2"* (**5,** 71–81).—Attention had been called[8] to the desirability of additional laboratory work on the Lyman-Birge-Hopfield system of N_2, which had heretofore been measured only up to λ 2162, the reason being that extrapolated wave lengths for high vibrational quantum numbers v'' seemed to agree with the wave lengths of unidentified bands in the night-sky spectrum. Renée and Louis Herman have succeeded in obtaining a discharge giving fairly intense Lyman-Birge-Hopfield bands up to λ 2600 and have shown that the previously adopted formula for the vibrational system must suffer important corrections. When these corrections are applied to the vibrational formula, the tentative identifications suggested for the night-sky features appear less convincing. Incidentally, these suggested identifications have been superseded in a more recent paper.[9] The reviewer is of the opinion that it might be a good plan to postpone all discussion of identifications of

[7] Link, *Bull. Astr.*, **8,** 77, 1932.

[8] *Ap. J.*, **93,** 337, 1941; also *C.R.*, **213,** 360, 1941.

[9] *Ap. J.*, **97,** 72, 1943.

night-sky bands until observations[10] are secured with spectrographs having a spectral purity at least twice as high as the highest heretofore used!

9. *J. Dufay (Lyons), "Remarks on the Spectral Distribution of Solar Energy in the Violet and Ultraviolet Regions"* (**5**, 85–92).—The author discusses Pettit's results[11] and suggests that the curve may have been undercorrected for the ozone absorption beyond λ 3200. He also attributes the three depressions found by Pettit near λλ 4200, 3900–3800, and 3500 to undercorrection of the cyanogen absorption in the solar atmosphere.

10. *J. Dufay (Lyons), "The Spectrum of the Setting Sun, from 4600 to 6900 A"* (**5**, 93–113).—This is the first paper of a series in which the author will discuss the selective absorption in the earth's atmosphere on the basis of (*a*) the light transmitted by the atmosphere through different masses of air (setting sun); (*b*) the light diffused at twilight by the higher layers (twilight spectrum); and (*c*) the light of the eclipsed lunar disk, at various distances from the center of the geometrical umbra. Since the ozone is mainly present in the high layers, water vapor in the low strata, and oxygen more or less uniformly over the whole mass, variations in the relative intensities of the absorption bands should be found among the three classes of atmospheric spectra mentioned above.

On low-dispersion spectrograms of the setting sun the telluric bands become so outstanding that they change entirely the appearance of the spectrum.[12] According to Dufay, all the absorption features receive satisfactory identification with bands of water vapor, oxygen, $(O_2)_2$, and ozone. Among the diffuse bands of $(O_2)_2$, only the λ 4774 band shows clearly on Dufay's plates, the others (λ 5770 and λ 6290) being superimposed over the δ bands of H_2O and the α and α' bands of O_2: the absorption by $(O_2)_2$ appears only when the sun is 2° or 3° above the horizon.

11. *P. Guintini, "Possibility of Improving the Statistical Determination of Distances of B-Type Stars"* (**5**, 114–22).—From the catalogue of color indices of 1332 B stars by Stebbins and collaborators, the author tries to establish a formula relating the interstellar absorption to the galactic longitude.

P. SWINGS

PASADENA, CALIFORNIA
October 14, 1943

SOLAR RESEARCH IN BELGIUM DURING 1942

A copy has been received of an important Liége publication, dated December 15, 1942, by Dr. Marcel V. Migeotte, entitled "First Application of a New Self-Recording Infrared Spectrograph of High Dispersion to the Solar Spectrum." The department of astrophysics of the University of Liége engaged in a program of astronomical infrared spectroscopy in 1933, the idea being to utilize a spectrograph having as high a resolving-power as possible. The solar tower equipped with a 12-inch vertical coelostat and the constant-temperature basement room were almost completed in 1940, as was also a self-recording spectrograph designed by Migeotte. This instrument consisted of a monochromator in KBr and of a large plane-grating spectrograph. It was intended to use four plane echelette gratings with 15,000, 3,600, 2,400, and 1,200 lines per inch, respectively, the last three of 225 × 175-mm size. In this way the whole spectrum from 1 to 20 μ could be covered with a resolving-power such that lines distant by about 1 cm^{-1} would be separated. At present only gratings with 15,000 and 2,400 lines per inch are available.

The spectrograph and all its accessories were installed in June, 1942, and the first re-

[10] Such as have been started by D. Barbier, according to one of the reports.

[11] *Ap. J.*, **91**, 159, 1940.

[12] The material collected by H. D. Babcock at the Mount Wilson Observatory illustrates this very clearly.

FIG. 1.—Region from λ 15,035, to λ 15,178 of the solar spectrum, recorded at the Observatory of Liége (Belgium), October 4, 1942, at three different hours. Scale 2/3.

cordings of the solar spectrum were made in July, 1942. The paper by Migeotte gives a general account of the results in the region from 1.35 to 2 μ, using a 15,000-line grating. In the region around 1.5 μ, absorption lines distant by 1.5 A can be separated, hence corresponding to a resolving-power of 10,000; this was still further ameliorated in 1943. The separation between solar and telluric lines is usually easy. As an example, the region from $\lambda\lambda$ 14,662–15,178, in which Abbot and Freeman's recordings gave only a dozen absorption features, shows at least 87 clearly separated lines on Migeotte's tracings. The reproducibility of the instrument is illustrated by Figure 1, showing the region from λ 15,035 to λ 15,178 A taken at three different hours.

Migeotte has almost completed a study of the water-vapor spectrum in the same region (thus extending Nielsen's work, which had not been received in Belgium). According to recent news, the new infrared spectrograph is in continuous operation.

P. SWINGS

PASADENA, CALIFORNIA
November 5, 1943

NOTES

PRELIMINARY NOTE ON THE BEHAVIOR OF HELIUM IN THE SOLAR ATMOSPHERE

ABSTRACT

The present data on the appearance of helium in the phenomena of the solar disk are reviewed. The possibility that the triplet helium lines behave like those of an element of low ionization potential under special conditions is suggested and discussed. A classification of eruptions based on the appearance of helium is suggested.

The infrared helium triplet λ 10830, $2^3S-2^3P^0$, was first identified in the normal solar spectrum by H. D. and H. W. Babcock[1] and was described by them as diffuse. M. and Mme d'Azambuja[2] studied the appearance of this line in detail, confirmed its diffuse character, and found an equivalent width of 1 A, its Fraunhofer intensity being estimated as 10. The line appears distinctly as a doublet, the shorter wave-length component being considerably more intense. Over the plages[3] λ 10830 clearly appears in absorption, and it is quite strong in the filaments, while in eruptions it is seen as an emission line.[4] Although λ 5876, $2^3P^0-3^3D$, does not appear in the normal disk spectrum, the absorption of this line over plages has been recorded by Waldmeier[5] and others. About 90 per cent of the plages viewed through the attachment to the spectrohelioscope[6] of the Whitin Observatory during a two-year period revealed it in absorption. The character of the line over a plage appears to be wide and diffuse. D_3 has been found in absorption over eruptions by a number of solar observers, and its appearance in emission over very bright ones has also been confirmed. Simultaneous observations of *Hα* and D_3[7] in 43 eruptive areas seem to indicate that λ 5876 occurs in absorption over the faint eruptions as well. Waldmeier[8] has found λ 5876 in absorption over filaments, and its presence there has been suspected by several others. The only singlet lines to appear on the disk are λ 6678, $2^1P^0-3^1D$, and λ 4388, $2^1P^0-5^1D$;[9] and they occur only over bright eruptions. The former has been observed in emission over the most intense portion of a very bright eruption.[10]

The helium lines are listed in Table 1, and the observational results are tabulated. The D lines of sodium are included as well as the hydrogen lines.

An examination of the data for helium in the phenomena of the solar atmosphere suggests that the so-called "helium problem" may be considered a singlet-triplet problem. In view of the great abundance of helium in the solar atmosphere and the low probability of transition from the metastable level 2^3S to the ground state, a possible explanation of the behavior of helium is suggested. If it is assumed that there is a general leakage of short-wave radiation sufficient to ionize singlet helium from the ground state, the meta-

[1] *Pub. A.S.P.*, **46**, 132, 1934.

[2] *B.A.*, **9**, 350, 1938.

[3] To avoid confusion, the European terms "filament" and "plage" are used rather than "dark flocculus" and "bright flocculus."

[4] D'Azambuja, *Observatory*, **63**, 269, 1940.

[5] *Naturwiss.*, **24**, 638, 1936.

[6] Dodson and van Dijke, *Pub. A.A.S.*, **10**, 122, 1941.

[7] Dodson and van Dijke, *Ap. J.*, **95**, 325, 1942.

[8] *B.A.*, **9**, 355, 1938.

[9] Allen, *M.N.*, **100**, 368, 1940.

[10] Dodson and van Dijke, *Ap. J.*, **95**, 325, 1942.

stable level 2^3S will become populated, provided the density is low enough to prevent frequent collisions—a condition which may be obtained in the higher atmosphere. Once the level 2^3S is fairly populated, the helium atom is comparable to an atom with an ionization potential of 4.67 volts. In Table 2 the singlet and triplet transitions are grouped according to quantum designations for purposes of intercomparison. The multiplet designation and data of excitation potentials are taken from Miss Moore's *Multiplet Table*,

TABLE 1

Line	Filament	Plage	Eruption
$H\alpha$	Absorption	Emission	Emission
$H\beta$, $H\gamma$	Absorption	Absorption	Emission
D_1, D_2	.....	.....	Emission
λ 4388 (singlet)	.....	.....	Absorption
λ 6678 (singlet)	.....	.....	Absorption, emission
λ 4471 (triplet)	.....	.....	Absorption*
λ 5876 (triplet)	(Absorption)	Absorption	Absorption, emission
λ 10830 (triplet)	Absorption	Absorption	Emission

* Allen, *M.N.*, **100**, 368, 1940.

TABLE 2

Multiplet	λ	Low E.P.	High E.P.	Lab. Int.	Chrom. Int.	Height (Km.)
$2^1S-3^1P^0$	5015	20.53	22.99	6	2	2500
$2^1S-4^1P^0$	3965	20.53	23.64	4	4	1200
$2^1P^0-3^1D$	6678	21.13	22.98	6	8	2200
$2^1P^0-4^1D$	4922	21.13	23.64	4	2	2500
$2^1P^0-5^1D$	4388	21.13	23.94	3	2	2000
$2^1P^0-3^1S$	7281	21.13	22.82	3	.....	.....
$2^1P^0-4^1S$	5048	21.13	23.57	2	.....	.....
$2^1P^0-5^1S$	4438	21.13	23.91	1	2	750
$2^3S-3^3P^0$	3888	19.74	22.91	10	.....	.....
$2^3S-4^3P^0$	3188	19.74	23.61	8	(High)*	.....
$2^3P^0-3^3D$	5876	20.87	22.98	10	40	7500
$2^3P^0-4^3D$	4471	20.87	23.63	6	40	7500
$2^3P^0-5^3D$	4026	20.87	23.94	5	15	5000
$2^3P^0-3^3S$	7065	20.87	22.62	5	1	1000
$2^3P^0-4^3S$	4713	20.87	23.49	3	5	5000
$2^3P^0-5^3S$	4120	20.87	23.87	3	2	2500
$2^3S-2^3P^0$	10830	19.74	20.87	(200)	(High)*	Above 7500*

* Mr. H. D. Babcock, in a private communication, states that he has observed λ 3188 in the chromosphere this summer; and, from the conditions under which it was observed, he estimates its intrinsic intensity must be high. He also estimates, from spectrograms made by H. W. Babcock on Mount Wilson in 1935, that the intensity of λ 10830 is perhaps ten times that of λ 5876 and that it probably attains a considerably greater height.

while laboratory and chromosphere intensities and heights are from the *Revision of Rowland's Preliminary Table.*

The triplet line λ 10830 acts as an ultimate line with an excitation potential of 1.13 volts, while λ 5876 acts as a subordinate line with an excitation potential of 3.24 volts. Thus, the behavior of the triplet series may be considered a low-ionization problem under special conditions, instead of one of high ionization.

The absence of λ 5876 from the normal disk spectrum could be due to an insufficient amount of excited helium or to the fact that the emission arising from cascading electrons compensates the absorption. The latter would also account in part for the relative

strengths of λ 5876 and λ 6678 in the flash spectrum. For, although the transition probabilities of these two lines are high and almost equal,[11] the probability of recapture as a triplet is 3 to 1.

In the case of the plages, where there is a general increase in temperature, the additional energy excites the atoms already present at the 2p level, so that λ 5876 appears in absorption. Since this results from an increase in temperature, we would expect to find the stronger absorption in λ 5876, corresponding to the brighter plage as seen in *Hα*—a relation which seems to be supported by observations taken simultaneously in hydrogen and helium. It is also possible that the increase in temperature of the region is accompanied by an increase in short-wave radiation, which in turn ionizes more helium. In this case the number of electrons captured as triplets must more than compensate for the proportional increase in ionization due to greater excitation. In the filaments, λ 10830 appears definitely in absorption, while λ 5876 does so only occasionally. The appearance of the infrared line is to be expected; and we might likewise expect that a very dark prominence (as seen in *Hα*), high in the solar atmosphere, would also yield faint λ 5876 absorption, which is apparently supported by observation.

While little of the nature of eruptions is known, a tremendous increase in energy is clearly indicated by the emission produced. In the case of faint eruptions, λ 5876 appears in absorption; and in more intense ones, it is seen in emission, and λ 6678 in absorption. In a very bright eruption both lines appear in emission. If we assume that an eruption is accompanied or characterized by a tremendous flow of short-wave radiation, at least sufficient to ionize the helium atoms present in the region, the observed spectral sequence can be accounted for.

In view of the behavior of helium, it would seem that a classification of eruptions based on the varied appearance of this element could be more significant than the present one, which is based on the integrated size-intensity of the region as seen in *Hα*. Since an eruption is not characterized by a general increase in the continuum, a classification based on excitation seems advisable. Observations in *Hα* are essential for the location of active areas and for the study of the fainter regions. The appearance of this line, however, is probably not so sensitive a criterion in the case of an eruption of any considerable brightness and for correlations with terrestrial magnetic deviations and short-wave radio fadeouts. There is certainly a great need for solar observations taken simultaneously in hydrogen, helium, and the metals.

SUZANNE E. A. VAN DIJKE

LICK OBSERVATORY
October 26, 1943

[11] Goldberg, *Ap. J.*, **90**, 432, 1939.

REVIEWS

Recent Advances in Galactic Dynamics. By A. C. BANERJI. ("Lucknow University Studies," No. 15.) Allahabad: Allahabad Law Journal Press, 1942. Pp. vi+116.

Professor Banerji divides his discussion of *Recent Advances in Galactic Dynamics* into three parts, dealing, respectively, with the topics "Polytropic Configurations of Gaseous Matter," "Spiral Nebulae," and "The Origin of the Solar System."

In the first chapter Professor Banerji emphasizes particularly the more recent developments on the equilibrium of distorted polytropic configurations in which the effects of rotation and tidal forces are treated as perturbations and are related to the structure of the unperturbed configuration.

In the second chapter the various theories which have been advanced in recent years to account for the spiral structure in extragalactic nebulae are reviewed. The discussion centers around those advances which have derived from Lindblad's original suggestion that the existence of spiral structure may have to be traced to the instability of circular orbits at the edges of flattened systems.

In the last chapter current theories regarding the origin of the solar system are critically reviewed and the difficulties encountered particulary by the "tidal theories" fully exposed. Toward the end of this chapter the author refers to his own theory in which the sun is presumed to have originally been a Cepheid. The sections dealing with this "Cepheid Theory" of the origin of the solar system are too brief to permit judging the merits of the case. But a full account has apparently been published in the *Proceedings of the National Academy of Sciences* (India).

On the whole, the present study is ably written and represents a sound piece of scholarship.

S. CHANDRASEKHAR

Navigation. By J. C. KINGSLAND and D. W. SEAGER. New York and Toronto: Oxford University Press, 1943. Pp. 95. $1.00.

This small book is designed to give a background of the art of navigation for the use of flyers whose training is obviously too short to allow a thorough study of the subject. A clear presentation is in this case of the utmost importance. The authors include a limited amount of material, which they treat in a very simple and understandable manner. The topics covered are maps and charts, rhumb-line bearings, the magnetic compass, wind drift, and dead reckoning. No mention is made of great-circle sailing or celestial navigation. The illustrations make the book very attractive and will be appreciated by the novice in the field.

JOHN TITUS

Yerkes Observatory

Norton's Star Atlas and Telescopic Handbook. By ARTHUR P. NORTON, B.A., and J. GALL INGLIS, F.R.A.S. 9th ed. London: Gall & Inglis, 1943. Pp. 56+18 maps.

This is the latest edition of the most useful of current star atlases. A wealth of practical information is included in the text, and the maps are clear and easy to use.

W. W. MORGAN

ERRATUM

On page 471 of Volume **98**, read λ 4160.6 instead of 4060.6.